AWARD NUMBER: W81XWH-15-1-0282

TITLE: HGF/c-MET Pathway in AIDS-Related Lymphoma

PRINCIPAL INVESTIGATOR: Zhiqiang Qin

CONTRACTING ORGANIZATION: Louisiana State University Health Sciences Center,
New Orleans, LA 70112-7021

REPORT DATE: September 2018

TYPE OF REPORT: Annual Report

PREPARED FOR: U.S. Army Medical Research and Materiel Command
Fort Detrick, Maryland 21702-5012

REPORT DOCUMENTATION PAGE

Form Approved
OMB No. 0704-0188

1. REPORT DATE	2. REPORT TYPE	3. DATES COVERED
SEPT 2018	Annual Report	15 AUG 2017 – 14 AUG 2018

4. TITLE AND SUBTITLE

HGF/c-MET Pathway in AIDS-Related Lymphoma

5a. CONTRACT NUMBER
W81XWH-15-1-0282

5b. GRANT NUMBER

5c. PROGRAM ELEMENT NUMBER

6. AUTHOR(S)
Lu Dai, Zhiqiang Qin

E-Mail: zqin@lsuhsc.edu

5d. PROJECT NUMBER

5e. TASK NUMBER

5f. WORK UNIT NUMBER

7. PERFORMING ORGANIZATION NAME(S) AND ADDRESS(ES)

Louisiana State University
Health Sciences Center, New
Orleans, LA 70112-7021

8. PERFORMING ORGANIZATION REPORT NUMBER

9. SPONSORING / MONITORING AGENCY NAME(S) AND ADDRESS(ES)

U.S. Army Medical Research and Materiel Command
Fort Detrick, Maryland 21702-5012

10. SPONSOR/MONITOR'S ACRONYM(S)

11. SPONSOR/MONITOR'S REPORT NUMBER(S)

12. DISTRIBUTION / AVAILABILITY STATEMENT

Approved for Public Release; Distribution Unlimited

13. SUPPLEMENTARY NOTES

14. ABSTRACT

In the third year of funding period, we have completed Specific Aim 3, and have almost completed Specific Aim 1 and Specific Aim 2. So we have achieved respective milestones listed in the SOW forms. In this year, we focus on targeting HGF/c-MET regulated downstream genes, especially the ribonucleotide reductase subunit M2 (RRM2) in KSHV+ tumor cells. We have found that one of RRM2 inhibitors, 3-AP, actively induces PEL cell cycle arrest through inhibiting the activity of the NF-κB pathway. 3-AP treatment effectively suppresses PEL progression in immunodeficient mice. Targeting RRM2 by 3-AP can also inhibit the growth of Kaposi's Sarcoma (another type of cancer caused by KSHV) cells in vitro and in vivo. During this year funding period, we have totally published 9 peer-reviewed articles about the molecular mechanisms of KSHV viral oncogenesis, and developing novel therapeutic strategies against these malignancies (including one in press now). In most of these publications, I serve as the corresponding or co-corresponding author. We also have published several meeting abstracts on national or international meetings. With the support by this DOD award, I recently got a NIH/NCI RO1 funding (as PI) and a NIH COBRE subproject (as project leader).

15. SUBJECT TERMS
HGF, c-MET, KSHV, primary effusion lymphoma, apoptosis, cell cycle

16. SECURITY CLASSIFICATION OF:			17. LIMITATION OF ABSTRACT	18. NUMBER OF PAGES	19a. NAME OF RESPONSIBLE PERSON
a. REPORT	b. ABSTRACT	c. THIS PAGE			USAMRMC
Unclassified	Unclassified	Unclassified	Unclassified	93	19b. TELEPHONE NUMBER *(include area code)*

Table of Contents

Page

1. INTRODUCTION

Viruses are the most common cause of lymphoma in patients with immune dysfunction, and virus-associated lymphomas incur high mortality for these patients due to a lack of effective therapeutic strategies. Studies in this proposal are designed to elucidate mechanisms for regulation of AIDS/KSHV-associated lymphoma (in particular KSHV+ PEL) pathogenesis by the oncogenic protein HGF/c-MET, and whether targeting HGF/c-MET reduce virus-associated lymphoma progression *in vivo*.

2. KEYWORDS

HGF, c-MET, KSHV, primary effusion lymphoma, apoptosis, cell cycle

3. ACCOMPLISHMENTS

3.1. What were the major goals of the project?

There are 3 specific aims in this project, Aim 1: To identify the complex mechanisms of the HGF/c-MET pathway controlling cell survival/growth for PEL tumor cells. Aim 2: To understand the mechanisms viral oncogenic proteins used to activate the HGF/c-MET pathway. Aim 3: To determine whether a selective small-molecule inhibitor of c-MET, PF-2341066, can repress PEL progression and/or reduce established tumor in an immune-deficient xenograft mice model.

The following are the condition of subtask completion as indicated in SOW:

Specific Aim 1(specified in proposal)	**Timeline**	**Site 1**
Major Task 1	Months	
Subtask 1: *HGF/c-MET affects viral gene expression (completed)*	2-3	Dr. Qin
Subtask 2: *HGF/c-MET affects downstream signaling pathways (ongoing)*	3-4	Dr. Qin
Subtask 3: *HGF/c-MET affects cell cycle checkpoints (completed)*	2-3	Dr. Qin
Subtask 4: *HGF/c-MET affects HGF secretion from PEL cells (completed)*	1-2	Dr. Qin
Specific Aim 2 (specified in proposal)	**Timeline**	**Site 1**
Major Task 2	Months	
Subtask 1: *viral proteins are essential for activation of HGF/c-MET (completed)*	2-3	Dr. Qin
Subtask 2: *key domain or amino acid residues essential for activation of HGF/c-MET (ongoing)*	4-6	Dr. Qin
Subtask 3: *the role of c-MET phosphorylation in*	2-3	Dr. Qin

signaling activation (completed)		
Specific Aim 3 (specified in proposal)	**Timeline**	**Site 1**
Major Task 3	Months	
Subtask 1: *c-MET inhibitor prevents PEL development in NOD/SCID mice model (completed)*	4-5	Dr. Qin
Subtask 2: *c-MET inhibitor reduces established PEL progression in NOD/SCID mice model (completed)*	5-7	Dr. Qin

3.2. What was accomplished under these goals?

In the third year of funding period, we have completed Specific Aim 3, and have almost completed Specific Aim 1 and Specific Aim 2 as listed in the SOW forms above. During this year funding period, we have totally published 9 peer-reviewed articles about the molecular mechanisms of KSHV viral oncogenesis, and developing novel therapeutic strategies against these malignancies (including one in press now). In most of these publications, I serve as the corresponding or co-corresponding author. We also have published several meeting abstracts on national or international meetings (please see below details in **PRODUCTS**).

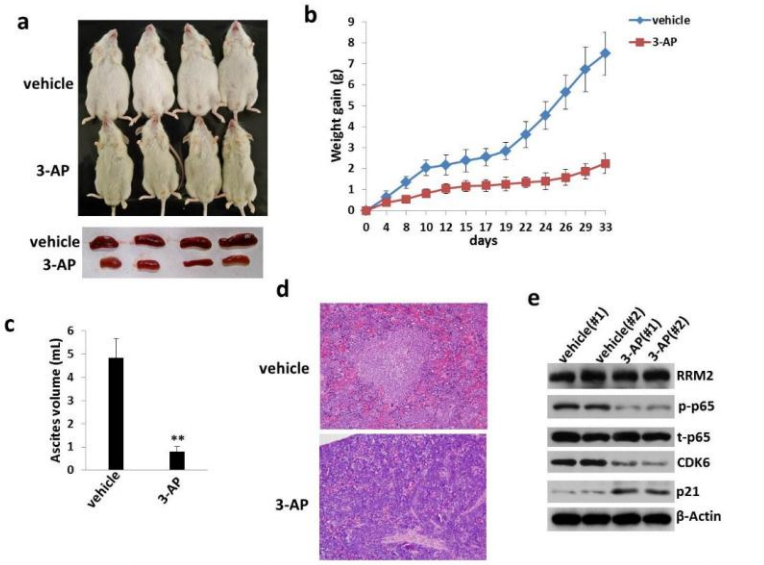

Figure 1. 3-AP treatment suppresses PEL progression *in vivo*. (**a-c**) NOD/SCID mice were injected i.p. with 1x10^7 BCBL-1 cells. 24 hours later, 20 mg/kg of 3-AP or vehicle (n=8 per group) were administered i.p., once daily, 3 days per week. Weights were recorded weekly. Images of representative animals and their spleens, as well as ascites fluid volumes, were collected at the conclusion of experiments on day 33. (**d**) Spleens from representative vehicle or 3-AP treated mice were prepared for the H&E staining. (**e**) Protein expression of the ascites PEL cells collected from the representative vehicle or 3-AP treated mice was analyzed by immunoblot analysis.

In this year, we focus on targeting HGF/c-MET regulated downstream genes, especially the ribonucleotide reductase subunit M2 (RRM2) in KSHV+ tumor cells. We have found that one of RRM2 inhibitors, 3-AP, actively induces PEL cell cycle arrest through inhibiting the activity of the nuclear factor-κB pathway. Using a xenograft model, we found that 3-AP effectively suppresses PEL progression in immunodeficient mice. Transcriptome analysis of 3-AP-treated PEL cell lines reveals altered cellular genes, most of whose roles in PEL have not yet been reported. The represented results have been shown in **Figure 1** & **2**.

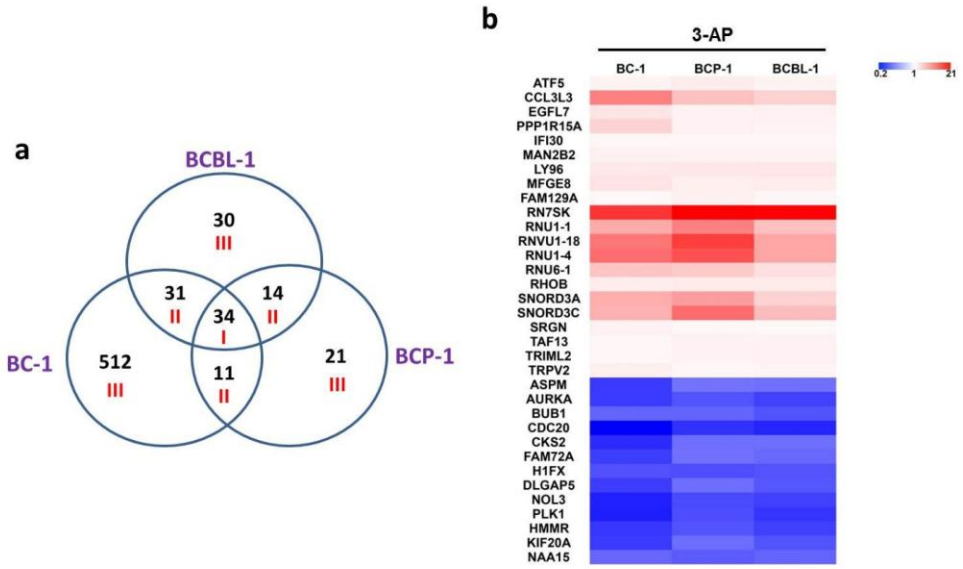

Figure 2. Transcriptome analysis of the 3-AP treated PEL cell lines. (**a**) The Human HT-12 v4 Expression BeadChip (Illumina) was used to investigate the transcriptome change between 3-AP and vehicle treated KSHV+ PEL cell lines (BCBL-1, BC-1 and BCP-1). The intersection analysis of significantly altered genes (expression change ≥ 2-fold and p<0.05) was conducted using Illumina GenomeStudio software. Set I: genes that were commonly altered in all three cell lines. Set II: genes that were altered in two cell lines. Set III: genes that were altered in only one cell line. (**b**) Heat map of genes commonly altered in all three 3-AP treated PEL cell lines (*vs* the vehicle treated controls). The heat map plot was generated by Microsoft Excel 2010.

We next found that 3-AP treatment selectively inhibited the proliferation of KSHV-infected endothelial cells, the major cellular components of Kaposi's Sarcoma (another cancer caused by KSHV), through inducing DNA damage, reducing the levels of intracellular iron and reactive oxygen species (ROS) and increasing viral lytic gene expression. By using a KS-like nude mouse model, we found that 3-AP treatment significantly suppressed KSHV induced tumorigenesis *in vivo* (**Figure 3**).

3.3. What opportunities for training and professional development has the project provided?

I have trained 2 postdoctors in my lab: Dr. Lu Dai has published 7 papers during this third year funding period (as the first author in most publications), and Dr. Jungang Chen has one paper in press now. We also have displayed our data in several national or international meetings such as International Conference on EBV & KSHV 2018. With the support by this DOD award, I recently got a NIH/NCI RO1 funding (as PI) and a NIH COBRE subproject (as project leader), although none of which is overlapped with the current project.

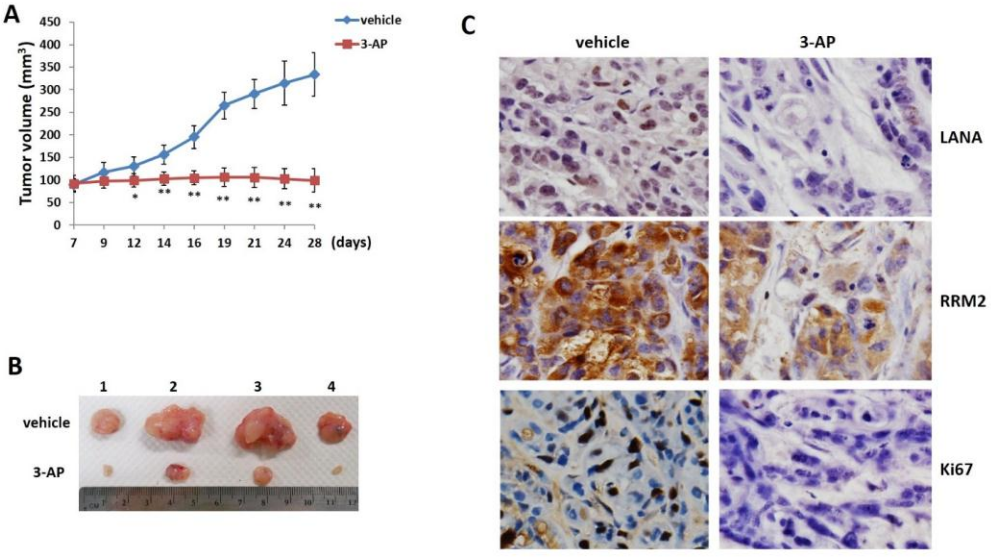

Figure 3. 3-AP treatment significantly represses KSHV induced tumorigenesis *in vivo*. (**A-B**) TIVE-LTC were injected subcutaneously into the flanks of nude mice (4 mice per group). When tumors reach ~10 mm in diameter for about one week, mice were received *in situ* subcutaneous injection with either vehicle or 3-AP (20 mg/kg), 3 days/week. The mice were observed and measured every 2~3 days for the size of palpable tumors for additional 3 weeks. At the end of experiment, the tumors were excised from the site of injection for subsequent analysis. Error bars represent the S.D. from one of 2 independent experiments. *=p<0.05, **=p<0.01. (**C**) Protein expression in tumor tissues from representative mice was measured by using the immunohistochemistry staining.

3.4. How were the results disseminated to communities of interest?

Nothing to Report.

3.5. What do you plan to do during the next reporting period to accomplish the goals?

We have asked 1-y no cost of extension to complete the rest experiments in Aim 2 & 3, data analysis and new manuscripts / grant proposals preparation.

4. IMPACT

4.1. What was the impact on the development of the principal discipline(s) of the project?

Our results have illuminated the complicated mechanisms through which the HGF/c-MET pathway regulates KSHV+ PEL cell survival. Our exciting *in vivo* data have provided the framework for development and implementation of clinical trials for evaluating strategies targeting HGF/c-MET (alone or combination of other therapies) for the treatment of lymphoma in HIV-infected patients including military personnel.

4.2. What was the impact on other disciplines?

Nothing to Report.

4.3. What was the impact on technology transfer?

Nothing to Report.

4.4. What was the impact on society beyond science and technology?

Nothing to Report.

5. CHANGES/PROBLEMS

Dr. Chris Parsons, the mentor of this project has left LSUHSC-NO and is no longer as key personnel in this project. Also, this project has asked 1-y no cost of extension.

6. PRODUCTS

6.1. Journal publications (total 9, * as the corresponding author, all have acknowledgement of DoD federal support):

1. Qiao J, Cao Y, Zabaleta J, Yang L, Dai L *, **Qin Z** *. Regulation of virus-associated lymphoma growth and gene expression by bacterial quorum sensing molecules. *J Virol*. 2018 May 9. pii: JVI.00478-18. doi: 10.1128/JVI.00478-18. [Epub ahead of print].
2. Dai L, Chen J, Cao Y, Del Valle L, **Qin Z** *. Ribonucleotide reductase inhibitor 3-AP induces oncogenic virus–infected cell death and represses tumor growth. *J Cancer*. 2018, *in press*.
3. Xu W, Luo Z, Alekseyenko AV, Martin L, Wan Z, Ling B, **Qin Z,** Heath SL, Maas K, Cong X, Jiang W. Distinct systemic microbiome and microbial translocation are associated with plasma level of anti-CD4 autoantibody in HIV infection. *Sci Rep.* 2018 Aug 27;8(1):12863. doi: 10.1038/s41598-018-31116-y.
4. Dai L, Del Valle L, Miley W, Whitby D, Ochoa AC, Flemington EK, **Qin Z** *. Transactivation of human endogenous retrovirus K (HERV-K) by KSHV promotes Kaposi's Sarcoma development. *Oncogene*. 2018 May 10. doi: 10.1038/s41388-018-0282-4. [Epub ahead of print].
5. Dai L, Qiao J, Del Valle L, **Qin Z** *. KSHV co-infection regulates HPV16+ cervical cancer cells pathogenesis *in vitro* and *in vivo*. *Am J Cancer Res*. 2018;8(4):708-714.

6. Dai L, Smith CD, Foroozesh M, Miele L, **Qin Z** *. The sphingosine kinase 2 inhibitor ABC294640 displays anti-non-small cell lung cancer activities *in vitro* and *in vivo*. *Int J Cancer*. 2018;142(10):2153-2162.

7. Dai L, Bai A, Smith CD, Rodriguez PC, Yu F *, **Qin Z** *. ABC294640, a novel sphingosine kinase 2 inhibitor induces oncogenic virus infected cell autophagic death and represses tumor growth. *Mol Cancer Ther*. 2017;16(12):2724-2734.

8. Luo Z, Zhou Z, Ogunrinde E, Zhang T, Li Z, Martin L, Wan Z, Wu H, **Qin Z,** Ou T, Zhang J, Ma L, Liao G, Heath S, Huang L, Jiang W *. The effect of plasma auto-IgGs on CD4+ T cell apoptosis in viral-suppressed HIV-infected patients under antiretroviral therapy. *J Leukoc Biol*. 2017;102(6):1481-1486.

9. Dai L, Lin Z, Jiang W, Flemington EK, **Qin Z *.** Lipids, lipid metabolism and Kaposi's sarcoma-associated herpesvirus pathogenesis. *Virol Sin.* 2017;32(5):369-375.

6.2. Other publications, conference papers, and presentations:

1. Dai L, Goldstein A and **Qin Z *.** "Periodontal Bacteria Promote the Pathogenesis of Kaposi's Sarcoma-associated Herpesvirus in HIV+ Patients". American Society for Microbiology South Central Branch Annual Meeting, Little Rock, AR, US, 2017.

2. Dai L, Del Valle L, Yang L and **Qin Z *.** "Pathogenic Bacteria PAMPs Promote Oncogenic Virus Pathogenesis". International Conference on EBV & KSHV, Madison, WI, US, 2018.

6.3. Other Products:

We have deposited our microarray data about the regulatory network of RRM2 inhibitor 3-AP treated KSHV+ PEL cell-lines to Gene Expression Omnibus (GEO) database (Accession number: GSE91389).

7. PARTICIPANTS & OTHER COLLABORATING ORGANIZATIONS

7.1. What individuals have worked on the project?

Name:	*Zhiqiang Qin*
Project Role:	*PI*
Researcher Identifier (e.g. ORCID ID):	*N/A*
Nearest person month worked:	*6*
Contribution to Project:	*Dr. Qin is responsible for experimental design, data analysis, animal work and manuscript preparation*
Funding Support:	*NIH COBRE subproject, NIH/NCI RO1 and LSU LIFT funding (NO-overlapping with the current project)*

Name:	*Lu Dai*
Project Role:	*Senior postdoctoral researcher*

Researcher Identifier (e.g. ORCID ID):	*N/A*
Nearest person month worked:	*6*
Contribution to Project:	*Dr. Dai is responsible for cell culture, qRT-PCR, immunoblots, animal work etc*
Funding Support:	*N/A*

7.2. Has there been a change in the active other support of the PD/PI(s) or senior/key personnel since the last reporting period?

For Dr. Zhiqiang Qin:

Completed:

P20GM103501 (PI: Augusto Ochoa) 01/01/2012-06/30/2015 2.5 CM
NIH-NIGMS $120,000
Mentoring Translational Researchers in Louisiana
Project 12: KSHV regulation of emmprin, drug resistance, and tumor progression
Role: Pilot Project Leader

Leukemia Research Foundation 07/01/2016-06/30/2017 1.0CM
$100,000
Targeting sphingolipid metabolism in AIDS-related lymphomas
Role: Principal Investigator

LA CaTS Pilot Funding 02/01/2017-01/31/2018 0.8 CM
$50,000
Developing new ceramide analogs as therapeutic agents against AIDS-related lymphomas
Role: Principal Investigator

Active:

NIH/NCI RO1 05/01/2018-04/30/2023 3.6 CM
1R01CA228166-01 $1,250,000
Title: Periodontal bacteria enhance oral KSHV pathogenesis and Kaposi's Sarcoma development in HIV+ patients
Role: Principal Investigator
NO-overlapping with the current project

NIH/NIGMS COBRE 01/01/2017-12/31/2021 2.4 CM
P20GM121288 (PI: Krzysztof Reiss) $1,201,926
Center for Translational Viral Oncology
Tier 1 Project 1 title: Role of HERV-K reactivation in AIDS-related Kaposi's Sarcoma
Role: Tier 1 project 1 leader
NO-overlapping with the current project

LSU LIFT funding 07/01/2017-06/30/2018 (6-month no cost extension) 0.8 CM
$50,000
Developing new ceramide analogous "lead-compounds" against AIDS-related lymphomas in vivo
Role: Principal Investigator
NO-overlapping with the current project

7.3. What other organizations were involved as partners?

Nothing to Report.

8. SPECIAL REPORTING REQUIREMENTS

N/A

9. APPENDICES

The original copies of total 8 journal articles published during this funding period, another one is in press now.

AMERICAN SOCIETY FOR MICROBIOLOGY | Journal of Virology®

Regulation of Virus-Associated Lymphoma Growth and Gene Expression by Bacterial Quorum-Sensing Molecules

Jing Qiao,[a] Yueyu Cao,[a] Jovanny Zabaleta,[b] Liang Yang,[c] Lu Dai,[a,d] Zhiqiang Qin[a,d]

[a]Department of Pediatrics, Research Center for Translational Medicine and Key Laboratory of Arrhythmias, East Hospital, Tongji University School of Medicine, Shanghai, China

[b]Department of Pediatrics, Louisiana State University Health Sciences Center, Louisiana Cancer Research Center, New Orleans, Louisiana, USA

[c]Singapore Centre for Environmental Life Sciences Engineering (SCELSE), Nanyang Technological University, Singapore, Singapore

[d]Department of Genetics, Louisiana State University Health Sciences Center, Louisiana Cancer Research Center, New Orleans, Louisiana, USA

ABSTRACT Kaposi's sarcoma-associated herpesvirus (KSHV) can cause several human cancers, including primary effusion lymphoma (PEL), which frequently occur in immunocompromised patients. KSHV-infected patients often suffer from polymicrobial infections caused by opportunistic bacterial pathogens. Therefore, it is crucial to understand how these coinfecting microorganisms or their secreted metabolites may affect KSHV infection and the pathogenesis of virus-associated malignancies. Quorum sensing (QS), a cell density-based intercellular communication system, employs extracellular diffusible signaling molecules to regulate bacterial virulence mechanisms in a wide range of bacterial pathogens, such as *Pseudomonas aeruginosa*, which is one of the most common opportunistic microorganisms found in immunocompromised individuals. In this study, we evaluated and compared the influence on PEL growth and the host/viral interactome of the major QS signaling molecules [*N*-(3-oxododecanoyl)-L-homoserine lactone (OdDHL), *N*-butyrylhomoserine lactone (BHL), and 2-heptyl-3-hydroxy-4-quinolone (PQS)] in conditioned medium from wild-type (wt) and QS mutant laboratory strains as well as clinical isolates of *P. aeruginosa*. Our data indicate that *P. aeruginosa* coinfection may facilitate virus dissemination and establishment of new infection and further promote tumor development through effectively inducing viral lytic gene expression by its QS systems.

IMPORTANCE Currently, most studies about KSHV infection and/or virus-associated malignancies depend on pure culture systems or immunodeficient animal models. However, the real situation should be much more complicated in KSHV-infected immunocompromised patients due to frequent polymicrobial infections. It is important to understand the interaction of KSHV and coinfecting microorganisms, especially opportunistic bacterial pathogens. Here we report for the first time that *P. aeruginosa* and its quorum-sensing signaling molecules display a complicated impact on KSHV-associated lymphoma growth as well as the intracellular host/viral gene expression profile. Our data imply that targeting of coinfecting pathogens is probably necessary during treatment of virus-associated malignancies in these immunocompromised patients.

KEYWORDS KSHV, primary effusion lymphoma, *Pseudomonas aeruginosa*, quorum sensing

Kaposi's sarcoma-associated herpesvirus (KSHV) represents a principal causative agent of several cancers arising in immunocompromised patients, including Kaposi's sarcoma (KS), primary effusion lymphoma (PEL), and multicentric Castleman disease

Received 20 March 2018 **Accepted** 4 May 2018

Accepted manuscript posted online 9 May 2018

Citation Qiao J, Cao Y, Zabaleta J, Yang L, Dai L, Qin Z. 2018. Regulation of virus-associated lymphoma growth and gene expression by bacterial quorum-sensing molecules. J Virol 92:e00478-18. https://doi.org/10.1128/JVI.00478-18.

Editor Jae U. Jung, University of Southern California

Address correspondence to Lu Dai, ldai@lsuhsc.edu, or Zhiqiang Qin, zqin@lsuhsc.edu.

J.Q. and Y.C. contributed equally to this article.

(MCD) (1–3). Among these malignancies, PEL, formerly known as body cavity lymphoma, usually comprises transformed B cells harboring viral episomes and presents as pleural, peritoneal, and pericardial neoplastic effusions. PEL is a rare but aggressive B-cell-derived lymphoma, with patients having a median survival time of approximately 6 months even under conventional chemotherapy (4). The exact mechanism by which KSHV promotes oncogenesis in PEL is an area under active investigation. Most infected cells express a latent pattern of viral gene expression, while a very small percentage expresses viral lytic genes (5). Even with the expression of latent genes, infected cells can undergo clonal expansion, eventually leading to neoplastic transformation through mechanisms including increased proliferation and impaired apoptosis (4).

It is well-known that KSHV-related malignancies, including PEL, usually occur in the setting of an immunocompromised subpopulation, especially HIV-positive (HIV^+) patients, who always suffer from polymicrobial infections, including those caused by opportunistic bacterial pathogens. Therefore, it is necessary and interesting to understand how these coinfecting microorganisms or their products may affect KSHV infection and the pathogenesis of virus-associated malignancies. One recent study has reported that the short-chain fatty acids produced by periodontal pathogens, including *Porphyromonas gingivalis* and *Fusobacterium nucleatum*, can induce KSHV lytic reactivation and promote virus replication (6). Our previous study reported that pretreatment of primary human oral fibroblasts with two prototypical pathogen-associated molecular patterns (PAMPs) produced by periodontal pathogenic bacteria, lipoteichoic acid (LTA) from *Staphylococcus aureus* and lipopolysaccharide (LPS) from *P. gingivalis*, increased KSHV entry and subsequent viral latent gene expression (7). We also demonstrated that *S. aureus* LTA and/or *P. gingivalis* LPS increased the level of several cellular receptors for KSHV entry (in particular, heparan sulfate proteoglycan [HSPG]) and increased the production of reactive oxygen species (ROS) as a cofactor facilitating virus entry, as well as the activation of intracellular signaling pathways, such as mitogen-activated protein kinase and NF-κB, which are required for KSHV latency establishment within oral cells (7).

Pseudomonas aeruginosa is a ubiquitous, Gram-negative bacterium that thrives in diverse habitats and environments. *P. aeruginosa* can act as an opportunistic pathogen, especially in patients who are intubated over long periods and immunocompromised and elderly individuals (8). More importantly, the infections caused by *P. aeruginosa* and its biofilms are usually resistant to multiple antibiotics, which can lead to severe and persistent infections (9, 10). For example, once established, the eradication of *P. aeruginosa* from the respiratory tract of HIV^+ individuals with advanced immunosuppression is problematic, and a chronic infective state appears to be common (11). Recent research progress has shown that quorum sensing (QS), a widely distributed bacterial population density-dependent cell-to-cell communication mechanism, plays a key role in modulating the expression of virulence genes as well as biofilm formation in bacterial pathogens, including *P. aeruginosa* (12–14). Typically, QS bacteria produce and release small diffusible signaling molecules, and at a high population density, the accumulated signals interact with cognate receptors to induce the transcriptional expression of various target genes, including genes that encode virulence factors. As a model organism for QS research, *P. aeruginosa* possesses three main QS systems (*las*, *rhl*, *pqs*), which regulate their target genes via three distinct QS signaling molecules, *N*-(3-oxododecanoyl)-L-homoserine lactone (OdDHL), *N*-butyrylhomoserine lactone (BHL), and 2-heptyl-3-hydroxy-4-quinolone (PQS), respectively. In the current study, we comparatively examined the impact of these QS signaling molecules in conditioned medium from wild-type (wt) and QS mutants of laboratory strains as well as clinical isolates of *P. aeruginosa* on PEL growth and the host/viral gene profile.

RESULTS

Regulation of PEL growth and viral gene expression by *P. aeruginosa* QS signaling molecules. By using WST-1 cell proliferation assays, we first tested and compared the regulation of PEL growth by 3 *P. aeruginosa* QS signaling molecules, OdDHL, BHL, and PQS (Fig. 1A). We found that among the 3 QS molecules, PQS

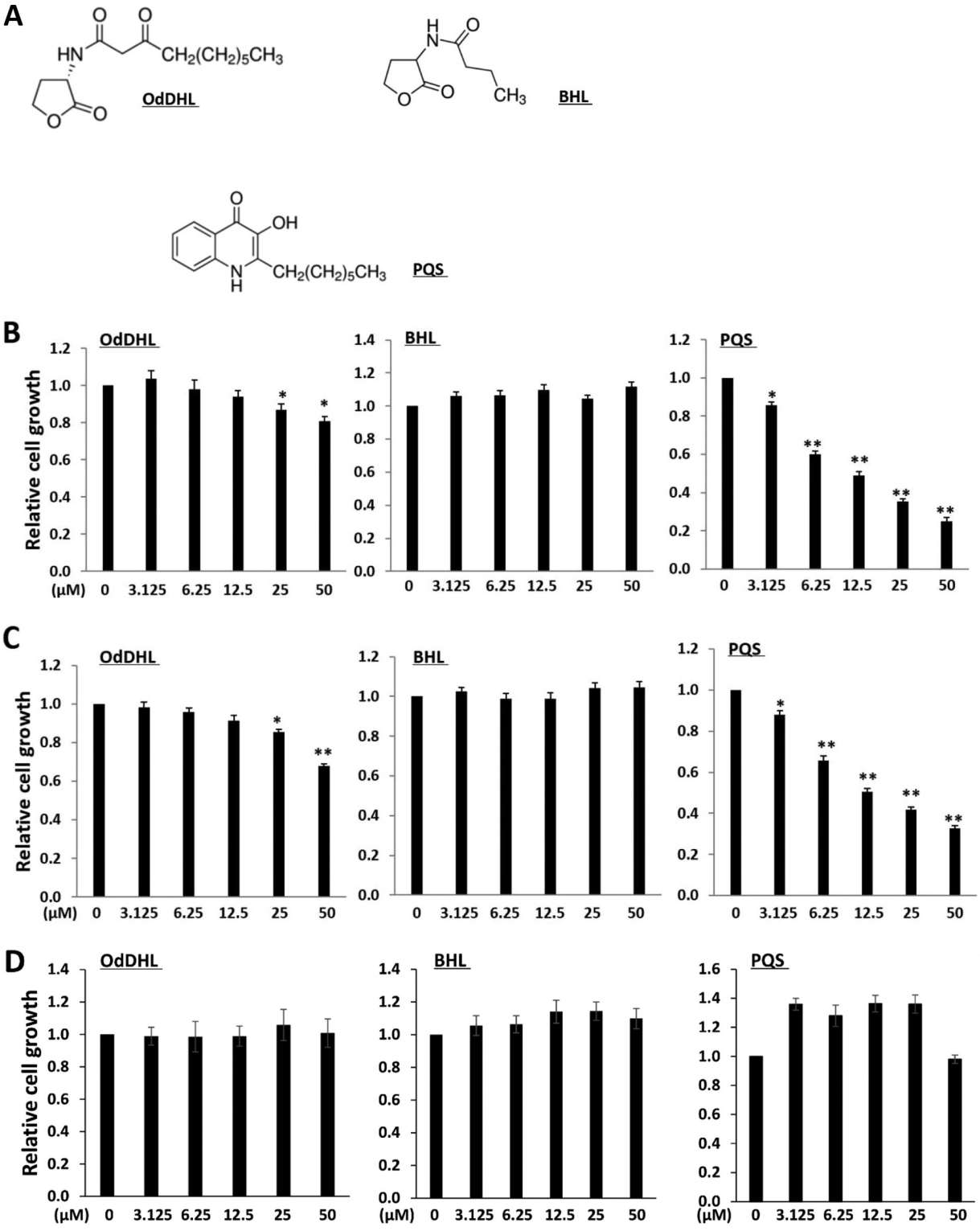

FIG 1 *P. aeruginosa* QS signaling molecules regulate the growth of KSHV$^+$ PEL cells. (A) Structures of major *P. aeruginosa* QS signaling molecules. OdDHL, *N*-(3-oxododecanoyl)-L-homoserine lactone; BHL, *N*-butyrylhomoserine lactone; PQS, 2-heptyl-3-hydroxy-4-quinolone. (B to D) Cells of the KSHV$^+$ PEL cell lines BCBL-1 (B) and BCP-1 (C) or a virus-negative lymphoma cell line, BL-41 (D), were incubated with the indicated concentrations of OdDHL, BHL, or PQS for 48 h. The cell proliferation status was examined using WST-1 cell proliferation assays (Roche). Error bars represent the SD from 3 independent experiments. *, $P < 0.05$; **, $P < 0.01$.

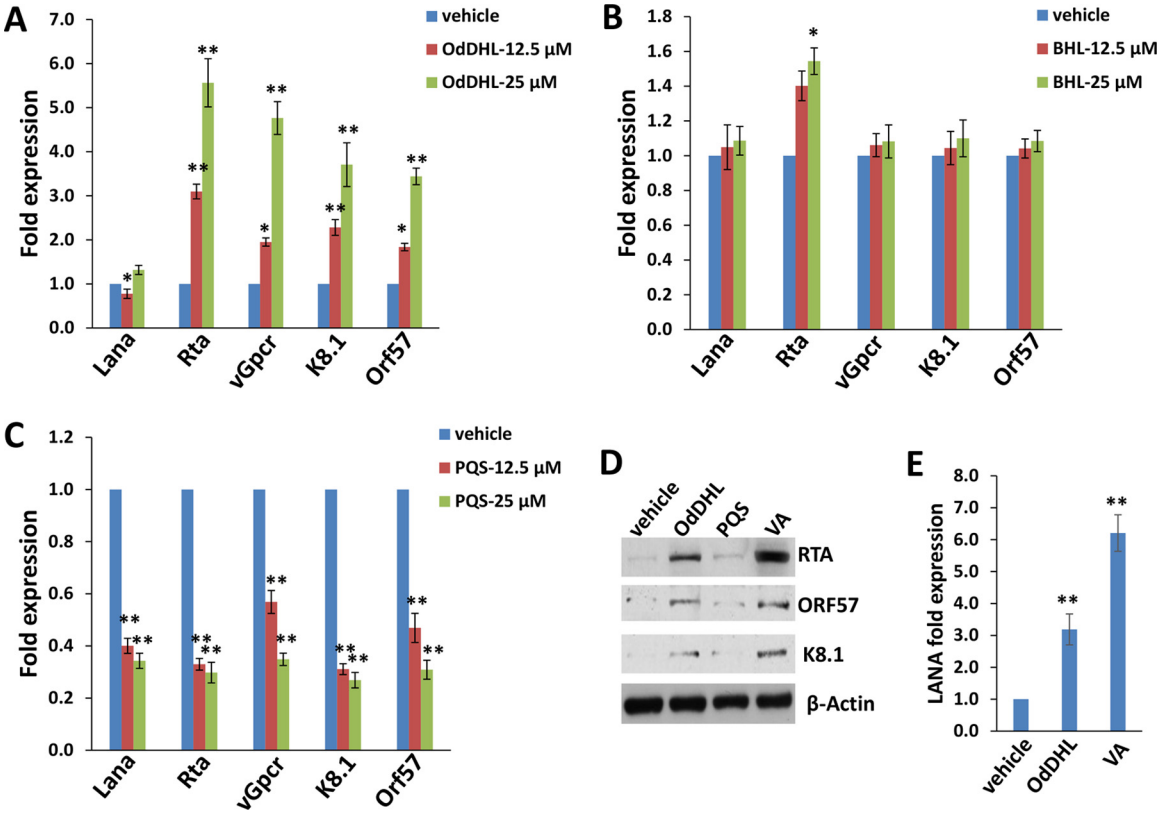

FIG 2 *P. aeruginosa* QS signaling molecules regulate KSHV gene expression from PEL cells. (A to C) BCBL-1 cells were incubated with the indicated concentrations of OdDHL (A), BHL (B), or PQS (C) for 48 h, and then quantitative real-time PCR (qRT-PCR) was used to quantify viral transcripts representing either latent (*Lana*) or lytic (*Rta*, *vGpcr*, *K8.1*, and *Orf57*) genes. Data were normalized to those for vehicle-treated cells, and β-actin was used as a loading control. (D) Protein expression was measured using immunoblots. (E) Released virions were isolated, purified from the supernatant of BCBL-1 cells that had been treated with OdDHL or valproic acid (VA; as the positive control) for 4 days, and then used to infect fresh HUVEC. After 24 h postinfection, *Lana* transcripts were quantified using qRT-PCR. Error bars represent the SD from 3 independent experiments. *, $P < 0.05$; **, $P < 0.01$.

significantly reduced the growth of KSHV-positive (KSHV$^+$) PEL cell lines, BCBL-1 and BCP-1, in a dose-dependent manner (Fig. 1B and C). OdDHL caused an intermediate reduction of PEL cell growth, especially at high concentrations (e.g., 50 μM). In contrast, BHL was almost not able to affect PEL cell growth over the dose range that we tested. Interestingly, all of the 3 QS molecules displayed little effect on the growth of a virus-negative lymphoma cell line, BL-41, over the same dose range (Fig. 1D). Although the concentrations of the QS molecules used here are higher than those reported in some human host samples (e.g., sputum from cystic fibrosis patients) (15, 16), the latter are likely to be underestimates since local OdDHL concentrations of up to 600 μM have been detected in the culture supernatants of *P. aeruginosa* biofilms grown *in vitro* (17).

Next, we measured the viral gene expression from PEL cells after being exposed to *P. aeruginosa* QS molecules using quantitative real-time PCR (qRT-PCR). We found that OdDHL significantly induced the expression of viral lytic genes (e.g., *Rta*, *vGpcr*, *K8.1*, *Orf57*) from PEL cells at concentrations of 12.5 and 25 μM (Fig. 2A). In contrast, PQS greatly reduced both latent (e.g., *Lana*) and lytic gene expression at similar concentrations (Fig. 2C). However, BHL was almost not able to affect viral gene expression within PEL cells (Fig. 2B). Immunoblot analysis confirmed the elevated expression of representative lytic proteins, such as RTA, ORF57, and K8.1, by OdDHL and valproic acid (VA; a positive control) from BCBL-1 cells (Fig. 2D). Furthermore, we found that both OdDHL and valproic acid induced PEL cells to release infectious KSHV particles, as demonstrated by increased LANA expression within fresh human umbilical vein endothelial cells (HUVEC) infected by purified virions isolated from OdDHL- or VA-treated PEL cell supernatants (Fig. 2E).

Transcriptomic analysis of the host gene profile altered within PEL cell lines exposed to QS signaling molecules. To determine the overall host gene profile affected by QS signaling molecules (especially OdDHL and PQS), we used a HumanHT-12 (v4) Expression BeadChip system (Illumina), which contains more than 47,000 probes derived from the NCBI Reference Sequence (RefSeq) database, release 38, and other sources, to analyze the gene profile altered between vehicle- and OdDHL- or PQS-treated BCBL-1 and BCP-1 cell lines. Intersection analysis indicated that there were 314 common genes significantly upregulated and 162 common genes downregulated ($\geq$2-fold and $P < 0.05$) within both PEL cell lines exposed to OdDHL; 256 were uniquely upregulated genes and 304 were uniquely downregulated in BCBL-1 cells, and 63 were uniquely upregulated genes and 133 were uniquely downregulated in BCP-1 cells (Fig. 3A). Within the common gene set, the top 20 upregulated genes and the top 20 downregulated genes in the OdDHL-treated PEL cell lines are listed in Tables 1 and 2, respectively. We also found that there were a total of 37 common genes whose expression was significantly altered (24 upregulated and 13 downregulated genes) within both PEL cell lines exposed to PQS; 29 genes were uniquely upregulated and 25 genes were uniquely downregulated in BCBL-1 cells, and 3 genes were uniquely upregulated and 6 genes were uniquely downregulated in BCP-1 cells (Fig. 3D). Within the common gene set, the top 10 upregulated and downregulated genes in PQS-treated PEL cell lines are listed in Table 3.

We also performed enrichment analysis of these significantly altered candidates by using the Gene Ontology (GO) Processes and Process Networks modules from Metacore software (Thompson Reuters). Notably, our analysis showed that both OdDHL and PQS treatment regulated cell growth-related functional categories in PEL, including varied phases of cell cycle and regulation, cytoskeleton_spindle microtubules, DNA damage, etc. (Fig. 3B, C, E, and F). Moreover, PQS treatment also regulated many cellular metabolism functional categories, such as glycolysis, fructose metabolism, glycogen metabolism, amino sugar metabolism, and iron metabolism (Fig. 3E and F). The top 2 scored pathway/network maps based on enrichment analysis of the common gene set are listed in Fig. S1 and S2 in the supplemental material, respectively. Since many cell cycle checkpoint or regulatory proteins were altered within OdDHL- or PQS-treated PEL cells, for functional validation, we demonstrated that both OdDHL and PQS treatment significantly caused G_1 cell cycle arrest for the BCBL-1 and BCP-1 cell lines by using flow cytometry analysis (Fig. 4A and B). Interestingly, only PQS dramatically induced PEL cell apoptosis, while OdDHL slightly increased cell apoptosis (with no statistical significance) (Fig. 4C).

Regulation of PEL growth and viral gene expression by conditioned medium from *P. aeruginosa* PAO1 wt and QS mutants. Since these QS signaling molecules are produced and secreted by *P. aeruginosa*, we next tested and compared the impact on PEL growth and viral gene expression of filtered conditioned medium from the *P. aeruginosa* PAO1 wild-type (wt) laboratory strain and its QS mutants (a *lasI* mutant deficient in OdDHL, an *rhlI* mutant deficient in BHL, and a *pqsC* mutant deficient in PQS). We found that conditioned medium from the PAO1 wt effectively inhibited PEL cell growth in a dose-dependent manner compared to the Luria-Bertani (LB) medium control (Fig. 5A and B). The conditioned medium from the various PAO1 QS mutants (especially the *lasI* and *pqsC* mutants) displayed a partially impaired ability to inhibit PEL growth compared to that from the PAO1 wt. However, we noticed that the conditioned medium from none of these single-QS-system mutants completely lost the ability to have an inhibitory effect on PEL growth. These data indicate that multiple QS systems may coordinate and/or some QS-independent factors of *P. aeruginosa* are able to regulate PEL cell growth. In contrast, the conditioned medium from the PAO1 wt and QS mutants displayed much less of an inhibitory effect on the growth of the virus-negative lymphoma cell line BL-41 (Fig. 5C). Instead, the conditioned medium from the PAO1 *pqsC* mutant increased BL-41 cell growth.

We next found that conditioned medium from the PAO1 wt significantly induced viral lytic gene expression from PEL cells compared to the LB medium control (Fig. 5D

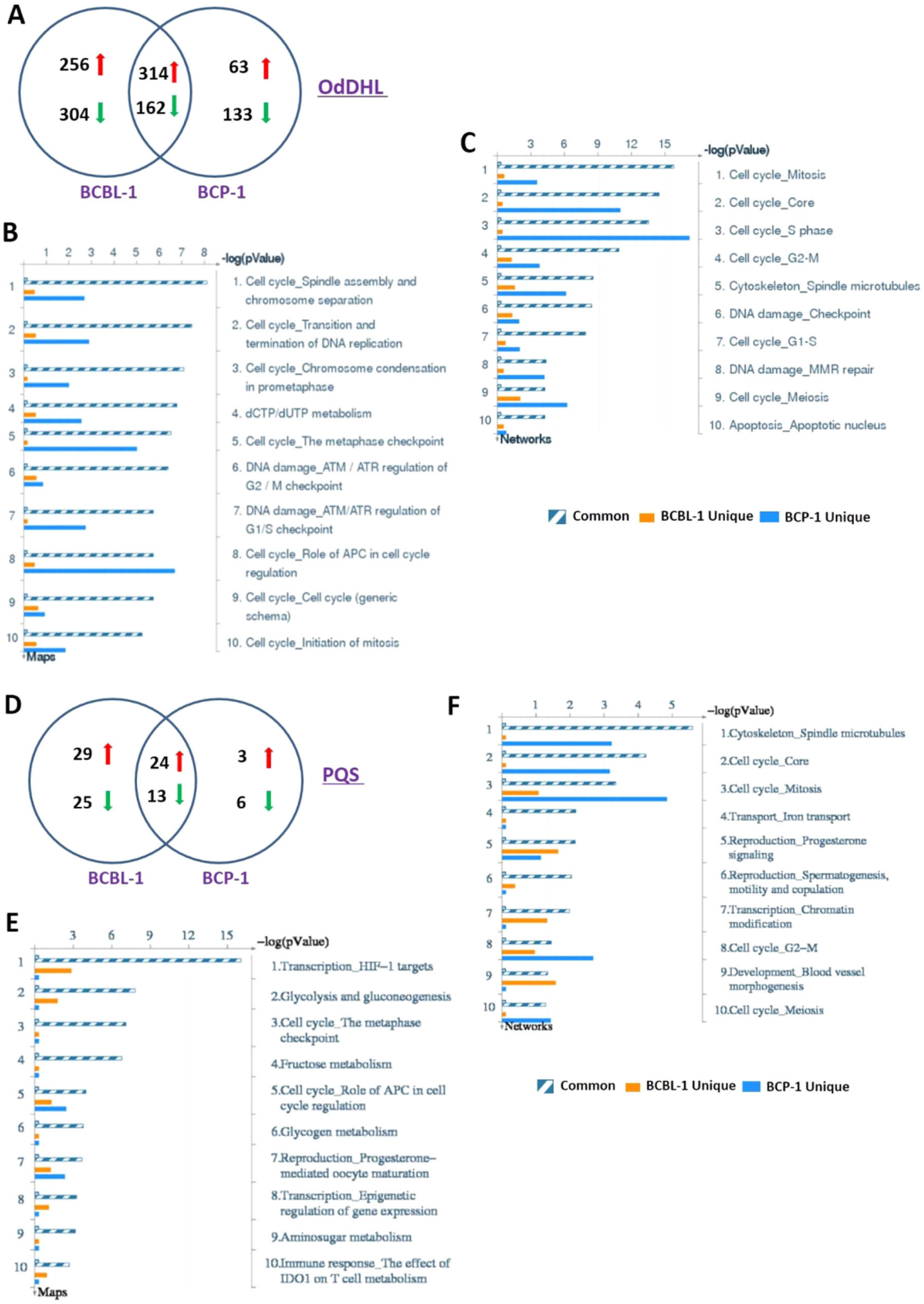

FIG 3 Transcriptome analysis of cells of OdDHL- or PQS-treated PEL cell lines. (A and D) BCBL-1 and BCP-1 cells were incubated with 25 μM OdDHL (A) or PQS (D) for 48 h, and then the HumanHT-12 (v4) Expression BeadChip system (Illumina) was used to detect the gene profile altered within OdDHL- or PQS-treated PEL cells compared to that in vehicle-treated cells. (B, C, E, and F) Enrichment analysis of the gene profile altered by OdDHL or PQS in PEL cell lines was performed using the MetaCore software modules of Gene Ontology Processes and Process Networks. APC, anaphase-promoting complex; ATM, ataxia-telangiectasia mutated; ATR, ATM and Rad3 related; MMR, mismatch repair.

TABLE 1 Top 20 common candidate genes upregulated in OdDHL-treated BCBL-1 and BCP-1 cell lines

Gene symbol	Description	Fold change in expression	
		BCBL-1 cells	BCP-1 cells
HSPA6	Heat shock 70-kDa protein 6 (HSP70B)	93.13	61.73
HSPA7	Putative heat shock 70-kDa protein 7	90.2	58.98
RN7SK	RNA, 7SK small nuclear	45.65	35.76
FOSB	Protein FosB	44.19	21.02
SNORD3C	Small nucleolar RNA, C/D box 3C	40.59	49.2
FOS	Proto-oncogene protein c-*fos*	37.3	37.56
SNORD3A	Small nucleolar RNA, C/D box 3A	34.66	39.87
RNU1-4	RNA, U1 small nuclear 4	30.77	36.16
RNU1-5	RNA, U1 small nuclear 5	26.12	34.75
RNU1-1	RNA, U1 small nuclear 1	22.29	28.62
IEX1	Radiation-inducible immediate early gene IEX-1	21.51	18
RGS2	Regulator of G-protein signaling 2	20.8	12.88
GADD45B	Growth arrest and DNA-damage-inducible protein GADD45 beta	19.77	12.94
PTGS2	Prostaglandin G/H synthase 2	19.75	16.78
HBEGF	Heparin-binding EGF[a]-like growth factor	18.57	14.98
DUSP12	Dual-specificity protein phosphatase 12	16.41	13.84
NR4A2	Nuclear receptor subfamily 4 group A member 2	13.31	9.87
MAFB	Transcription factor MafB	12.88	12.18
PPP1R15A	Protein phosphatase 1 regulatory subunit 15A	12.18	9.84
HSPA1A	Heat shock 70-kDa protein 1	11.42	6.97

[a]EGF, epidermal growth factor.

to F). The conditioned medium from the PAO1 *lasI* or *rhlI* mutant partially reduced such induction abilities, while the conditioned medium from the *pqsC* mutant induced viral lytic gene expression at levels similar to those for the conditioned medium from the wt. Again, the conditioned medium from none of these single-QS-system mutants completely lost the ability to induce viral lytic gene expression. We further confirmed that all the conditioned media from the PAO1 wt and QS mutants effectively induced PEL

TABLE 2 Top 20 common candidate genes downregulated in OdDHL-treated BCBL-1 and BCP-1 cell lines

Gene symbol	Description	Fold change in expression	
		BCBL-1 cells	BCP-1 cells
RRM2	Ribonucleoside diphosphate reductase subunit M2	0.29	0.35
CyclinA2	Cyclin-A2	0.29	0.49
RAB36	Ras-related protein Rab-36	0.29	0.37
TPX2	Targeting protein for Xklp2	0.29	0.46
TNFRSF17	Tumor necrosis factor receptor superfamily member 17	0.3	0.49
FAM81A	Protein FAM81A	0.29	0.35
GPRC5D	G-protein-coupled receptor family C group 5 member D	0.29	0.49
EMP3	Epithelial membrane protein 3	0.29	0.37
HDGF	Hepatoma-derived growth factor	0.29	0.46
DLGAP5	Disks large-associated protein 5	0.3	0.49
SFN	14-3-3 protein sigma	0.29	0.35
ITGA4	Integrin alpha 4	0.29	0.49
TYMS	Thymidylate synthase	0.29	0.37
ACTB	Actin, cytoplasmic 1	0.29	0.46
POLE2	DNA polymerase epsilon subunit 2	0.3	0.49
CCR7	C-C chemokine receptor type 7	0.29	0.35
SPAG5	Sperm-associated antigen 5	0.29	0.49
FOXM1	Forkhead box protein M1	0.29	0.37
IGFBP4	Insulin-like growth factor-binding protein 4	0.29	0.46
APOBEC3B	Probable DNA dC->dU-editing enzyme APOBEC3B	0.3	0.49

TABLE 3 Top 10 common candidate genes up- and downregulated in PQS-treated BCBL-1 and BCP-1 cell lines

Gene symbol	Description	Fold change in expression	
		BCBL-1 cells	BCP-1 cells
PFKFB4	6-Phosphofructo-2-kinase/fructose-2,6-bisphosphatase 4	9.58	8.85
ALDOC	Fructose-bisphosphate aldolase C	5.04	4.97
CA9	Carbonic anhydrase 9	4.24	6.41
BNIP3L	BCL2/adenovirus E1B 19-kDa protein-interacting protein 3-like	3.81	3.57
CCDC151	Coiled-coil domain-containing protein 151	3.36	3.64
SLC2A1	Solute carrier family 2, facilitated glucose transporter member 1	3.29	3.56
SLC2A3	Solute carrier family 2, facilitated glucose transporter member 3	2.88	2.42
PLOD2	Procollagen-lysine, 2-oxoglutarate 5-dioxygenase 2	2.76	2.55
TXNIP	Thioredoxin-interacting protein	2.75	3.45
PFKFB3	6-Phosphofructo-2-kinase/fructose-2,6-bisphosphatase 3	2.54	2.42
HIST1H3J	Histone H3.1	0.24	0.24
CDC20	Cell division cycle protein 20 homolog	0.38	0.36
HIST1H2BC	Histone H2B type 1-C/E/F/G/I	0.39	0.4
HIST2H2AC	Histone H2A type 2-C	0.4	0.45
AURKA	Aurora kinase A	0.42	0.4
CENPA	Histone H3-like centromeric protein A	0.44	0.43
ZCCHC12	Zinc finger CCHC domain-containing protein 12	0.45	0.36
HMMR	Hyaluronan-mediated motility receptor	0.46	0.46
PLK1	Serine/threonine-protein kinase PLK1	0.47	0.39
KIF20A	Kinesin-like protein KIF20A	0.47	0.47

cell release of infectious KSHV particles, although the conditioned medium from the *lasI* or *rhlI* mutant displayed a partially reduced ability (Fig. 5G).

Regulation of PEL growth and viral gene expression by conditioned medium from *P. aeruginosa* clinical isolates. For further study of clinical relevance for our findings, we tested the regulation of PEL growth and viral gene expression by conditioned medium from several *P. aeruginosa* clinical isolates. PA-CF230 (also named CF57388A) was isolated from the sputum of a cystic fibrosis patient (18); PA-D16 and PA-D23 were both isolated from ventilator-associated pneumonia patients (19). We found that filtered conditioned medium from all 3 of these clinical isolates (especially PA-CF230) dramatically inhibited PEL cell growth compared to the LB medium control (Fig. 6A). In contrast, the conditioned medium from these *P. aeruginosa* clinical isolates displayed much less of an inhibitory effect on the growth of the virus-negative lymphoma cell line BL-41 (Fig. 6B). Furthermore, conditioned medium from these clinical isolates significantly induced viral lytic gene expression and the release of infectious KSHV particles from PEL cells (Fig. 6C to E).

DISCUSSION

KSHV-related malignancies usually occur in immunocompromised individuals, such as HIV$^+$ patients, who frequently suffer polymicrobial infections, including infections caused by opportunistic bacteria. However, there are limited data about how these opportunistic bacteria or their products can regulate KSHV infection as well as virus-related cancer development. QS systems have been found to regulate many virulence factors in both Gram-positive and Gram-negative bacteria. In the current study, we report for the first time the diverse impacts on KSHV$^+$ PEL cell growth and host/viral gene expression of 3 major QS molecules (OdDHL, BHL, and PQS) from *P. aeruginosa*, an opportunistic pathogen commonly seen in immunocompromised individuals. Recently, a fourth QS system, 2-(2-hydroxyphenyl)-thiazole-4-carbaldehyde, also named an integrated quorum-sensing system (IQS), has been identified in *P. aeruginosa* (20). IQS synthesis depends on a nonribosomal

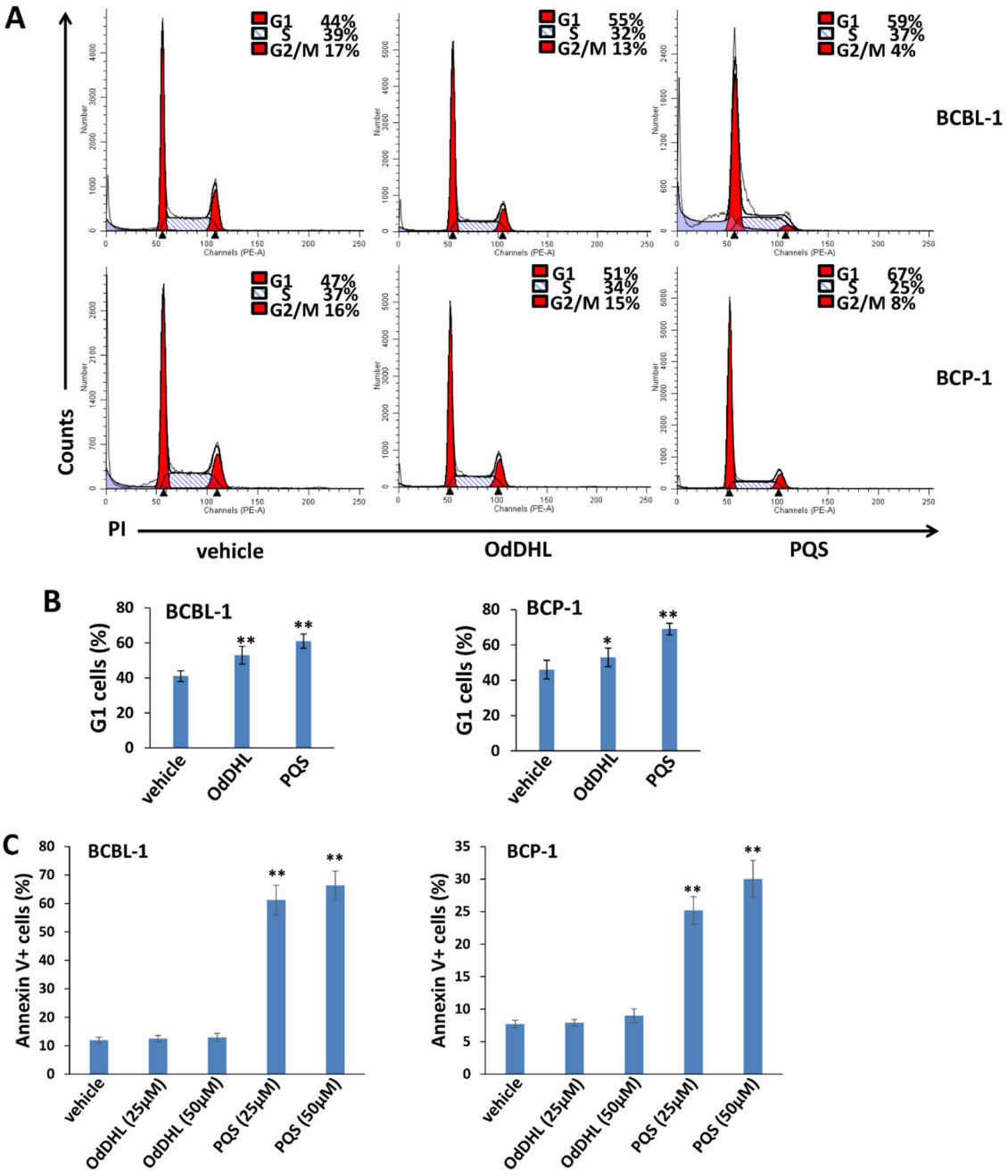

FIG 4 OdDHL or PQS regulates PEL cell cycle and apoptosis. (A and B) BCBL-1 and BCP-1 cells were incubated with 25 μM OdDHL or PQS for 48 h and then stained by propidium iodide (PI) and analyzed by flow cytometry. The solid blue area in panel A represents cell debris, which was excluded from analysis, and the G_1, S, and G_2/M subpopulations were calculated only for diploid cells. (C) Cell apoptosis was measured by using flow cytometry, as described in Materials and Methods. Error bars represent the SD from 3 independent experiments. *, $P < 0.05$; **, $P < 0.01$.

peptide synthase gene cluster, *ambBCDE*, which has been shown to contribute to the virulence of *P. aeruginosa* in different animal host models. However, since the purified IQS molecule of *P. aeruginosa* is currently not available, we did not involve it in this study.

We notice that the results obtained with conditioned medium from the *P. aeruginosa* wt and QS mutants were not fully expected on the basis of the data that we obtained with pure QS molecules. One of the major reasons is the complex interconnection among these different QS systems. *las* governs the expression of both the *pqs*

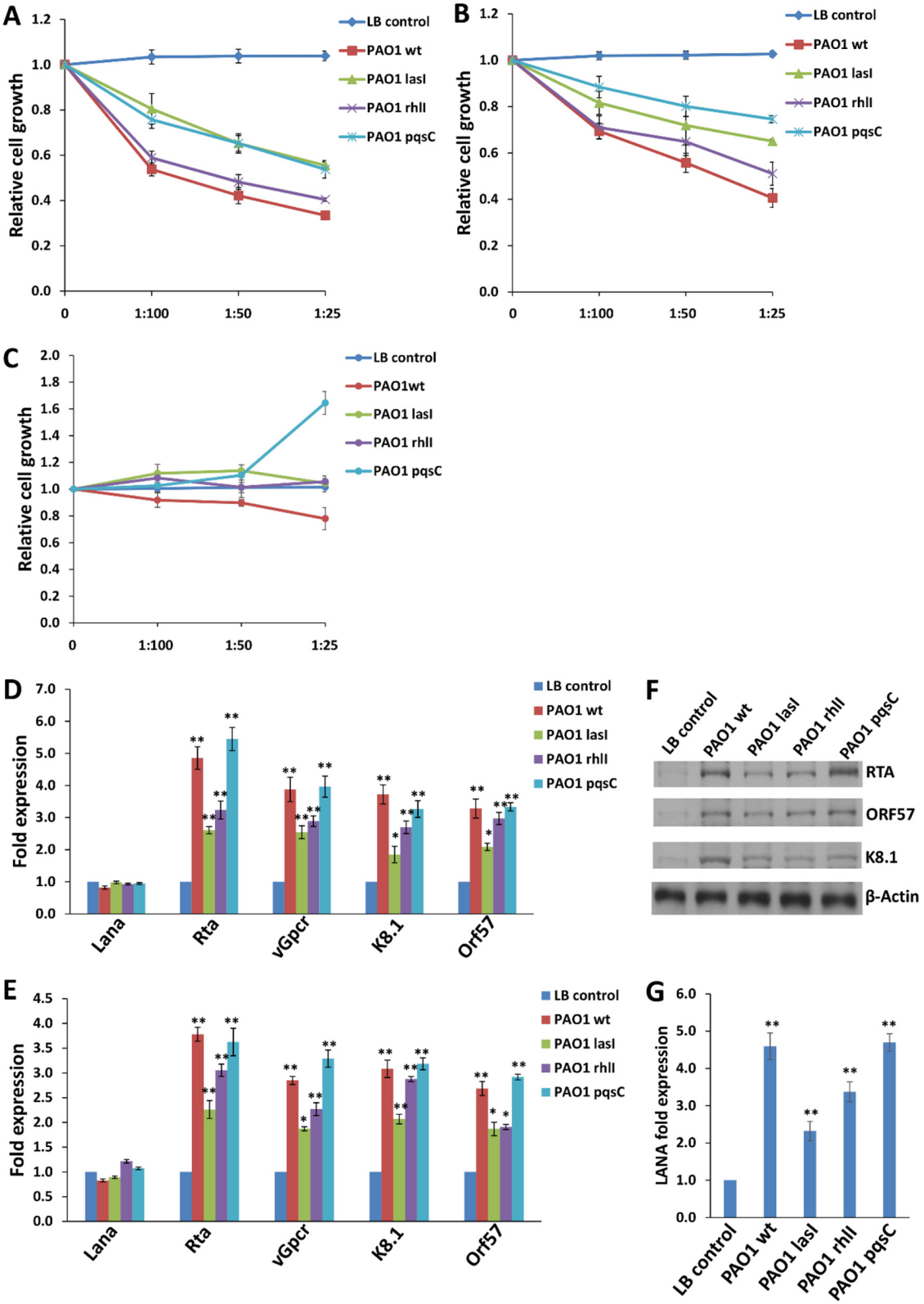

FIG 5 The conditioned medium from the *P. aeruginosa* PAO1 wild type and QS mutants regulates PEL cell growth and viral gene expression. (A to C) BCBL-1 (A), BCP-1 (B), or BL-41 (C) cells were incubated with filtered conditioned medium from overnight *P. aeruginosa* PAO1 wt or QS mutant (*lasI*, *rhlI*, *pqsC*) cultures (diluted 1:100, 1:50, and 1:25) for 48 h. The cell proliferation status was examined using WST-1 cell proliferation assays (Roche). (D and E) BCBL-1 (D) and BCP-1 (E) cells were incubated with filtered conditioned medium from overnight *P. aeruginosa* PAO1 wt or QS mutants cultures (diluted 1:25) for 48 h, and then qRT-PCR was used to quantify viral transcripts representing either latent or lytic genes. Data were normalized to those for vehicle-treated cells, and

(Continued on next page)

and *rhl* systems; on the other hand, the *rhl* system is under the control of both *las* and *pqs* (21, 22). Even the recently identified IQS has also been found to be tightly controlled by *lasRI* under rich medium conditions (20). Besides the QS signaling molecules mentioned above, the conditioned medium of *P. aeruginosa* cultures may contain a variety of QS-controlled virulence factors, such as pyocyanin and rhamnolipids (23, 24), although we found that conditioned medium from the *P. aeruginosa* PAO1 *rhlA* mutant (25) (deficient in rhamnolipid production) still effectively inhibited PEL cell growth (data not shown). Therefore, the construction of double- or even triple-knockout QS mutants in future studies will be helpful to answer these questions. Of course, we cannot exclude the possibility that some QS-independent factors, such as the type III secretion system of *P. aeruginosa* (26), may also affect PEL cell growth and/or viral gene expression.

Although both the QS molecules (e.g., PQS) and the conditioned medium of *P. aeruginosa* cultures displayed inhibitory effects on PEL cell growth, we think that coinfection by *P. aeruginosa* should not be enough to eliminate all the tumor cells in patients (due to their highly aggressive progression). On the other hand, these QS molecules and/or conditioned medium from *P. aeruginosa* laboratory strains and clinical isolates displays a strong ability to induce viral lytic gene expression and the release of viral infectious particles from PEL cells, which may greatly facilitate virus dissemination, the establishment of new infection, and, finally, the promotion of tumor development. We are now working on determining the underlying mechanisms by which *P. aeruginosa* or its QS molecules induce viral lytic gene expression. One of the possible mechanisms is the repression of some KSHV microRNAs, which have been shown to maintain viral latency in infected cells through either direct targeting of the viral lytic reactivation activator Rta or indirect mechanisms targeting some host factors (27–29). Since our methods used in this study represent an indirect evaluation of virion release, there are several alternative interpretations for the increased LANA expression in HUVEC exposed to QS molecules or conditioned medium-induced supernatant; for example, QS molecules enhance KSHV attachment to HUVEC or relieve heterochromatin formation on incoming virions to enhance LANA transcription. Therefore, we will design respective experiments to test these alternative interpretations in future studies.

Interestingly, the QS molecules of *P. aeruginosa* have been found to regulate host immune cell functions and cytokine production (30), which may modify the tumor microenvironment to accelerate tumor development. For example, during *P. aeruginosa* infection, innate immune cells can migrate toward the site of infection and remain in close proximity to the bacterial biofilms, but their functions are inhibited rather than stimulated by enhanced concentrations of QS molecules and QS-controlled bacterial traits (31, 32). In other studies, it has been reported that the expression and secretion of different pro- and anti-inflammatory cytokines in host cells are influenced by bacterial QS molecules (33–35). So, it will be interesting to explore the role of the immunoregulatory function of *P. aeruginosa* QS molecules in KSHV pathogenesis and tumorigenesis in future studies.

The current study focused only on KSHV$^+$ PEL cells, but it will be interesting to find out the impacts of *P. aeruginosa* or its QS molecules on other KSHV-related malignancies, such as KS and MCD. For example, *P. aeruginosa* is one of most common pathogens causing skin and soft tissue infections (36, 37), which may also affect KS development.

FIG 5 Legend (Continued)
β-actin was used as a loading control. (F and G) BCBL-1 cells were incubated with the filtered conditioned medium described above for 4 days, and then protein expression was measured using immunoblots. Released virions were isolated, purified from the supernatant, and used to infect fresh HUVEC. After 24 h postinfection, *Lana* transcripts were quantified using qRT-PCR. Error bars represent the SD from 3 independent experiments. *, $P < 0.05$; **, $P < 0.01$.

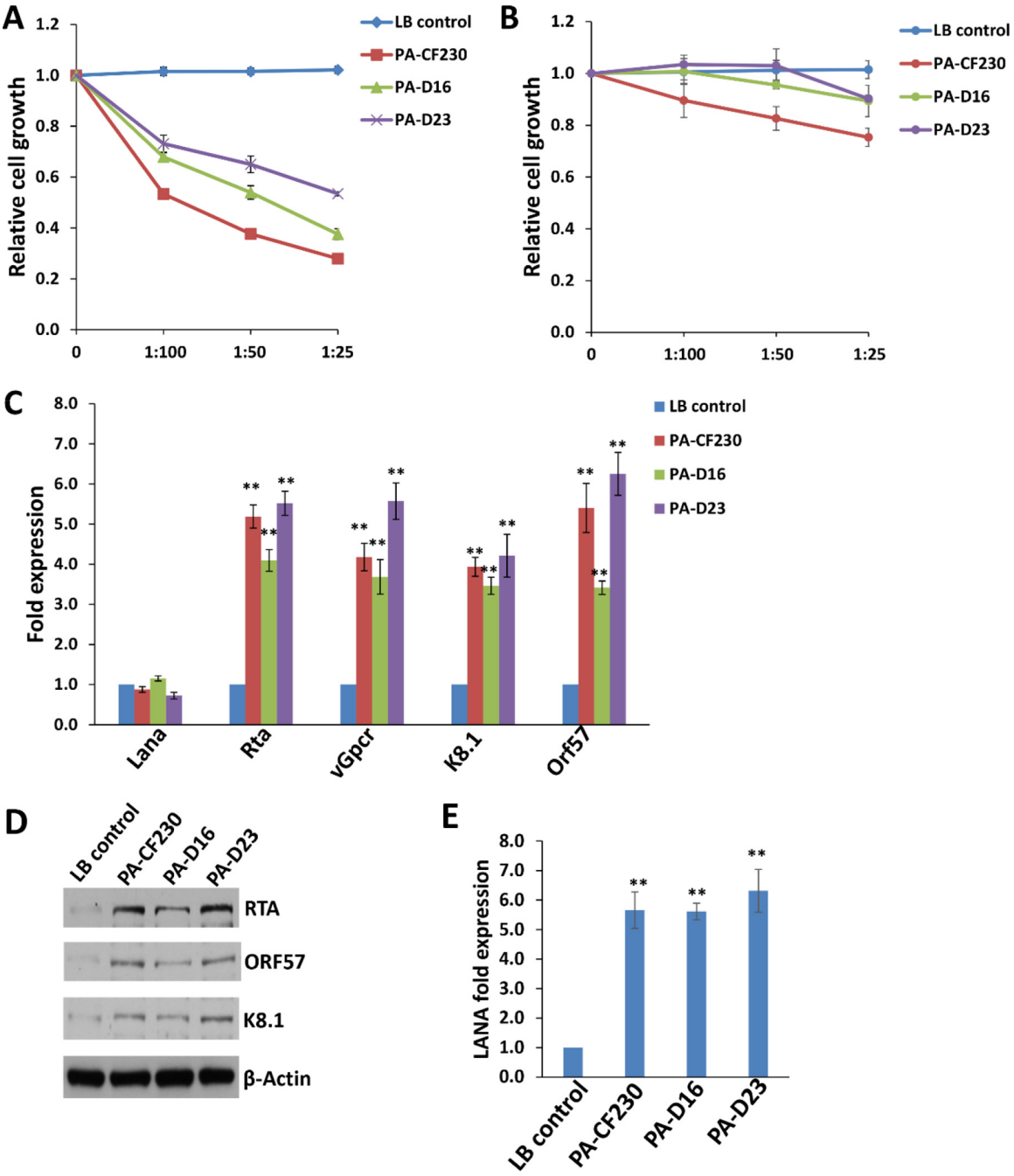

FIG 6 Conditioned medium from *P. aeruginosa* clinical isolates regulates PEL cell growth and viral gene expression. (A and B) BCBL-1 or BL-41 cells were incubated with filtered conditioned medium from overnight *P. aeruginosa* clinical isolate (PA-CF230, PA-D16, PA-D23) cultures (diluted 1:100, 1:50, and 1:25) for 48 h. The cell proliferation status was examined as described in the legend to Fig. 5. (C) BCBL-1 cells were incubated with filtered conditioned medium from overnight *P. aeruginosa* clinical isolate cultures (diluted 1:25) for 48 h, and then qRT-PCR was used to quantify the viral transcripts. (D and E) BCBL-1 cells were incubated with filtered conditioned medium from clinical isolates for 4 days, and then protein expression was measured using immunoblots. Released virions were isolated, purified from the supernatant, and used to infect fresh HUVEC. After 24 h postinfection, *Lana* transcripts were quantified using qRT-PCR. Error bars represent the SD from 3 independent experiments. **, $P < 0.01$.

MATERIALS AND METHODS

Cell culture, bacterial strains, and reagents. Cells of the KSHV$^+$ PEL cell line BCBL-1 and Burkitt's lymphoma cell line BL-41 (KSHV negative, Epstein-Barr virus negative) were kindly provided by Dean Kedes (University of Virginia) and maintained in RPMI 1640 medium (Gibco) with supplements as described previously (38). Cells of another KSHV$^+$ PEL cell line, BCP-1, were purchased from the American Type Culture Collection (ATCC) and maintained in complete RPMI 1640 medium (ATCC) supplemented

with 20% fetal bovine serum. Primary human umbilical vein endothelial cells (HUVEC) were cultured as described previously (7). All the cells were cultured at 37°C in 5% CO_2. All experiments were carried out using cells harvested at low passage numbers (<20). *P. aeruginosa* PAO1 (strain PAO0001) was obtained from the Pseudomonas Genetic Stock Center (East Carolina University School of Medicine, Greenville, NC, USA). The *lasI* and *rhlI* mutants were constructed by allelic displacement in PAO1 as described previously (39). The *pqsC* mutant was constructed via transposon insertion in PAO1 (40). *P. aeruginosa* clinical isolates were collected as described previously (18, 19). Luria-Bertani (LB; Oxoid) broth was used as the culture medium for *P. aeruginosa* growth. Purified QS molecules from *P. aeruginosa*, OdDHL, BHL, and PQS, were purchased from Sigma.

Cell proliferation assays. Cell proliferation was measured by using the WST-1 assay (Roche) according to the manufacturer's instructions. Briefly, after the period of treatment, 10 μl/well of the WST-1 cell proliferation reagent was added into the 96-well microplate, and the plate was incubated for 3 h at 37°C in 5% CO_2. The absorbance of the samples was measured by using a microplate reader at 450 nm.

Microarray analysis. Microarray analysis was performed by and the results were analyzed at the Stanley S. Scott Cancer Center Translational Genomics Core at LSUHSC. Total RNA was isolated using a Qiagen RNeasy kit (Qiagen), and 500 ng of total RNA was used to synthesize double-stranded cDNA. Biotin-labeled RNA was generated using a TargetAmp-Nano labeling kit (Epicentre) for the Illumina Expression BeadChip system and hybridized to the HumanHT-12 (v4) Expression BeadChip system (Illumina) at 58°C for 16 h. The chip was washed, stained with streptavadin-Cy3, and scanned with Illumina BeadStation 500 and BeadScan systems. Using Illumina's GenomeStudio software, we normalized the signals using the cubic spline algorithm, which assumes that the distribution of the transcript abundance is similar in all samples. The background signal was removed using the detection *P* value algorithm to remove targets with signal intensities equal to or lower than those of irrelevant probes (which have no known targets in the human genome but which are thermodynamically similar to the relevant probes). The microarray experiments were performed twice for each group, and the average values were used for analysis. Common and unique sets of genes and enrichment analysis were performed using MetaCore software (Thompson Reuters).

Cell cycle analysis. PEL cell pellets were fixed in 70% ethanol and incubated at 4°C overnight. Cell pellets were resuspended in 0.5 ml of 0.05 mg/ml propidium iodide (PI) plus 0.2 mg/ml RNase A and incubated at 37°C for 30 min. The cell cycle distribution was analyzed on a FACSCalibur 4-color flow cytometer (BD Bioscience).

Cell apoptosis assays. Flow cytometry was used for quantitative assessment of apoptosis using a fluorescein isothiocyanate-annexin V-propidium iodide (PI) apoptosis detection kit I (BD Pharmingen).

qRT-PCR. Total RNA was isolated using an RNeasy minikit (Qiagen), and cDNA was synthesized from equivalent total RNA using a SuperScript III first-strand synthesis SuperMix kit (Invitrogen) according to the manufacturer's instructions. The primers used for amplification of the target genes are listed in Table S1 in the supplemental material. Amplification was carried out using an iCycler IQ real-time PCR detection system, and cycle threshold (C_T) values were tabulated in duplicate for each gene of interest in each experiment. No-template (water) controls were used to ensure minimal background contamination. Using the mean C_T values tabulated for each gene and paired C_T values for β-actin as a loading control, fold changes in expression for experimental groups relative to the assigned controls were calculated using automated iQ5 (v2.0) software (Bio-Rad).

Immunoblotting. Cells were lysed in buffer containing 20 mM Tris (pH 7.5), 150 mM NaCl, 1% NP-40, 1 mM EDTA, 5 mM NaF, and 5 mM Na_3VO_4. Total cell lysates (30 μg) were resolved by 10% SDS-PAGE, transferred to nitrocellulose membranes, and incubated with 100 to 200 μg/ml of K8.1 (ABI), KSHV ORF57 (Santa Cruz), and RTA (Abbiotec). For loading controls, lysates were also incubated with antibodies detecting β-actin (Sigma). Immunoreactive bands were developed using an enhanced chemiluminescence reaction (Perkin-Elmer).

Statistical analysis. Significance for differences between the experimental and control groups was determined using the two-tailed Student's *t* test (Excel software, v8.0), and *P* values of <0.05 or <0.01 were considered significant or highly significant, respectively.

Accession number(s). The microarray original data have been submitted to the Gene Expression Omnibus (GEO) database (accession number GSE110076).

SUPPLEMENTAL MATERIAL

Supplemental material for this article may be found at https://doi.org/10.1128/JVI.00478-18.

SUPPLEMENTAL FILE 1, PDF file, 0.4 MB.

ACKNOWLEDGMENTS

This work was supported by grants from NIH/NCI 1R01CA228166-01, a DOD Career Development Award (CA140437), a Louisiana Clinical and Translational Science Center Pilot grant (U54GM104940 from NIH), LSU LIFT^2 funding, and an NIH P20-GM121288-01 subproject (Tier 1) to Z. Qin, as well as awards from the National Natural Science Foundation of China (81472547 and 81672924 to Z. Qin and 81400164 and 81772930 to L. Dai).

The funding sources had no role in study design, data collection and analysis, decision to publish, or preparation of the manuscript.

REFERENCES

1. Chang Y, Cesarman E, Pessin MS, Lee F, Culpepper J, Knowles DM, Moore PS. 1994. Identification of herpesvirus-like DNA sequences in AIDS-associated Kaposi's sarcoma. Science 266:1865–1869. https://doi.org/10.1126/science.7997879.
2. Cesarman E, Chang Y, Moore PS, Said JW, Knowles DM. 1995. Kaposi's sarcoma-associated herpesvirus-like DNA sequences in AIDS-related body-cavity-based lymphomas. N Engl J Med 332:1186–1191. https://doi.org/10.1056/NEJM199505043321802.
3. Soulier J, Grollet L, Oksenhendler E, Cacoub P, Cazals-Hatem D, Babinet P, d'Agay MF, Clauvel JP, Raphael M, Degos L, Sigaux F. 1995. Kaposi's sarcoma-associated herpesvirus-like DNA sequences in multicentric Castleman's disease. Blood 86:1276–1280.
4. Chen YB, Rahemtullah A, Hochberg E. 2007. Primary effusion lymphoma. Oncologist 12:569–576. https://doi.org/10.1634/theoncologist.12-5-569.
5. Judde JG, Lacoste V, Briere J, Kassa-Kelembho E, Clyti E, Couppie P, Buchrieser C, Tulliez M, Morvan J, Gessain A. 2000. Monoclonality or oligoclonality of human herpesvirus 8 terminal repeat sequences in Kaposi's sarcoma and other diseases. J Natl Cancer Inst 92:729–736. https://doi.org/10.1093/jnci/92.9.729.
6. Yu X, Shahir AM, Sha J, Feng Z, Eapen B, Nithianantham S, Das B, Karn J, Weinberg A, Bissada NF, Ye F. 2014. Short-chain fatty acids from periodontal pathogens suppress histone deacetylases, EZH2, and SUV39H1 to promote Kaposi's sarcoma-associated herpesvirus replication. J Virol 88:4466–4479. https://doi.org/10.1128/JVI.03326-13.
7. Dai L, DeFee MR, Cao Y, Wen J, Wen X, Noverr MC, Qin Z. 2014. Lipoteichoic acid (LTA) and lipopolysaccharides (LPS) from periodontal pathogenic bacteria facilitate oncogenic herpesvirus infection within primary oral cells. PLoS One 9:e101326. https://doi.org/10.1371/journal.pone.0101326.
8. Van Delden C, Iglewski BH. 1998. Cell-to-cell signaling and Pseudomonas aeruginosa infections. Emerg Infect Dis 4:551–560. https://doi.org/10.3201/eid0404.980405.
9. Chernish RN, Aaron SD. 2003. Approach to resistant gram-negative bacterial pulmonary infections in patients with cystic fibrosis. Curr Opin Pulm Med 9:509–515. https://doi.org/10.1097/00063198-200311000-00011.
10. Bonomo RA, Szabo D. 2006. Mechanisms of multidrug resistance in Acinetobacter species and Pseudomonas aeruginosa. Clin Infect Dis 43(Suppl 2):S49–S56. https://doi.org/10.1086/504477.
11. Asboe D, Gant V, Aucken HM, Moore DA, Umasankar S, Bingham JS, Kaufmann ME, Pitt TL. 1998. Persistence of Pseudomonas aeruginosa strains in respiratory infection in AIDS patients. AIDS 12:1771–1775. https://doi.org/10.1097/00002030-199814000-00008.
12. Jakobsen TH, Bjarnsholt T, Jensen PO, Givskov M, Hoiby N. 2013. Targeting quorum sensing in Pseudomonas aeruginosa biofilms: current and emerging inhibitors. Future Microbiol 8:901–921. https://doi.org/10.2217/fmb.13.57.
13. Lee J, Zhang L. 2015. The hierarchy quorum sensing network in Pseudomonas aeruginosa. Protein Cell 6:26–41. https://doi.org/10.1007/s13238-014-0100-x.
14. Rasamiravaka T, El Jaziri M. 2016. Quorum-sensing mechanisms and bacterial response to antibiotics in P. aeruginosa. Curr Microbiol 73:747–753. https://doi.org/10.1007/s00284-016-1101-1.
15. Middleton B, Rodgers HC, Camara M, Knox AJ, Williams P, Hardman A. 2002. Direct detection of *N*-acylhomoserine lactones in cystic fibrosis sputum. FEMS Microbiol Lett 207:1–7. https://doi.org/10.1111/j.1574-6968.2002.tb11019.x.
16. Collier DN, Anderson L, McKnight SL, Noah TL, Knowles M, Boucher R, Schwab U, Gilligan P, Pesci EC. 2002. A bacterial cell to cell signal in the lungs of cystic fibrosis patients. FEMS Microbiol Lett 215:41–46. https://doi.org/10.1111/j.1574-6968.2002.tb11367.x.
17. Charlton TS, de Nys R, Netting A, Kumar N, Hentzer M, Givskov M, Kjelleberg S. 2000. A novel and sensitive method for the quantification of *N*-3-oxoacyl homoserine lactones using gas chromatography-mass spectrometry: application to a model bacterial biofilm. Environ Microbiol 2:530–541. https://doi.org/10.1046/j.1462-2920.2000.00136.x.
18. Hoiby N. 2006. P. aeruginosa in cystic fibrosis patients resists host defenses, antibiotics. Microbe (Wash, DC) 1:571–577.
19. Wang K, Chen YQ, Salido MM, Kohli GS, Kong JL, Liang HJ, Yao ZT, Xie YT, Wu HY, Cai SQ, Drautz-Moses DI, Darling AE, Schuster SC, Yang L, Ding Y. 2017. The rapid in vivo evolution of Pseudomonas aeruginosa in ventilator-associated pneumonia patients leads to attenuated virulence. Open Biol 7:170029. https://doi.org/10.1098/rsob.170029.
20. Lee J, Wu J, Deng Y, Wang J, Wang C, Wang J, Chang C, Dong Y, Williams P, Zhang LH. 2013. A cell-cell communication signal integrates quorum sensing and stress response. Nat Chem Biol 9:339–343. https://doi.org/10.1038/nchembio.1225.
21. Whiteley M, Lee KM, Greenberg EP. 1999. Identification of genes controlled by quorum sensing in Pseudomonas aeruginosa. Proc Natl Acad Sci U S A 96:13904–13909.
22. Schuster M, Greenberg EP. 2007. Early activation of quorum sensing in Pseudomonas aeruginosa reveals the architecture of a complex regulon. BMC Genomics 8:287. https://doi.org/10.1186/1471-2164-8-287.
23. Lau GW, Hassett DJ, Ran H, Kong F. 2004. The role of pyocyanin in Pseudomonas aeruginosa infection. Trends Mol Med 10:599–606. https://doi.org/10.1016/j.molmed.2004.10.002.
24. Reis RS, Pereira AG, Neves BC, Freire DM. 2011. Gene regulation of rhamnolipid production in Pseudomonas aeruginosa—a review. Bioresour Technol 102:6377–6384. https://doi.org/10.1016/j.biortech.2011.03.074.
25. Qin Z, Yang L, Qu D, Molin S, Tolker-Nielsen T. 2009. Pseudomonas aeruginosa extracellular products inhibit staphylococcal growth, and disrupt established biofilms produced by Staphylococcus epidermidis. Microbiology 155:2148–2156. https://doi.org/10.1099/mic.0.028001-0.
26. Diaz MR, King JM, Yahr TL. 2011. Intrinsic and extrinsic regulation of type III secretion gene expression in Pseudomonas aeruginosa. Front Microbiol 2:89. https://doi.org/10.3389/fmicb.2011.00089.
27. Qin Z, Jakymiw A, Findlay V, Parsons C. 2012. KSHV-encoded microRNAs: lessons for viral cancer pathogenesis and emerging concepts. Int J Cell Biol 2012:603961. https://doi.org/10.1155/2012/603961.
28. Plaisance-Bonstaff K, Choi HS, Beals T, Krueger BJ, Boss IW, Gay LA, Haecker I, Hu J, Renne R. 2014. KSHV miRNAs decrease expression of lytic genes in latently infected PEL and endothelial cells by targeting host transcription factors. Viruses 6:4005–4023. https://doi.org/10.3390/v6104005.
29. Piedade D, Azevedo-Pereira JM. 2016. The role of microRNAs in the pathogenesis of herpesvirus infection. Viruses 8:E156. https://doi.org/10.3390/v8060156.
30. Pacheco AR, Sperandio V. 2009. Inter-kingdom signaling: chemical language between bacteria and host. Curr Opin Microbiol 12:192–198. https://doi.org/10.1016/j.mib.2009.01.006.
31. Jesaitis AJ, Franklin MJ, Berglund D, Sasaki M, Lord CI, Bleazard JB, Duffy JE, Beyenal H, Lewandowski Z. 2003. Compromised host defense on Pseudomonas aeruginosa biofilms: characterization of neutrophil and biofilm interactions. J Immunol 171:4329–4339. https://doi.org/10.4049/jimmunol.171.8.4329.
32. Jensen PO, Givskov M, Bjarnsholt T, Moser C. 2010. The immune system vs. Pseudomonas aeruginosa biofilms. FEMS Immunol Med Microbiol 59:292–305. https://doi.org/10.1111/j.1574-695X.2010.00706.x.
33. Telford G, Wheeler D, Williams P, Tomkins PT, Appleby P, Sewell H, Stewart GS, Bycroft BW, Pritchard DI. 1998. The Pseudomonas aeruginosa quorum-sensing signal molecule *N*-(3-oxododecanoyl)-L-homoserine lactone has immunomodulatory activity. Infect Immun 66:36–42.
34. Smith RS, Harris SG, Phipps R, Iglewski B. 2002. The Pseudomonas aeruginosa quorum-sensing molecule *N*-(3-oxododecanoyl)homoserine lactone contributes to virulence and induces inflammation in vivo. J Bacteriol 184:1132–1139. https://doi.org/10.1128/jb.184.4.1132-1139.2002.
35. Hooi DS, Bycroft BW, Chhabra SR, Williams P, Pritchard DI. 2004. Differential immune modulatory activity of Pseudomonas aeruginosa quorum-sensing signal molecules. Infect Immun 72:6463–6470. https://doi.org/10.1128/IAI.72.11.6463-6470.2004.
36. Chiller K, Selkin BA, Murakawa GJ. 2001. Skin microflora and bacterial infections of the skin. J Investig Dermatol Symp Proc 6:170–174. https://doi.org/10.1046/j.0022-202x.2001.00043.x.
37. Wu DC, Chan WW, Metelitsa AI, Fiorillo L, Lin AN. 2011. Pseudomonas

skin infection: clinical features, epidemiology, and management. Am J Clin Dermatol 12:157–169. https://doi.org/10.2165/11539770-000000000-00000.
38. Qin Z, Kearney P, Plaisance K, Parsons CH. 2010. Pivotal advance: Kaposi's sarcoma-associated herpesvirus (KSHV)-encoded microRNA specifically induce IL-6 and IL-10 secretion by macrophages and monocytes. J Leukoc Biol 87:25–34. https://doi.org/10.1189/jlb.0409251.
39. Hentzer M, Wu H, Andersen JB, Riedel K, Rasmussen TB, Bagge N, Kumar N, Schembri MA, Song Z, Kristoffersen P, Manefield M, Costerton JW, Molin S, Eberl L, Steinberg P, Kjelleberg S, Hoiby N, Givskov M. 2003. Attenuation of Pseudomonas aeruginosa virulence by quorum sensing inhibitors. EMBO J 22:3803–3815. https://doi.org/10.1093/emboj/cdg366.
40. D'Argenio DA, Calfee MW, Rainey PB, Pesci EC. 2002. Autolysis and autoaggregation in Pseudomonas aeruginosa colony morphology mutants. J Bacteriol 184:6481–6489. https://doi.org/10.1128/JB.184.23.6481-6489.2002.

SCIENTIFIC REPORTS

OPEN

Distinct systemic microbiome and microbial translocation are associated with plasma level of anti-CD4 autoantibody in HIV infection

Received: 14 November 2017
Accepted: 3 August 2018
Published online: 27 August 2018

Wanli Xu[1], Zhenwu Luo[2], Alexander V. Alekseyenko[3], Lisa Martin[4], Zhuang Wan[2], Binhua Ling[5,6], Zhiqiang Qin[7], Sonya L. Heath[8], Kendra Maas[9], Xiaomei Cong[1] & Wei Jiang[2,4]

Microbial signals have been linked to autoantibody induction. Recently, we found that purified anti-CD4 autoantibodies from the plasma of chronic HIV-1-infected patients under viral-suppressed antiretroviral therapy (ART) play a pathologic role in poor CD4+ T cell recovery. The purpose of the study was to investigate the association of systemic microbiome and anti-CD4 autoantibody production in HIV. Plasma microbiome from 12 healthy controls and 22 HIV-infected subjects under viral-suppressed ART were analyzed by MiSeq sequencing. Plasma level of autoantibodies and microbial translocation (LPS, total bacterial 16S rDNA, soluble CD14, and LPS binding protein) were analyzed by ELISA, limulus amebocyte assay, and qPCR. We found that plasma level of anti-CD4 IgGs but not anti-CD8 IgGs was increased in HIV+ subjects compared to healthy controls. HIV+ subjects with plasma anti-CD4 IgG $>$ 50 ng/mL (high) had reduced microbial diversity compared to HIV+ subjects with anti-CD4 IgG $\leq$ 50 ng/mL (low). Moreover, plasma anti-CD4 IgG level was associated with elevated microbial translocation and reduced microbial diversity in HIV+ subjects. The *Alphaproteobacteria* class was significantly enriched in HIV+ subjects with low anti-CD4 IgG compared to patients with high anti-CD4 IgG even after controlling for false discovery rate (FDR). The microbial components were different from the phylum to genus level in HIV+ subjects with high anti-CD4 IgGs compared to the other two groups, but these differences were not significant after controlling for FDR. These results suggest that systemic microbial translocation and microbiome may associate with anti-CD4 autoantibody production in ART-treated HIV disease.

Chronic inflammation or immune dysfunction has been a critical issue in human immunodeficiency virus (HIV) disease even in patients under viral suppressive antiretroviral therapy (ART). ART significantly suppresses HIV viral replication, improves immune function, and decreases morbidity and mortality in HIV disease[1,2]. However, a substantial number of patients fail to reconstitute their peripheral CD4+ T cell counts even after

[1]University of Connecticut School of Nursing, Storrs, Connecticut, 06269, USA. [2]Department of Microbiology and Immunology, Medical University of South Carolina, Charleston, SC, 29425, USA. [3]Program for Human Microbiome Research, Biomedical Informatics Center, Department of Public Health Sciences, Department of Oral Health Sciences, Medical University of South Carolina, Charleston, SC, 29425, USA. [4]Division of Infectious Diseases, Department of Medicine, Medical University of South Carolina, Charleston, SC, 29425, USA. [5]Department of Microbiology and Immunology, Tulane University School of Medicine, New Orleans, LA, 70112, USA. [6]Tulane National Primate Research Center, New Orleans, LA, 70433, USA. [7]Departments of Genetics, Louisiana State University Health Sciences Center, Louisiana Cancer Research Center, 1700 Tulane Ave., New Orleans, LA, 70112, USA. [8]Division of Infectious Diseases, Department of Medicine, University of Alabama at Birmingham, Birmingham, AL, 35294, USA. [9]Microbial Analysis, Resources, and Services, University of Connecticut, Storrs, CT, 06269, USA. Wanli Xu and Zhenwu Luo contributed equally. Correspondence and requests for materials should be addressed to X.C. (email: xiaomei.cong@uconn.edu) or W.J. (email: jianw@musc.edu)

long-term viral-suppressive ART treatment, and exhibit increased risks of complications, morbidity and mortality[3–7]. Previous studies have shown that thymic and lymphatic fibrosis, low nadir CD4+ T cell counts, sustained increases in inflammation, and microbial translocation may account for patients with poor CD4+ T cell recovery under viral suppressive ART treatment[5,8–21]. However, the exact mechanism governing poor CD4+ T cell recovery is still unknown. In our recent work, we studied the anti-CD4 autoreactive IgGs purified from plasma of ART-treated aviremic patients with peripheral CD4+ T cell counts less than 350 cells/μL. Our study has shown that anti-CD4 autoreactive IgGs induce CD4+ T cell death through antibody-mediated natural killer (NK) cell cytotoxicity *in vitro*, suggesting that anti-CD4 autoantibodies play a role in blunted CD4+ T cell reconstitution after ART treatment[22]. Consistently, we have found that purified NK cells from patients with blunted CD4+ T cell recovery were enriched in cytotoxic cells and were able to mediate uninfected CD4+ T cell death *ex vivo*[23].

Prior to ART treatment, HIV infection results in significant B cell depletion, especially memory B cell depletion, B cell hyperactivation and heightened plasma levels of autoantibodies, as well as impaired vaccine responsiveness[24–28]. These B cell perturbations cannot be completely explained by the lack of contribution from CD4+ T cells; B cell intrinsic defects have been observed[29,30]. For example, our previous work has shown that purified B cells from HIV-infected subjects had reduced proliferation capacities in response to toll-like receptor (TLR) 9 ligand stimulation compared to B cells from healthy controls *in vitro*[30]. Another study from Moir's group reported that purified B cells from HIV-infected patients had reduced antigen-presenting function compared to B cells from healthy controls when co-culturing with purified T cells from the same healthy donors[29]. These results suggest B cell intrinsic dysfunction in HIV disease. Furthermore, B cells have been reported activated even after long-term viral-suppressive ART treatment, which may account for inconsistent serologic antibody responses and cellular responses in patients given seasonal influenza vaccination[31].

The underlying mechanisms of long-term humoral immune perturbations in HIV-infected patients, despite undergoing ART treatment, are still largely unknown. The fecal microbiota and microbial translocation from the gastrointestinal (GI) tract to systemic circulation have been recently investigated as a major driver of immune perturbations and persistent systemic inflammation in HIV disease[32–35]. Increased intestinal permeability due to mucosal barrier dysfunction, GI immune dysregulation and/or altered intestinal microbiome are considered to be significant factors related to microbial translocation and HIV pathogenesis. Differences in fecal microbiome in HIV-infected patients versus healthy controls are associated with systemic inflammation[32]. Mechanistically, microbial products such as TLR ligands can induce autoantibody production and may play a pathogenic role in autoimmune diseases[36–38]. Increased systemic microbial translocation and its associated inflammation may result in B cell hyperactivation and perturbation in HIV disease. After long-term repeated stimulation by low concentrations of TLR ligands (compared to one dose and high concentration as vaccine adjuvants) and other microbial products released from the gut[24–26,39], B cells may be polyclonally activated as reflected by increased total IgM and IgG[26,40].

In the current study, we hypothesize that microbial translocation of specific bacterial strains may play a role in B cell activation and anti-CD4 autoantibody production. We, therefore, investigate systemic bacterial microbiome, the magnitude of microbial translocation, and plasma anti-CD4 autoantibodies in HIV+ subjects under long-term viral suppressive ART treatment.

Methods

Study Design, Subjects, and Data Collection. This study was approved by the Institutional Review Board at Medical University of South Carolina. All methods were performed in accordance with the relevant guidelines and regulations. All participants provided written informed consents. In the present study, 12 healthy volunteers and 22 HIV+ ART-treated aviremic (plasma HIV RNA < 50 copies/mL) patients were enrolled. The clinical characteristics of participants are shown in Table 1.

Inclusion and exclusion criteria. All participants were age 18 years and older. All patients had documented HIV infection and were receiving a stable antiretroviral regimen with plasma HIV RNA < 50 copies/mL more than two years prior to study entry. Transient viremic blips did not exclude participation if flanked by viral levels below detection limits. Exclusion criteria included pregnancy, breast-feeding, surgery, chemotherapy, inflammatory bowel diseases, and uses of steroids more than 10 mg per day for more than 120 days or uses of antibiotics within 14 days prior to enrollment.

ELISA for detection of anti-CD4 IgGs and anti-CD8 IgGs. Human soluble CD4 protein (sCD4, Progenics Tarrytown, NY) or human soluble CD8B/P37/LEU2 protein (sCD8, Sino Biological Inc. Beijing, China) were diluted at the concentration of 16 μg/ml and added to microtiter wells, and incubated at 4 °C overnight. Microwells were washed three times with phosphate buffered saline wash buffer (PBS with 0.1% Tween 20), and then blocked with PBS containing 3% bovine serum albumin (BSA) for 120 min at 37 °C. Plasma was diluted 1:40 in PBS containing 3% BSA and 100 μl of the dilution were added to the wells. The plate was incubated at room temperature for 60 min. Biotin-labeled goat anti-human IgG was added at 1:5000 dilution in PBS containing 3% BSA. The plate was then incubated for 60 min at room temperature. Horseradish peroxidase conjugated streptavidin (HRP-Streptavidin) was added at a 1:1000 dilution in PBS containing 3% BSA, and then incubated for 30 min at room temperature. After washing, 100 μl 2,2′-Azino-di (3-ethylbenzthiazoline-6-sulfonate) were added and incubated for 30 min, and 405 nm emission was read within 30 min. PBS containing 3% BSA alone was used as a negative control and anti-CD4 and anti-CD8 antibodies were used as positive controls.

The 40th percentile (50 ng/mL) of anti-CD4 IgG was used to define the cutoff for high and low levels of the IgG. Therefore, patients with plasma anti-CD4 IgG level above 50 mg/mL were defined as the high anti-CD4 IgG group; and patients with plasma anti-CD4 IgG level equal or below 50 ng/mL were defined as the low anti-CD4 IgG group.

	Healthy control	HIV+/αCD4^{low}	HIV+/αCD4^{high}	P1	P2	P3
Number	12	13	9			
Age	43.5 (33.5–56)	43 (26–46.5)	47 (36–56.5)	0.25	0.77	0.21
Gender (Male/%)	3 (25%)	11 (84.6%)	3 (33.3%)	0.005	>0.99	0.04
Race (AA/%)	7 (44%)	8 (57%)	7 (58%)	0.72	0.7	0.52
Nadir CD4 count (cells/μL)		361 (226–490)	229 (124–426)			0.19
Duration of ART (yr)		4 (3.5–6.5)	6 (4–6)			0.82
CD4 count (cells/μL)	828 (523–1043)	634 (514–744)	450 (321–677)	0.50	0.07	0.07
%ki67+ CD4	1.0 (0.7–1.6)	2.8 (1.9–3.8)	2.5 (1.7–3.9)	<0.0001	0.001	0.73
%annexin V+ CD4	19 (13.5–37.7)	29.4 (27.1–43)	26.9 (15.7–32)	0.14	0.60	0.18
B cell count (cells/μL)	219 (112–235)	239 (132–314)	185 (130–245)	0.29	0.65	0.37
%ki67+ B cells	0.9 (0.7–1.1)	1.5 (0.9–2.0)	1.3 (0.9–2.7)	0.03	0.03	0.84
%annexin V+ B cells	9 (5.5–18)	19.4 (12.6–27.8)	17.6 (13.3–33)	0.007	0.04	0.86
Plasma soluble CD4 (ng/mL)	2.1 (1.2–4.9)	1.7 (0–2.7)	1.8 (0.3–2.7)	0.37	0.39	0.66
Current ART regimen						
Multi-Class Combination		11 (84.6%)	4 (44.4%)			>0.99
NRTIs		2 (15.4%)	3 (33.3%)			0.71
PIs		3 (23%)	3 (33.3%)			>0.99
Metabolic abnormities						
BMI		26.1 (23.3–29.7)	32.3 (24.9–38.3)			0.14
Diabetes mellitus		1 (0.08%)	1 (0.11%)			>0.99
Hypertension		4 (30.8%)	2 (22.2%)			0.67
Abnormal lipid metabolism		5 (38.5%)	3 (33.3%)			0.67

Table 1. Demographic and clinical characteristics of the participants. P1: HIV- vs HIV+/αCD4^{low}. P2: HIV- vs HIV+/αCD4^{high}. P3: HIV+/αCD4^{high} vs HIV+/αCD4^{low}. Non-parametric Mann-Whitney tests. Abnormal lipid metabolism: hyperlipidemia, hyperlipidemia, hypertriglyceridemia, hypercholesterolemia. Multi-Class Combination ART: Two different groups in a complete HIV drug regimen (e.g., Atripla (bictegravir + tenofovir DF + emtricitabine)).

Plasma levels of LPS, soluble CD14 (sCD14), LPS binding protein (LBP). Plasma samples were collected into tubes containing EDTA and stored at −80 °C until they were thawed once. The method was described in our previous studies[41–43]. Briefly, the plasma samples were diluted to 10% with endotoxin-free water, and LPS was quantified using a commercially available limulus amebocyte assay kit (Lonza Inc., Allendale, NJ) according to the manufacturer's protocol. sCD14 and LBP were quantified using kits from R&D (Minneapolis, MN) and Hycult Biotech (Plymouth Meeting, PA) respectively following manufacturers' protocols.

Quantitative polymerase chain reaction (PCR) for measurement of bacterial 16S rDNA. DNA was extracted from 400 μL endotoxin-free water and 400 μL plasma using QIAamp UCP pathogen Mini kit (Qiagen, Valencia, CA) according to the manufacturer's instructions. The method was described in our previous studies[31,41]. Briefly, a 20 μL amplification reaction consisted of 10 μL of 2x Perfecta qPCR ToughMix (Quanta, Gaithersburg, MD), 0.3 μmol/L forward and reverse primers, 0.175 μmol/L probe (338 P: 5′-FAM-GCTGCCTCCCGTAGGAGT-BHQ1-3′), and 5 μL of the template plasma DNA. Degenerate forward (8 F: 5′-AGTTTGATCCTGGCTCAG-3′) and reverse (515 R: 5′-GWATTACCGCGGCKGCTG-3′) primers were used to amplify DNA templates encoding 16S rRNA. The DNA was amplified in duplicate, and mean values were calculated by subtracting values in the water control. A standard curve was created from serial dilutions of plasmid DNA containing known copy numbers of the template. The reaction conditions for amplification of DNA were 95 °C for 5 min, followed by 40 cycles at 95 °C for 15 s and at 60 °C for 1 min[41].

Plasma microbial DNA extraction, sequencing and data process. Microbial DNA extraction was described above in 16S rDNA assay. The 16S rRNA gene V4 variable region PCR primers 515/806 with barcode on the forward primer were used in a 30 cycle PCR (5 cycle used on PCR products) using the HotStarTaq Plus Master Mix Kit (Qiagen, USA) under the following conditions: 94 °C for 3 minutes, followed by 28 cycles of 94 °C for 30 seconds, 53 °C for 40 seconds and 72 °C for 1 minute, after which a final elongation step at 72 °C for 5 minutes was performed. After amplification, PCR products were checked in 2% agarose gel to determine the success of amplification and the relative intensity of bands. Multiple samples were pooled together (e.g., 100 samples) in equal proportions based on their molecular weight and DNA concentrations. Pooled samples were purified using calibrated Ampure XP beads. Then the pooled and purified PCR product was used to prepare the DNA library by following Illumina TruSeq DNA library preparation protocol. Sequencing was performed at MR DNA (www.mrdnalab.com, Shallowater, TX, USA) on a MiSeq following the manufacturer's guidelines.

The Q25 sequence data derived from the sequencing process was processed using a proprietary analysis pipeline (www.mrdnalab.com, MR DNA, Shallowater, TX). Sequences were depleted of barcodes and primers, then short sequences <200 bp and sequences with ambiguous base calls, and sequences with homopolymer runs exceeding 6 bp were removed. Next, sequences were denoised and operational taxonomic units (OTUs)

were defined clustering at 3% divergence (97% similarity) followed by removal of singleton sequences and chimeras[44–48]. Final OTUs were taxonomically classified using BLASTn against a curated database derived from GreenGenes, RDPII and NCBI[49]. The data has been summarized at each taxonomic level by both raw counts and relative abundances. For each plasma sample and water control, absolute and relative abundance in OTU tables were generated. To control for contamination, two water samples were used as negative controls for DNA extraction. ß-diversity is different from the samples of patients, healthy and water controls (Supplemental Fig. 1). In the data analysis, we used both methods of subtracting the mean abundance of the OTUs and removing any OTUs that are present in the water control. The PERMANOVA variability from both methods are the same. The results in this paper were presented based on the method of removing the mean absolute abundance of OTUs. See Supplemental Table 1 for the raw data of the read counts and relative abundance from each sample including water controls.

Statistical Analysis. In the pre-specified hypothesis, we were interested in the comparisons of HIV+ high anti-CD4 antibody group versus HIV+ low anti-CD4 antibody group or healthy controls; therefore, P values from comparing HIV+ high anti-CD4 antibody group to each control group were not adjusted for multiple comparisons[50]. Non-parametric Mann-Whitney U tests were applied to the current study.

For microbiome analysis, OTU tables and different levels of taxonomy tables derived from the sequencing process described above were imported to R (version 3.3.1) for statistical analysis[51]. The mean values of two negative controls were subtracted from each sample's OTU to control for the contamination. Simpson index of diversity was calculated using Vegan package[52] to measure α diversity of each sample. Spearman's Correlation test was used to assess the association among Simpson diversity index, clinical and demographic characters and autoreactive antibody. Bray-Curtis and Jaccard dissimilarity were calculated using Vegan package to evaluate ß-diversity, the compositional dissimilarity among the microbial community. Jaccard dissimilarity measures the dissimilarity between samples based on the presence/absence of the data, whereas Bray-Curtis dissimilarity was calculated based on both presence/absence and abundance. The relationships between ß-diversity of the microbial community and autoreactive antibody titer were assessed using PERMANOVA in Vegan package. Analysis of indicator species (Indicspecis package) was used to assess the relationship between the occurrence/abundance of species at the genus level with different clinical characters. False discovery rate (FDR) correction was applied to control for multiple comparisons.

Accession codes. The data are available at the NCBI Sequence Read Archive (SRA) under accession no. SRP120355 (http://www.ncbi.nlm.nih.gov/sra).

Results

A total of 34 participants completed the study, including 22 HIV patients and 12 healthy controls. Demographic characteristics of the participants are illustrated in Table 1.

Plasma anti-CD4 IgG level but not anti-CD8 IgG level was increased in aviremic ART-treated HIV+ subjects compared to healthy controls. Following our recent work, we investigated the mechanism of anti-CD4 autoantibody production in well-controlled ART-treated HIV infection. We first analyzed plasma levels of anti-CD4 IgG as well as anti-CD8 IgG in age-matched healthy controls and aviremic ART-treated HIV-infected subjects. We found that the plasma level of autoreactive anti-CD8 IgG was similar in controls and HIV+ subjects, but the level of anti-CD4 IgG increased in the HIV+ subjects compared to controls (Fig. 1A,B), suggesting that B cell function is still abnormal even after long-term ART treatment and successful viral suppression.

Plasma microbial translocation was elevated in HIV+ subjects with high plasma anti-CD4 IgGs compared to healthy controls. Next, to investigate the association of systemic microbial translocation and plasma anti-CD4 IgGs level in HIV-infected subjects, we stratified patients to either high plasma autoantibody level or low plasma autoantibody level group. The cutoff value of 50 ng/mL plasma anti-CD4 IgG was defined based on 40 up-percentile, and no healthy controls were above that value. Notably, both plasma LPS level and bacterial 16S rDNA level, markers of microbial translocation[41], tended to increase in HIV+ subjects with plasma anti-CD4 IgG below 50 ng/mL compared to healthy controls but have not achieved significant differences (Fig. 1C,D). Importantly, HIV+ subjects with high plasma level of anti-CD4 IgGs exhibited significantly elevated plasma microbial translocation (Fig. 2), suggesting that residual increased systemic microbial products may be associated with autoantibody production. In addition, we have evaluated the other two markers related to microbial translocation, sCD14 and LBP in plasma. Indeed, HIV+ subjects with high anti-CD4 IgGs had increased plasma sCD14 (Fig. 1E) and LBP (Fig. 1F) levels compared to the other two study groups. These results suggest that HIV+ subjects with high plasma anti-CD4 IgGs, but not HIV+ subjects with low plasma anti-CD4 IgGs, had increased systemic microbial translocation compared to healthy controls.

Distinct plasma microbial profiles in HIV+ subjects with high anti-CD4 IgGs compared to controls. To investigate the difference of microbial translocation in healthy controls and HIV+ subjects, we performed and analyzed plasma microbiome (Fig. 2A–E). The samples yielded a total of 1,218,338 reads with an average of 34758.15 ($\pm$15380.71) reads per subject and 18280.5 ($\pm$10127.89) reads for water control. A total of 2408 OTUs were found in samples of all 34 subjects. On average, 400 ($\pm$98) OTUs were found in each sample. In contrast, 439 OTUs (average 272 $\pm$ 76) were found in the water control, and the top phyla were *Proteobacteria* (79.3%), *Firmicutes* (12.5%), *Deinococcus-Thermus* (7.3%), *Cuampbacteroa* (0.7%) and *Actinobacteria* (0.2%). In the phylum levels among all samples, 57.4% were *Proteobacteria*, 19.2% were *Firmicutes*, 10.5% were

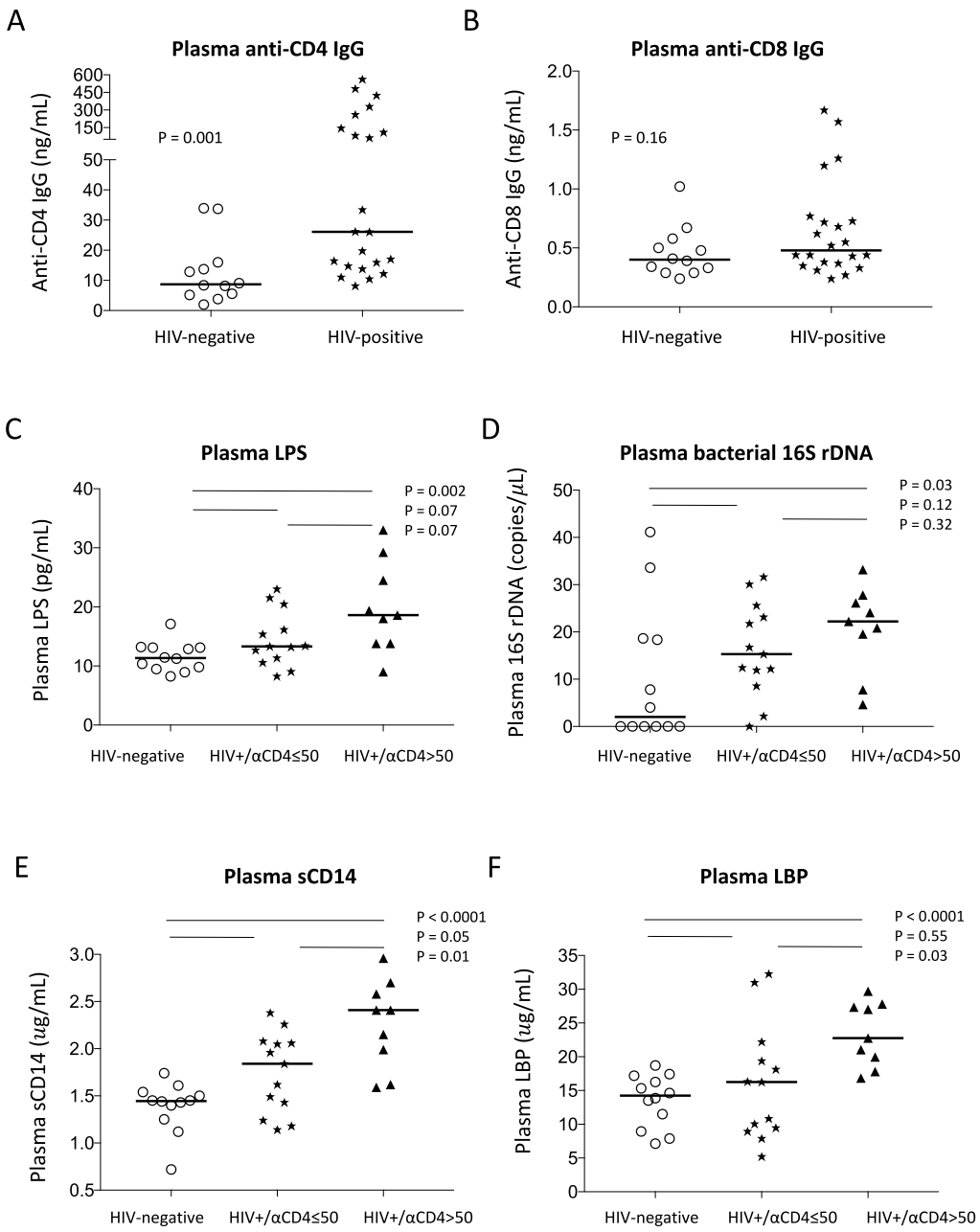

Figure 1. Plasma level of anti-CD4 IgG and its association with microbial translocation in HIV+ subjects. sCD4 and sCD8 proteins were used to detect plasma anti-CD4 IgGs (**A**) and anti-CD8 IgGs (**B**) by ELISA. Plasma levels of LPS were detected by limulus amebocyte assay (**C**), bacterial 16S rDNA were detected by qPCR (**D**), sCD14 (**E**) and LBP (**F**) by ELISA in healthy controls and HIV+ subjects with plasma anti-CD4 IgG > 50 ng/mL and ≤50 ng/mL. Non-parametric Mann-Whitney tests.

Actinobacteria, and 6.4% *Bacteroidetes* in plasma (Fig. 2A). A decreased ratio of *Firmicutes/Bacteroidetes* was reported on the fecal microbiome in autoantibody-derived autoimmune disease such as systemic lupus erythematosus (SLE)[53,54]. In this study, the ratios of *Firmicutes/Bacteroidetes* were 0.58 ± 0.45 in healthy controls, 0.37 ± 0.38 in the low anti-CD4 IgG HIV+ subjects, and 0.32 ± 0.30 in the high anti-CD4 IgG HIV+ subjects, respectively, but did not achieve significant difference between any two groups (mean ± SD, $P > 0.05$). At the class level, *Gammaproteobateria, Betaproteobacteria, Bacilli* and *Alphaproteobacteria* were predominant (80.3%) in the low anti-CD4 IgG group (Fig. 2B). Notably, the plasma enrichment of *Alphaproteobacteria* class was significantly higher in the low anti-CD4 IgG patient group compared to the high anti-CD4 IgG patient group after controlling for FDR ($t = 3.22$, $P < 0.05$, Fig. 2B). At the family level, *Staphylococcaceae* and *Pseudomonadaceae* were increased in the high anti-CD4 IgG patient group compared to the other two groups (Fig. 2D). At the genus level, *Alicycliphilus, Pseudomonas*, and *Staphylococcus* had increased relative abundance in the high anti-CD4 IgG

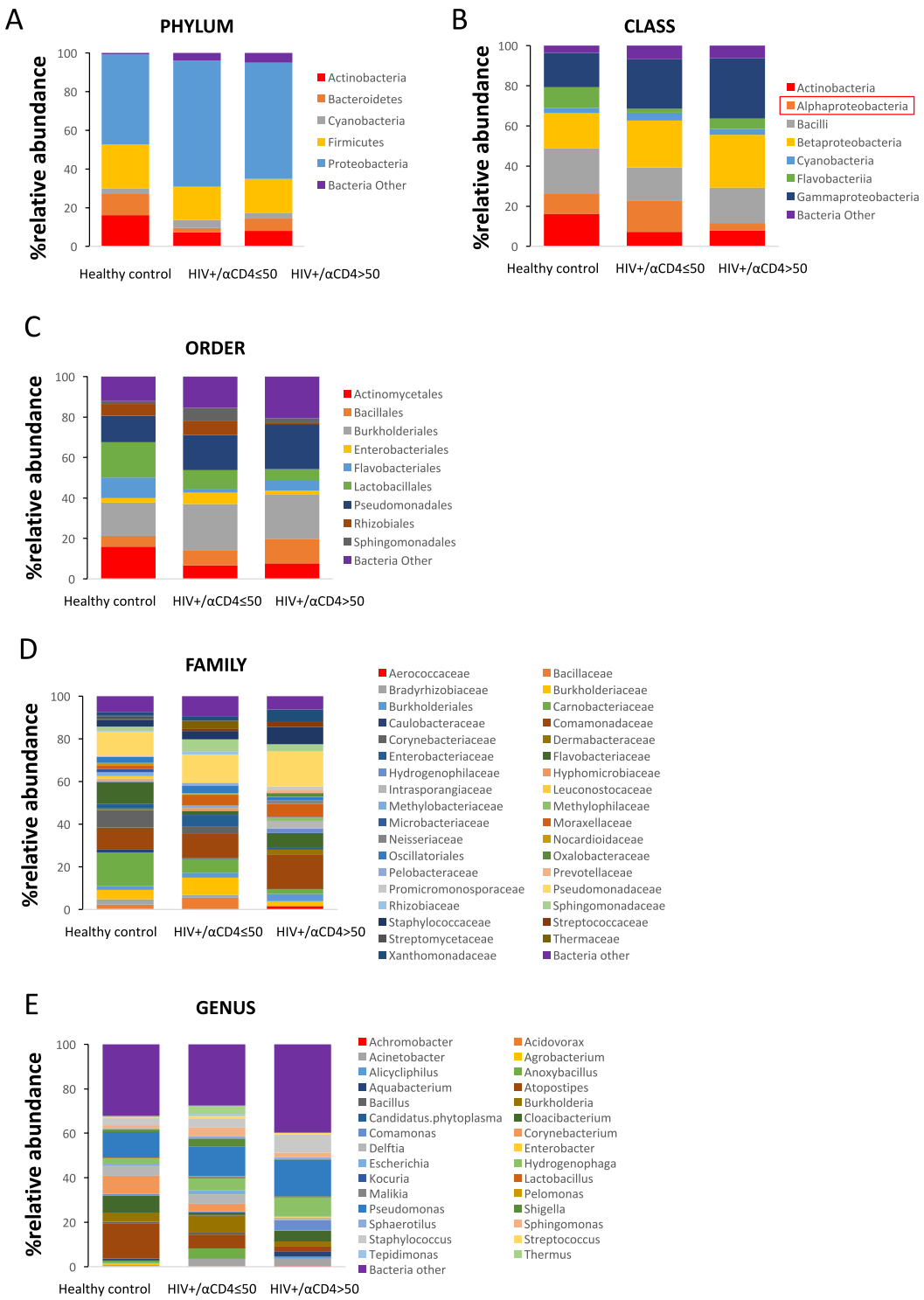

Figure 2. Circulating microbiome relative abundance analysis in healthy controls and HIV+ subjects. Microbial DNA was extracted from plasma and V4 variable region of bacterial 16S rDNA gene was amplified. The relative abundance of phylum (**A**), class (**B**), order (**C**), family (**D**), and genus (**E**) level bacteria (>1%) were shown in plasma from healthy controls, HIV+ subjects with plasma anti-CD4 IgG level ≤ 50 ng/mL and HIV+ subjects with anti-CD4 IgG > 50 ng/mL. The plasma enrichment of *Alphaproteobacteria* class was significantly higher in the low anti-CD4 IgG patient group compared to the high anti-CD4 IgG patient group after controlling for FDR.

patient group compared to the low anti-CD4 IgG patient group. (Fig. 2E). Although the microbial components were different from the phylum to genus levels in HIV+ subjects with high anti-CD4 IgGs compared to the other two groups, these differences were not significant after controlling for FDR.

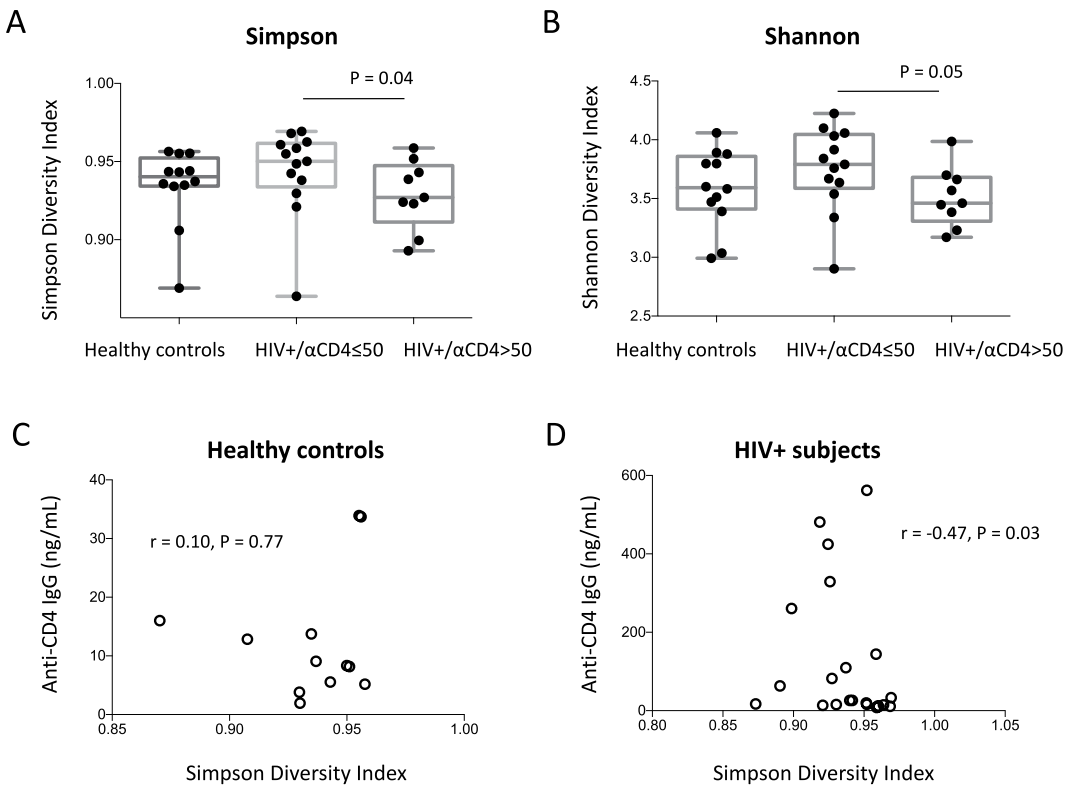

Figure 3. Reduced diversity was associated with increased plasma level of anti-CD4 autoantibody in HIV+ subjects. Box and whiskers plots of the Simpson (**A**) and Shannon (**B**) diversity indexes of plasma samples from HIV+ subjects with anti-CD4 IgG levels ≤ 50 ng/mL, >50 ng/mL and healthy controls. The top and bottom boundaries of each box indicate the 3rd and 1st quartile values, respectively. The central horizontal line represents the median values. The dot represents Simpson and Shannon diversity index of each sample. Non-parametric Mann-Whitney U tests. Correlations between the Simpson diversity index and plasma anti-CD4 IgG levels in healthy controls (**C**) and HIV+ subjects (**D**). Spearman correlation tests.

Reduced plasma microbial diversity was associated with increased plasma anti-CD4 antibodies in HIV-infected individuals. Next, to investigate the difference of composition in plasma microbiome in the three study groups, we analyzed microbial diversity including Simpson Diversity Index, Shannon index and species number observed. The Simpson and Shannon diversity indexes in the high anti-CD4 IgG HIV+ subject group were significantly lower compared to the low anti-CD4 IgG HIV+ subject group ($P = 0.04$ and $P = 0.05$ respectively, Fig. 3A,B). The numbers of species were 365.8 ± 99.6 in healthy controls, 373.5 ± 91.2 in the low anti-CD4 IgG HIV+ subjects, and 362.1 ± 85.7 in the high anti-CD4 IgG HIV+ subjects, respectively (mean $\pm$ SD, $P > 0.05$). There was an inverse correlation between plasma anti-CD4 IgG level and the Simpson diversity index in HIV+ subjects but not in healthy controls (Fig. 3C,D). Moreover, ß-diversity, the compositional dissimilarity among the microbial community was assessed using nonmetric dimensional scaling with both Bray-Curtis Coefficient and Jaccard Index, and revealed significant clusters between HIV-infected subjects with plasma anti-CD4 IgG level >50 ng/mL and their counterparts (Fig. 4). Nonetheless, anti-CD4 IgG level explained 6.8% of the variation of Bray-Curtis coefficient among HIV-infected individuals after controlling for plasma LPS level, duration of the ART treatment and CD4 counts (PERMANOVA, $n = 22$, $P < 0.05$); PERANOVA test of anti-CD4 IgG level on Jaccard Index yielded a similar result. Indicator species analysis showed that patients who had a higher level of anti-CD4 IgG (>50 ng/mL) had significantly higher levels of *Alicycliphilus* ($P < 0.05$) and *Hylemonella* ($P < 0.05$). However, the significances disappeared after controlling for FDR.

Discussion

Increased levels of autoreactive antibodies or autoimmune diseases have been shown in HIV/SIV infection[55–62]. ART treatment reduces B cell hyperactivation[63]. Our recent study shows that anti-CD4 autoantibodies purified from plasma of immunologic non-responders (undetectable plasma viral load, ART-treated, and CD4+ T cell counts <350 cells/μL) mediated CD4+ T cell death through antibody-dependent NK cell cytotoxicity, suggesting that anti-CD4 IgG plays a role in poor CD4+ T cell recovery under viral suppressive ART treatment[22]. In the current study, we found that both quantity and quality of plasma microbial products in ART-treated HIV-infected subjects was associated with anti-CD4 autoantibodies.

Microbial TLR and its agonists play a role in autoantibody production and autoimmune diseases[64,65]. Our previous study showed that plasma level of TLR4 ligand LPS was associated with inflammation and B cell activation in HIV disease[43]. Although ART treatment greatly reduces cell apoptosis and activation and thus limits

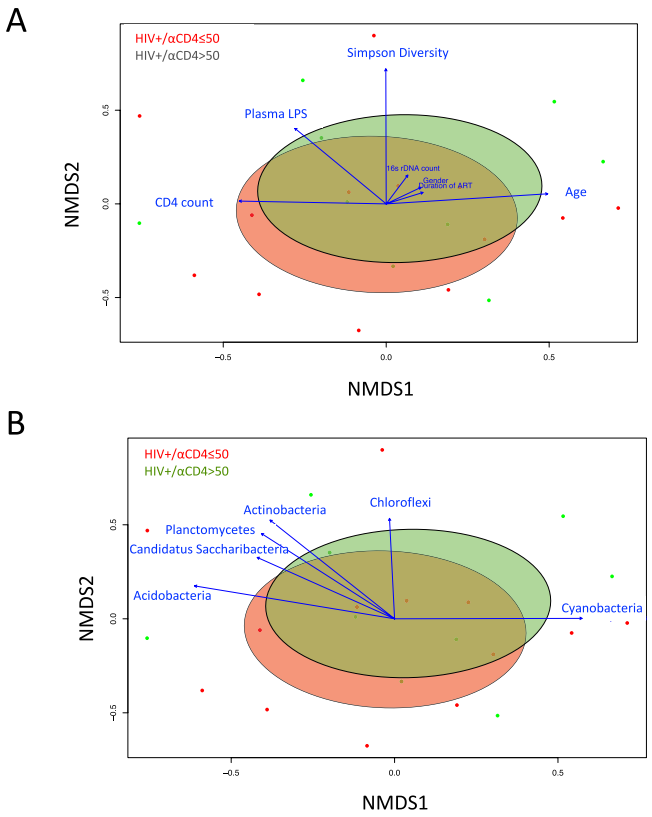

Figure 4. Nonmetric multidimensional scaling ordination (NMDS) plot of the OTUs with fitted vectors of clinical variables (**A**), and based on the abundance of bacterial phyla (**B**). Dots with different colors represent data from each plasma sample in HIV+ subjects with anti-IgG level ≤ 50 ng/mL (red) and HIV+ subjects with anti-CD4 IgG > 50 ng/mL (green). Ellipses denote the standard deviation of the weighted average NDMS score of anti-IgG level ≤ 50 ng/mL group (red) and anti-CD4 IgG > 50 ng/mL group (green). Community differences were verified by PERMONOVA test (Adonis, $P < 0.05$). Arrows represent the direction and magnitude of correlation of each clinical variable (**A**) and the abundance of bacterial phyla (**B**) with the ordination axes.

autoantibody production[43,66–69], we found that anti-CD4 specific antibody is a key exception (Fig. 1A). Moreover, altered B cell receptor (BCR) and TLR signals (e.g., MyD88) may promote autoreactive B cell selection[70]. Indeed, HIV+ subjects had elevated levels of microbial translocation (Fig. 1C,D) and cycling B cells[31] compared to healthy controls, implying that bacterial products (e.g., LPS) may play a role in activating B cells. Nonetheless, how microenvironmental and inflammatory factors drive the breakdown of B cell tolerance, especially in humans, is not fully understood. Notably, autoimmune diseases in HIV are often observed after ART[55,71,72], implying that pathologic autoantibodies are developed post the ART treatment.

Interestingly, a diverse bacterial DNAs were found in the plasma of healthy controls (Fig. 2). These findings are consistent with the study from Païssé S[73]. Low levels of microbial translocation occur in healthy individuals but increase when there is a GI barrier disruption. On the other hand, dysbiosis of gut microbiome community may result in mucosal immune dysfunction and intestinal mucosal barrier damage, which allows gut microbial translocation to the bloodstream[74–78]. Increased "leakiness" of microbial products (e.g., LPS) from the intestinal barrier further may cause systemic immune cell activation and drives immune perturbations[32]. Interestingly, we observed a trend decrease in the *Firmicutes/Bacteroidetes* ratio in HIV+ subjects with high anti-CD4 IgG level compared to the other two groups, which is consistent with prior reports on the fecal microbiome in autoimmune disease such as systemic lupus erythematosus (SLE)[53,54].

Most microbiome studies used stool, saliva, or cervical-vaginal lavage fluid samples, very rare study was done on plasma microbiome due to highly technical demands[32,79–81]. A recent study reported that HIV-infected patients had different fecal microbial community composition compared to healthy controls[32]. Fecal microbiome from HIV-infected patients was enriched in *Enterobacteriales, Erysipelotrichaceae, Proteobacteria, Enterobacteriaceae, Gammaproteobacteria, Erysipelotrichi, Barnesiella*, and *Erysipelotrichales*, but was depleted in *Rikenellaceae* and *Alistipes*, relative to healthy controls[32]. Another study showed that HIV-infected patients with low peripheral CD4+ T cell counts exhibited reduced enteric bacterial diversity, which is consistent with our findings[79]. Both studies indicate that enrichment of *Enterobacteriaceae* was associated with systemic inflammation[32,79]. Consistently, plasma enrichment of *Proteobacteria, Gammaproteobacteria* and *Betaproteobacteria* was also observed in HIV+ individuals compared to healthy controls in the current study, but the difference did not achieve statistical significance (Fig. 2). However, we did not observe enrichment in other bacteria products

reported in the fecal microbiome study besides *Proteobacteria, Gammaproteobacteria* and *Betaproteobacteria* in plasma from HIV+ individuals relative to healthy controls[32]. Nonetheless, it is important to investigate microbiome simultaneously in plasma and mucosal sites in HIV in the future.

TLR4 signaling was increased with transgenic mice for a TLR chaperone molecule (gp96), which resulted in a lupus-like autoimmune glomerulonephritis[26]. Flares of autoimmune diseases have been observed with infection[82] in humans and also is an inducer of autoimmunity in mice. Decreased anti-dsDNA antibodies were observed in TLR2 and TLR4 knockout C57BL/6 (lpr/lpr) mice; and autoantibodies were induced by LPS stimulation through the TLR4-dependent cell signaling pathway in lupus-prone mice[83,84]. Therefore, increased bacterial product translocation may play a key role to induce autoantibodies in HIV. However, the association of plasma bacterial products (e.g., LPS) and anti-CD4 IgG level we observed in the current study does not prove causality. Next, we will give HIV-infected humanized animal models with specific bacterial products (e.g., LPS) found in plasma of the high HIV+ subjects to evaluate anti-CD4 autoantibody production. The other possibility of this association can be high anti-CD4 autoantibody-mediated immunodeficiency (poor CD4+ T cell recovery[22]) and increased inflammation favor particular bacterial survival. Furthermore, plasma soluble CD4 level was similar among the three study groups[22], suggesting that increased anti-CD4 IgG in some patients may not result from increased antigens in plasma. However, we do not know whether the level of CD4 antigen and HIV proteins (e.g., gp120[85]) with CD4 binding capacity is increased in lymph nodes, raising the question that increased anti-CD4 IgG may be due to increased antigens in the patients with high anti-CD4 IgG level.

Women in general have higher humoral and cellular immune responses relative to men, as well as higher prevalence of autoimmune diseases[86]. Mechanisms accounting for sex differences in autoimmune diseases include sex-induced breaks in tolerance and increases in peripheral cell activity, such as TLR responsiveness, T regulatory cells, environmental and genetic factors[87–90]. Consistently, we found that there were more women in the high HIV+ anti-CD4 autoantibody group compared to the low HIV+ anti-CD4 autoantibody group (Table 1). Whether anti-CD4 autoantibody induced by female sex hormones or sex hormone-mediated immune responses is worth further investigation.

This is the first study to date to report plasma microbiome and microbial products (e.g., LPS) in relation to autoantibodies in HIV patients. One of its limitations remains a small sample size. Due to the small sample size and large amount of microbial species observed in the plasma, most significant differences of microbiome among the study groups were not demonstrable after FDR correction. Another limitation is that other factors that may influence gut microbiota composition and bacterial translocation, such as diet, usage of probiotics and antibiotics, and the comorbidity of the patients were not controlled in the study. Therefore, the interpretation and generalization of findings may be limited. Future studies with large and diverse sample sizes are needed to lead a greater understanding of the concept of microbial translocation and auto-immune responses. In addition, the contributing factors for microbiome including sex should be considered.

In summary, we found that elevated plasma anti-CD4 IgG in HIV-infected subjects was associated with the magnitude of systemic microbial translocation and systemic microbiome. At the class level, *Gammaproteobateria, Betaproteobacteria, Bacilli* and *Alphaproteobacteria* were predominant in the low anti-CD4 IgG group. At the genus level, *Alicycliphilus*, and *Hylemonella* had elevated relative abundance in the high anti-CD4 IgG patient group compared to the low anti-CD4 IgG patient group. These results suggest that systemic microbial translocation and microbiome may play a role in anti-CD4 autoantibody production in HIV infection. However, the small sample size in the current study prevents us to draw further conclusions.

References

1. Keiser, O. *et al.* All cause mortality in the Swiss HIV Cohort Study from 1990 to 2001 in comparison with the Swiss population. *AIDS* **18**, 1835–1843 (2004).
2. Palella, F. J. Jr *et al.* Mortality in the highly active antiretroviral therapy era: changing causes of death and disease in the HIV outpatient study. *J Acquir Immune Defic Syndr* **43**, 27–34, https://doi.org/10.1097/01.qai.0000233310.90484.16 (2006).
3. Baker, J. V. *et al.* CD4+ count and risk of non-AIDS diseases following initial treatment for HIV infection. *Aids* **22**, 841–848, https://doi.org/10.1097/QAD.0b013e3282f7cb76 (2008).
4. Lewden, C. *et al.* HIV-infected adults with a CD4 cell count greater than 500 cells/mm3 on long-term combination antiretroviral therapy reach same mortality rates as the general population. *J Acquir Immune Defic Syndr* **46**, 72–77, https://doi.org/10.1097/QAI.0b013e318134257a (2007).
5. Lederman, M. M. *et al.* Immunologic failure despite suppressive antiretroviral therapy is related to activation and turnover of memory CD4 cells. *The Journal of infectious diseases* **204**, 1217–1226, https://doi.org/10.1093/infdis/jir507 (2011).
6. Kelley, C. F. *et al.* Incomplete peripheral CD4+ cell count restoration in HIV-infected patients receiving long-term antiretroviral treatment. *Clinical infectious diseases: an official publication of the Infectious Diseases Society of America* **48**, 787–794, https://doi.org/10.1086/597093 (2009).
7. Gutierrez, F. *et al.* Patients' characteristics and clinical implications of suboptimal CD4 T-cell gains after 1 year of successful antiretroviral therapy. *Current HIV research* **6**, 100–107 (2008).
8. Moore, R. D. & Keruly, J. C. CD4+ cell count 6 years after commencement of highly active antiretroviral therapy in persons with sustained virologic suppression. *Clinical infectious diseases: an official publication of the Infectious Diseases Society of America* **44**, 441–446, https://doi.org/10.1086/510746 (2007).
9. Tuboi, S. H. *et al.* Discordant responses to potent antiretroviral treatment in previously naive HIV-1-infected adults initiating treatment in resource-constrained countries: the antiretroviral therapy in low-income countries (ART-LINC) collaboration. *J Acquir Immune Defic Syndr* **45**, 52–59, https://doi.org/10.1097/QAI.0b013e318042e1c3 (2007).
10. Hunt, P. W. *et al.* T cell activation is associated with lower CD4+ T cell gains in human immunodeficiency virus-infected patients with sustained viral suppression during antiretroviral therapy. *The Journal of infectious diseases* **187**, 1534–1543, https://doi.org/10.1086/374786 (2003).
11. Fernandez, S., Price, P., McKinnon, E. J., Nolan, R. C. & French, M. A. Low CD4+ T-cell counts in HIV patients receiving effective antiretroviral therapy are associated with CD4+ T-cell activation and senescence but not with lower effector memory T-cell function. *Clinical immunology* **120**, 163–170, https://doi.org/10.1016/j.clim.2006.04.570 (2006).

12. Benveniste, O. *et al*. Mechanisms involved in the low-level regeneration of CD4+ cells in HIV-1-infected patients receiving highly active antiretroviral therapy who have prolonged undetectable plasma viral loads. *J Infect Dis* **191**, 1670–1679, https://doi.org/10.1086/429670 (2005).
13. Marchetti, G. *et al*. Comparative analysis of T-cell turnover and homeostatic parameters in HIV-infected patients with discordant immune-virological responses to HAART. *Aids* **20**, 1727–1736, https://doi.org/10.1097/01.aids.0000242819.72839.db (2006).
14. Marchetti, G. *et al*. Microbial translocation is associated with sustained failure in CD4+ T-cell reconstitution in HIV-infected patients on long-term highly active antiretroviral therapy. *Aids* **22**, 2035–2038, https://doi.org/10.1097/QAD.0b013e3283112d29 (2008).
15. Rajasuriar, R. *et al*. Biological determinants of immune reconstitution in HIV-infected patients receiving antiretroviral therapy: the role of interleukin 7 and interleukin 7 receptor alpha and microbial translocation. *J Infect Dis* **202**, 1254–1264, https://doi.org/10.1086/656369 (2010).
16. Gandhi, R. T. *et al*. Effect of baseline- and treatment-related factors on immunologic recovery after initiation of antiretroviral therapy in HIV-1-positive subjects: results from ACTG 384. *J Acquir Immune Defic Syndr* **42**, 426–434, https://doi.org/10.1097/01.qai.0000226789.51992.3f (2006).
17. Anthony, K. B. *et al*. Incomplete CD4 T cell recovery in HIV-1 infection after 12 months of highly active antiretroviral therapy is associated with ongoing increased CD4 T cell activation and turnover. *J Acquir Immune Defic Syndr* **33**, 125–133 (2003).
18. Valdez, H. *et al*. Limited immune restoration after 3 years' suppression of HIV-1 replication in patients with moderately advanced disease. *AIDS* **16**, 1859–1866 (2002).
19. Negredo, E. *et al*. Nadir CD4 T cell count as predictor and high CD4 T cell intrinsic apoptosis as final mechanism of poor CD4 T cell recovery in virologically suppressed HIV-infected patients: clinical implications. *Clinical infectious diseases: an official publication of the Infectious Diseases Society of America* **50**, 1300–1308, https://doi.org/10.1086/651689 (2010).
20. Teixeira, L. *et al*. Poor CD4 T cell restoration after suppression of HIV-1 replication may reflect lower thymic function. *Aids* **15**, 1749–1756 (2001).
21. Molina-Pinelo, S. *et al*. Premature immunosenescence in HIV-infected patients on highly active antiretroviral therapy with low-level CD4 T cell repopulation. *J Antimicrob Chemother* **64**, 579–588, https://doi.org/10.1093/jac/dkp248 (2009).
22. Luo Z. W. *et al*. Pathological role of anti-CD4 antibodies in HIV-infected immunologic non-responders under viral suppressive antiretroviral therapy. *Journal of Infectious Diseases* Epub ahead of print, https://doi.org/10.1093/infdis/jix223 (2017).
23. Luo, Z. *et al*. Increased Natural Killer Cell Activation in HIV-Infected Immunologic Non-Responders Correlates with CD4+ T Cell Recovery after Antiretroviral Therapy and Viral Suppression. *PLoS One* **12**, e0167640, https://doi.org/10.1371/journal.pone.0167640 (2017).
24. Titanji, K. *et al*. Loss of memory B cells impairs maintenance of long-term serologic memory during HIV-1 infection. *Blood* **108**, 1580–1587 (2006).
25. De Milito, A., Morch, C., Sonnerborg, A. & Chiodi, F. Loss of memory (CD27) B lymphocytes in HIV-1 infection. *AIDS (London, England)* **15**, 957–964 (2001).
26. De Milito, A. *et al*. Mechanisms of hypergammaglobulinemia and impaired antigen-specific humoral immunity in HIV-1 infection. *Blood* **103**, 2180–2186 (2004).
27. Titanji, K. *et al*. Primary HIV-1 infection sets the stage for important B lymphocyte dysfunctions. *AIDS (London, England)* **19**, 1947–1955 (2005).
28. Guan, Y. *et al*. Discordant memory B cell and circulating anti-Env antibody responses in HIV-1 infection. *Proceedings of the National Academy of Sciences of the United States of America* **106**, 3952–3957 (2009).
29. Malaspina, A. *et al*. Deleterious effect of HIV-1 plasma viremia on B cell costimulatory function. *J Immunol* **170**, 5965–5972 (2003).
30. Jiang, W. *et al*. Impaired naive and memory B-cell responsiveness to TLR9 stimulation in human immunodeficiency virus infection. *J Virol* **82**, 7837–7845, https://doi.org/10.1128/JVI.00660-08 (2008).
31. Luo, Z. *et al*. Key differences in B cell activation patterns and immune correlates among treated HIV-infected patients versus healthy controls following influenza vaccination. *Vaccine* **34**, 1945–1955, https://doi.org/10.1016/j.vaccine.2015.12.038 (2016).
32. Dinh, D. M. *et al*. Intestinal microbiota, microbial translocation, and systemic inflammation in chronic HIV infection. *J Infect Dis* **211**, 19–27, https://doi.org/10.1093/infdis/jiu409 (2015).
33. Mutlu, E. A. *et al*. A compositional look at the human gastrointestinal microbiome and immune activation parameters in HIV infected subjects. *PLoS Pathog* **10**, e1003829, https://doi.org/10.1371/journal.ppat.1003829 (2014).
34. Nowak, P. *et al*. Gut microbiota diversity predicts immune status in HIV-1 infection. *AIDS* **29**, 2409–2418, https://doi.org/10.1097/QAD.0000000000000869 (2015).
35. Villanueva-Millan, M. J., Perez-Matute, P., Recio-Fernandez, E., Lezana Rosales, J. M. & Oteo, J. A. Differential effects of antiretrovirals on microbial translocation and gut microbiota composition of HIV-infected patients. *J Int AIDS Soc* **20**, 21526, https://doi.org/10.7448/IAS.20.1.21526 (2017).
36. Umiker, B. R. *et al*. Dosage of X-linked Toll-like receptor 8 determines gender differences in the development of systemic lupus erythematosus. *European journal of immunology* **44**, 1503–1516, https://doi.org/10.1002/eji.201344283 (2014).
37. Wong, C. K. *et al*. Activation profile of Toll-like receptors of peripheral blood lymphocytes in patients with systemic lupus erythematosus. *Clin Exp Immunol* **159**, 11–22, https://doi.org/10.1111/j.1365-2249.2009.04036.x (2010).
38. Thibault, D. L. *et al*. IRF9 and STAT1 are required for IgG autoantibody production and B cell expression of TLR7 in mice. *The Journal of clinical investigation* **118**, 1417–1426, https://doi.org/10.1172/JCI30065 (2008).
39. Brenchley, J. M. *et al*. Microbial translocation is a cause of systemic immune activation in chronic HIV infection. *Nature medicine* **12**, 1365–1371 (2006).
40. Nagase, H. *et al*. Mechanism of hypergammaglobulinemia by HIV infection: circulating memory B-cell reduction with plasmacytosis. *Clinical immunology Orlando, Fla* **100**, 250–259 (2001).
41. Jiang, W. *et al*. Plasma levels of bacterial DNA correlate with immune activation and the magnitude of immune restoration in persons with antiretroviral-treated HIV infection. *J Infect Dis* **199**, 1177–1185, https://doi.org/10.1086/597476 (2009).
42. Jiang, W. *et al*. Cycling memory CD4+ T cells in HIV disease have a diverse T cell receptor repertoire and a phenotype consistent with bystander activation. *J Virol* **88**, 5369–5380, https://doi.org/10.1128/JVI.00017-14 (2014).
43. Zhang, L. *et al*. Plasmacytoid dendritic cells mediate synergistic effects of HIV and lipopolysaccharide on CD27+ IgD- memory B cell apoptosis. *Journal of virology* **88**, 11430–11441, https://doi.org/10.1128/JVI.00682-14 (2014).
44. Dowd, S. E. *et al*. Evaluation of the bacterial diversity in the feces of cattle using 16S rDNA bacterial tag-encoded FLX amplicon pyrosequencing (bTEFAP). *BMC Microbiol* **8**, 125, https://doi.org/10.1186/1471-2180-8-125 (2008).
45. Dowd, S. E., Sun, Y., Wolcott, R. D., Domingo, A. & Carroll, J. A. Bacterial tag-encoded FLX amplicon pyrosequencing (bTEFAP) for microbiome studies: bacterial diversity in the ileum of newly weaned Salmonella-infected pigs. *Foodborne Pathog Dis* **5**, 459–472, https://doi.org/10.1089/fpd.2008.0107 (2008).
46. Capone, K. A., Dowd, S. E., Stamatas, G. N. & Nikolovski, J. Diversity of the human skin microbiome early in life. *J Invest Dermatol* **131**, 2026–2032, https://doi.org/10.1038/jid.2011.168 (2011).
47. Eren, A. M. *et al*. Exploring the diversity of Gardnerella vaginalis in the genitourinary tract microbiota of monogamous couples through subtle nucleotide variation. *PLoS One* **6**, e26732, https://doi.org/10.1371/journal.pone.0026732 (2011).
48. Swanson, K. S. *et al*. Phylogenetic and gene-centric metagenomics of the canine intestinal microbiome reveals similarities with humans and mice. *ISME J* **5**, 639–649, https://doi.org/10.1038/ismej.2010.162 (2011).
49. DeSantis, T. Z. *et al*. Greengenes, a chimera-checked 16S rRNA gene database and workbench compatible with ARB. *Appl Environ Microbiol* **72**, 5069–5072, https://doi.org/10.1128/AEM.03006-05 (2006).

50. Rothman, K. J. No adjustments are needed for multiple comparisons. *Epidemiology* **1**, 43–46 (1990).
51. Team, R. C. *R: A language and environment for statistical computing. R Foundation for Statistical Computing* (2016).
52. Jari Oksanen, F. G. B. *et al*. Eduard Szoecs and Helene Wagner vegan: Community Ecology Package. *R package version* 2.4–1. doi:CRAN.R-project.org/package=vegan (2016).
53. Hevia, A. *et al*. Intestinal Dysbiosis Associated with Systemic Lupus Erythematosus. *mBio* **5**, 14, https://doi.org/10.1128/mbio.01548-14 (2014).
54. He, Z., Shao, T., Li, H., Xie, Z. & Wen, C. Alterations of the gut microbiome in Chinese patients with systemic lupus erythematosus. *Gut pathogens* **8**, 64, https://doi.org/10.1186/s13099-016-0146-9 (2016).
55. Sheikh, V. *et al*. Graves' disease as immune reconstitution disease in HIV-positive patients is associated with naive and primary thymic emigrant CD4(+) T-cell recovery. *AIDS* **28**, 31–39, https://doi.org/10.1097/QAD.0000000000000006 (2014).
56. Shah, I. Immune thrombocytopenic purpura: a presentation of HIV infection. *Journal of the International Association of Providers of AIDS Care* **12**, 95–97, https://doi.org/10.1177/1545109712462068 (2013).
57. Visser, R., de Mast, Q., Netea-Maier, R. T. & van der Ven, A. J. Hashimoto's thyroiditis presenting as acute painful thyroiditis and as a manifestation of an immune reconstitution inflammatory syndrome in a human immunodeficiency virus-seropositive patient. *Thyroid: official journal of the American Thyroid Association* **22**, 853–855, https://doi.org/10.1089/thy.2012.0055 (2012).
58. Bonsignori, M. *et al*. An autoreactive antibody from an SLE/HIV-1 individual broadly neutralizes HIV-1. *The Journal of clinical investigation* **124**, 1835–1843, https://doi.org/10.1172/JCI73441 (2014).
59. Levesque, M. C. *et al*. Polyclonal B cell differentiation and loss of gastrointestinal tract germinal centers in the earliest stages of HIV-1 infection. *PLoS medicine* **6**, e1000107, https://doi.org/10.1371/journal.pmed.1000107 (2009).
60. Kuwata, T. *et al*. Association of progressive CD4(+) T cell decline in SIV infection with the induction of autoreactive antibodies. *PLoS pathogens* **5**, e1000372, https://doi.org/10.1371/journal.ppat.1000372 (2009).
61. Stahl, D. *et al*. Alterations of self-reactive antibody repertoires in HIV disease: an insight into the role of T cells in the selection of autoreactive B cells. *Immunol Lett* **99**, 198–208, https://doi.org/10.1016/j.imlet.2005.02.018 (2005).
62. Rodriguez-Mahou, M. *et al*. Autoimmune phenomena in children with human immunodeficiency virus infection and acquired immunodeficiency syndrome. *Acta paediatrica* **400**, 31–34 (1994).
63. Nilssen, D. E., Oktedalen, O. & Brandtzaeg, P. Intestinal B cell hyperactivity in AIDS is controlled by highly active antiretroviral therapy. *Gut* **53**, 487–493 (2004).
64. Lartigue, A. *et al*. Critical role of TLR2 and TLR4 in autoantibody production and glomerulonephritis in lpr mutation-induced mouse lupus. *Journal of immunology* **183**, 6207–6216, https://doi.org/10.4049/jimmunol.0803219 (2009).
65. Simchoni, N. & Cunningham-Rundles, C. TLR7- and TLR9-Responsive Human B Cells Share Phenotypic and Genetic Characteristics. *J Immunol* **194**, 3035–3044, https://doi.org/10.4049/jimmunol.1402690 (2015).
66. du Toit, R., Whitelaw, D., Taljaard, J. J., du Plessis, L. & Esser, M. Lack of specificity of anticyclic citrullinated peptide antibodies in advanced human immunodeficiency virus infection. *J Rheumatol* **38**, 1055–1060, https://doi.org/10.3899/jrheum.100713 (2011).
67. Fust, G. *et al*. Antibodies against heat shock proteins and cholesterol in HIV infection. *Mol Immunol* **42**, 79–85, https://doi.org/10.1016/j.molimm.2004.07.003 (2005).
68. Pereda, I. *et al*. Antitissue transglutaminase antibodies in HIV infection and effect of highly active antiretroviral therapy. *J Acquir Immune Defic Syndr* **27**, 507–508 (2001).
69. Horvath, A. *et al*. High level of anticholesterol antibodies (ACHA) in HIV patients. Normalization of serum ACHA concentration after introduction of HAART. *Immunobiology* **203**, 756–768, https://doi.org/10.1016/S0171-2985(01)80004-8 (2001).
70. Kolhatkar, N. S. *et al*. Altered BCR and TLR signals promote enhanced positive selection of autoreactive transitional B cells in Wiskott-Aldrich syndrome. *J Exp Med* **212**, 1663–1677, https://doi.org/10.1084/jem.20150585 (2015).
71. Zandman-Goddard, G. & Shoenfeld, Y. HIV and autoimmunity. *Autoimmun Rev* **1**, 329–337 (2002).
72. Iordache, L. *et al*. Autoimmune diseases in HIV-infected patients: 52 cases and literature review. *Autoimmun Rev* **13**, 850–857, https://doi.org/10.1016/j.autrev.2014.04.005 (2014).
73. Paisse, S. *et al*. Comprehensive description of blood microbiome from healthy donors assessed by 16S targeted metagenomic sequencing. *Transfusion* **56**, 1138–1147, https://doi.org/10.1111/trf.13477 (2016).
74. Barlow, G. M., Yu, A. & Mathur, R. Role of the Gut Microbiome in Obesity and Diabetes Mellitus. *Nutr Clin Pract* **30**, 787–797, https://doi.org/10.1177/0884533615609896 (2015).
75. Mathur, R. & Barlow, G. M. Obesity and the microbiome. *Expert Rev Gastroenterol Hepatol* **9**, 1087–1099, https://doi.org/10.1586/17474124.2015.1051029 (2015).
76. Chiriac, M. T., Mahapatro, M., Neurath, M. F. & Becker, C. The Microbiome in Visceral Medicine: Inflammatory Bowel Disease, Obesity and Beyond. *Visc Med* **33**, 153–162, https://doi.org/10.1159/000470892 (2017).
77. Bischoff, S. C. [The intestinal microbiome and metabolic diseases: From obesity to diabetes and nonalcoholic steatohepatitis]. *Internist (Berl)* **58**, 441–448, https://doi.org/10.1007/s00108-017-0229-9 (2017).
78. Bouter, K. E., van Raalte, D. H., Groen, A. K. & Nieuwdorp, M. Role of the Gut Microbiome in the Pathogenesis of Obesity and Obesity-Related Metabolic Dysfunction. *Gastroenterology* **152**, 1671–1678, https://doi.org/10.1053/j.gastro.2016.12.048 (2017).
79. Monaco, C. L. *et al*. Altered Virome and Bacterial Microbiome in Human Immunodeficiency Virus-Associated Acquired Immunodeficiency Syndrome. *Cell host & microbe* **19**, 311–322, https://doi.org/10.1016/j.chom.2016.02.011 (2016).
80. Lelouvier, B. *et al*. Changes in blood microbiota profiles associated with liver fibrosis in obese patients: A pilot analysis. *Hepatology* **64**, 2015–2027, https://doi.org/10.1002/hep.28829 (2016).
81. Ericsen, A. J. *et al*. Microbial Translocation and Inflammation Occur in Hyperacute Immunodeficiency Virus Infection and Compromise Host Control of Virus Replication. *PLoS Pathog* **12**, e1006048, https://doi.org/10.1371/journal.ppat.1006048 (2016).
82. Segal, Y., Calabro, M., Kanduc, D. & Shoenfeld, Y. Human papilloma virus and lupus: the virus, the vaccine and the disease. *Current opinion in rheumatology* **29**, 331–342, https://doi.org/10.1097/BOR.0000000000000398 (2017).
83. Qing, X. *et al*. Pathogenic anti-DNA antibodies modulate gene expression in mesangial cells: involvement of HMGB1 in anti-DNA antibody-induced renal injury. *Immunol Lett* **121**, 61–73, https://doi.org/10.1016/j.imlet.2008.08.007 (2008).
84. Zhai, J. X. *et al*. PDTC attenuate LPS-induced kidney injury in systemic lupus erythematosus-prone MRL/lpr mice. *Mol Biol Rep* **39**, 6763–6771, https://doi.org/10.1007/s11033-012-1501-7 (2012).
85. Zhang, Y. *et al*. The glycan-mediated mechanism on the interactions of gp120 with CD4 and antibody: Insights from molecular dynamics simulation. *Chem Biol Drug Des*, https://doi.org/10.1111/cbdd.13045 (2017).
86. Alpizar-Rodriguez, D., Pluchino, N., Canny, G., Gabay, C. & Finckh, A. The role of female hormonal factors in the development of rheumatoid arthritis. *Rheumatology (Oxford)* **56**, 1254–1263, https://doi.org/10.1093/rheumatology/kew318 (2017).
87. Afshan, G., Afzal, N. & Qureshi, S. CD4+ CD25(hi) regulatory T cells in healthy males and females mediate gender difference in the prevalence of autoimmune diseases. *Clinical laboratory* **58**, 567–571 (2012).
88. Pisitkun, P. *et al*. Autoreactive B cell responses to RNA-related antigens due to TLR7 gene duplication. *Science* **312**, 1669–1672, https://doi.org/10.1126/science.1124978 (2006).
89. Rullo, O. J. & Tsao, B. P. Recent insights into the genetic basis of systemic lupus erythematosus. *Annals of the rheumatic diseases* **72**(Suppl 2), ii56–61, https://doi.org/10.1136/annrheumdis-2012-202351 (2013).
90. Brusca, S. B., Abramson, S. B. & Scher, J. U. Microbiome and mucosal inflammation as extra-articular triggers for rheumatoid arthritis and autoimmunity. *Current opinion in rheumatology* **26**, 101–107, https://doi.org/10.1097/BOR.0000000000000008 (2014).

Acknowledgements

This work was supported by the National Institutes of Health grants AI091526 (Jiang), AI128864 (Jiang), K23NR014674 (Cong), R01NR016928 (Cong), AI093307 (Ling), R01LM012517 (Alekseyenko), R01CA164964, R01CA164964, U54CA210962, P50AR070591, a DOD Career Development Award CA140437 (Qin), a Louisiana Clinical and Translational Science Center Pilot grant U54GM104940, and P30 AI027767 (Saag/Health). We thank NIH AIDS Reagent Program, Division of AIDS, NIAID, NIH: Human Soluble CD4 Recombinant Protein (sCD4) from Progenics. Human monoclonal anti-CD4 antibody Zanolimumab (HuMax-CD4) was kindly provided by Dr. Paul Parren from Genmab.

Author Contributions

W.X. Wrote the first version of manuscript and analyzed the microbiome data. Z.L. Performed experiments. A.A. Analyzed the microbiome data and assisted statistical analysis. L.M.: Recruited donors and helped study design. Z.W. Statistic data analysis. B.L. Designed the study and revised manuscript. Z.Q. Designed the study and revised manuscript. S.H. Designed the study and revised manuscript. K.M. Analyzed the microbiome data and designed the study. X.C. Analyzed the microbiome data, revised manuscript and designed the study. W.J. Designed the study and revised manuscript.

Additional Information

Supplementary information accompanies this paper at https://doi.org/10.1038/s41598-018-31116-y.

Competing Interests: The authors declare no competing interests.

Publisher's note: Springer Nature remains neutral with regard to jurisdictional claims in published maps and institutional affiliations.

Oncogene
https://doi.org/10.1038/s41388-018-0282-4

ARTICLE

Transactivation of human endogenous retrovirus K (HERV-K) by KSHV promotes Kaposi's sarcoma development

Lu Dai[1,2] · Luis Del Valle[3] · Wendell Miley[4] · Denise Whitby[4] · Augusto C. Ochoa[5] · Erik K. Flemington[6] · Zhiqiang Qin[1,2]

Received: 2 February 2018 / Revised: 23 March 2018 / Accepted: 2 April 2018

Abstract

Kaposi's sarcoma-associated herpesvirus (KSHV) is the causative agent of several human cancers such as Kaposi's sarcoma (KS), which represents the most common AIDS-associated malignancy that lacks effective treatment options. Despite its clear role in AIDS malignancies, the fact that only a small set of KSHV-infected patients will eventually develop these tumors implies that additional co-factors are required for the development of KSHV-related cancers. In the current study, we demonstrate for the first time that KSHV de novo infection or viral latent proteins are able to transactivate human endogenous retrovirus K (HERV-K) through a variety of cellular signaling pathways and transcriptional factors. Moreover, we found that HERV-K transactivation, particularly activation of its encoded oncogenic NP9 protein, plays an important role in KSHV pathogenesis and tumorigenesis in vitro and in vivo. Our data provide innovative insights into the mechanisms of HERV-K transactivation contributing to viral oncogenesis, which may represent a promising target for KS treatment.

Introduction

Approximately 20% of human cancers have been found related to viral infections, including Kaposi's sarcoma-associated herpesvirus (KSHV, also named as human herpesvirus 8) [1]. KSHV is the causative agent of several cancers arising in patients with compromised immune systems, including Kaposi's sarcoma (KS) and primary effusion lymphoma (PEL) [2, 3]. Despite the reduced incidence of KS since the invention of highly active antiretroviral therapy (HAART) for human immunodeficiency virus (HIV), KS remains the most common acquired immunodeficiency syndrome (AIDS)-associated tumor [4, 5]. The prevalence of KSHV in the United States (US) HIV-infected population remains high and incidence of new infections has increased in the HAART era [6]. A longitudinal study of solid organ transplant recipients in the US reported 15% of KSHV seropositivity in this specific subpopulation [7]. Transplant recipients who develop primary KSHV infection after the transplantation will have a relatively high probability of developing these KSHV-related malignancies, especially KS [8, 9]. Since its discovery about 25 years ago, KSHV has now become a model pathogen for viral oncogenesis research, but many key questions regarding its mechanisms of pathogenesis and oncogenesis still remain unclear, hindering the identification

Electronic supplementary material The online version of this article (https://doi.org/10.1038/s41388-018-0282-4) contains supplementary material, which is available to authorized users.

✉ Zhiqiang Qin
zqin@lsuhsc.edu

1 Department of Genetics, Louisiana State University Health Sciences Center, Louisiana Cancer Research Center, 1700 Tulane Avenue, New Orleans, LA 70112, USA

2 Department of Pediatrics, Research Center for Translational Medicine and Key Laboratory of Arrhythmias, East Hospital, Tongji University School of Medicine, 200120 Shanghai, China

3 Department of Pathology, Louisiana State University Health Sciences Center, Louisiana Cancer Research Center, 1700 Tulane Avenue, New Orleans, LA 70112, USA

4 Viral Oncology Section, AIDS and Cancer Virus Program, Leidos Biomedical Research, Frederick National Laboratory for Cancer Research, PO Box B, Frederick, MD 21702, USA

5 Department of Pediatrics, Louisiana State University Health Sciences Center, Louisiana Cancer Research Center, 1700 Tulane Avenue, New Orleans, LA 70112, USA

6 Department of Pathology, Tulane University Health Sciences Center, Tulane Cancer Center, 1700 Tulane Avenue, New Orleans, LA 70112, USA

Published online: 10 May 2018

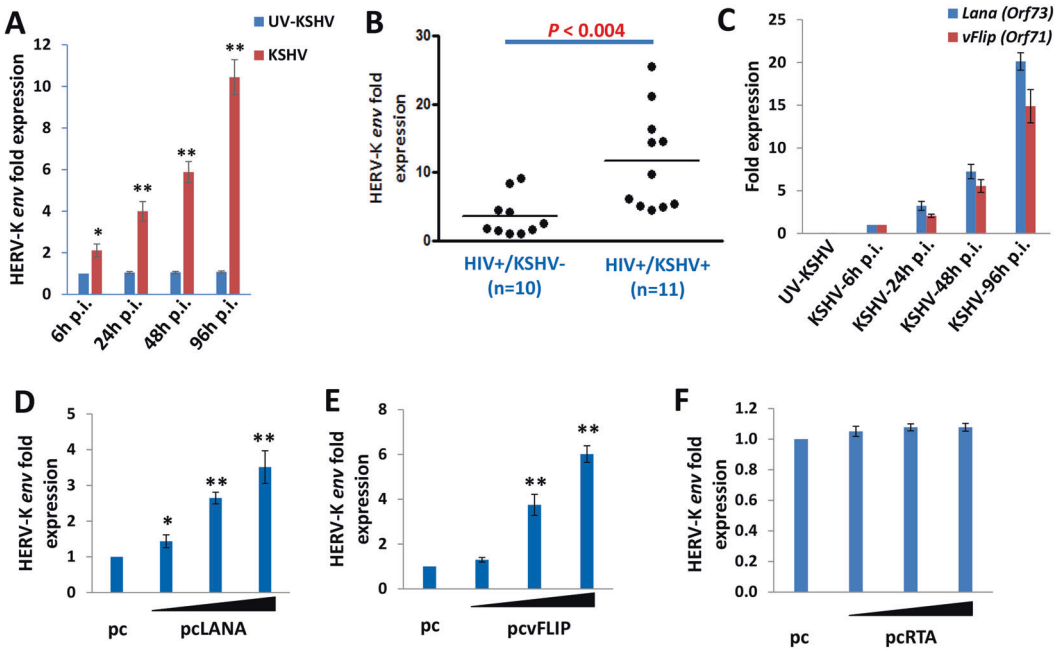

Fig. 1 KSHV de novo infection or viral latent proteins transactivate HERV-K in vitro and in vivo. **a** Human umbilical vein endothelial cells (HUVEC) were infected with purified KSHV (MOI ~ 10) or UV-inactivated KSHV for 2 h, then the induction of HERV-K reactivation at the indicated time points postinfection (p.i.) was measured and compared to UV-inactivated KSHV-infected cells control by qRT-PCR with the specific primers for HERV-K *env* gene. **b** The levels of HERV-K transactivation within peripheral blood mononuclear cells (PBMCs) from HIV+ patients with or without KSHV co-infection were quantified using qRT-PCR. KSHV infection status was identified using ELISA as described in Methods. **c** HUVEC were infected by purified KSHV as described above, then the transcripts of viral latent genes *Lana* (*Orf73*) and *vFlip* (*Orf71*) at the indicated time points p.i. were measured and compared to control mock cells by using qRT-PCR. **d**–**f** HUVEC were transfected with control vector (pc) or vectors encoding LANA (pcLANA), vFLIP (pcvFLIP), or RTA (pcRTA) at 0.2, 1.0, or 2.5 μg, respectively, for 48 h, then the induction of HERV-K transactivation was quantified by using qRT-PCR. Error bars represent the S.D. from three independent experiments. $*p < 0.05$, $**p < 0.01$

of rational targets or the development of effective therapeutic strategies against these malignancies. Although KSHV has been closely linked to several human malignancies, only a small portion of KSHV-infected patients will eventually develop these tumors [1], implying that additional host or environmental co-factors such as co-infecting pathogens are required for the development of KSHV-related malignancies.

Human endogenous retrovirus (HERV) sequences occupy ~6–8% of the human genome and have resided in our genome for several million years [10, 11]. Owing to the accumulation of multiple nonsense mutations, the majority of HERVs are dysfunctional; however, some are still active and may play a role in human disease, in particular the HERV type K (HML-2) family [12–14]. HERV-K transactivation has been observed in a variety of human cancers, such as leukemia [15], lymphoma [16], breast cancer [17, 18], and melanoma [19]. For instance, the expression of the HERV-K envelope (*env*) protein in malignant breast cancer cell lines have been found higher than in non-malignant breast cells, and some anti-HERV-K-specific monoclonal antibodies effectively inhibited breast cancer cells' growth and induced their apoptosis of in vitro and in vivo [17]. Interestingly, several herpesviruses have been reported to induce HERV-K transactivation. For instance, HERV-K18 can be transactivated as a superantigen (SAg) by Epstein–Barr virus (EBV) infection and subsequently activates TCRVB13 T cells through major histocompatibility complex-II, which plays a central role in EBV infection and pathogenesis [20–22]. However, currently there are no data describing the role of HERV-K transactivation in viral oncogenesis, especially KSHV-related malignancies. In the current study, we demonstrate for the first time that KSHV de novo infection or viral latent proteins are able to transactivate HERV-K through a complex of mechanisms. Moreover, HERV-K transactivation (in particular activation of its oncogenic NP9 protein) are required for KSHV pathogenesis and tumorigenesis in vitro and in vivo.

Results

KSHV de novo infection or encoded latent proteins transactivate HERV-K in vitro and in vivo

During an infection time course analysis, we found that KSHV de novo infection gradually increased HERV-K

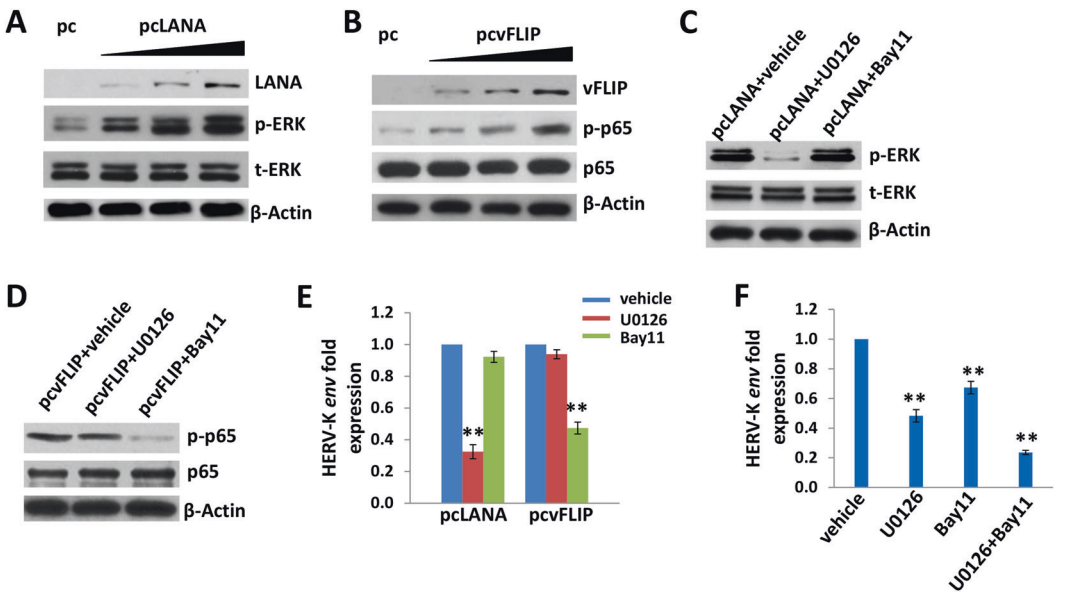

Fig. 2 Activation of intracellular signaling pathways is involved in HERV-K transactivation by KSHV. **a**, **b** HUVEC were transfected with control vector (pc) or vectors encoding LANA (pcLANA) or vFLIP (pcvFLIP) at 0.2, 1.0, or 2.5 μg, respectively, for 48 h, then the protein expression was analyzed by using immunoblots. **c–f** HUVEC were first incubated with either vehicle or MEK inhibitor (10 μM of U0126) or NF-κB inhibitor (10 μM of Bay11–7082) for 1 h, then transfected or infected as described above. The induction of HERV-K transactivation was quantified by using qRT-PCR and the protein expression was detected by immunoblots. Error bars represent the S.D. from three independent experiments. $^{**}p < 0.01$

envelope gene (*env*) transcripts from primary human umbilical vein endothelial cells (HUVEC) when compared to the ultraviolet (UV)-inactivated KSHV-infected cells by using quantitative reverse transcription polymerase chain reaction (qRT-PCR; Fig. 1a). Currently, the qRT-PCR-based detection of HERV-K *env* transcripts is the most common and reliable method to evaluate the level of HERV-K transactivation in host cells [15–17]. Our qRT-PCR primers were designed to measure the total levels of HERV-K *env* transcripts, including type 1 and 2 proviruses. Interestingly, our data indicate that KSHV+PEL tumor cell lines (BC-1, BC-3, BCP-1. and BCBL-1) also have significantly higher levels of HERV-K *env* transcripts when compared with the virus-negative lymphoma cell line, BL-41 (Fig. S1). To understand the clinical relevance of HERV-K transactivation in KSHV-infected HIV+ patients, we examined the levels of HERV-K *env* transcripts in peripheral blood mononuclear cell (PBMC) samples collected from a cohort of HIV+ patients prior to undergoing the HAART. KSHV infection status have been determined by measuring the titers of anti-KSHV-encoded LANA and K8.1 circulating immunoglobulin G as described previously [23, 24]. Our results indicated a higher level of HERV-K *env* transcripts in the KSHV+ group ($n = 11$) than those in the KSHV− group ($n = 10$, Fig. 1b). Since there are no significant differences in HIV viral loads and CD4 counts between these two groups (data not shown), we think that KSHV infection may be responsible for the HERV-K transactivation in these patients.

KSHV has two infection phases: a latent phase with only a limited number of viral genes expressed and a lytic phase in which most viral genes are expressed that ultimately produces infectious virions [25]. In most KSHV-infected host cells (>90%), the virus exists in the latency stage [26], suggesting that some virus-encoded latent proteins are potentially responsible for HERV-K transactivation. We detected the expression of two major KSHV-encoded latent genes, Latency-associated nuclear antigen (*Lana*, *Orf73*) [27] and viral FADD-like interferon converting enzyme inhibitory protein (*vFlip*, *Orf71*) [28] during KSHV de novo infection. Notably, we found that the expression of these two latent genes displayed an increase in expression that was relatively concordant with HERV-K *env* expression during the time course of KSHV infection (Fig. 1c). To further determine whether these latent genes are indeed responsible for KSHV-induced HERV-K transactivation, we transfected HUVEC with a recombinant LANA or vFLIP construct [29, 30], respectively. We found that ectopic expression of LANA or vFLIP significantly increased HERV-K *env* transcripts from HUVEC in a dose-dependent manner (Fig. 1d, e). As a comparison, we found that the ectopic expression of RTA, a viral lytic protein that initially controls KSHV "latent to lytic" switch [31], almost does not induce HERV-K *env* expression (Fig. 1f).

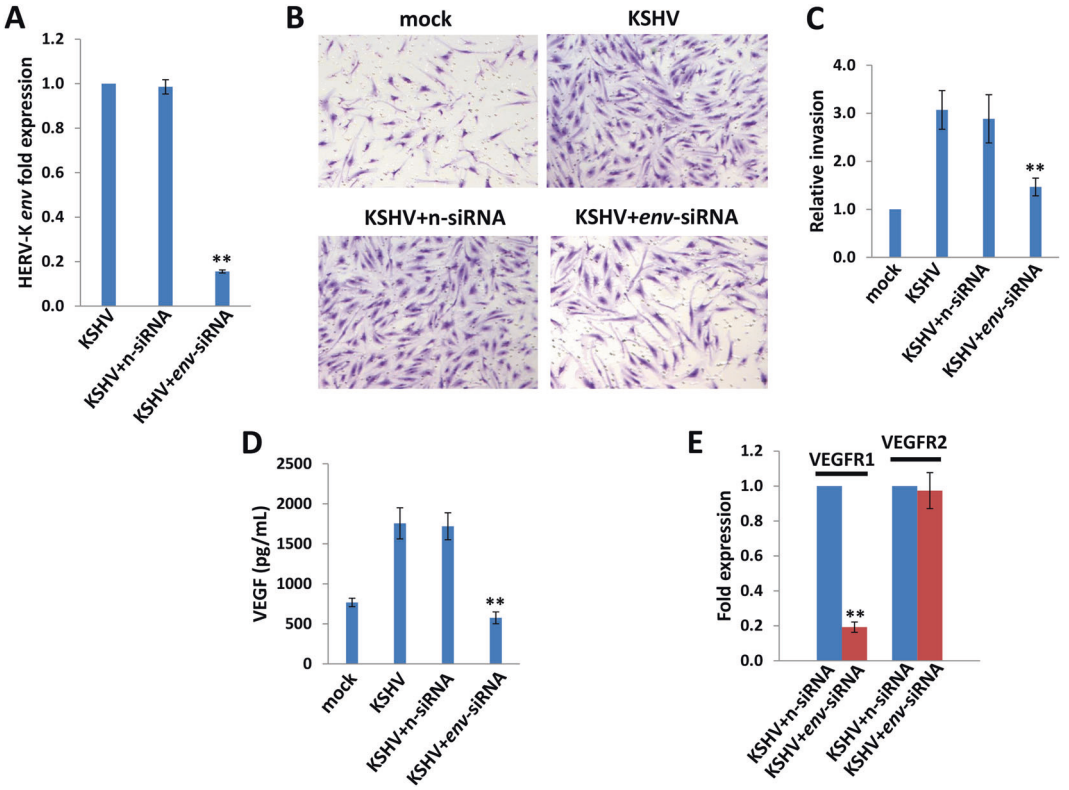

Fig. 3 Targeting HERV-K transactivation significantly reduces KSHV-induced primary endothelial cell invasiveness. **a**–**c** HUVEC cells were incubated with purified KSHV (MOI ~ 10) for 2 h, then transfected with non-target control siRNA (n-siRNA) or HERV-K *env* siRNA for additional 48 h. The transwell assays were performed to determine relative invasiveness as described in Methods. **d** The concentrations of VEGF in culture supernatants were determined using ELISA. **e** The gene transcripts were quantified by using qRT-PCR. Error bars represent the S.D. from three independent experiments. $^{**}p < 0.01$

Identification of cellular mechanisms for KSHV latent protein induction of HERV-K expression

We next sought to understand the underlying mechanisms for LANA- or vFLIP-induced HERV-K transactivation in primary endothelial cells. We and others have reported that KSHV latent proteins are capable of activating several intracellular signaling pathways, e.g., LANA can activate the mitogen-activated protein kinase (MAPK) pathway [32] and vFLIP can activate the nuclear factor (NF)-κB pathway [28]. Our data here confirmed that ectopic expression of LANA or vFLIP induced the phosphorylation of MAPK-ERK (extracellular signal–regulated kinase) or NF-κB p65, respectively, from transfected HUVEC (Fig. 2a, b). Next, we found that only inhibition of MAPK by U0126 effectively reduced HERV-K *env* transcripts from LANA-transfected cells, while inhibition of NF-κB by Bay11–7082 had no effects (Fig. 2c, e). In contrast, only inhibition of NF-κB but not of MAPK effectively reduced HERV-K *env* transcripts from vFLIP-transfected cells (Fig. 2d, e). Furthermore, inhibition of either MAPK or NF-κB can partially reduce HERV-K *env* transcripts from KSHV-infected cells, and dual inhibition of these pathways has synergistic effects on reduction of HERV-K *env* transcripts (Fig. 2f). These data demonstrate that the MAPK and/or NF-κB pathways are indeed required for KSHV- or viral latent protein-induced HERV-K transactivation.

In fact, HERV-K transactivation largely depends on the transcriptional regulatory elements within its retroviral long terminal repeats (LTRs), which have potential binding sites for both viral and cellular transcriptional factors (TRs) [33]. Currently, there are a few TRs that have been experimentally shown to modulate HERV-K LTR activities, including Sp1 and YY1 proteins [34, 35]. A previous study has shown that LANA directly interacts with Sp1 in the nucleus of KSHV+ lymphoma cells [36]. Here we confirmed the interaction of LANA and Sp1 in KSHV-infected HUVEC by using immunofluorescence and co-immunoprecipitation assays (Fig. S2A-B). Moreover, knockdown of Sp1 by RNA interference (RNAi) partially reduced HERV-K *env* transcripts from LANA-transfected cells (Fig. S2C). These data provide additional mechanistic insights into viral latent protein-mediated induction of HERV-K expression through interaction with cellular TRs.

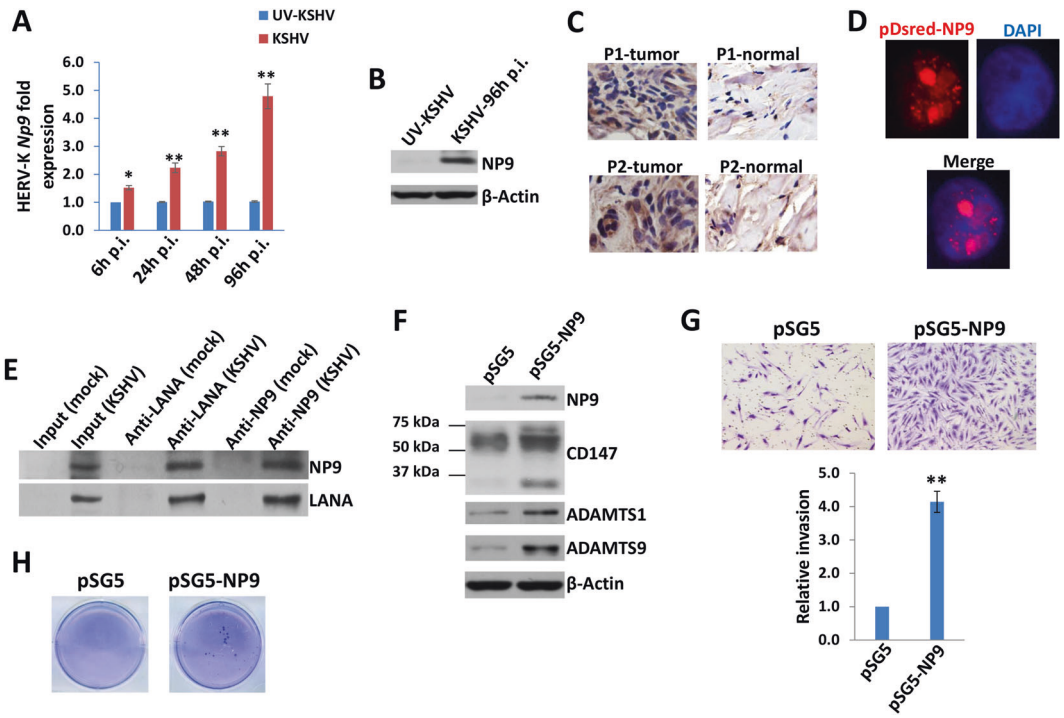

Fig. 4 KSHV infection induces HERV-K encoded oncogenic NP9 expression, which enhances primary endothelial cells invasion and colony formation. **a**, **b** HUVEC were infected with purified KSHV (MOI ~ 10) or UV-inactivated KSHV for 2 h, then the induction of HERV-K NP9 at the indicated time points postinfection (p.i.) was measured and compared to UV-inactivated KSHV-infected cells control using qRT-PCR and immunoblots. **c** The strong expression of NP9 protein in KS tissues from our cohort of two AIDS-KS patients without any treatment by immunohistochemical staining. **d**, **e** HUVEC were transfected with the pDsred-NP9 vector for 48 h, then protein expression was detected by immunofluorescence and nuclear was shown by DAPI. Immunoprecipitation assays in both directions were performed using the Catch and Release Immunoprecipitation Kit (Millipore) with anti-LANA or anti-NP9 antibodies, respectively. **f**–**h** HUVEC were transfected with pSG5 control vector or pSG5-NP9 for 48 h, then the protein expression was detected by immunoblots. Cell invasiveness was determined using the transwell assays. Anchorage-independent growth ability was determined using the soft agar assays. Error bars represent the S.D. from three independent experiments. *$p < 0.05$, **$p < 0.01$

HERV-K transactivation is closely related to KSHV-induced primary endothelial cell invasiveness

One hallmark of KSHV-infected endothelial cells is displaying a migratory or invasive phenotype, which can facilitate viral dissemination and angiogenesis during KS development [36]. Our data indicated that knockdown of HERV-K *env* by RNAi significantly blocked the invasiveness of KSHV-infected HUVEC by using the transwell assays (Fig. 3a–c). This reduction is independent of cell growth, since we do not observe silencing of HERV-K *env* affecting HUVEC cell growth (data not shown). Our previous study has demonstrated that vascular endothelial growth factor (VEGF) is one of the major pro-angiogenic cytokines responsible for KSHV-induced primary endothelial cell invasiveness [37]. Here we found that silencing of HERV-K *env* significantly reduced the VEGF production and the expression of VEGF receptor 1 (VEGFR1) but not the VEGF receptor 2 (VEGFR2) from KSHV-infected HUVEC (Fig. 3d, e). Together, these data indicate that HERV-K transactivation is closely related to KSHV-induced primary endothelial cell malignant behaviors.

KSHV infection activates HERV-K-encoded oncogenic NP9 expression, which enhances viral pathogenesis in endothelial cells

Among HERV-K (HML-2) elements, there are two major types of proviruses (type 1 and 2). Unlike type 2 proviruses, type 1 elements share a 292-nt fragment deletion in the *env* region, which gives rise to a difference between two isoforms of regulatory proteins encoded by the double-spliced transcripts. Type 2 proviral transcripts, 1.8 kb long, code the 15-kDa accessory protein Rec [38], which is a functional homolog of Rex and Rev from other retroviruses [39]. Type 1-specific double-spliced RNA product, NP9, is a 9-kDa protein that shares only the N-terminal 15 amino acid residues with Rec [18, 40, 41]. Furthermore, the NP9 protein has been found as a oncogenic protein and is present in a variety of tumors and transformed cells [18, 40, 41]. Our data here indicate that KSHV de novo infection induced a gradient increase of *Np9* transcripts from HUVEC using qRT-PCR with *Np9*-specific primers [42], which was subsequently confirmed by immunoblots with a NP9 polyclonal antibody (kindly provided by Dr. Friedrich A. Grasser from

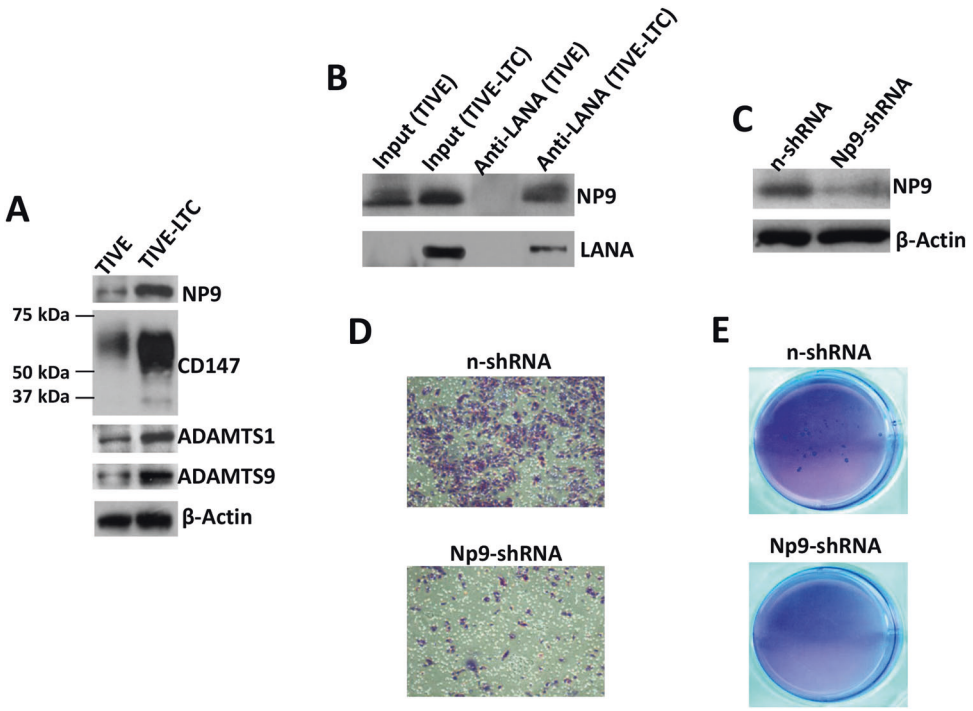

Fig. 5 The HERV-K NP9 protein is involved in the pathogenesis of KSHV long-term-infected endothelial cells. **a** The protein expression in KSHV long-term-infected telomerase-immortalized human umbilical vein endothelial (TIVE-LTC) and parental uninfected TIVE cells was detected and compared by immunoblots. **b** Immunoprecipitation assays were performed with anti-LANA antibody as described previously. **c–e** The stably "knockdown" of Np9 in TIVE-LTC were established by using lentiviral vector containing shRNA specifically targeting Np9 (Np9-shRNA) as described in the Methods. A non-silencing (n)-shRNA was used as a negative control. Protein expression, cell invasiveness, and anchorage-independent growth abilities were measured as described above

Universitatsklinikum des Saarlandes, Germany) [43] (Fig. 4a, b). Notably, NP9 protein is only expressed in KSHV-infected cells, whereas none in the uninfected cells. In contrast, we found that KSHV de novo infection slightly induced the increase of *Rec* transcripts (with no statistical significance) using qRT-PCR with *Rec*-specific primers [42] (Fig. S3). Next, we observed the strong expression of NP9 within AIDS-KS tumor tissues while only low levels of expression in adjacent normal tissues from two HIV+ patients without any HAART treatment (Fig. 4c). Additionally, we found that NP9 was exclusively expressed in the nucleus by transfecting HUVEC with the pDsred-NP9 construct [43] (Fig. 4d), although we observed some cytoplasmic staining of NP9 in AIDS-KS tissues (Fig. 4c). Since this is a self-made polyclonal antibody that has not been tested for immunohistochemical staining, we cannot exclude the existence of some non-specific staining in the immunohistochemical assays. The results from co-immunoprecipitation assays in both directions revealed the protein interaction between NP9 and LANA in KSHV-infected HUVEC (Fig. 4e). Moreover, ectopic expression of NP9 from the recombinant construct pSG5-NP9 [43] significantly increased HUVEC invasion and anchorage-independent growth (Fig. 4f–h). Interestingly, we found that ectopic expression of NP9 greatly upregulated the expression of one cellular glycoprotein, CD147 (also named as Emmprin), and its downstream proteins, ADAMTS1 (A disintegrin and metalloproteinase with thrombospondin motifs 1) and ADAMTS9 (A disintegrin and metalloproteinase with thrombospondin motifs 9) (Fig. 4f). Both high and low molecular weight (~65 and ~35 kDa, respectively) CD147 glycoforms were elevated in NP9-transfected cells, in particular the mature high molecular weight glycoform related to biological activities [44]. qRT-PCR analysis indicated that the ectopic expression of NP9 also increased the transcripts of these genes (Fig. S4). Our previous studies reported that KSHV infection or ectopic expression of LANA induced CD147 expression, which enhances primary endothelial cell invasiveness [29]. Our recent transcriptomic analysis has determined that ADAMTS1 and ADAMTS9 are two novel CD147-regulated downstream proteins, and they are all highly expressed in AIDS-KS tissues [45]. Moreover, silencing of CD147, ADAMTS1, or ADAMTS9 by RNAi significantly reduced KSHV-induced primary endothelial cell invasiveness [29, 45]. Here we also found that silencing of CD147, ADAMTS1, or ADAMTS9 by RNAi significantly blocked the NP9-induced HUVEC invasion (Fig. S5), indicating that CD147–ADAMTS1/

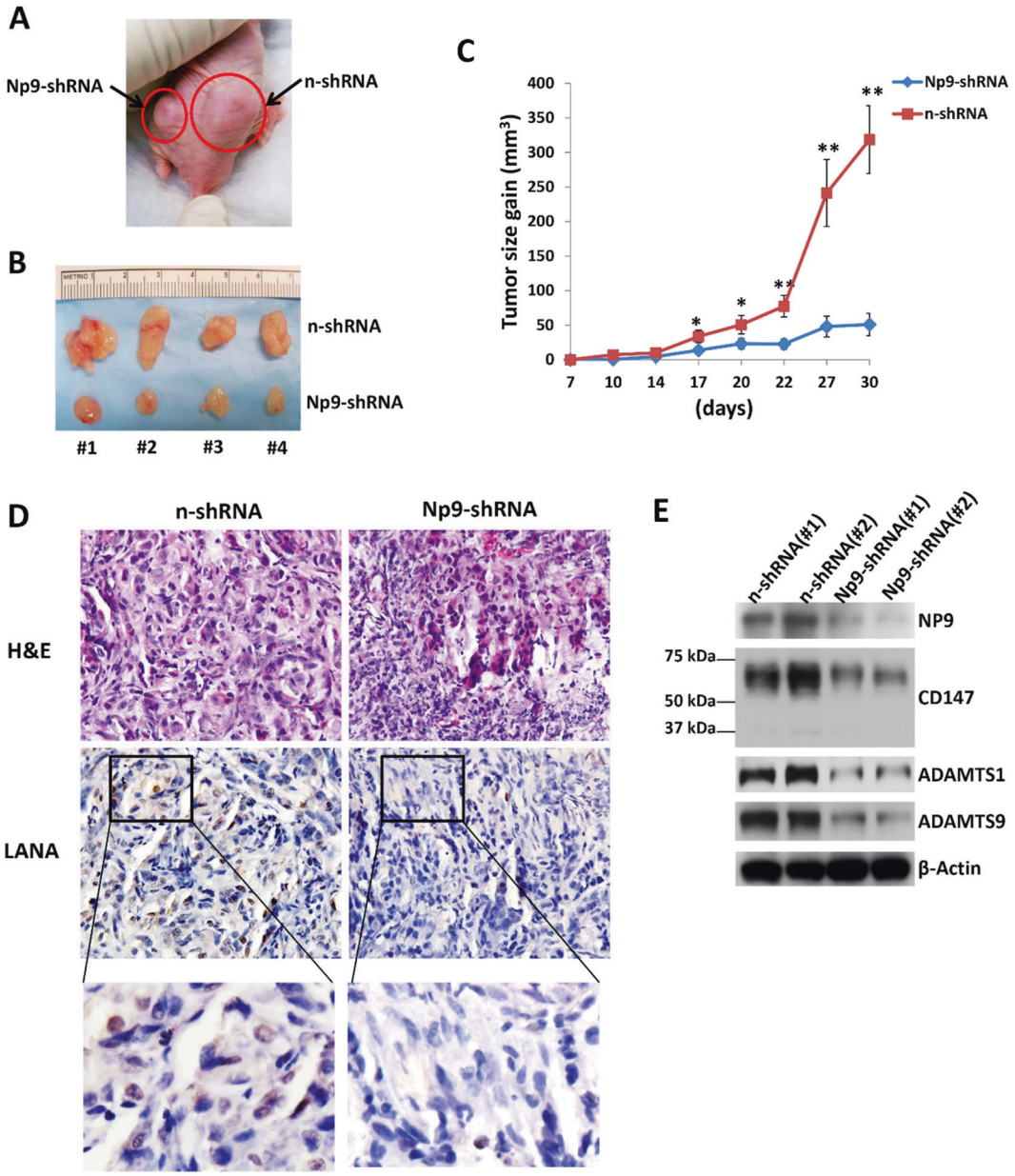

Fig. 6 Targeting HERV-K NP9 significantly suppresses KSHV-induced tumorigenesis in vivo. **a**–**c** The Np9 stably "knockdown" TIVE-LTC or control cells (approximately 5×10^5 cells were mixed at a ratio of 1:1 with growth factor-depleted Matrigel) were injected subcutaneously into the right and left flanks of nude mice, respectively. The mice were observed and measured every 2–3 days for the presence of palpable tumors for 30 days. Error bars represent the S.D. from two independent experiments. $*p < 0.05$, $**p < 0.01$. **d**, **e** Protein expression within tumor tissues from representative injected mice was measured by using immunohistochemistry or immunoblots, respectively

ADAMTS9 axis is indeed contributed to NP9-mediated cellular functions.

Since KSHV-infected primary endothelial cells (e.g., HUVEC) usually are not able to form tumors in mice [25], we recently established a KS-like xenograft model using a KSHV long-term-infected *t*elomerase-*i*mmortalized human umbilical *v*ein endothelial (TIVE-LTC) cell line, which stably supports KSHV latency (kindly provided by Dr. Rolf Renne at the University of Florida) [45, 46]. Our data indicated that TIVE-LTC have much higher levels of NP9, CD147, and downstream protein expression than the parental non-infected TIVE cells (Fig. 5a). Co-immunoprecipitation assays confirmed the interaction of LANA and NP9 in TIVE-LTC (Fig. 5b). We previously showed that TIVE-LTC displayed much stronger abilities of cell invasiveness and anchorage-independent growth than its parental TIVE cells, the latter almost cannot form colonies in soft agar assays [45]. To further study the functional

role of NP9 in TIVE-LTC, we first directly silenced it by using lentiviral vector containing short hairpin RNA (shRNA) specifically targeting Np9 (Np9-shRNA) to obtain stably "knockdown" cells. A non-silencing (n)-shRNA was used as a negative control, and we do not observe silencing of Np9 affecting TIVE-LTC cell growth (data not shown). Here we demonstrated that silencing of Np9 by RNAi dramatically reduced TIVE-LTC invasion and anchorage-independent growth abilities (Fig. 5c–e).

Targeting HERV-K NP9 significantly suppresses KSHV-induced tumorigenesis in vivo

We next seek to determine the role of HERV-K NP9 in KSHV-induced tumorigenesis in vivo by using the established KS-like xenograft model [45]. We injected the Np9 stably "knockdown" TIVE-LTC or control cells subcutaneously into the two sides of flanks of nude mice, respectively. These mice were checked and measured every 2–3 days for the presence of palpable tumors for 30 days. Our results indicate that silencing of Np9 significantly repressed KSHV-induced tumorigenesis in nude mice. Mice injected with Np9 stably "knockdown" cells formed much smaller tumors, when compared to mice injected with control "n-shRNA" cells at 30 days (Fig. 6a–c). Hematoxylin–eosin (H&E) staining confirmed that there were significantly fewer tumor cells or tumor biomass with more immune cell infiltrated in the tumor tissues from mice injected with Np9 stably "knockdown" cells (Fig. 6d). Of note, we also observed dramatically reduced LANA expression in tumor tissues from mice injected with Np9 stably "knockdown" cells, although the underlying mechanisms remain unclear and we do not observe the similar phenotype in in vitro cultures (data not shown). Immunoblot results confirmed the reduced levels of NP9, CD147, ADAMTS1, and ADAMTS9 expression in tumor lysates from mice injected with Np9 stably "knockdown" cells (Fig. 6e). Taken together, these data strongly support the important role of HERV-K transactivation (in particular activation of NP9 and related signaling) as the cellular co-factors for KSHV-induced tumorigenesis in this in vivo model.

Discussion

In the current study, we demonstrate for the first time that the KSHV-encoded latent proteins LANA and vFLIP can induce HERV-K transactivation through both intracellular signaling pathways (e.g., MAPK and NF-κB) and cellular transactional factors (TRs, e.g., Sp1), resulting in enhanced cell invasion, anchorage-independent growth, and KSHV-induced tumorigenesis (summarized in Fig. 7). In silico

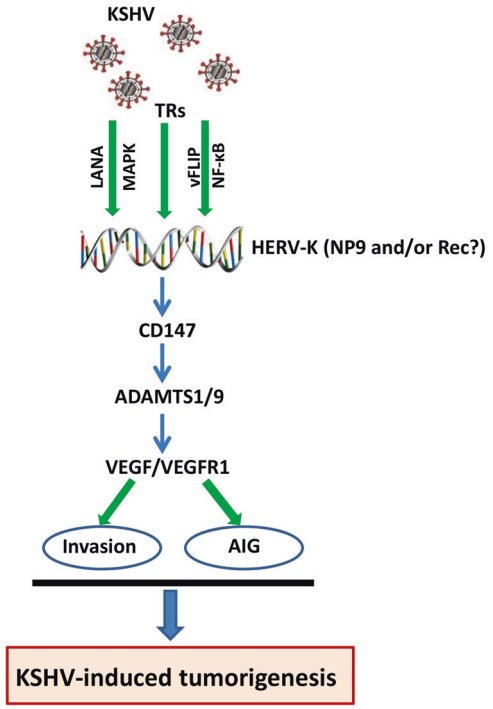

Fig. 7 Schematic diagram of potential mechanisms for HERV-K transactivation promoting KSHV-induced tumorigenesis. AIG anchorage-independent growth, TRs transcriptional factors

analysis of HERV-K 5' LTR regions has found >40 cellular TRs with putative binding sites, including Sp1 [33]. Future work will explore which TRs are indeed responsible for KSHV-induced HERV-K transactivation. Besides TRs interacting with HERV-K LTRs, the expression of HERV-K can also be regulated by some epigenetic mechanisms, including DNA methylation and histone modification [47]. Interestingly, LANA has been found to interact with or regulate a variety of epigenetic factors, such as EZH2, KDM3a, and DNMT3a [48–51]. Therefore, it will be interesting to determine whether these epigenetic factors are also involved in KSHV-induced HERV-K transactivation. One recent study reports that the expression of HERV-K correlates with the expression of genes in retinoblastoma (Rb) pathway including p16INK4A-CDK4 in melanoma cells [52]. In fact, LANA can interact with Rb and regulate the Rb/E2F pathway, protecting lymphoid cells from p16 INK4A-induced cell cycle arrest and inducing S-phase entry [53, 54]. Therefore, it will be important to determine the potential involvement of Rb/E2F pathway in KSHV/LANA-induced HERV-K transactivation.

Based on the types of proviruses, two different isoforms of regulatory proteins are encoded by the double-spliced transcripts of HERV-K *env* region, Rec and NP9, both of which have been reported to link with cancer development [55, 56]. In the current study, we found that KSHV de novo infection prominently increases the expression of NP9,

which is also highly expressed in AIDS-KS tumor tissues. Interestingly, NP9 has been found to not only activate the Akt, ERK, and Notch1 pathways but also to upregulate β-catenin, which is essential for survival of leukemia stem cells [41]. More importantly, all of these pathways are closely related to KSHV pathogenesis and/or KS development [57–60]. However, it still requires to understand the role of Rec in the KSHV-related tumorigenesis in future studies, since we found that our RNAi silencing of HERV-K *env* caused the reduction of both *Rec* and *Np9* transcripts (data not shown).

We here report that "knockdown" of Np9 by RNAi effectively suppresses KSHV-induced tumorigenesis in vivo. Dr. Anil Sood at the MD Anderson Cancer Center has validated the use of 1,2-dioleoyl-snglycero-3-phosphatidylcholine (DOPC) for the efficient systemic delivery of EphA2-specific small interfering RNA (siRNA) (EphA2-siRNA-DOPC) in an established xenograft model for intraperitoneal ovarian cancer [61]. This work has revealed a significant reduction in intra-abdominal tumor expression of EphA2 48 h after intravenous injection of EphA2-siRNA-DOPC, and twice-weekly dosing results in sustained target knockdown and significant antitumor efficacy using EphA2-siRNA-DOPC alone or in combination with paclitaxel. Therefore, the use of siRNA-DOPC or siRNA-nanoparticles targeting oncogenic NP9 protein may represent a novel and clinically feasible approach for the treatment of KSHV-associated tumors.

Our H&E staining images indicated that there is more immune cells' infiltration in the tumor tissues from mice injected with Np9 "knockdown" cells when compared to control mice (Fig. 6d), although the underlying mechanisms need further investigation. Actually, HERVs can promote an immunosuppressive response that may lead to cancer formation and spreading [62]. For instance, HERV Env protein contains an immunosuppressive domain, which was confirmed in animal models as a cause of tumor growth for tumor cells harboring the insertion of Moloney MLV and in *env* knockdown in B16 melanoma cells and Neuro-2a neuroblastoma cell lines [63]. Therefore, whether targeting HERV-K transactivation can be part of immunotherapy for KSHV-related malignancies may represent an interesting direction.

Materials and methods

Cell culture and reagents

KSHV+PEL cell line, BCBL-1 as well as a Burkitt's lymphoma cell line, BL-41, were kindly provided by Dr. Dean Kedes (University of Virginia), which are cultured as described previously [64]. The other PEL cell lines including BC-1, BC-3, and BCP-1 were purchased from American Type Culture Collection (ATCC) and cultured as recommended by the manufacturer. KSHV long-term-infected telomerase-immortalized HUVEC (TIVE-LTC) and the parental non-infected TIVE and cells were cultured as previously described [46]. All the cells were cultured at the conditions of 37 °C with 5% CO_2.

KSHV purification and infection

BCBL-1 cells were incubated with valproic acid (0.6 mM) for 5 days, and KSHV virions in the culture supernatants was purified using ultracentrifugation as described previously [65]. HUVEC were incubated with purified virus for 2 h at 37 °C. The concentration of viral particles (multiplicity of infection) was calculated as described previously [65].

Patients and ethics statement

The study was approved by the Institutional Review Boards for Human Research at Louisiana State University Health Science Center—New Orleans (No. 8079). All subjects have been provided the written informed consent. A total of 21 HIV+ patients with HAART treatment in our HIV Outpatient Clinic are involved. There are 8 females and 13 males; the average age is 50.2 years (range 23–65 years). The average CD4 T-cell counts of these patients are 544/mL (range 33–1775/mL), and the average viral loads of HIV is 5904 copies/mL (range 30–63,367 copies/mL).

Plasma and PBMC preparation

Whole blood from HIV+ patients was collected and stored in heparin-coated tubes, then PBMCs were isolated using a Ficoll-Hypaque cushion. Plasma was obtained through the centrifugation. The KSHV infection status is determined by using the quantitative enzyme-linked immunosorbent assays as described previously [23, 24].

Immunoblotting and immunoprecipitation

The following antibodies (100–200 μg/mL) were used in immunoblotting: p-ERK/t-ERK, p-p65/t-p65, ADAMTS1 (Cell Signaling, Cat. #4370, #4695, #3033, #8242, #12897), ADAMTS9 (Thermo, Cat. #PA1-1760), CD147 (BD, Cat. #555961), LANA (ABI, Cat. #13-210-100), vFLIP (Ximbio, Cat. #151778), and HERV-K NP9 (kindly provided by Dr. Friedrich A. Grasser from Universitatsklinikum des Saarlandes, Germany) [43]. The antibody-detecting β-Actin (Cell Signaling, Cat. #4970) was used as the loading control. Immunoprecipitation assays were carried out using the Catch and Release Immunoprecipitation Kit (Milipore).

Plasmid transfection and RNA interference

HUVEC were transfected with control vectors, pcDNA3.1-LANA (pcLANA), pcDNA3.1-vFLIP (pcvFLIP), pcDNA3.1-RTA (pcRTA), pDsred-NP9, and pSG5-NP9 (both are kindly provided by Dr. Friedrich A. Grasser) [43] in 12-well plates using Lipofectamine 3000 (Invitrogen). Transfection efficiency was determined as described previously [66]. For RNAi assays, ON-TARGET plus SMART pool siRNA for HERV-K *Env*, *Sp1* (Dharmacon), or the negative control siRNA were delivered by using the DharmaFECT transfection reagent. To establish stable HERV-K knockdown cells, we used Dharmacon SMARTvector Lentiviral *Np9*-shRNA and a non-silencing (n)-shRNA as a negative control.

qRT-PCR

Total cellular RNA was isolated and purified using the RNeasy Mini Kit (QIAGEN). cDNA was synthesized using the SuperScript III First-Strand Synthesis SuperMix Kit (Invitrogen). Primers used for amplification of target genes are listed in Table. S1. Amplification was performed on an iCycler IQ Real-Time PCR Detection System and analyzed as described previously [64].

Transwell invasion and soft agar assays

Transwell invasion assays were performed using Matrigel invasion chambers (BD) and the relative invasion was calculated as described previously [65, 67]. The anchorage-independent growth abilities were assessed using soft agar assays as described previously [65].

KS-like nude mouse model

In all, 5×10^5 TIVE-LTC cells in 50 µL phosphate-buffered saline plus 50 µL growth factor-depleted Matrigel (BD Biosciences) were together injected subcutaneously into the flanks of nude mice, 6–8-week old, male (Jackson Laboratory), 4 mice for each group. At the end of experiment, the tumors were excised for immunoblots and immunohistochemical analyses. All protocols were approved by the LSUHSC Institutional Animal Care and Use Committee in accordance with the national guidelines.

Statistical analyses

Significance for differences among the experimental groups was calculated and determined using the two-tailed Student's *t*-test (Excel 2016). *p*-Values <0.05 or <0.01 were considered significant or highly significant, respectively.

Acknowledgements We thank Dr. Rolf Renne at the University of Florida for his kind gifts of TIVE-LTC and TIVE cells and Dr. Friedrich A. Grasser from Universitatsklinikum des Saarlandes, Germany for kindly providing HERV-K NP9 plasmids and antibody. This work was supported by grants from a DOD Career Development Award to (CA140437 to ZQ); a Louisiana Clinical and Translational Science Center Pilot grant (U54GM104940 from NIH), a LSU LIFT^2 funding, and NIH P20-GM121288-01 (PI: Krzysztof Reiss) subproject to ZQ; NIH RO1-AI101046, R01-AI106676, and P01CA214091 and Department of Defense W81XWH-16-1-0318 to EKF; the federal funds from the National Cancer Institute, NIH, under Contract No. HHSN261200800001E to DW; and the awards from the National Natural Science Foundation of China (81472547, 81672924 to ZQ and 81400164, 81772930 to LD). Funding sources had no role in study design, data collection and analysis, decision to publish, or preparation of the manuscript.

Authors contribution LD and ZQ designed and performed experiments, analyzed results, and wrote the manuscript. LDV and WM performed experiments. DW, ACO, and EKF performed statistical analysis and provided critical input.

Compliance with ethical standards

Conflict of interest The authors declare that they have no conflict of interest.

References

1. Mesri EA, Feitelson MA, Munger K. Human viral oncogenesis: a cancer hallmarks analysis. Cell Host Microbe. 2014;15:266–82.
2. Chang Y, Cesarman E, Pessin MS, Lee F, Culpepper J, Knowles DM, et al. Identification of herpesvirus-like DNA sequences in AIDS-associated Kaposi's sarcoma. Science. 1994;266:1865–9.
3. Cesarman E, Chang Y, Moore PS, Said JW, Knowles DM. Kaposi's sarcoma-associated herpesvirus-like DNA sequences in AIDS-related body-cavity-based lymphomas. N Engl J Med. 1995;332:1186–91.
4. Engels EA, Biggar RJ, Hall HI, Cross H, Crutchfield A, Finch JL, et al. Cancer risk in people infected with human immunodeficiency virus in the United States. Int J Cancer. 2008;123:187–94.
5. Bonnet F, Lewden C, May T, Heripret L, Jougla E, Bevilacqua S, et al. Malignancy-related causes of death in human immunodeficiency virus-infected patients in the era of highly active antiretroviral therapy. Cancer. 2004;101:317–24.
6. Labo N, Miley W, Benson CA, Campbell TB, Whitby D. Epidemiology of Kaposi's sarcoma-associated herpesvirus in HIV-1-infected US persons in the era of combination antiretroviral therapy. AIDS. 2015;29:1217–25.
7. Jenkins FJ, Hoffman LJ, Liegey-Dougall A. Reactivation of and primary infection with human herpesvirus 8 among solid-organ transplant recipients. J Infect Dis. 2002;185:1238–43.
8. Luppi M, Barozzi P, Santagostino G, Trovato R, Schulz TF, Marasca R, et al. Molecular evidence of organ-related transmission of Kaposi sarcoma-associated herpesvirus or human herpesvirus-8 in transplant patients. Blood. 2000;96:3279–81.
9. Ariza-Heredia EJ, Razonable RR. Human herpes virus 8 in solid organ transplantation. Transplantation. 2011;92:837–44.
10. Lander ES, Linton LM, Birren B, Nusbaum C, Zody MC, Baldwin J, et al. Initial sequencing and analysis of the human genome. Nature. 2001;409:860–921.
11. Hughes JF, Coffin JM. Evidence for genomic rearrangements mediated by human endogenous retroviruses during primate evolution. Nat Genet. 2001;29:487–9.

12. Dewannieux M, Harper F, Richaud A, Letzelter C, Ribet D, Pierron G, et al. Identification of an infectious progenitor for the multiple-copy HERV-K human endogenous retroelements. Genome Res. 2006;16:1548–56.
13. Lee YN, Bieniasz PD. Reconstitution of an infectious human endogenous retrovirus. PLoS Pathog. 2007;3:e10.
14. Kraus B, Boller K, Reuter A, Schnierle BS. Characterization of the human endogenous retrovirus K Gag protein: identification of protease cleavage sites. Retrovirology. 2011;8:21.
15. Depil S, Roche C, Dussart P, Prin L. Expression of a human endogenous retrovirus, HERV-K, in the blood cells of leukemia patients. Leukemia. 2002;16:254–9.
16. Contreras-Galindo R, Kaplan MH, Leissner P, Verjat T, Ferlenghi I, Bagnoli F, et al. Human endogenous retrovirus K (HML-2) elements in the plasma of people with lymphoma and breast cancer. J Virol. 2008;82:9329–36.
17. Wang-Johanning F, Rycaj K, Plummer JB, Li M, Yin B, Frerich K, et al. Immunotherapeutic potential of anti-human endogenous retrovirus-K envelope protein antibodies in targeting breast tumors. J Natl Cancer Inst. 2012;104:189–210.
18. Armbruester V, Sauter M, Krautkraemer E, Meese E, Kleiman A, Best B, et al. A novel gene from the human endogenous retrovirus K expressed in transformed cells. Clin Cancer Res. 2002;8:1800–7.
19. Buscher K, Trefzer U, Hofmann M, Sterry W, Kurth R, Denner J. Expression of human endogenous retrovirus K in melanomas and melanoma cell lines. Cancer Res. 2005;65:4172–80.
20. Sutkowski N, Conrad B, Thorley-Lawson DA, Huber BT. Epstein-Barr virus transactivates the human endogenous retrovirus HERV-K18 that encodes a superantigen. Immunity. 2001;15:579–89.
21. Sutkowski N, Chen G, Calderon G, Huber BT. Epstein-Barr virus latent membrane protein LMP-2A is sufficient for transactivation of the human endogenous retrovirus HERV-K18 superantigen. J Virol. 2004;78:7852–60.
22. Hsiao FC, Lin M, Tai A, Chen G, Huber BT. Cutting edge: Epstein-Barr virus transactivates the HERV-K18 superantigen by docking to the human complement receptor 2 (CD21) on primary B cells. J Immunol. 2006;177:2056–60.
23. Mbisa GL, Miley W, Gamache CJ, Gillette WK, Esposito D, Hopkins R, et al. Detection of antibodies to Kaposi's sarcoma-associated herpesvirus: a new approach using K8.1 ELISA and a newly developed recombinant LANA ELISA. J Immunol Methods. 2010;356:39–46.
24. Benavente Y, Mbisa G, Labo N, Casabonne D, Becker N, Maynadie M, et al. Antibodies against lytic and latent Kaposi's sarcoma-associated herpes virus antigens and lymphoma in the European EpiLymph case-control study. Br J Cancer. 2011;105:1768–71.
25. Mesri EA, Cesarman E, Boshoff C. Kaposi's sarcoma and its associated herpesvirus. Nat Rev Cancer. 2010;10:707–19.
26. Ye F, Lei X, Gao SJ. Mechanisms of Kaposias sarcoma-associated herpesvirus latency and reactivation. Adv Virol. 2011;2011:193860
27. Kellam P, Boshoff C, Whitby D, Matthews S, Weiss RA, Talbot SJ. Identification of a major latent nuclear antigen, LNA-1, in the human herpesvirus 8 genome. J Hum Virol. 1997;1:19–29.
28. Grossmann C, Podgrabinska S, Skobe M, Ganem D. Activation of NF-kappaB by the latent vFLIP gene of Kaposi's sarcoma-associated herpesvirus is required for the spindle shape of virus-infected endothelial cells and contributes to their proinflammatory phenotype. J Virol. 2006;80:7179–85.
29. Qin Z, Dai L, Slomiany MG, Toole BP, Parsons C. Direct activation of emmprin and associated pathogenesis by an oncogenic herpesvirus. Cancer Res. 2010;70:3884–9.
30. Liu L, Eby MT, Rathore N, Sinha SK, Kumar A, Chaudhary PM. The human herpes virus 8-encoded viral FLICE inhibitory protein physically associates with and persistently activates the Ikappa B kinase complex. J Biol Chem. 2002;277:13745–51.
31. Sun R, Lin SF, Gradoville L, Yuan Y, Zhu F, Miller G. A viral gene that activates lytic cycle expression of Kaposi's sarcoma-associated herpesvirus. Proc Natl Acad Sci USA. 1998;95:10866–71.
32. Dai L, Chen Y, Toole B, Parsons C, Qin Z. Induction of hyaluronan production by oncogenic KSHV and the contribution to viral pathogenesis in AIDS patients. Cancer Lett. 2015;362:158–66.
33. Manghera M, Douville RN. Endogenous retrovirus-K promoter: a landing strip for inflammatory transcription factors? Retrovirology. 2013;10:16.
34. Fuchs NV, Kraft M, Tondera C, Hanschmann KM, Lower J, Lower R. Expression of the human endogenous retrovirus (HERV) group HML-2/HERV-K does not depend on canonical promoter elements but is regulated by transcription factors Sp1 and Sp3. J Virol. 2011;85:3436–48.
35. Kim JD, Yu S, Kim J. YY1 is autoregulated through its own DNA-binding sites. BMC Mol Biol. 2009;10:85.
36. Verma SC, Borah S, Robertson ES. Latency-associated nuclear antigen of Kaposi's sarcoma-associated herpesvirus up-regulates transcription of human telomerase reverse transcriptase promoter through interaction with transcription factor Sp1. J Virol. 2004;78:10348–59.
37. Qian LW, Xie J, Ye F, Gao SJ. Kaposi's sarcoma-associated herpesvirus infection promotes invasion of primary human umbilical vein endothelial cells by inducing matrix metalloproteinases. J Virol. 2007;81:7001–10.
38. Lower R, Tonjes RR, Korbmacher C, Kurth R, Lower J. Identification of a Rev-related protein by analysis of spliced transcripts of the human endogenous retroviruses HTDV/HERV-K. J Virol. 1995;69:141–9.
39. Magin C, Lower R, Lower J. cORF and RcRE, the Rev/Rex and RRE/RxRE homologues of the human endogenous retrovirus family HTDV/HERV-K. J Virol. 1999;73:9496–507.
40. Buscher K, Hahn S, Hofmann M, Trefzer U, Ozel M, Sterry W, et al. Expression of the human endogenous retrovirus-K transmembrane envelope, Rec and Np9 proteins in melanomas and melanoma cell lines. Melanoma Res. 2006;16:223–34.
41. Chen T, Meng Z, Gan Y, Wang X, Xu F, Gu Y, et al. The viral oncogene Np9 acts as a critical molecular switch for co-activating beta-catenin, ERK, Akt and Notch1 and promoting the growth of human leukemia stem/progenitor cells. Leukemia. 2013;27:1469–78.
42. Gonzalez-Hernandez MJ, Swanson MD, Contreras-Galindo R, Cookinham S, King SR, Noel RJ Jr, et al. Expression of human endogenous retrovirus type K (HML-2) is activated by the Tat protein of HIV-1. J Virol. 2012;86:7790–805.
43. Gross H, Barth S, Pfuhl T, Willnecker V, Spurk A, Gurtsevitch V, et al. The NP9 protein encoded by the human endogenous retrovirus HERV-K(HML-2) negatively regulates gene activation of the Epstein-Barr virus nuclear antigen 2 (EBNA2). Int J Cancer. 2011;129:1105–15.
44. Tang W, Chang SB, Hemler ME. Links between CD147 function, glycosylation, and caveolin-1. Mol Biol Cell. 2004;15:4043–50.
45. Dai L, Qiao J, Nguyen D, Struckhoff AP, Doyle L, Bonstaff K, et al. Role of heme oxygenase-1 in the pathogenesis and tumorigenicity of Kaposi's sarcoma-associated herpesvirus. Oncotarget. 2016;7:10459–71.
46. An FQ, Folarin HM, Compitello N, Roth J, Gerson SL, McCrae KR, et al. Long-term-infected telomerase-immortalized endothelial cells: a model for Kaposi's sarcoma-associated herpesvirus latency in vitro and in vivo. J Virol. 2006;80:4833–46.

47. Maksakova IA, Mager DL, Reiss D. Keeping active endogenous retroviral-like elements in check: the epigenetic perspective. Cell Mol Life Sci. 2008;65:3329–47.
48. He M, Zhang W, Bakken T, Schutten M, Toth Z, Jung JU, et al. Cancer angiogenesis induced by Kaposi sarcoma-associated herpesvirus is mediated by EZH2. Cancer Res. 2012;72:3582–92.
49. Kim KY, Huerta SB, Izumiya C, Wang DH, Martinez A, Shevchenko B, et al. Kaposi's sarcoma-associated herpesvirus (KSHV) latency-associated nuclear antigen regulates the KSHV epigenome by association with the histone demethylase KDM3A. J Virol. 2013;87:6782–93.
50. Di Bartolo DL, Cannon M, Liu YF, Renne R, Chadburn A, Boshoff C, et al. KSHV LANA inhibits TGF-beta signaling through epigenetic silencing of the TGF-beta type II receptor. Blood. 2008;111:4731–40.
51. Shamay M, Krithivas A, Zhang J, Hayward SD. Recruitment of the de novo DNA methyltransferase Dnmt3a by Kaposi's sarcoma-associated herpesvirus LANA. Proc Natl Acad Sci USA. 2006;103:14554–9.
52. Li Z, Sheng T, Wan X, Liu T, Wu H, Dong J. Expression of HERV-K correlates with status of MEK-ERK and p16INK4A-CDK4 pathways in melanoma cells. Cancer Invest. 2010;28:1031–7.
53. Friborg J Jr., Kong W, Hottiger MO, Nabel GJ. p53 inhibition by the LANA protein of KSHV protects against cell death. Nature. 1999;402:889–94.
54. An FQ, Compitello N, Horwitz E, Sramkoski M, Knudsen ES, Renne R. The latency-associated nuclear antigen of Kaposi's sarcoma-associated herpesvirus modulates cellular gene expression and protects lymphoid cells from p16 INK4A-induced cell cycle arrest. J Biol Chem. 2005;280:3862–74.
55. Hohn O, Hanke K, Bannert N. HERV-K(HML-2), the best preserved family of HERVs: endogenization, expression, and implications in health and disease. Front Oncol. 2013;3:246.
56. Downey RF, Sullivan FJ, Wang-Johanning F, Ambs S, Giles FJ, Glynn SA. Human endogenous retrovirus K and cancer: Innocent bystander or tumorigenic accomplice? Int J Cancer. 2015;137:1249–57.
57. Wong JP, Damania B. Modulation of oncogenic signaling networks by Kaposi's sarcoma-associated herpesvirus. Biol Chem. 2017;398:911–8.
58. Li W, Jia X, Shen C, Zhang M, Xu J, Shang Y, et al. A KSHV microRNA enhances viral latency and induces angiogenesis by targeting GRK2 to activate the CXCR2/AKT pathway. Oncotarget. 2016;7:32286–305.
59. Li S, Hu H, He Z, Liang D, Sun R, Lan K. Fine-tuning of the Kaposi's sarcoma-associated herpesvirus life cycle in neighboring cells through the RTA-JAG1-Notch pathway. PLoS Pathog. 2016;12:e1005900.
60. Angelova M, Ferris M, Swan KF, McFerrin HE, Pridjian G, Morris CA, et al. Kaposi's sarcoma-associated herpesvirus G-protein coupled receptor activates the canonical Wnt/beta-catenin signaling pathway. Virol J. 2014;11:218.
61. Landen CN Jr., Chavez-Reyes A, Bucana C, Schmandt R, Deavers MT, Lopez-Berestein G, et al. Therapeutic EphA2 gene targeting in vivo using neutral liposomal small interfering RNA delivery. Cancer Res. 2005;65:6910–8.
62. Gonzalez-Cao M, Iduma P, Karachaliou N, Santarpia M, Blanco J, Rosell R. Human endogenous retroviruses and cancer. Cancer Biol Med. 2016;13:483–8.
63. Mangeney M, Heidmann T. Tumor cells expressing a retroviral envelope escape immune rejection in vivo. Proc Natl Acad Sci USA. 1998;95:14920–5.
64. Dai L, Trillo-Tinoco J, Cao Y, Bonstaff K, Doyle L, Del Valle L, et al. Targeting HGF/c-MET induces cell cycle arrest, DNA damage, and apoptosis for primary effusion lymphoma. Blood. 2015;126:2821–31.
65. Qin Z, Freitas E, Sullivan R, Mohan S, Bacelieri R, Branch D, et al. Upregulation of xCT by KSHV-encoded microRNAs facilitates KSHV dissemination and persistence in an environment of oxidative stress. PLoS Pathog. 2010;6:e1000742.
66. Qin Z, Dai L, Defee M, Findlay VJ, Watson DK, Toole BP, et al. Kaposi's sarcoma-associated herpesvirus suppression of DUSP1 facilitates cellular pathogenesis following de novo infection. J Virol. 2013;87:621–35.
67. Dai L, Bratoeva M, Toole BP, Qin Z, Parsons C. KSHV activation of VEGF secretion and invasion for endothelial cells is mediated through viral upregulation of emmprin-induced signal transduction. Int J Cancer. 2012;131:834–43.

Am J Cancer Res 2018;8(4):708-714
www.ajcr.us /ISSN:2156-6976/ajcr0075984

Original Article

KSHV co-infection regulates HPV16+ cervical cancer cells pathogenesis *in vitro* and *in vivo*

Lu Dai[1,2,3], Jing Qiao[1], Luis Del Valle[4], Zhiqiang Qin[1,2,3]

[1]Department of Pediatrics, [2]Research Center for Translational Medicine and Key Laboratory of Arrhythmias, East Hospital, School of Medicine, Tongji University, Shanghai 200120, China; Departments of [3]Genetics, [4]Pathology, Louisiana State University Health Sciences Center, Louisiana Cancer Research Center, 1700 Tulane Ave., New Orleans, LA 70112, USA

Received March 13, 2018; Accepted March 20, 2018; Epub April 1, 2018; Published April 15, 2018

Abstract: High-risk human papillomavirus (HPV) infection is the etiological agent of cervical, oral and oropharyngeal cancers. Another oncogenic virus, Kaposi sarcoma-associated herpesvirus (KSHV) can cause several human cancers arising in those immunocompromised patients. KSHV DNA has been detected in the oral cavity and the female genital tract, although its detection rate in cervical samples is relatively low. Therefore, it remains unclear about the role of KSHV co-infection in the development of HPV-related neoplasia. We recently report that KSHV infection of HPV16+ cervical cancer cell line SiHa induces several pro-inflammatory factors production while reducing HPV16 E6 and E7 expression through the manipulation of cellular microRNA function. In the current study, we focus on determining the influence of KSHV co-infection on cervical cancer cells pathogenesis *in vitro* and *in vivo*. We found that KSHV co-infection is able to maintain SiHa and/or CaSki cells pathogenesis and tumorigenesis, although hijacking HPV oncogenic proteins expression. In mechanisms, KSHV co-infection is capable of increasing Macrophage migration inhibitory factor (MIF) and its receptor CXCR2 expression from cervical cancer cells, which may contribute to cervical cancer development. Our data indicate that KSHV co-infection may act as a potential co-factor to promote HPV-related neoplasia development.

Keywords: HPV, KSHV, SiHa, MIF

Introduction

Cervical cancer represents one of the most common malignancies in females worldwide. The pathogenesis of cervical cancer occurs following persistent infection with high-risk human papillomavirus (HPV) in particular subtype 16 and 18 [1]. E6 and E7 proteins represent the major high-risk HPV-encoded oncoproteins, which are closely associated with cervical carcinogenesis [2]. Mechanistically, E6 and E7 proteins can bind to the p53 and retinoblastoma (Rb) family proteins, respectively, resulting in the regulation of cell cycle and final transformation [3]. In addition, high-risk HPV infection is prevalent in oral cavity and related to oral and oropharyngeal cancer development [4-6].

Kaposi sarcoma-associated herpesvirus (KSHV) represents a principal causative agent of several human cancers arising in those immunocompromised patients, including Kaposi's Sarcoma (KS) and Primary Effusion Lymphoma (PEL) [7, 8]. Published literatures have reported that KSHV DNA sequences are detected in the prostate, semen, oral cavity and the female genital tract [9-13]. In contrast to the high prevalence of KSHV shedding in oral cavity, the detection rate of KSHV DNA or virus infection in cervical samples are relatively low (< 2%), even in those high-risk population such as sex workers and HIV+ patients [13, 14]. Furthermore, currently there are few studies reporting the co-infection of KSHV and HPV in cervical samples or cervical cancer cells. Therefore, it remains unclear about the role of KSHV co-infection in the development of HPV-related neoplasia. Recently, we have reported that HPV16+ cervical cancer cell line SiHa is susceptible to KSHV initial infection and supports virus replication [15]. Interestingly, we have found that KSHV *de novo* infection or ectopic expression of viral

latent proteins can significantly reduce HPV16 E6 and E7 expression (~50%-70% of reduction) through the up-regulation of one cellular microRNA, miR129-5p [15, 16]. In the current study, we focus on determining the influence of KSHV co-infection on HPV16+ cervical cancer cells pathogenesis *in vitro* and *in vivo*.

Materials and methods

Cell culture and KSHV purification/infection

Body cavity-based lymphoma cells (BCBL-1, $KSHV^{+}/EBV^{neg}$) were kindly provided by Dr. Dean Kedes (University of Virginia) and maintained in RPMI 1640 medium (Gibco) with supplements as described previously [17]. SiHa and CaSki cells were purchased from ATCC and maintained in Eagle's Minimum Essential Medium or RMPI 1640 medium (ATCC) supplemented with 10% FBS, respectively. All cells were incubated at 37°C in 5% CO_2. All experiments were carried out using cells harvested at low passages (< 20). To obtain KSHV for infection experiments, BCBL-1 cells were incubated with 0.6 mM valproic acid for 6 days, and purified virus was concentrated from culture supernatants and infectious titers were determined as described previously [18].

Cell proliferation and apoptosis assays

Cell proliferation was measured by using the WST-1 assays (Roche) according to the manufacturers' instructions. Flow cytometry was used for quantitative assessment of apoptosis using the FITC-Annexin V/propidium iodide (PI) Apoptosis Detection Kit I (BD Pharmingen).

Transwell invasion assays

Matrigel Invasion Chambers (BD) were hydrated for 4 h at 37°C with culture media. Following hydration, media in the bottom of the well was replaced with fresh media, then 2×10^4 tumor cells were plated in the top of the chamber. After 24 h, cells were fixed with 4% formaldehyde for 15 min at room temperature and chambers rinsed in PBS prior to staining with 0.2% crystal violet for 10 min. After washing the chambers, cells at the top of the membrane were removed and cells at the bottom of the membrane counted using a phase contrast microscope.

Soft agar assays

A base layer containing 0.5% agarose medium and 5% FCS was poured into six-well plates. Then, 1×10^5 cells were mixed with 0.4% agarose in Earl's minimal essential medium (EMEM) containing 5% FCS to form a single-cell suspension. After being seeded, the plates were incubated for 2 weeks. Colonies were stained with 0.005% crystal violet and photographed under a phase-contrast microscope (Leica DFC320).

ELISA

Concentrations of MIF in culture supernatants were determined using the human MIF ELISA kit (R&D Systems), according to the manufacturer's instructions.

qRT-PCR

Total RNA was isolated using the RNeasy Mini kit (QIAGEN), and cDNA was synthesized from equivalent total RNA using a SuperScript III First-Strand Synthesis SuperMix Kit (Invitrogen) according to the manufacturer's instructions. Primers used for amplification of HPV16 E6 and E7 are described previously [15]. Amplification was carried out using an iCycler IQ Real-Time PCR Detection System, and cycle threshold (Ct) values were tabulated in duplicate for each gene of interest in each experiment. "No template" (water) controls were used to ensure minimal background contamination. Using mean Ct values tabulated for each gene, and paired Ct values for β-actin as a loading control, fold changes for experimental groups relative to assigned controls were calculated using automated iQ5 2.0 software (Bio-rad).

Nude mouse xenograft model

Cells were counted and washed once in ice-cold PBS, and 2×10^6 cells in 50 μL PBS plus 50 μL growth factor-depleted Matrigel (BD Biosciences) were injected subcutaneously into the flanks of nude mice (Jackson Laboratory). The mice were observed and measured every 2~3 d for the presence of palpable tumors. At the end of experiment, the tumors were excised for subsequent analysis such as hematoxylin & eosin (H&E) and immunohistochemistry staining as described previously [19]. Images were collected using an Olympus BX61 microscope

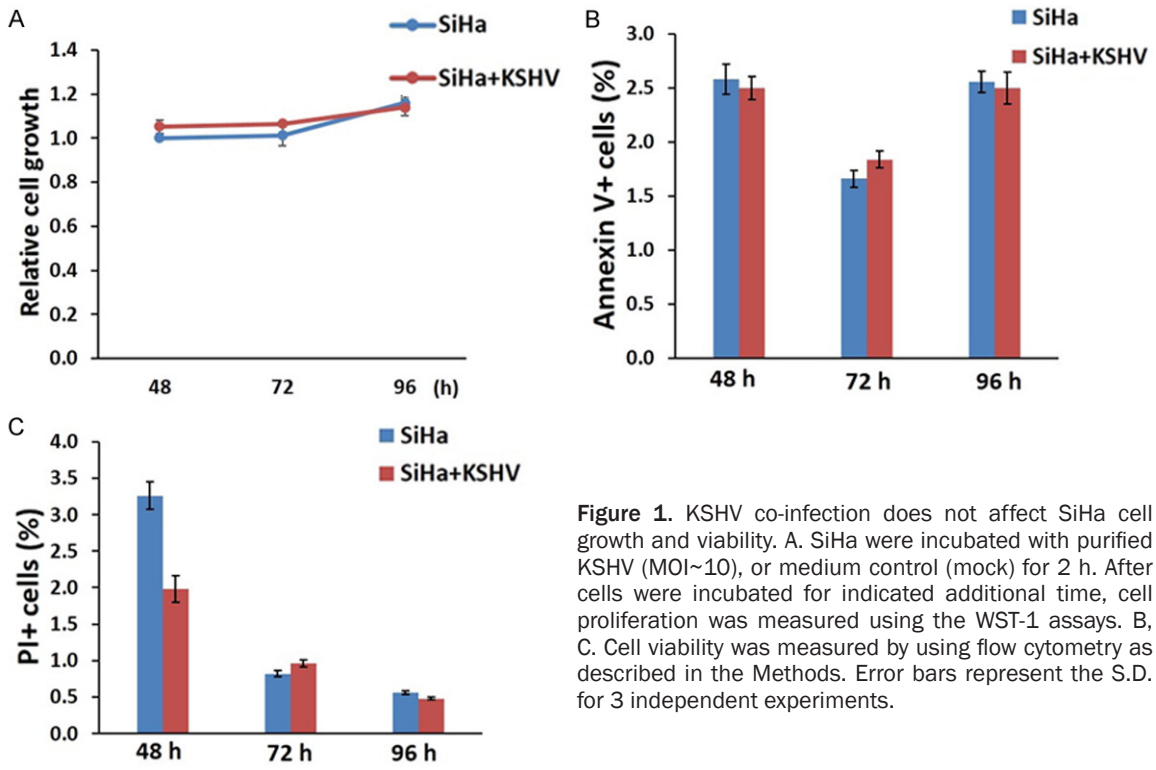

Figure 1. KSHV co-infection does not affect SiHa cell growth and viability. A. SiHa were incubated with purified KSHV (MOI~10), or medium control (mock) for 2 h. After cells were incubated for indicated additional time, cell proliferation was measured using the WST-1 assays. B, C. Cell viability was measured by using flow cytometry as described in the Methods. Error bars represent the S.D. for 3 independent experiments.

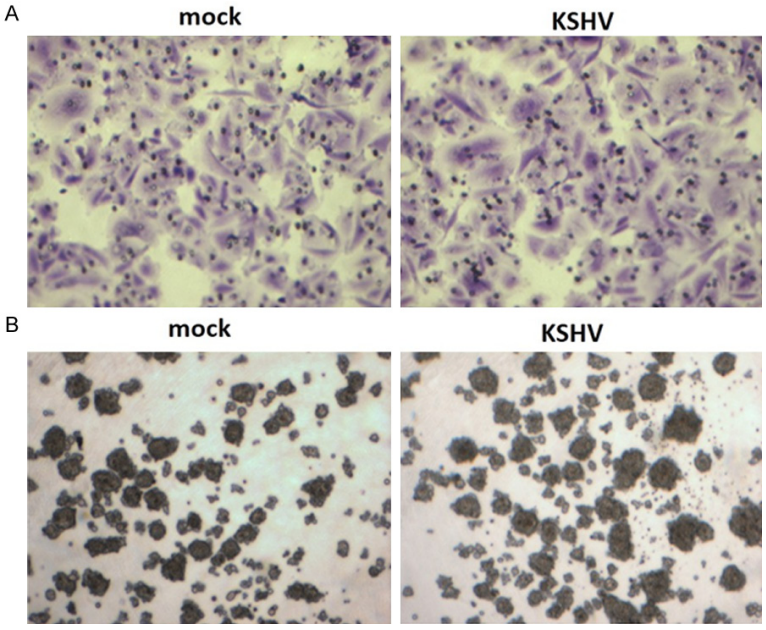

Figure 2. Comparison of cell invasiveness and anchorage-independent growth abilities between mock and KSHV co-infected SiHa cells. A. SiHa were incubated with or without purified KSHV (MOI~10) for 2 h, after additional 48 h incubation, the transwell assays were performed to determine cell invasiveness ability as described in the Methods. B. The anchorage-independent growth ability was determined using the soft agar assays as described in the Methods.

equipped with a high resolution DP72 camera and CellSense image capture software. All protocols were approved by the LSUHSC Animal Care and Use Committee in accordance with national guidelines.

Statistical analyses

Significance for differences between experimental and control groups was determined using the two-tailed Student's t-test (Excel 8.0), and p values < 0.05 or < 0.01 were considered significant or highly significant, respectively.

Results and discussion

During a time-course culture, we first have confirmed that KSHV co-infection does not affect SiHa cell growth and viability when compared to non-infected mock cells (**Figure 1**), therefore which are not responsible for any differences between these two groups of cells in cellular functional assays if have. Next, by using the transwell and soft agar assays, respectively, we

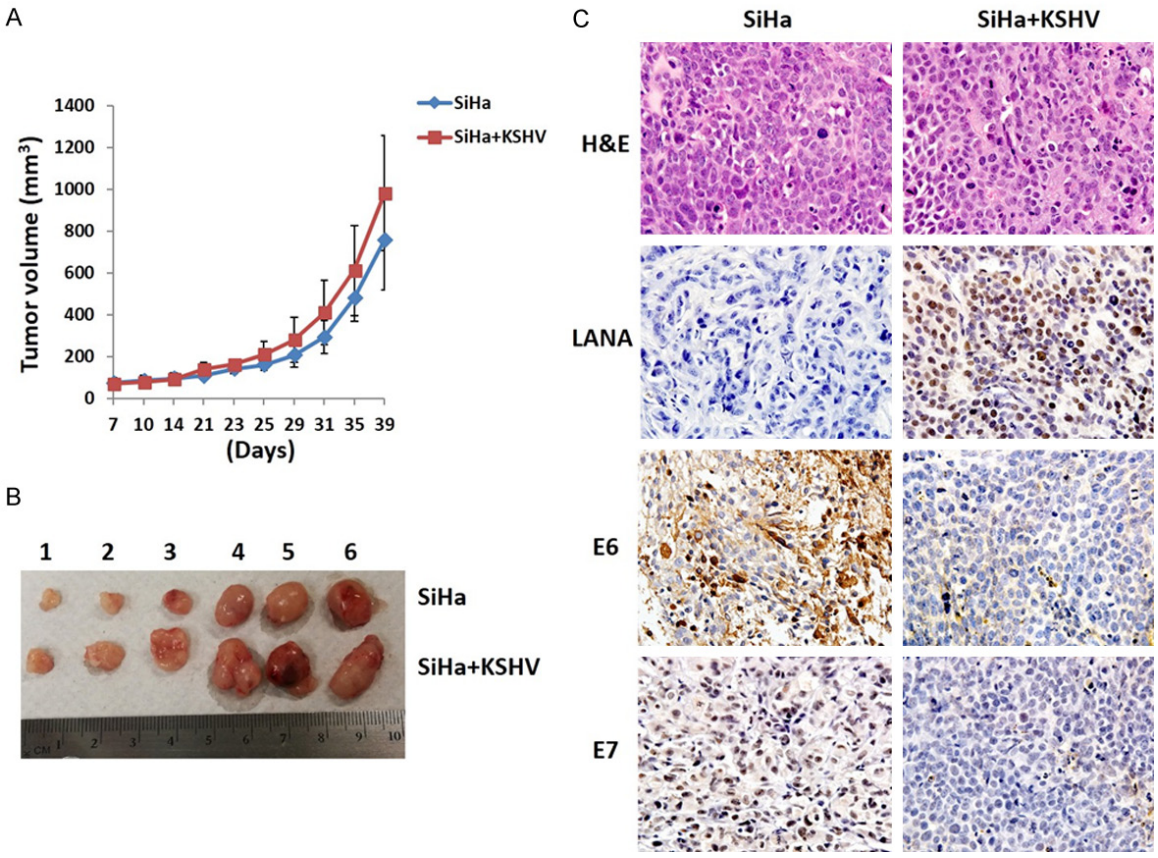

Figure 3. Comparison of tumorigenesis ability between mock and KSHV co-infected SiHa cells in a nude mice xenograft model. A, B. The mock and KSHV co-infected SiHa cells (approximately 5 × 10^5 cells were mixed at a ratio of 1:1 with growth factor-depleted Matrigel) were injected subcutaneously into the right flanks of nude mice, respectively. The mice were observed and measured every 2~3 d for the presence of palpable tumors for ~40 d. Error bars represent the S.D. from 2 independent experiments. C. Protein expression within tumor tissues from representative injected mice was measured by using immunohistochemistry staining as described in the Methods.

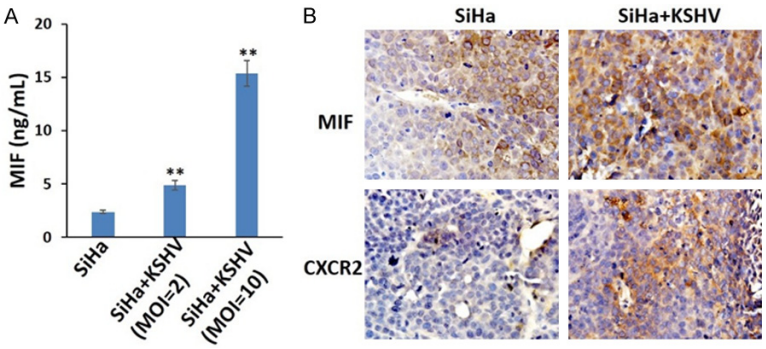

Figure 4. The up-regulation of MIF and its receptor by KSHV co-infection *in vitro* and *in vivo*. A. SiHa were incubated with purified KSHV (MOI~2 or 10), or medium control (mock) for 2 h. After cells were incubated for additional 72 h, MIF concentrations in supernatant were determined by using ELISA. Error bars represent the S.D. for 3 independent experiments, **=P < 0.01. B. The mock and KSHV co-infected SiHa cells were injected subcutaneously into the nude mice as described previously. Protein expression within tumor tissues from representative injected mice was measured by using immunohistochemistry staining.

have observed that there is no difference in cell invasiveness and anchorage-independent growth abilities between mock and KSHV co-infected SiHa cells (**Figure 2**), although KSHV co-infected cells seem to form a little larger size of colonies. Therefore, we think that KSHV or viral latent proteins can hijack HPV-encoded oncogenic proteins expression in cervical cancer cells, however, the new co-infected virus may use its unique mechanisms to maintain cervical cancer cells pathogenesis.

We next have compared the tumorigenesis ability between

mock and KSHV co-infected SiHa cells in a nude mice xenograft model. Our data indicate that the tumors formed by KSHV co-infected SiHa cells are a little bigger than those from mock cells during ~40 d growth in mice, but with no statistical significance (**Figure 3A**, **3B**). There are no architecture difference in the H&E staining tumor tissues between these two groups of mice (**Figure 3C**). By using immunohistochemistry staining, we confirm that more than 90% of tumor cells from KSHV co-infected SiHa injected mice are LANA+, which means these cells are still latently infected by KSHV [20]. In contrast, none of tumor cells from SiHa mock cells injected mice are LANA+ (**Figure 3C**). We also confirm that E6 and E7 proteins expression are dramatically repressed in tumor cells from KSHV co-infected SiHa injected mice (**Figure 3C**), which is consistent with what we have previously observed *in vitro* cultures (a 50%-70% of reduction of HPV16 E6 and E7 expression in KSHV co-infected SiHa cells) [15].

By using a cytokine/chemokine array, we recently have identified a global signature altered within KSHV co-infected SiHa when compared to the control mock cells [15]. We have found that KSHV co-infection increases several pro-inflammatory factors production, including an induction of ~8-fold increasing of Macrophage migration inhibitory factor (MIF) [15]. By using ELISA in the current study, we confirm that KSHV co-infection significantly increases MIF secretion from SiHa cells in a dose-dependent manner (**Figure 4A**). MIF is well recognized as a cancer biomarker protein [21-23], since its expression in normal cells is several orders of magnitude lower than levels observed in cancer cells [24]. For example, MIF protein levels can be 100-fold higher in lung cancer tissue over normal lung tissue, and MIF mRNA levels rise 7- to 24-fold in tumors [24]. Soluble MIF produced by cancer cells is imported into the cytoplasm and nucleus of its target cancer cells via an autocrine loop [25, 26]. MIF enters its target cells by binding to its cellular receptor such as CXCR2 and CD74 [26, 27]. Our data indicate that the obvious up-regulation of MIF and its receptor CXCR2 in tumor tissues from KSHV co-infected SiHa injected mice (**Figure 4B**). Interestingly, published literature has reported the overexpression of MIF in invasive cervical cancer samples compared to cervical dysplasias samples [28].

To test the cell line relevance, we also used purified KSHV to infect another HPV16+ cell line, CaSki. Similarly, we have also found that KSHV co-infection maintains CaSki cell growth, pathogenesis (invasion), increase MIF secretion while decreasing HPV16 E6 and E7 expression (Figure S1).

In conclusion, our data indicate that KSHV may manipulate some unique mechanisms (e.g., MIF/CXCR2) to maintain cervical cancer cells pathogenesis, although its co-infection hijacking HPV-encoded oncogenic proteins expression. Therefore, we still cannot exclude the possibility that KSHV as one of co-factors for cervical cancer development, even the detection rate of its co-infection in cervical samples are relatively low.

Acknowledgements

This work was supported by grants from a DOD Career Development Award (CA140437), a Louisiana Clinical and Translational Science Center Pilot grant (U54GM104940 from NIH), a LSU LIFT^2 funding and a NIH P20-GM1212-88-01 subproject as well as the awards from National Natural Science Foundation of China (81472547, 81400164, 81672924 and 8177-2930) and the Health Industry Project PW2-013E-1 from Pudong Health Bureau of Shanghai, China. Funding sources had no role in study design, data collection and analysis, decision to publish, or preparation of the manuscript.

Disclosure of conflict of interest

None.

Address correspondence to: Zhiqiang Qin, Suite 902, Louisiana Cancer Research Center, 1700 Tulane Ave., New Orleans, LA 70112, USA. Tel: 504-210-3327; E-mail: zqin@lsuhsc.edu

References

[1] Munoz N, Castellsague X, de Gonzalez AB and Gissmann L. Chapter 1: HPV in the etiology of human cancer. Vaccine 2006; 24 Suppl 3: S3/1-10.

[2] Narisawa-Saito M and Kiyono T. Basic mechanisms of high-risk human papillomavirus-induced carcinogenesis: roles of E6 and E7 proteins. Cancer Sci 2007; 98: 1505-1511.

[3] Longworth MS and Laimins LA. Pathogenesis of human papillomaviruses in differentiating

epithelia. Microbiol Mol Biol Rev 2004; 68: 362-372.
[4] Chaitanya NC, Allam NS, Gandhi Babu DB, Waghray S, Badam RK and Lavanya R. Systematic meta-analysis on association of human papilloma virus and oral cancer. J Cancer Res Ther 2016; 12: 969-974.
[5] Kim SM. Human papilloma virus in oral cancer. J Korean Assoc Oral Maxillofac Surg 2016; 42: 327-336.
[6] Mallen-St Clair J, Alani M, Wang MB and Srivatsan ES. Human papillomavirus in oropharyngeal cancer: the changing face of a disease. Biochim Biophys Acta 2016; 1866: 141-150.
[7] Chang Y, Cesarman E, Pessin MS, Lee F, Culpepper J, Knowles DM and Moore PS. Identification of herpesvirus-like DNA sequences in AIDS-associated Kaposi's sarcoma. Science 1994; 266: 1865-1869.
[8] Cesarman E, Chang Y, Moore PS, Said JW and Knowles DM. Kaposi's sarcoma-associated herpesvirus-like DNA sequences in AIDS-related body-cavity-based lymphomas. N Engl J Med 1995; 332: 1186-1191.
[9] Diamond C, Brodie SJ, Krieger JN, Huang ML, Koelle DM, Diem K, Muthui D and Corey L. Human herpesvirus 8 in the prostate glands of men with Kaposi's sarcoma. J Virol 1998; 72: 6223-6227.
[10] Howard MR, Whitby D, Bahadur G, Suggett F, Boshoff C, Tenant-Flowers M, Schulz TF, Kirk S, Matthews S, Weller IV, Tedder RS and Weiss RA. Detection of human herpesvirus 8 DNA in semen from HIV-infected individuals but not healthy semen donors. AIDS 1997; 11: F15-19.
[11] Koelle DM, Huang ML, Chandran B, Vieira J, Piepkorn M and Corey L. Frequent detection of Kaposi's sarcoma-associated herpesvirus (human herpesvirus 8) DNA in saliva of human immunodeficiency virus-infected men: clinical and immunologic correlates. J Infect Dis 1997; 176: 94-102.
[12] Calabro ML, Fiore JR, Favero A, Lepera A, Saracino A, Angarano G, Schulz TF and Chieco-Bianchi L. Detection of human herpesvirus 8 in cervicovaginal secretions and seroprevalence in human immunodeficiency virus type 1-seropositive and -seronegative women. J Infect Dis 1999; 179: 1534-1537.
[13] Whitby D, Smith NA, Matthews S, O'Shea S, Sabin CA, Kulasegaram R, Boshoff C, Weiss RA, de Ruiter A and Best JM. Human herpesvirus 8: seroepidemiology among women and detection in the genital tract of seropositive women. J Infect Dis 1999; 179: 234-236.
[14] de Sanjose S, Marshall V, Sola J, Palacio V, Almirall R, Goedert JJ, Bosch FX and Whitby D. Prevalence of Kaposi's sarcoma-associated herpesvirus infection in sex workers and women from the general population in Spain. Int J Cancer 2002; 98: 155-158.
[15] Dai L, Cao Y, Jiang W, Zabaleta J, Liu Z, Qiao J and Qin Z. KSHV co-infection down-regulates HPV16 E6 and E7 from cervical cancer cells. Oncotarget 2017; 8: 35792-35803.
[16] Zhang J, Li S, Yan Q, Chen X, Yang Y, Liu X and Wan X. Interferon-beta induced microRNA-129-5p down-regulates HPV-18 E6 and E7 viral gene expression by targeting SP1 in cervical cancer cells. PLoS One 2013; 8: e81366.
[17] Dai L, Trillo-Tinoco J, Cao Y, Bonstaff K, Doyle L, Del Valle L, Whitby D, Parsons C, Reiss K, Zabaleta J and Qin Z. Targeting HGF/c-MET induces cell cycle arrest, DNA damage, and apoptosis for primary effusion lymphoma. Blood 2015; 126: 2821-2831.
[18] Qin Z, Dai L, Toole B, Robertson E and Parsons C. Regulation of Nm23-H1 and cell invasiveness by Kaposi's sarcoma-associated herpesvirus. J Virol 2011; 85: 3596-3606.
[19] Dai L, Trillo-Tinoco J, Chen Y, Bonstaff K, Del Valle L, Parsons C, Ochoa AC, Zabaleta J, Toole BP and Qin Z. CD147 and downstream ADAMTSs promote the tumorigenicity of Kaposi's sarcoma-associated herpesvirus infected endothelial cells. Oncotarget 2016; 7: 3806-3818.
[20] Cotter MA 2nd and Robertson ES. The latency-associated nuclear antigen tethers the Kaposi's sarcoma-associated herpesvirus genome to host chromosomes in body cavity-based lymphoma cells. Virology 1999; 264: 254-264.
[21] Grieb G, Merk M, Bernhagen J and Bucala R. Macrophage migration inhibitory factor (MIF): a promising biomarker. Drug News Perspect 2010; 23: 257-264.
[22] Chang KP, Lin SJ, Liu SC, Yi JS, Chien KY, Chi LM, Kao HK, Liang Y, Lin YT, Chang YS and Yu JS. Low-molecular-mass secretome profiling identifies HMGA2 and MIF as prognostic biomarkers for oral cavity squamous cell carcinoma. Sci Rep 2015; 5: 11689.
[23] Gamez-Pozo A, Sanchez-Navarro I, Calvo E, Agullo-Ortuno MT, Lopez-Vacas R, Diaz E, Camafeita E, Nistal M, Madero R, Espinosa E, Lopez JA and Fresno Vara JA. PTRF/cavin-1 and MIF proteins are identified as non-small cell lung cancer biomarkers by label-free proteomics. PLoS One 2012; 7: e33752.
[24] Tomiyasu M, Yoshino I, Suemitsu R, Okamoto T and Sugimachi K. Quantification of macrophage migration inhibitory factor mRNA expression in non-small cell lung cancer tissues and its clinical significance. Clin Cancer Res 2002; 8: 3755-3760.
[25] Verjans E, Noetzel E, Bektas N, Schutz AK, Lue H, Lennartz B, Hartmann A, Dahl E and Bernhagen J. Dual role of macrophage migration inhibitory factor (MIF) in human breast cancer. BMC Cancer 2009; 9: 230.

[26] Leng L, Metz CN, Fang Y, Xu J, Donnelly S, Baugh J, Delohery T, Chen Y, Mitchell RA and Bucala R. MIF signal transduction initiated by binding to CD74. J Exp Med 2003; 197: 1467-1476.

[27] Bernhagen J, Krohn R, Lue H, Gregory JL, Zernecke A, Koenen RR, Dewor M, Georgiev I, Schober A, Leng L, Kooistra T, Fingerle-Rowson G, Ghezzi P, Kleemann R, McColl SR, Bucala R, Hickey MJ and Weber C. MIF is a noncognate ligand of CXC chemokine receptors in inflammatory and atherogenic cell recruitment. Nat Med 2007; 13: 587-596.

[28] Krockenberger M, Engel JB, Kolb J, Dombrowsky Y, Hausler SF, Kohrenhagen N, Dietl J, Wischhusen J and Honig A. Macrophage migration inhibitory factor expression in cervical cancer. J Cancer Res Clin Oncol 2010; 136: 651-657.

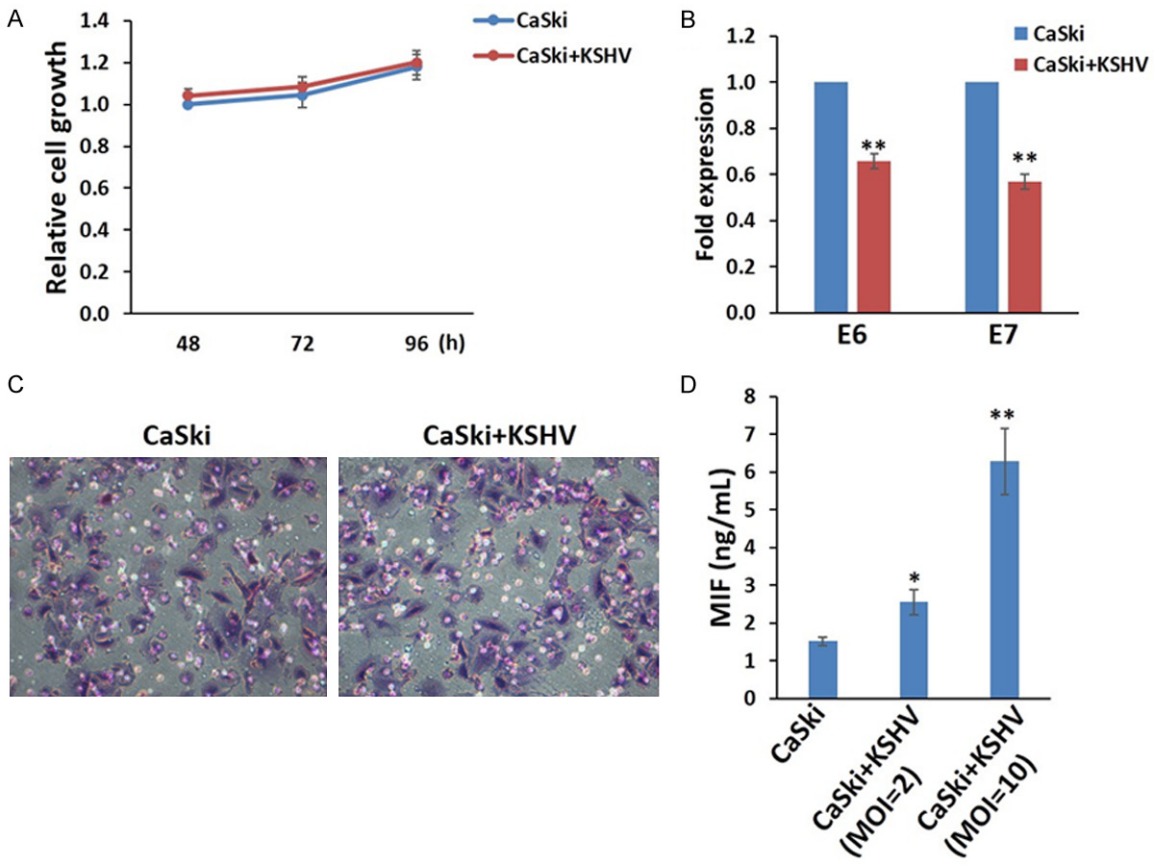

Figure S1. KSHV co-infection maintains CaSki cell pathogenesis although hijacking HPV-encoded oncogenic proteins expression. A. CaSki cells were incubated with purified KSHV (MOI~10), or medium control for 2 h. After cells were incubated for indicated additional time, cell proliferation was measured using the WST-1 assays. B, C. The gene transcripts were quantified by using qRT-PCR and the transwell assays were performed to determine cell invasiveness ability. D. CaSki were incubated with purified KSHV (MOI~2 or 10), or medium control for 2 h. After cells were incubated for additional 72 h, MIF concentrations in supernatant were determined by using ELISA. Error bars represent the S.D. for 3 independent experiments, *=P < 0.05; **=P < 0.01.

IJC
International Journal of Cancer

The sphingosine kinase 2 inhibitor ABC294640 displays anti-non-small cell lung cancer activities *in vitro* and *in vivo*

Lu Dai[1,2], Charles D. Smith[3], Maryam Foroozesh[4], Lucio Miele[1] and Zhiqiang Qin[1,2]

[1] Department of Genetics, Louisiana State University Health Sciences Center, Louisiana Cancer Research Center, 1700 Tulane Ave., New Orleans, LA
[2] Department of Pediatrics, Research Center for Translational Medicine and Key Laboratory of Arrhythmias, East Hospital, Tongji University School of Medicine, Shanghai 200120, China
[3] Apogee Biotechnology Corporation, Hummelstown, PA
[4] Department of Chemistry, Xavier University of Louisiana, 1 Drexel Drive, New Orleans, LA

Non-small cell lung cancer (NSCLC) accounts for about 85-90% of lung cancer cases, and is the number one killer among cancers in the United States. The majorities of lung cancer patients do not respond well to conventional chemo- and/or radiotherapeutic regimens, and have a dismal 5-year survival rate of ~15%. The recent introduction of targeted therapy and immunotherapy gives new hopes to NSCLC patients, but even with these agents, not all patients respond, and responses are rarely complete. Thus, there is still an urgent need to identify new therapeutic targets in NSCLC and develop novel anti-cancer agents. Sphingosine kinase 2 (SphK2) is one of the key enzymes in sphingolipid metabolism. SphK2 expression predicts poor survival in NSCLC patients, and is associated with Gefitinib-resistance. In this study, the anti-NSCLC activities of ABC294640, the only first-in-class orally available inhibitor of SphK2, were explored. The results obtained indicate that ABC294640 treatment causes significant NSCLC cell apoptosis, cell cycle arrest and suppression of tumor growth *in vitro* and *in vivo*. Moreover, lipidomics analyses revealed the complete signature of ceramide and dihydro(dh)-ceramide species in the NSCLC cell-lines with or without ABC294640 treatment. These findings indicate that sphingolipid metabolism targeted therapy may be developed as a promising strategy against NSCLC.

Key words: non-small cell lung cancer, sphingosine kinase, sphingolipid, ceramide
Additional Supporting Information may be found in the online version of this article.
Conflicts of interest: C.D. Smith is the President and Chief Executive Officer and has ownership interests (including patents) in Apogee Biotechnology Corporation. No potential conflicts of interest were disclosed by the other authors.
Grant sponsor: NIH; **Grant numbers:** P30-CA016059 and S10RR031535; **Grant sponsor:** Dr. Hua Lu at Tulane University (NSCLC cell-lines); **Grant sponsor:** DOD Career Development Award; **Grant number:** CA140437 (to Z. Qin); **Grant sponsor:** Louisiana Clinical and Translational Science Center Pilot; **Grant sponsor:** NIH; **Grant number:** U54GM104940; **Grant sponsor:** LSU LIFT; **Grant number:** P20-GM121288-01 (PI: Krzysztof Reiss) subproject to Z. Qin; **Grant sponsor:** National Natural Science Foundation of China; **Grant numbers:** 81472547 and 81672924 (to Z. Qin) and 81400164, 81772930 (to L. Dai); **Grant sponsor:** DoD Breast Cancer grant (M. Foroozesh group); **Grant number:** W81XWH-11–1-0105; **Grant sponsor:** NIH awards; **Grant numbers:** TL4GM118968, R25GM060926 and G12MD007595; **Grant sponsor:** Louisiana Cancer Research Center
DOI: 10.1002/ijc.31234
History: Received 22 Sep 2017; Accepted 14 Dec 2017; Online 26 Dec 2017
Correspondence to: Dr. Zhiqiang Qin, Suite 902, Louisiana Cancer Research Center, 1700 Tulane Ave., New Orleans, LA 70112, E-mail: zqin@lsuhsc.edu; Tel: (504)-210-3327

Introduction

Lung cancer is the number one killer among cancers in the United States with an estimated 155,870 deaths expected to occur in 2017.[1] It is also the second most diagnosed cancer in the United States, and is responsible for approximate 222,500 new cases in 2017.[1] Based on histological features and cells of origin, lung cancers can be classified as small cell lung cancer (SCLC), a neuro-endocrine tumor and non-small cell lung cancer (NSCLC), a group of epithelial-derived carcinomas including several subtypes. NSCLC accounts for about 85–90% of lung cancer cases. Clinically, the majority of lung cancer patients do not respond well to current chemo- and/or radiotherapeutic regimens, and have a very low 5-year survival rate of ~15%.[2] Recently, targeted therapy and immunotherapy have given new hopes to NSCLC patients, but the outcome/prognosis for most patients remains far from satisfactory. For instance, targeted therapeutic drugs such as Gefitinib that inhibits mutant epidermal growth factor receptor (EGFR), exhibit good initial effects. However, drug-resistance inevitably develops after 10 months of treatment, and patients eventually succumb to the disease.[3] Inhibition of immune checkpoint receptors or ligands such as PD-1 and PD-L1 has yielded good clinical responses and improved overall survival in certain NSCLC patients, primarily in squamous carcinomas. However, only 15–20% of NSCLC patients respond to such therapy, and affordability is a serious issue, since a single-course (7-month) treatment will cost more than $100,000.[4,5] Thus, there is an

What's new?

Therapeutic resistance and poor survival in non-small cell lung cancer (NSCLC) are associated with expression of sphingosine kinase 2 (SphK2), an enzyme involved in sphingolipid metabolism. Anti-tumor activity via SphK2 inhibition with the small molecule ABC294640 is possible, though data are limited for NSCLC. Here, in NSCLC cell lines and a mouse xenograft model, ABC294640 treatment was associated with tumor cell apoptosis, cell cycle arrest and reduced tumor growth. In NSCLC cells, ABC294640 treatment resulted in increased levels of bioactive sphingolipids, specifically ceramides and dihydro(dh)-ceramides. The data indicate that ABC294640 exerts significant anti-NSCLC activity *in vitro* and *in vivo*.

urgent need to better understand the mechanisms of lung carcinogenesis and to identify new therapeutic targets to improve the treatment of NSCLC.

Sphingolipid biosynthesis involves the hydrolysis of ceramides to generate sphingosine, which is subsequently phosphorylated by one of two sphingosine kinase isoforms (SphK1 or SphK2) to generate sphingosine-1-phosphate (S1P).[6,7] Bioactive sphingolipids including ceramides and S1P, can act as signaling molecules that regulate apoptosis and tumor cell survival.[6] In contrast to the generally pro-apoptotic function of ceramides, S1P promotes cell proliferation and survival.[7] S1P has been reported to promote the expansion of cancer stem cells through ligand-independent activation of Notch.[8] Given the importance of SphKs in sphingolipid metabolism, a highly selective and well-characterized small molecule inhibitor of SphK2, ABC294640, has been recently developed,[9,10] which displays significant anti-tumor activities for a variety of cancers such as lymphoma, prostate cancer, colorectal cancer, pancreatic cancer and cholangiocarcinoma.[11–15] However, there are limited data about the sphingolipid metabolism and targeted therapy in NSCLC. Johnson *et al.* examined 25 NSCLC tumor samples and reported that they all overwhelmingly exhibited positive immunostaining for SphK1 as compared with patient-matched normal tissues.[16] Wang *et al.* reported that NSCLC patients with SphK2 overexpression in their tissues had lower overall survival (OS) and disease-free survival (DFS) rates than those with low SphK2 expression.[17] Recently, Suzuki *et al.* reported that combined treatment with l-α-dimyristoylphosphatidylcholine liposome and the glucosylceramide synthase inhibitor D-PDMP induced NSCLC cell death associated with ceramide accumulation, and promoted cancer cell apoptosis and tumor regression in murine models.[18] In general, there is still limited information on the lipidomics of ceramide species in NSCLC cells or sphingolipid metabolism targeted therapy for NSCLC. In this study, lipidomics analyses were performed to identify the ceramide signature in NSCLC cell-lines with or without ABC294640 treatment. The anti-NSCLC activities of ABC294640 were also assessed *in vitro* and *in vivo*, and the underlying mechanisms were explored.

Materials and Methods

Cell culture and reagents

NSCLC cell lines (A549, H460, H1299) were kindly provided by Dr. Hua Lu at Tulane University, and cultured in RPMI-1640 medium supplemented with 10% fetal bovine serum and 1% penicillin & streptomycin. All experiments were carried out using cells harvested at low (<20) passages. 3–(4-chlorophenyl)-adamantane-1-carboxylic acid (pyridin-4-ylmethyl) amide (ABC294640) was synthesized as previously described.[9] The pan-caspase inhibitor, Z-VAD-FMK, was purchased from Sigma (St. Louis, MO).

Cell proliferation and apoptosis assays

Cell proliferation was measured using the WST-1 assays (Roche, Indianapolis, IN) according to the manufacturer's instructions. Flow cytometry was used for quantitative assessment of apoptosis with the FITC-Annexin V/propidium iodide (PI) Apoptosis Detection Kit I (BD Pharmingen, San Jose, CA).

Cell cycle analysis

NSCLC cell pellets were fixed in 70% ethanol, and incubated at 4°C overnight. Cell pellets were resuspended in 0.5 ml of 0.05 mg/ml PI plus 0.2 mg/ml RNaseA, and incubated at 37°C for 30 min. Cell cycle distribution was analyzed on a FACS Calibur 4-color flow cytometer (BD Bioscience, San Jose, CA).

RNA interference

For RNA interference (RNAi) assays, SphK2 ON-TARGETplus SMARTpool siRNA (Dharmacon, Lafayette, CO) or negative control siRNA (n-siRNA), were delivered using the DharmaFECT transfection reagent according to the manufacturer's instructions.

Immunoblotting

Total cell lysates (20 μg) were resolved by 10% SDS–PAGE, transferred to nitrocellulose membranes and immunoblotted with antibodies for SphK2, cleaved Caspase3/9, Myt1, phosphor-Cdc2, Cyclin B1, Cyclin D1, phosphor-Rb (Cell Signaling, Danvers, MA) and β-Actin (Sigma, St. Louis, MO) for loading controls. Immunoreactive bands were identified using an enhanced chemiluminescence reaction (Perkin-Elmer, Waltham, MA), and visualized by autoradiography.

Quantitative real-time PCR

Total RNA was isolated using the RNeasy Mini kit (Qiagen, Germantown, MD), and cDNA was synthesized from equivalent total RNA using a SuperScript III First-Strand Synthesis SuperMix Kit (Invitrogen, Waltham, MA) according to the manufacturer's instructions. Primers used for amplification of target genes are displayed in Supporting Information Table

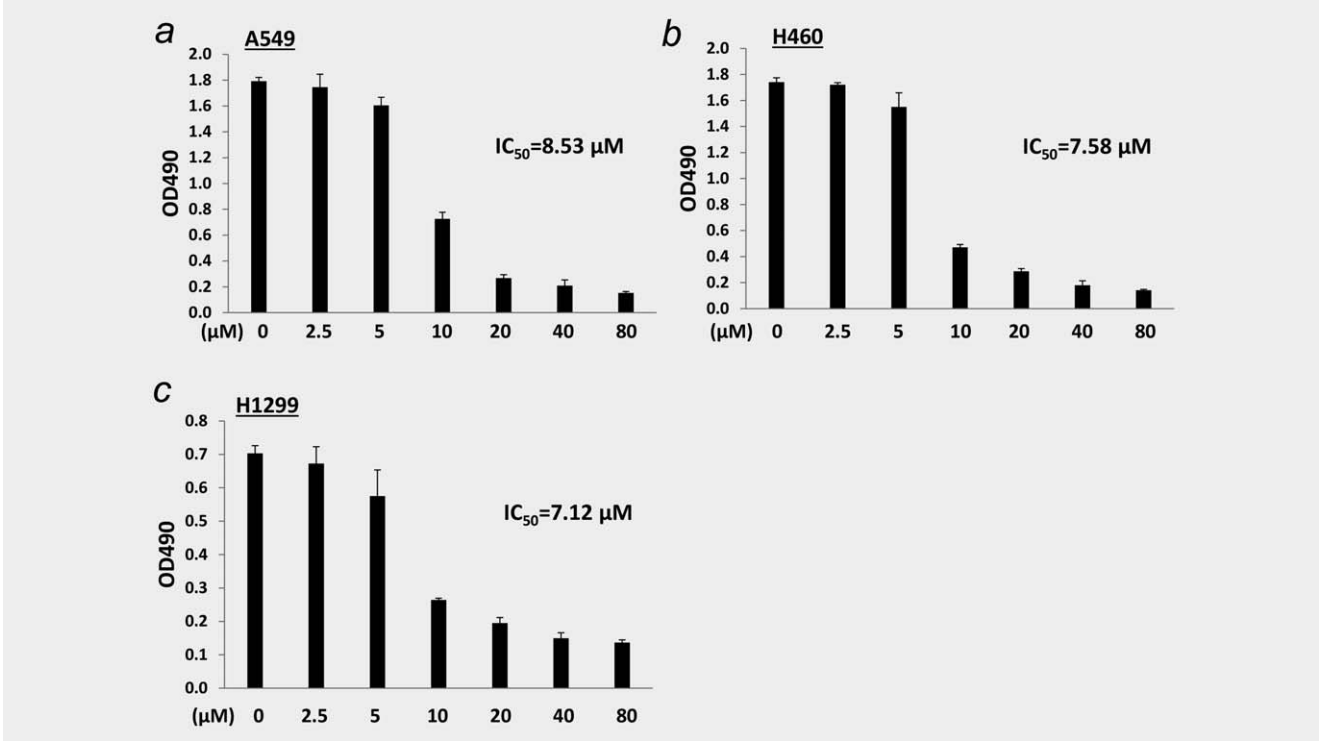

Figure 1. ABC294640 treatment represses the proliferation of NSCLC cell-lines. (*a–c*) NSCLC cell-lines A549, H460 and H1299 were incubated with the indicated concentrations of ABC294640 (ABC) for 72 hr; cell proliferation was measured using the WST-1 assays. Error bars represent the SD from three independent experiments. The 50% Inhibitory Concentration (IC_{50}) was calculated using SPSS 20.0 (Armonk, NY).

S1. Amplification was carried out using an iCycler IQ Real-Time PCR Detection System, and cycle threshold (*Ct*) values were tabulated in duplicate for each gene of interest in each experiment. "No template" (water) controls were used to ensure minimal background contamination. Using mean Ct values tabulated for each gene, and paired *Ct* values for β-actin as a loading control, fold changes for experimental groups relative to assigned controls were calculated using automated iQ5 2.0 software (Bio-Rad, Hercules, CA).

Sphingolipid analyses

Quantification of sphingolipid species was performed using a Thermo Finnigan TSQ 7000 triple-stage quadruple mass spectrometer operating in Multiple Reaction Monitoring positive ionization mode (Thermo Fisher Scientific, Waltham, MA). Quantification was based on calibration curves generated by spiking an artificial matrix with known amounts of target standards and an equal amount of the internal standard. The target analyte:internal standard peak area ratios from each sample were compared with the calibration curves using linear regression. Final results were expressed as the ratio of sphingolipid normalized to total phospholipid phosphate level using the Bligh and Dyer lipid extract method.[19]

Nude mice xenograft models

Cells were counted and washed once in ice-cold PBS. 5×10^5 H460 cells in 50 μl PBS plus 50 μl growth factor-depleted Matrigel (BD Biosciences, San Jose, CA) were injected subcutaneously into the flank of nude mice (Jackson Laboratory, Sacramento, CA). Five days after this injection, the mice were randomly separated into two groups and received i.p. injection with either vehicle or ABC294640 (75 mg/kg of body weight dissolved in PEG:ddH_2O as 1:1), 3 days/week. The mice were observed and measured every 2–3 days for the presence of palpable tumors. At the end of the experiment, the tumors were excised for subsequent analyses. The animal experiments were repeated twice. All protocols were approved by the LSUHSC Animal Care and Use Committee in accordance with national guidelines.

Statistical analysis

Significance for differences between experimental and control groups was determined using the two-tailed Student's *t* test (Excel 8.0), and *p* values <0.05 or <0.01 were considered significant or highly significant, respectively.

Results

Targeting SphK2 reduces NSCLC cell-lines proliferation in a dose-dependent manner

ABC294640 treatment alone was found to dramatically reduce the proliferation in NSCLC cell-lines (A549, H460, H1299) in a dose-dependent manner as determined by the WST-1 cell proliferation assays (Fig. 1). Notably, although H1299 cells have a homozygous partial deletion of p53 and

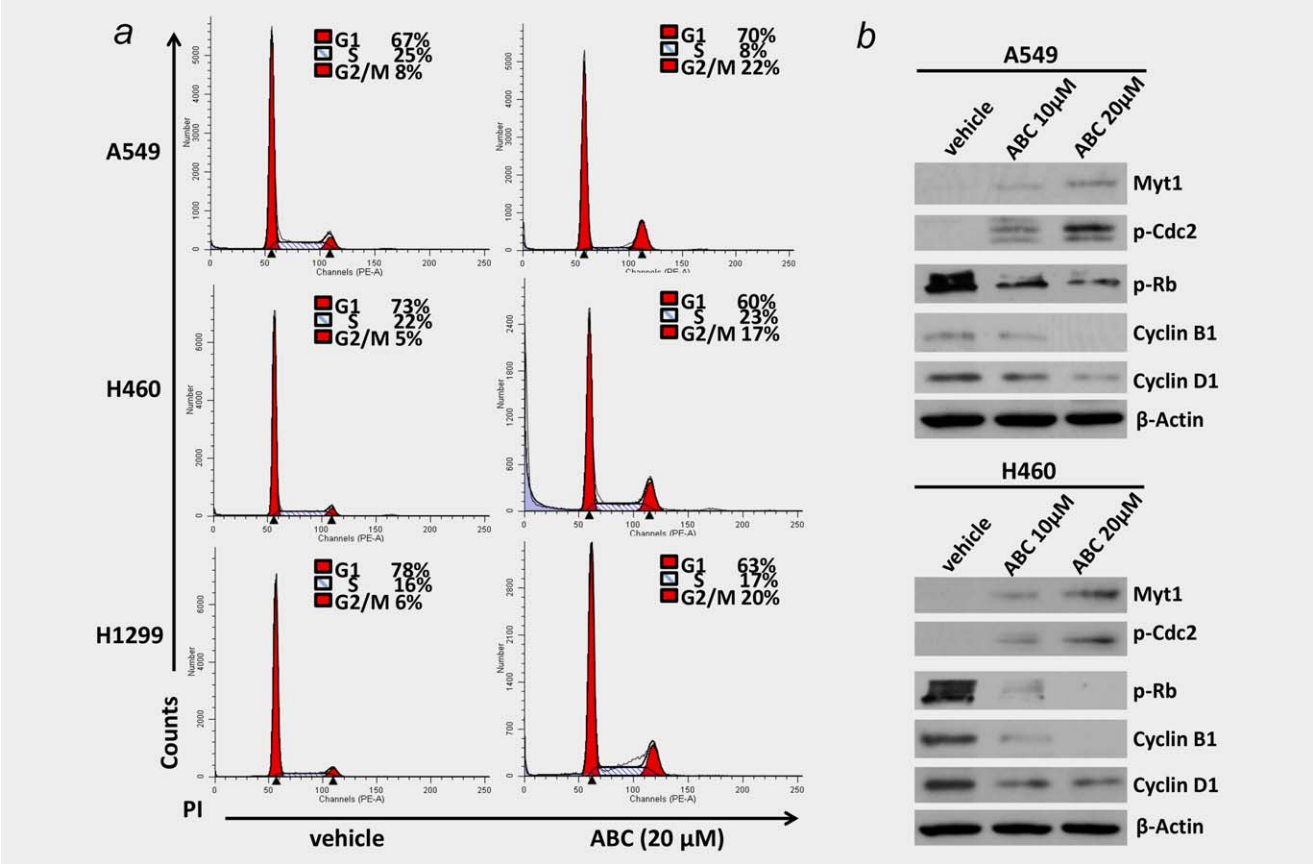

Figure 2. ABC294640 treatment causes NSCLC cell-lines G2 cell cycle arrest. (*a* and *b*) NSCLC cell-lines A549, H460 and H1299 were incubated with 10 or 20 μM of ABC294640 (ABC) or vehicle for 48 hr, then stained by propidium iodide (PI) and analyzed by flow cytometry. Protein expression was analyzed by immunoblot analysis. The experiments were repeated twice, and one representative experiment results were shown. [Color figure can be viewed at wileyonlinelibrary.com]

mutant *NRAS*,[20] ABC294640 displayed similar efficacy among these three NSCLC cell-lines (IC_{50} ranges 7.0–8.0 μM). To further confirm the impact of targeting SphK2 in the NSCLC cell proliferation, RNAi was used to directly silence SphK2, which also significantly reduced NSCLC cell-lines proliferation (Supporting Information Fig. S1).

Targeting SphK2 induces NSCLC cell cycle arrest and apoptosis

To further investigate the mechanisms through which ABC294640 reduces NSCLC cell proliferation, cell cycle distribution was analyzed by flow cytometry. It was found that ABC294640 treatment causes significant G2 phase arrest in all of the 3 NSCLC cell-lines tested (Fig. 2*a*). Subsequent immunoblot analyses indicated that ABC294640 regulates the expression of several cell cycle check-point factors, including the upregulation of Myt1 and phospho-Cdc2, as well as the downregulation of phosphor-Rb, Cyclin B1 and Cyclin D1 in A549 and H460 cells (Fig. 2*b*). Subsequent qRT-PCR analyses demonstrated that ABC294640 downregulates Cyclin B1 and Cyclin D1 at the transcriptional level as well (Supporting Information Fig. S2). Furthermore, silencing SphK2 by RNAi also induced G2 cell cycle arrest in NSCLC cells, although at a lower extent than those caused by ABC294640 (Supporting Information Fig. S3).

ABC294640 treatment was found to cause apparent apoptosis in NSCLC cell-lines as detected by Annexin-V/PI staining and flow cytometry analysis (Fig. 3*a*). The data obtained indicated that ABC294640 induces a dose-dependent increase of cleaved caspase 3 and caspase 9 levels in A549 and H460 cells, while a pan-caspase inhibitor, Z-VAD-FMK (Z-VAD), almost completely protects NSCLC cells from the apoptosis induced by ABC294640 (Figs. 3*b* and 3*c*). In addition, silencing of SphK2 by RNAi caused significant cell apoptosis in A549 and H460 cell-lines (Supporting Information Fig. S4). Taken together, the results demonstrate that targeting SphK2 reduces NSCLC cell proliferation through inducing cell cycle arrest and caspase-dependent apoptosis.

ABC294640 increases the production of intracellular ceramides and dihydro(dh)-ceramides and alters their composition in NSCLC cells

Mass spectrometric-based lipidomics analyses were used to quantify intracellular levels of bioactive ceramide/dh-ceramide species in NSCLC cell-lines. It was observed that

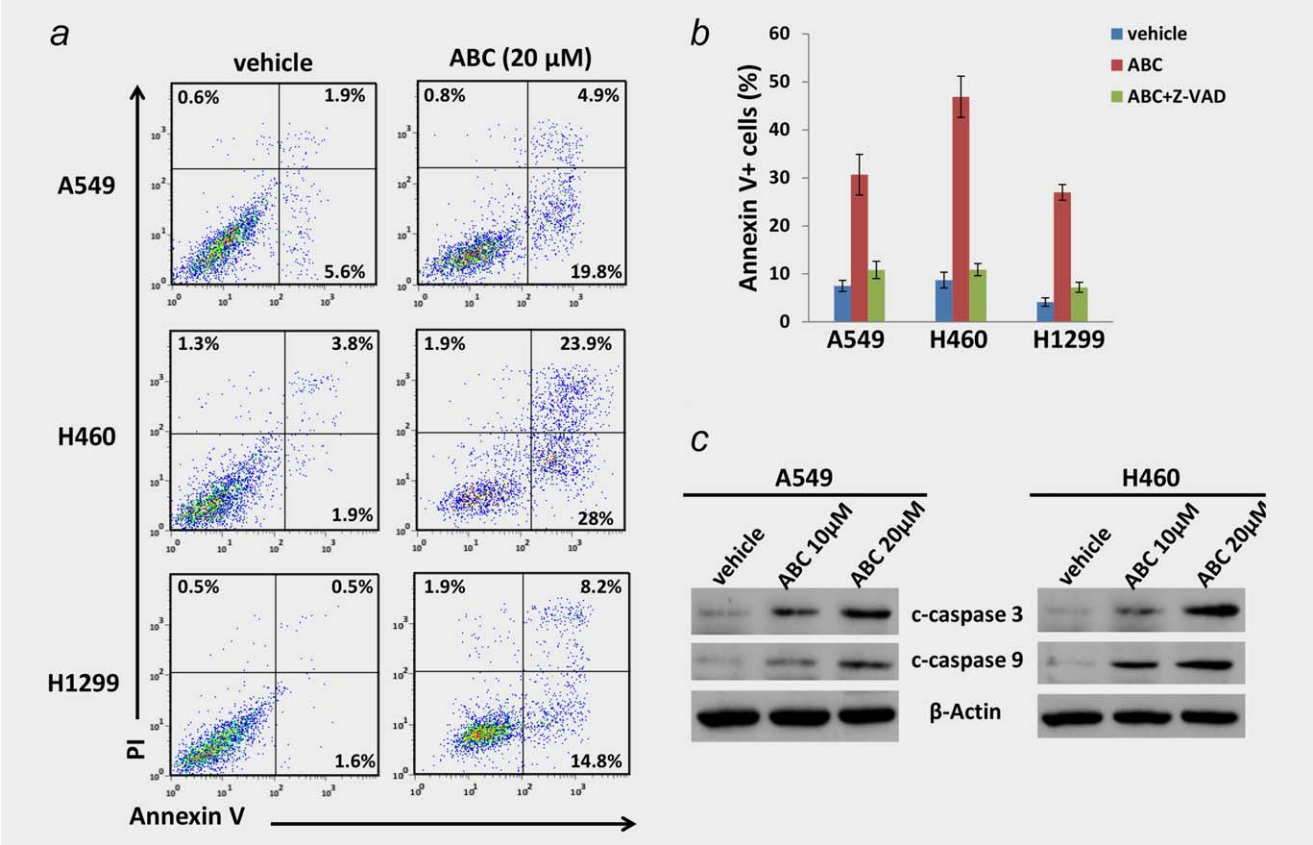

Figure 3. ABC294640 treatment induces NSCLC cell-lines apoptosis. (*a* and *b*) NSCLC cell-lines A549, H460 and H1299 were incubated with 20 μM of ABC294640 (ABC) or vehicle in the presence or absence of the pan-caspase inhibitor Z-VAD-FMK (Z-VAD, 10 μM) for 48 hr; cell apoptosis was measured using Annexin V-PI staining and flow cytometry analysis. Error bars represent the SD from three independent experiments. (*c*) NSCLC cell-lines were incubated with 10 or 20 μM of ABC294640 (ABC) or vehicle for 48 hr; protein expression was analyzed using immunoblot analysis.

ABC294640 increases total levels of intracellular ceramides (1.5–3.5 folds) and dh-ceramides (3.0–7.5 folds) in the 3 NSCLC cell-lines tested (Fig. 4*a*). The lipidomics analyses of individual ceramide and dh-ceramide species indicated that most species including C14∼C26-Cer and dhC14∼dhC26-Cer were upregulated in the 3 NSCLC cell-lines exposed to ABC294640, although the extent of the increases varies among these cell-lines (Figs. 4b–4d). Since SphKs are responsible for phosphorylating sphingosine and generating S1P, it is not surprising to observe that ABC294640 treatment significantly reduces intracellular S1P levels and increases sphingosine levels in all the 3 NSCLC cell-lines (Supporting Information Fig. S5). Interestingly, a reduction of total sphingomyelin levels in NSCLC cell-lines exposed to ABC294640 was also observed (Supporting Information Fig. S6), implying that sphingomyelin hydrolysis[21] may contribute to ABC294640-induced ceramides production.

The composition and proportion of individual ceramide and dh-ceramide species were calculated within the total lipid mass of NSCLC cell-lines with or without ABC294640 treatment (Figs. 5*a* and 5*b*). First, the top predominant ceramide/dh-ceramide species were identified within the NSCLC cell-lines studied, including C16-, C22-, C24:1-, C24-, dhC16-, dhC18-, dhC22-, dhC24:1- and dhC24-Cer (Fig. 5*c*). Despite subtle differences, NSCLC cell-lines display a consistent ceramide signature. Second, it was found that ABC294640 treatment greatly alters the proportion of individual ceramide and dh-ceramide species within the NSCLC cell-lines studied (Fig. 5*d*). The most common proportional changes observed in all 3 NSCLC cell-lines include increased dhC22-Cer, and decreased C16-Cer and dhC16-Cer.

ABC294640 treatment effectively represses NSCLC tumor growth *in vivo*

By using an established H460 xenograft mice model, the effect of ABC294640 on NSCLC tumor growth was tested *in vivo*. H460 cells (5×10^5 cells, 1:1 with growth factor-depleted Matrigel) were injected subcutaneously into the flank of nude mice (5 mice per group). Five days after injection, the mice were randomly separated into two groups and received i.p. injections with either vehicle or ABC294640 (75 mg/kg of body weight), 3 days/week. The mice were observed every 2–3 days, and palpable tumors were measured over an additional 3 weeks. Results obtained indicate that

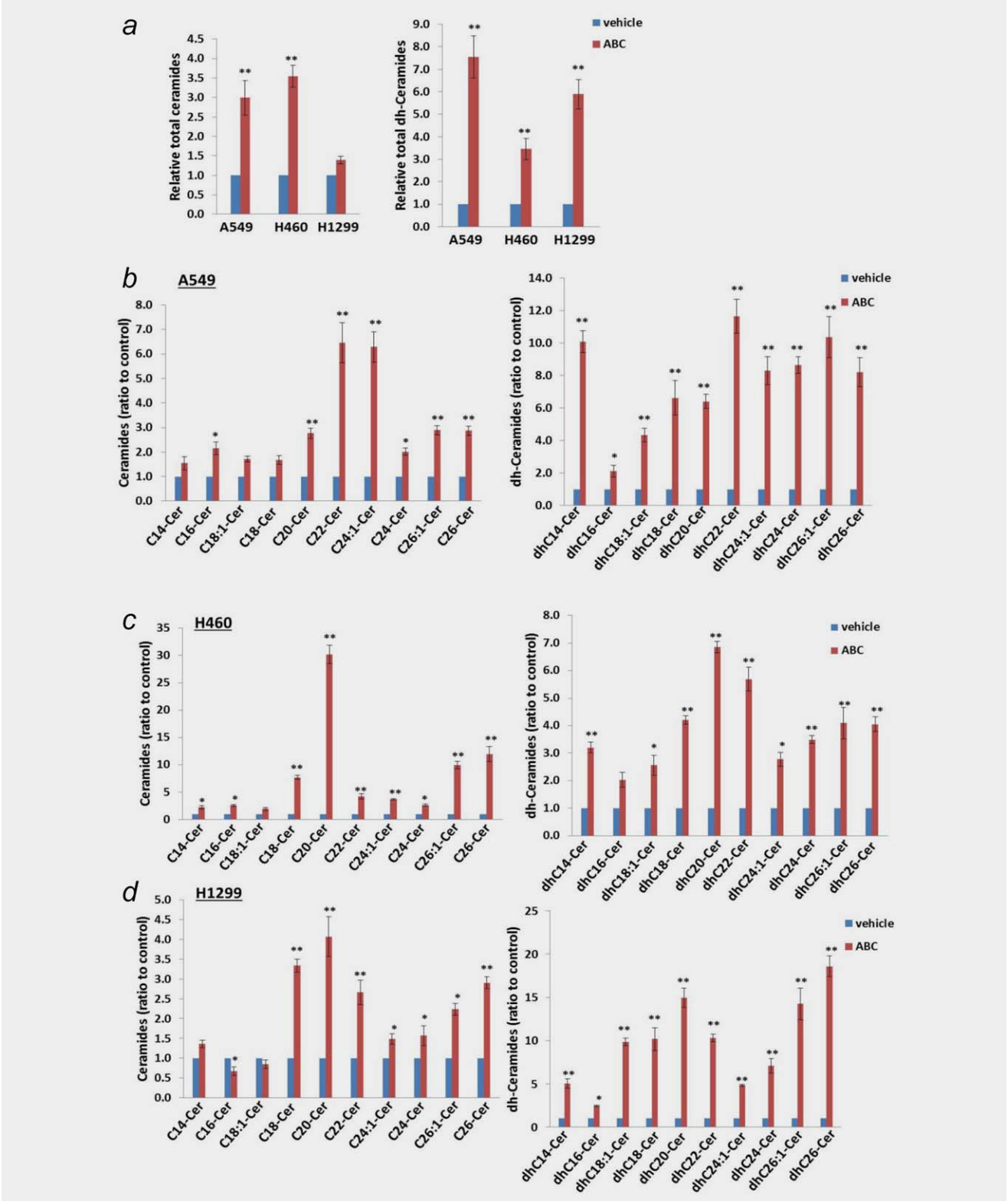

Figure 4. ABC294640 treatment induces intracellular ceramides production from NSCLC cell-lines. (*a–d*) NSCLC cell-lines A549, H460 and H1299 were incubated with vehicle or 20 μM of ABC294640 (ABC) for 48 hr; ceramide and dihydro(dh)-ceramide species were quantified using lipidomics analysis as described in the Methods. Error bars represent the SD from three independent experiments. * = $p < 0.05$, ** = $p < 0.01$. [Color figure can be viewed at wileyonlinelibrary.com]

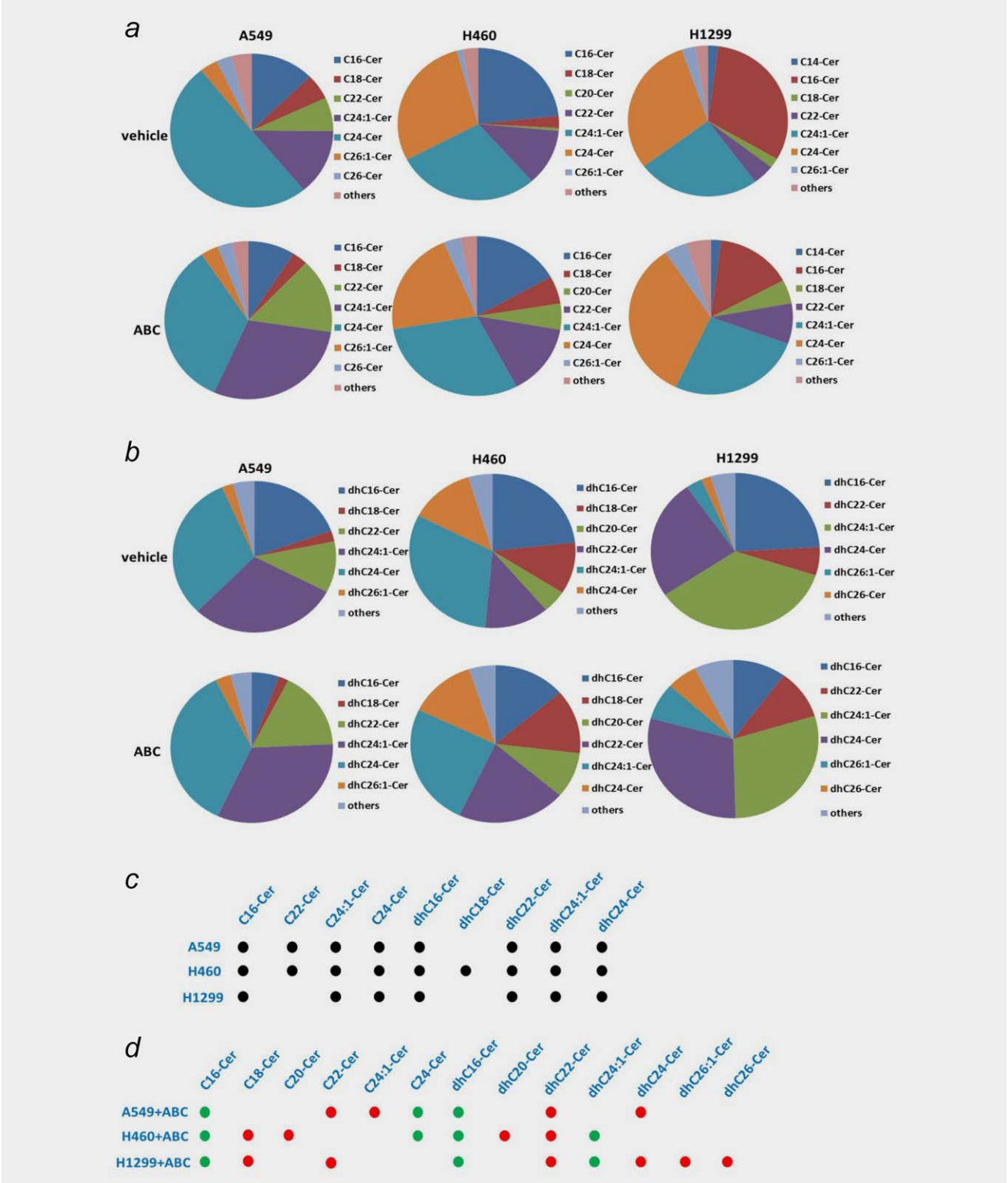

Figure 5. The compositions and proportions of ceramide/dh-ceramide species in NSCLC cell-lines are altered by ABC294640. (*a* and *b*) Relative compositions and proportions of specific ceramide and dh-ceramide species present within vehicle- or ABC-treated NSCLC cell-lines are shown. Each color is representing a specific ceramide species and is labeled beside the pie chart. (*c* and *d*) Black dots represent the top prominent ceramide/dh-ceramide species present in NSCLC cell-lines. Red and green dots represent upregulated or downregulated ceramide/dh-ceramide species in NSCLC cell-lines exposed to ABC, respectively.

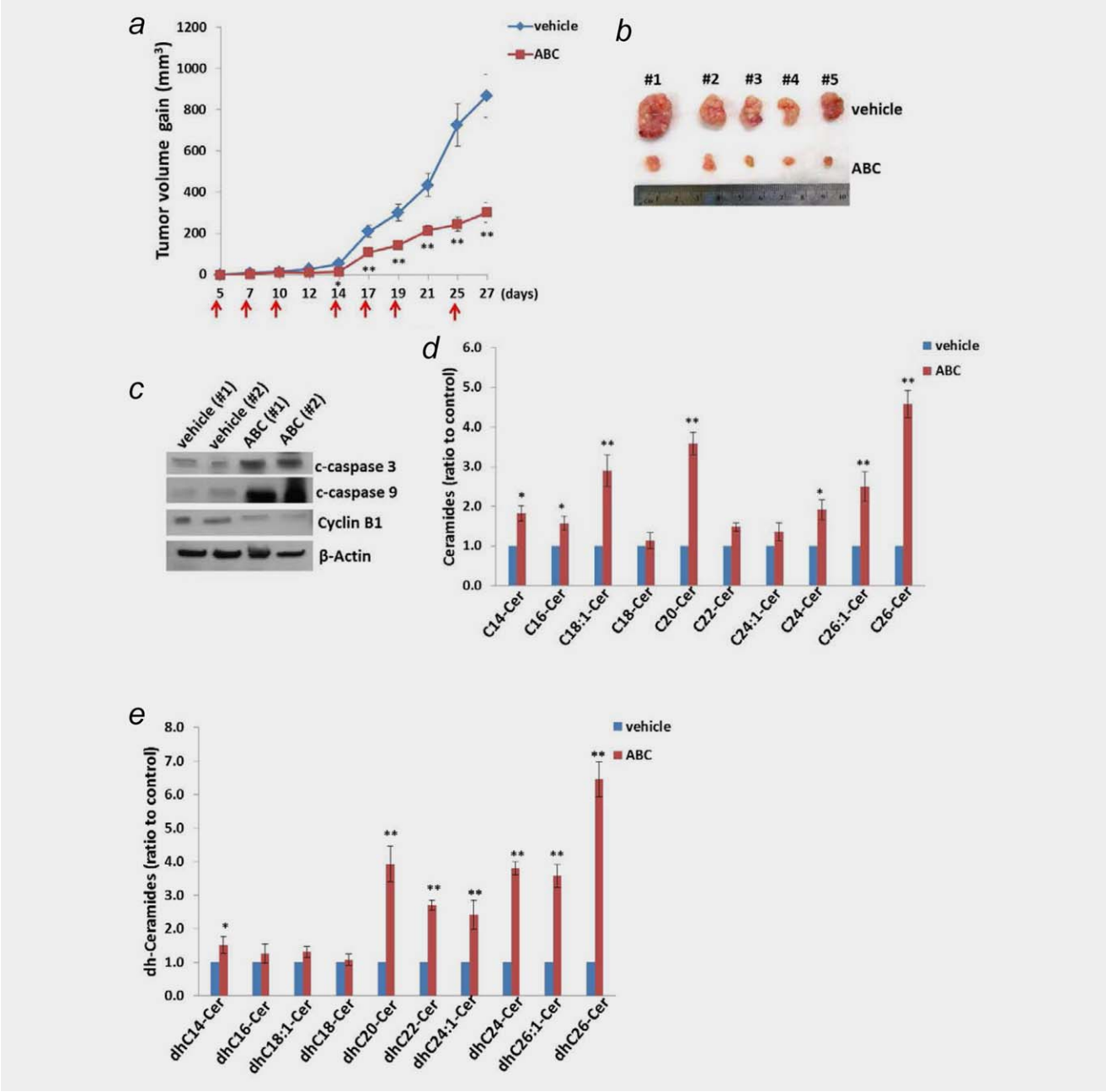

Figure 6. ABC294640 treatment effectively represses NSCLC growth *in vivo*. (*a* and *b*) NSCLC H460 cells (5×10^5 cells, 1:1 with growth factor-depleted Matrigel) were injected subcutaneously into the flank of nude mice. Five days after this injection, the mice were randomly separated into two groups and received i.p. injection with either vehicle or ABC294640 (75 mg/kg of body weight), 3 days/week. The arrows indicate the time points when ABC294640 or vehicle was administered. The mice were observed and measured every 2–3 days for the size of palpable tumors over an additional 3 weeks. At the end of the experiment, the tumors were excised for subsequent analyses. The numbers 1–5 represent different mice from the same group. Error bars represent the SD from one of the two independent experiments. (*c*–*e*) Protein expression in tumor tissues from representative mice was measured using immunoblots. The ceramide and dihydro(dh)-ceramide species within tumor tissues were quantified using lipidomics analysis as described in the Methods. Error bars represent the SD from three mice from each group. * = $p < 0.05$, ** = $p < 0.01$. [Color figure can be viewed at wileyonlinelibrary.com]

ABC294640 treatment alone significantly represses tumor growth in mice compared to those observed in vehicle-treated mice (Fig. 6*a*). After the 3-week treatment period, the tumors isolated from ABC294640-treated mice had significantly smaller size than those from vehicle-treated mice (Fig. 6*b*). Immunoblot analyses confirmed increased expression of cleaved caspase 3 and caspase 9, and reduced expression of Cyclin B1 within tumor tissues from representative ABC294640-treated mice when compared to those from the vehicle-treated mice (Fig. 6*c*). Lipidomics analyses indicated

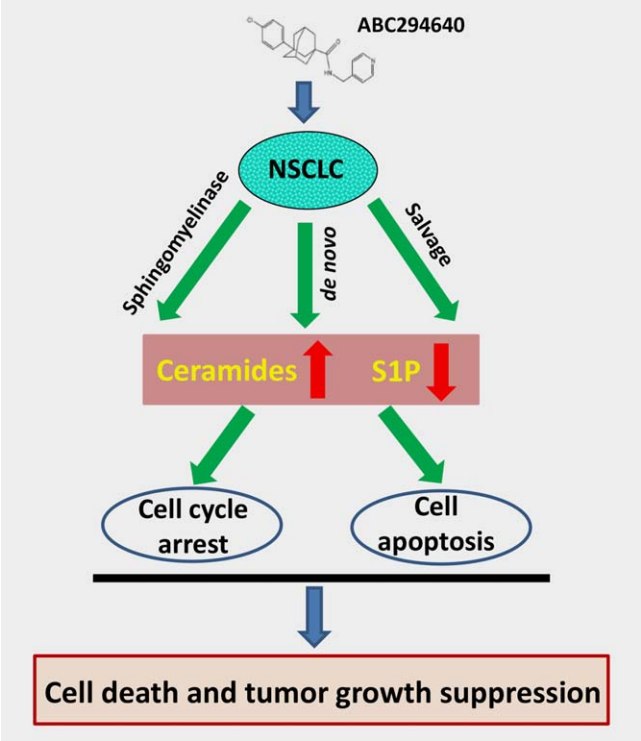

Figure 7. Schematic diagram of the possible mechanisms for anti-NSCLC activities of ABC294640. [Color figure can be viewed at wileyonlinelibrary.com]

that many ceramide and dh-ceramide species were upregulated in tumor tissues of the ABC294640-treated mice when compared to those of the vehicle-treated mice (Figs. 6*d* and 6*e*), although the extents of these increases and sphingolipids patterns were subtly different from what we observed *in vitro*.

Discussion

There are three major pathways of ceramide generation: the sphingomyelinase pathway (sphingomyelin→ceramide); the *de novo* pathway (3-keto-dihydrosphingosine→dihydrosphingosine→dihydroceramide→ceramide); and the salvage pathway (S1P→sphingosine→ceramide).[22,23] ABC294640, a selective inhibitor of SphK2 (an enzyme responsible for phosphorylating sphingosine and generating S1P), significantly reduces intracellular S1P levels and increases sphingosine levels in NSCLC cell-lines, through blocking the salvage pathway. ABC294640 treatment also greatly reduces the total levels of sphingomyelin, implying that the *de novo* pathway and sphingomyelinase pathway are also indirectly affected by ABC294640 in NSCLC cell-lines (Fig. 7). Our group is currently determining which ceramide synthases (CerSs, the key enzymes for ceramide generation in both the *de novo* pathway and the salvage pathway) and/or sphingomyelinases (SMases, the key enzymes for ceramide generation in the sphingomyelinase pathway) are responsible for ABC294640-induced ceramide production in NSCLC cells. At present, six different CerSs have been identified, CerS1–6,[24] and different isoforms of CerS generate an array of ceramide species with distinct chain lengths of fatty acids.[25] Previous data have shown that ABC294640 treatment increases the levels of several CerSs in a virus-associated lymphoma *in vitro* and *in vivo*.[26] The SMases are divides into acidic, neutral and alkaline forms dependent on their pH optimum.[27] For example, acidic SMase is localized in the lysosomal compartment and can also be secreted in the extracellular space.[28] Neutral SMase is present in the plasma membrane, cytoplasm and the nucleus.[21] In this study, it was also found that ABC294640 treatment increases a variety of dihydroceramides production in NSCLC cells. Interestingly, recent data have shown that ABC294640 can also inhibit dihydroceramide desaturase activity, resulting in the accumulation of dihydroceramides in prostate cancer cells, which is dispensable with SphK2 expression.[12,29]

Here, it is reported that ABC294640 treatment can induce significant caspase-dependent apoptosis in NSCLC cells, which is closely related to increased intracellular production of ceramides. In fact, published reports have shown that ceramides can activate protein phosphatase 2A (PP2A) directly by binding inhibitor 2 of PP2A (I2PP2A/SET), thereby reducing the association between PP2A and its inhibitors.[30,31] The effect of ceramides on PP2A leads to inactivation of Akt through dephosphorylation. In addition, apoptosis signal-regulating kinase 1 (Ask1) is a member of the mitogen-activated protein kinase kinase kinase (MAPKKK) family, which can be activated by ceramide, and initiates apoptosis.[32] Our results have previously shown that ABC294640 treatment can affect the activities of the Akt and MAPK pathways in a virus-associated lymphoma.[11] Mitochondrial outer membrane permeabilization (MOMP) is a critical step in apoptosis. Ceramide is considered to be the main substance that induces MOMP, which is a key event in apoptotic signaling through the formation of ceramide channels to facilitate the passage of proteins released during MOMP.[33] Ganesan *et al.* have indicated that ceramides are the key permeabilizing entity, and that Bax and ceramides can synergistically generate MOMP.[34] Ceramides can also contribute to MOMP by inducing the translocation to the mitochondria and activation of protein kinase C δ (PKC δ), which in turn promotes caspase 9 activation and cytochrome c release.[35] Further studies will determine which of these mechanisms is most prominent for the pro-apoptotic activity of ABC294640 in NSCLC cells.

The study reported here only focuses on single-agent ABC294640 treatment of NSCLC cells. A recent study reports that ABC294640 combined with tumor necrosis factor-related apoptosis-inducing ligand (TRAIL) can enhance the apoptosis of NSCLC cells.[36] Another recent study reports that inhibition of ceramide glucosylation by either a glucosylceramide synthase (GCS) inhibitor or GCS shRNA/siRNA knockdown can enhance ABC294640-induced NSCLC cell apoptosis.[37] Li and Zhang have summarized recent studies on combinations of chemotherapeutic drugs and ceramide-generating agents (e.g., CerS or SMase inducers) or modulators of ceramide metabolism (e.g., GCS or SphK inhibitors).[27] Generally,

ceramide inducers sensitize cancer cells to anticancer agents resulting in enhanced cell apoptosis and death.[27] Very recently, Britten *et al.* have reported promising results from a Phase I Study of ABC294640 in patients with advanced solid tumors.[38] They found that at 500 mg bid, ABC294640 was well tolerated and achieves biologically relevant plasma concentrations. These data together with the findings reported here indicate that sphingolipid metabolism targeted therapy may have broad prospects for clinical applications in oncology. An important question to be addressed is whether these agents target cancer stem-like cells, which are typically resistant to standard of care chemotherapy and are thought to be responsible for relapse and metastasis in many malignancies including lung cancer.

Acknowledgements

Funding sources had no role in study design, data collection and analysis, decision to publish or preparation of the manuscript.

References

1. American Cancer Society. Cancer facts & figures 2017. Atlanta: American Cancer Society, 2017.
2. Molina JR, Yang P, Cassivi SD, *et al.* Non-small cell lung cancer: epidemiology, risk factors, treatment, and survivorship. *Mayo Clin Proc* 2008;83: 584–94.
3. Ware KE, Hinz TK, Kleczko E, *et al.* A mechanism of resistance to gefitinib mediated by cellular reprogramming and the acquisition of an FGF2-FGFR1 autocrine growth loop. *Oncogenesis* 2013;2:e39.
4. Sundar R, Cho BC, Brahmer JR, *et al.* Nivolumab in NSCLC: latest evidence and clinical potential. *Ther Adv Med Oncol* 2015;7:85–96.
5. Andrews A. Treating with checkpoint inhibitors-figure $1 million per patient. *Am Health Drug Benefits* 2015;8:9.
6. Ogretmen B, Hannun YA. Biologically active sphingolipids in cancer pathogenesis and treatment. *Nat Rev Cancer* 2004;4:604–16.
7. Takabe K, Paugh SW, Milstien S, *et al.* Inside-out" signaling of sphingosine-1-phosphate: therapeutic targets. *Pharmacol Rev* 2008;60:181–95.
8. Hirata N, Yamada S, Shoda T, *et al.* Sphingosine-1-phosphate promotes expansion of cancer stem cells via S1PR3 by a ligand-independent Notch activation. *Nat Commun* 2014;5:4806.
9. French KJ, Schrecengost RS, Lee BD, *et al.* Discovery and evaluation of inhibitors of human sphingosine kinase. *Cancer Res* 2003;63:5962–9.
10. French KJ, Zhuang Y, Maines LW, *et al.* Pharmacology and antitumor activity of ABC294640, a selective inhibitor of sphingosine kinase-2. *J Pharmacol Exp Ther* 2010;333:129–39.
11. Qin Z, Dai L, Trillo-Tinoco J, *et al.* Targeting sphingosine kinase induces apoptosis and tumor regression for KSHV-associated primary effusion lymphoma. *Mol Cancer Ther* 2014;13:154–64.
12. Venant H, Rahmaniyan M, Jones EE, *et al.* The sphingosine kinase 2 inhibitor ABC294640 reduces the growth of prostate cancer cells and results in accumulation of dihydroceramides in vitro and in vivo. *Mol Cancer Ther* 2015;14:2744–52.
13. Xun C, Chen MB, Qi L, *et al.* Targeting sphingosine kinase 2 (SphK2) by ABC294640 inhibits colorectal cancer cell growth in vitro and in vivo. *J Exp Clin Cancer Res* 2015;34:94.
14. Lewis CS, Voelkel-Johnson C, Smith CD. Suppression of c-Myc and RRM2 expression in pancreatic cancer cells by the sphingosine kinase-2 inhibitor ABC294640. *Oncotarget* 2016;7: 60181–92.
15. Ding X, Chaiteerakij R, Moser CD, *et al.* Antitumor effect of the novel sphingosine kinase 2 inhibitor ABC294640 is enhanced by inhibition of autophagy and by sorafenib in human cholangiocarcinoma cells. *Oncotarget* 2016;7:20080–92.
16. Johnson KR, Johnson KY, Crellin HG, *et al.* Immunohistochemical distribution of sphingosine kinase 1 in normal and tumor lung tissue. *J Histochem Cytochem* 2005;53:1159–66.
17. Wang Q, Li J, Li G, *et al.* Prognostic significance of sphingosine kinase 2 expression in non-small cell lung cancer. *Tumour Biol* 2014;35:363–8.
18. Suzuki M, Cao K, Kato S, *et al.* Targeting ceramide synthase 6-dependent metastasis-prone phenotype in lung cancer cells. *J Clin Invest* 2015; 126:254–65.
19. Bielawski J, Szulc ZM, Hannun YA, *et al.* Simultaneous quantitative analysis of bioactive sphingolipids by high-performance liquid chromatography-tandem mass spectrometry. *Methods* 2006;39:82–91.
20. Phelps RM, Johnson BE, Ihde DC, *et al.* NCI-navy medical oncology branch cell line data base. *J Cell Biochem Suppl* 1996;24:32–91.
21. Huwiler A, Zangemeister-Wittke U. Targeting the conversion of ceramide to sphingosine 1-phosphate as a novel strategy for cancer therapy. *Crit Rev Oncol Hematol* 2007;63:150–9.
22. Liu J, Beckman BS, Foroozesh M. A review of ceramide analogs as potential anticancer agents. *Future Med Chem* 2013;5:1405–21.
23. Hannun YA, Obeid LM. Principles of bioactive lipid signaling: lessons from sphingolipids. *Nat Rev Mol Cell Biol* 2008;9:139–50.
24. Stiban J, Tidhar R, Futerman AH. Ceramide synthases: roles in cell physiology and signaling. *Adv Exp Med Biol* 2010;688:60–71.
25. Hannun YA, Obeid LM. Many ceramides. *J Biol Chem* 2011;286:27855–62.
26. Dai L, Trillo-Tinoco J, Bai A, *et al.* Ceramides promote apoptosis for virus-infected lymphoma cells through induction of ceramide synthases and viral lytic gene expression. *Oncotarget* 2015;6: 24246–60.
27. Li F, Zhang N. Ceramide: therapeutic potential in combination therapy for cancer treatment. *Curr Drug Metab* 2015;17:37–51.
28. Aureli M, Murdica V, Loberto N, *et al.* Exploring the link between ceramide and ionizing radiation. *Glycoconj J* 2014;31:449–59.
29. McNaughton M, Pitman M, Pitson SM, *et al.* Proteasomal degradation of sphingosine kinase 1 and inhibition of dihydroceramide desaturase by the sphingosine kinase inhibitors, SKi or ABC294640, induces growth arrest in androgen-independent LNCaP-AI prostate cancer cells. *Oncotarget* 2016;7:16663–75.
30. Mukhopadhyay A, Saddoughi SA, Song P, *et al.* Direct interaction between the inhibitor 2 and ceramide via sphingolipid-protein binding is involved in the regulation of protein phosphatase 2A activity and signaling. *FASEB J* 2009;23:751–63.
31. Oaks J, Ogretmen B. Regulation of PP2A by sphingolipid metabolism and signaling. *Front Oncol* 2014;4:388.
32. Chen CL, Lin CF, Chang WT, *et al.* Ceramide induces p38 MAPK and JNK activation through a mechanism involving a thioredoxin-interacting protein-mediated pathway. *Blood* 2008;111:4365–74.
33. Chang KT, Anishkin A, Patwardhan GA, *et al.* Ceramide channels: destabilization by Bcl-xL and role in apoptosis. *Biochim Biophys Acta* 2015; 1848:2374–84.
34. Ganesan V, Perera MN, Colombini D, *et al.* Ceramide and activated Bax act synergistically to permeabilize the mitochondrial outer membrane. *Apoptosis* 2010;15:553–62.
35. Sumitomo M, Ohba M, Asakuma J, *et al.* Protein kinase Cdelta amplifies ceramide formation via mitochondrial signaling in prostate cancer cells. *J Clin Invest* 2002;109:827–36.
36. Yang J, Yang C, Zhang S, *et al.* ABC294640, a sphingosine kinase 2 inhibitor, enhances the antitumor effects of TRAIL in non-small cell lung cancer. *Cancer Biol Ther* 2015;16:1194–204.
37. Guan S, Liu YY, Yan T, *et al.* Inhibition of ceramide glucosylation sensitizes lung cancer cells to ABC294640, a first-in-class small molecule SphK2 inhibitor. *Biochem Biophys Res Commun* 2016; 476:230–6.
38. Britten CD, Garrett-Mayer E, Chin SH, *et al.* A phase I study of ABC294640, a first-in-class sphingosine kinase-2 inhibitor, in patients with advanced solid tumors. *Clin Cancer Res* 2017;23: 4642–50.

Published OnlineFirst September 22, 2017; DOI: 10.1158/1535-7163.MCT-17-0485

Small Molecule Therapeutics

Molecular Cancer Therapeutics

ABC294640, A Novel Sphingosine Kinase 2 Inhibitor, Induces Oncogenic Virus–Infected Cell Autophagic Death and Represses Tumor Growth

Lu Dai[1,2], Aiping Bai[3], Charles D. Smith[4], Paulo C. Rodriguez[5], Fangyou Yu[6], and Zhiqiang Qin[1,2]

Abstract

Kaposi sarcoma–associated herpes virus (KSHV) is the etiologic agent of several malignancies, including Kaposi sarcoma and primary effusion lymphoma (PEL), which preferentially arise in HIV$^+$ patients and lack effective treatment. Sphingosine kinase 2 (SphK2) is a key factor within sphingolipid metabolism, responsible for the conversion of proapoptotic ceramides to antiapoptotic sphingosine-1-phosphate (S1P). We have previously demonstrated that targeting SphK2 using a novel selective inhibitor, ABC294640, leads to the accumulation of intracellular ceramides and induces apoptosis in KSHV-infected primary endothelial cells and PEL tumor cells but not in uninfected cells. In this study, we found that ABC294640 induces autophagic death instead of apoptosis in a KSHV long-term–infected immortalized endothelial cell-line, TIVE-LTC, but not in uninfected TIVE cells, through the upregulation of LC3B protein. Transcriptomic analysis indicates that many genes related to cellular stress responses, cell cycle/proliferation, and cellular metabolic process are altered in TIVE-LTC exposed to ABC294640. One of the candidates, *Egr-1*, was found to directly regulate LC3B expression and was required for the ABC294640-induced autophagic death. By using a Kaposi sarcoma–like nude mice model with TIVE-LTC, we found that ABC294640 treatment significantly suppressed KSHV-induced tumor growth *in vivo*, which indicates that targeting sphingolipid metabolism, especially SphK2, may represent a promising therapeutic strategy against KSHV-related malignancies. *Mol Cancer Ther; 16(12); 1–11. ©2017 AACR.*

Introduction

Kaposi sarcoma–associated herpesvirus (KSHV) represents a principal causative agent of several cancers arising in those immunocompromised patients, such as Kaposi sarcoma (1). Currently, there are 4 Kaposi sarcoma isoforms: classic Kaposi sarcoma, affecting elderly men of Mediterranean; endemic Kaposi sarcoma, existing in some countries of Central and Eastern Africa; iatrogenic Kaposi sarcoma, usually developed in organ transplant receipts with immunosuppression; and epidemic or AIDS- Kaposi sarcoma with more aggressive features (2). Even though the reduced incidence of KS due to combined antiretroviral therapy (cART) developed in the Western world, Kaposi sarcoma still remains the most common AIDS-associated malignancy and a leading cause of morbidity and mortality in this setting (3). Interestingly, some AIDS- Kaposi sarcoma patients receive little or no benefit from cART alone or combined with conventional chemotherapy (4). Recently, the issues of Kaposi sarcoma in the context of immune reconstitution inflammatory syndrome (IRIS) and its impact on cART rollout initiatives have become increasingly apparent (5, 6). Furthermore, although treatments for Kaposi sarcoma exist, none are curative, which requires the identification of rational targets and development of novel therapeutic strategies against these malignancies.

Sphingolipid biosynthesis involves hydrolysis of ceramides to generate sphingosine, which is subsequently phosphorylated by one of two sphingosine kinase isoforms (SphK1 or SphK2) to generate sphingosine-1-phosphate (S1P; refs. 7, 8). Bioactive sphingolipids, including ceramides and S1P, act as signaling molecules that regulate apoptosis and tumor cell survival (7). In contrast to the generally proapoptotic function of ceramides, S1P promotes cell proliferation and survival (8). Given the importance of SphKs in sphingolipid metabolism, a highly selective and well-characterized small-molecule inhibitor of SphK2, ABC294640, has been recently developed (9, 10), which displays significant antitumor activities for a variety of cancers (11, 12). ABC294640 is currently under evaluation in a phase I clinical trial for patients with solid tumors (Clinicaltrials.gov identifier: NCT01488513) and in a phase I/II clinical trial for HIV$^+$ patients with diffuse large B-cell lymphoma (Clinicaltrials.gov identifier: NCT02229981). Moreover, we recently have reported that pharmacologic inhibition of SphK2 using ABC294640 induces

[1]Department of Pediatrics, Research Center for Translational Medicine and Key Laboratory of Arrhythmias, East Hospital, Tongji University School of Medicine, Shanghai, China. [2]Department of Genetics, Louisiana State University Health Sciences Center, Louisiana Cancer Research Center, New Orleans, Louisiana. [3]Department of Biochemistry and Molecular Biology, Hollings Cancer Center, Medical University of South Carolina, Charleston, South Carolina. [4]Apogee Biotechnology Corporation, Hershey Center for Applied Research, Hummelstown, Pennsylvania. [5]H. Lee Moffitt Cancer Center and Research Institute, Tampa, Florida. [6]Department of Clinical Laboratory, Shanghai Pulmonary Hospital, Tongji University School of Medicine, Shanghai, China.

Note: Supplementary data for this article are available at Molecular Cancer Therapeutics Online (http://mct.aacrjournals.org/).

Corresponding Authors: Zhiqiang Qin, Louisiana Cancer Research Center, 1700 Tulane Avenue, New Orleans, LA 70112. Phone: 504-210-3327; Fax: 504-210-2970; E-mail: zqin@lsuhsc.edu; and Fangyou Yu, wzjxyfy@163.com

doi: 10.1158/1535-7163.MCT-17-0485

Published OnlineFirst September 22, 2017; DOI: 10.1158/1535-7163.MCT-17-0485

dose-dependent, caspase-mediated apoptosis in primary effusion lymphoma (PEL, another type of cancer caused by KSHV), and suppresses PEL tumor progression *in vivo* (13). Interestingly, our additional data indicated that targeting SphK2 by ABC294640 selectively induces apoptosis in KSHV-infected primary human dermal microvascular endothelial cells (pDMVEC), but not in noninfected cells, through induction of viral lytic gene expression (14). However, a major obstacle for this study is that KSHV-infected primary endothelial cells usually fail to form tumors even in immunodeficiency mice (2). Recently, a KSHV long-term-infected *t*elomerase-immortalized human umbilical vein endothelial cell line (TIVE-LTC) has been established, which stably supports KSHV latency (15). The TIVE-LTC, but not the uninfected parental TIVE cells, efficiently induces Kaposi sarcoma–like tumor formation in nude mice, which express Kaposi sarcoma phenotypic markers such as CD31, CD34, and LYVE-1 (15, 16). In this study, we aim to understand the impact of ABC294640 on the TIVE-LTC proliferation/survival and determine whether targeting sphingolipid metabolism, in particular SphK2, can be developed as a novel therapeutic strategy against Kaposi sarcoma *in vivo*.

Materials and Methods

Cell culture and reagents

TIVE and TIVE-LTC were kindly provided by Dr. Rolf Renne at University of Florida (Gainesville, FL) in 2015 and cultured as described previously (15). The cell lines have been tested by using MycoAlert PLUS Mycoplasma Detection Kit (Lonza) in our laboratory once we received them, and the results are negative. All experiments were carried out using cells harvested at low (<20) passages. 3-(4-chlorophenyl)-adamantane-1-carboxylic acid (pyridin-4-ylmethyl) amide (ABC294640) was synthesized as described previously (9). The other chemicals such as chloroquine, bafilomycin A1, rapamycin, and the pan-caspase inhibitor, Z-VAD-FMK, were purchased from Sigma.

Cell proliferation and apoptosis assays

Cell proliferation was measured by using the WST-1 assays (Roche) according to the manufacturers' instructions. Flow cytometry was used for quantitative assessment of apoptosis with the FITC-Annexin V/propidium iodide (PI) Apoptosis Detection Kit I (BD Pharmingen).

Microarray

Microarray analysis was performed and analyzed at the Stanley S. Scott Cancer Center's Translational Genomics Core at LSUHSC. Total RNA was isolated using Qiagen RNeasy kit (Qiagen), and 500 ng of total RNA was used to synthesize dscDNA. Biotin-labeled RNA was generated using the TargetAmp-Nano Labeling Kit for Illumina Expression BeadChip (Epicentre), and hybridized to the HumanHT-12 v4 Expression BeadChip (Illumina) at 58°C for 16 hours. The chip was washed, stained with streptavadin-Cy3, and scanned with the Illumina BeadStation 500 and BeadScan. Using the Illumina GenomeStudio software, we normalized the signals using the "cubic spline algorithm" that assumes that the distribution of transcript abundance is similar in all samples. The background signal was removed using the "detection *P* value algorithm" to remove targets with signal intensities equal or lower than that of irrelevant probes (with no known targets in the human genome but thermodynamically similar to the relevant probes). The microarray experiments were performed twice for each group and the average values were used for analysis. Common and unique sets of genes and enrichment analysis were performed using the MetaCore Software (Thompson Reuters). The microarray original data have been submitted to Gene Expression Omnibus (GEO) database (accession number: GSE74338).

Transfection assays

For RNA interference, *Egr1*, *SphK2*, *LC3B*, and *Atg5* ON-TARGET plus SMART pool siRNA, or negative control siRNA (n-siRNA; Dharmacon), were delivered using the DharmaFECT transfection reagent according to the manufacturer's instructions.

Cell-cycle analysis

TIVE-LTC pellets were fixed in 70% ethanol, and incubated at 4°C overnight. Cell pellets were resuspended in 0.5 mL of 0.05 mg/mL PI plus 0.2 mg/mL RNaseA and incubated at 37°C for 30 minutes. Cell-cycle distribution was analyzed on a FACSCalibur 4-color flow cytometer (BD Biosciences).

Immunoblotting

Total cell lysates (20 μg) were resolved by 10% SDS-PAGE, transferred to nitrocellulose membranes, and immunoblotted with antibodies for cleaved caspase-3/9, LC3B, p62, Beclin-1, Atg5, Atg12, Egr1, Cyclin D1, CDK6, phospho-Rb, p21 (Cell Signaling Technology), SphK2 (Abgent), and β-actin (Sigma) for loading controls. Immunoreactive bands were identified using an enhanced chemiluminescence reaction (PerkinElmer), and visualized by autoradiography.

Immunofluorescence

Cells were incubated in 1:1 methanol-acetone at −20°C for fixation and permeabilization, then with a blocking reagent (10% normal goat serum, 3% BSA, and 1% glycine) for an additional 30 minutes. Cells were then incubated for 1 hour at 25°C with 1:400 dilution of a rabbit anti-LC3B antibody (Cell Signaling Technology) followed by 1:200 dilution of a goat anti-rabbit secondary antibody conjugated to Texas Red (Invitrogen). For identification of nuclei, cells were subsequently counterstained with 0.5 mg/mL 4′,6-diamidino-2-phenylindole (DAPI) in 180 mmol/L Tris-HCl (pH 7.5). Slides were washed once in 180 mmol/L Tris-HCl for 15 minutes and prepared for visualization using a Leica TCPS SP5 AOBS confocal microscope. LysoTracker red (Invitrogen) was used to visualize lysosomes as described previously (17), which was added to achieve final concentrations of 50 nmol/L. After 1 hour of incubation, the medium was replaced with fresh media, and confocal imaging was performed.

Electron microscopy

Cells were fixed in primary fixative (1.6% paraformaldehyde, 2.5% glutaraldehyde, 0.03% $CaCl_2$ in 0.05 mol/L cacodylate buffer, pH 7.4), pelleted, and embedded in 3% agarose. Agar blocks were cut in 1-mm^3 cubes and transferred to a fresh portion of the fixative for 2 hours at room temperature. Samples were then washed in 0.1 mol/L cacodylate buffer supplemented with 5% sucrose, postfixed in 1% osmium tetroxide for 1 hour, washed in water, and in-block stained with 2% uranyl acetate in 0.2 mol/L sodium acetate buffer, pH 3.5. Specimens were dehydrated in ascending ethanol series and propylene oxide, and embedded in Epon-Araldite mixture. Blocks were sectioned with the Ultratome

Published OnlineFirst September 22, 2017; DOI: 10.1158/1535-7163.MCT-17-0485

Leica EM UC7. Thin (80 nm) sections were stained with lead citrate for 5 minutes and examined in JEOL JEM 1011 microscope with the attached HAMAMATSU ORCA-HR digital camera.

qRT-PCR

Total RNA was isolated using the RNeasy Mini kit (Qiagen), and cDNA was synthesized from equivalent total RNA using a SuperScript III First-Strand Synthesis SuperMix Kit (Invitrogen) according to the manufacturer's instructions. Primers used for amplification of target genes are listed in Supplementary Table S1. Amplification was carried out using an iCycler IQ Real-Time PCR Detection System, and cycle threshold (C_t) values were tabulated in duplicate for each gene of interest in each experiment. "No template" (water) controls were used to ensure minimal background contamination. Using mean C_t values tabulated for each gene, and paired C_t values for *β-actin* as a loading control, fold changes for experimental groups relative to assigned controls were calculated using automated iQ5 2.0 software (Bio-Rad).

Sphingolipid analyses

Quantification of ceramide and dihydro-ceramide species was performed using a Thermo Finnigan TSQ 7000 triple-stage quadruple mass spectrometer operating in Multiple Reaction Monitoring positive ionization mode (Thermo Fisher Scientific). Quantification was based on calibration curves generated by spiking an artificial matrix with known amounts of target standards and an equal amount of the internal standard. The target analyte:internal standard peak area ratios from each sample were compared with the calibration curves using linear regression. Final results were expressed as the ratio of sphingolipid normalized to total phospholipid phosphate level using the Bligh and Dyer lipid extract method (18).

Kaposi sarcoma–like nude mice model

Cells were counted and washed once in ice-cold PBS, and 5×10^5 TIVE-LTC in 50-μL PBS plus 50-μL growth factor–depleted Matrigel (BD Biosciences) were injected subcutaneously into the two flanks of nude mice (The Jackson Laboratory). The mice were observed and measured every 2–3 days for the presence of palpable tumors. When tumors reach 10–15 mm in diameter (~1.5 weeks), the mice received *in situ* subcutaneous injection with either vehicle or ABC294640 (50 mg/kg of body weight dissolved in PEG:ddH_2O as 1:1), 5 days/week. At the end of experiment, the tumors were excised from the site of injection for subsequent analysis such as IHC. All protocols were approved by the LSUHSC Animal Care and Use Committee in accordance with national guidelines.

Statistical analysis

Significance for differences between experimental and control groups was determined using the two-tailed Student *t* test (Microsoft Excel 8.0), and *P* values <0.05 or <0.01 were considered significant or highly significant, respectively.

Results

Targeting SphK2 by ABC294640 induces KSHV-infected immortalized endothelial cell death

By using the WST-1 assays, we found that ABC294640 treatment dramatically reduced TIVE-LTC proliferation in a dose-dependent manner, while it only slightly suppressed TIVE cell growth (Fig. 1A). We further found that TIVE-LTC had higher expressional level of SphK2 than the parental TIVE cells (Supplementary Fig. S1A), which may represent one of potential mechanisms that making TIVE-LTC more sensitive to ABC294640 than TIVE cells. We also found that KSHV *de novo* infection greatly upregulated SphK2 expression from TIVE cells (Supplementary Fig. S1B). We next used flow cytometry to monitor cell viability and apoptosis. Interestingly, we found that ABC294640 induced significant cell death in TIVE-LTC (PI^+ subpopulation) but not in TIVE cells, which was almost independent of cell apoptosis (Annexin V^+ subpopulation) even at high concentration (Fig. 1B). These results are opposite to our previous data showing that ABC294640 triggered apoptosis in KSHV-infected primary endothelial cells (14). These data indicate ABC294640-induced deleterious effects in TIVE-LTC through some apoptosis-independent mechanisms.

As ABC294640 is a selective SphK2 inhibitor, we also measured the levels of intracellular ceramide and dihydro(dh)-ceramide species within ABC294640-treated TIVE and TIVE-LTC cells through lipidomics analysis (13, 14). Our results indicated that ABC294640 caused the accumulation of total and individual ceramide species, in particular dh-ceramides, such as dhC14-Cer, dhC24-Cer, and dhC24:1-Cer (Fig. 1C and D; Supplementary Fig. S2A). In contrast to this, we found that ABC294640 only slightly increased total ceramides/dh-ceramides but with no statistical significance within TIVE cells (Supplementary Fig. S2B). Ceramide/dh-ceramide composition analysis indicated that the prominent species within TIVE-LTC were C16-Cer, C24-Cer, C24:1-Cer, dhC14-Cer, dhC16-Cer, and dhC20-Cer; ABC294640 treatment mainly increased the relative composition percentage of C14-Cer, dhC14-Cer, whereas reducing the relative composition percentage of C24-Cer, dhC16-Cer, and dhC20-Cer, respectively (Fig. 1F and G). Ceramides are synthesized by a family of ceramide synthases (CerSs), CerS1–CerS6 (19). Accordingly, our qRT-PCR analysis indicated that ABC294640 treatment mainly increased the transcripts of *CerS1*, *CerS2*, and *CerS6* from TIVE-LTC (Fig. 1E).

ABC294640 causes TIVE-LTC programmed cell death through autophagy

To further seek the mechanisms through which ABC294640 induced cell death in TIVE-LTC, we found that ABC294640 significantly induced LC3B expression, one of the autophagic markers, while reducing p62 expression, a ubiquitin binding protein degraded in autophagy (ref. 12; Fig. 2A). In contrast, the expression of other autophagy-related proteins including Atg5, Atg12, and Beclin-1 was not affected by ABC294640. Immunofluorescence data with a LC3B-specific antibody confirmed the increased signal of LC3B and the puncta structures were readily observed in the cytoplasm of ABC294640-treated TIVE-LTC when compared with vehicle-treated cells (Fig. 2B). Because basic lipophilic compounds can act as lysosomotropic agents and are thus possible autophagy modulators (12), lysosomal morphology was assessed to gain further insight into the mechanisms through which ABC294640 induces autophagy. Compared with vehicle-treated cells, ABC294640 treatment for 24 hours resulted in enhanced accumulation of LysoTracker Red dye and increased in the size of lysosomes ("swelling"; Fig. 2C). We also confirmed that ABC294640 induced autophagy within TIVE-LTC by using electron microscopy. Exposure of TIVE-LTC

Published OnlineFirst September 22, 2017; DOI: 10.1158/1535-7163.MCT-17-0485

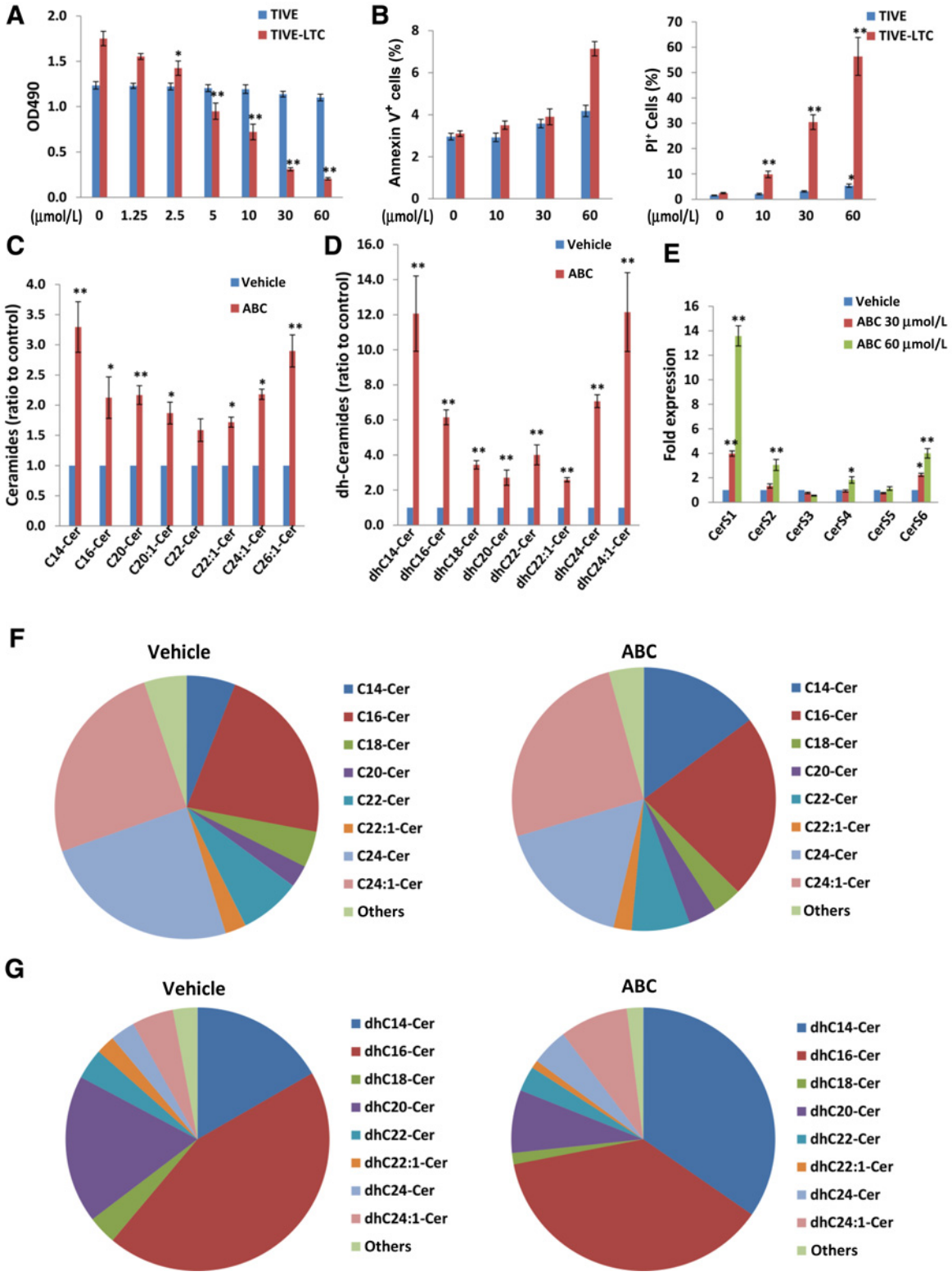

Figure 1.

Targeting SphK2 by ABC294640 induces KSHV-infected immortalized endothelial cell death. **A,** TIVE-LTC and TIVE were incubated with indicated concentrations of ABC294640 (ABC) for 24 hours, and then cell proliferation was measured using the WST-1 assays. **B,** Cell viability and apoptosis were measured using Annexin V-PI staining and flow cytometry analysis. **C** and **D,** TIVE-LTC were incubated with 60 μmol/L of ABC294640 or vehicle for 24 hours, then ceramide and dihydro(dh)-ceramide species were quantified as described in Materials and Methods. **E,** The transcripts of ceramide synthases (*CerS1–CerS6*) were quantified using qRT-PCR. **F** and **G,** The composition of ceramide/dh-ceramide species was calculated and analyzed by using Excel 8.0 software. Error bars, SD from three independent experiments. *, $P < 0.05$; **, $P < 0.01$.

Published OnlineFirst September 22, 2017; DOI: 10.1158/1535-7163.MCT-17-0485

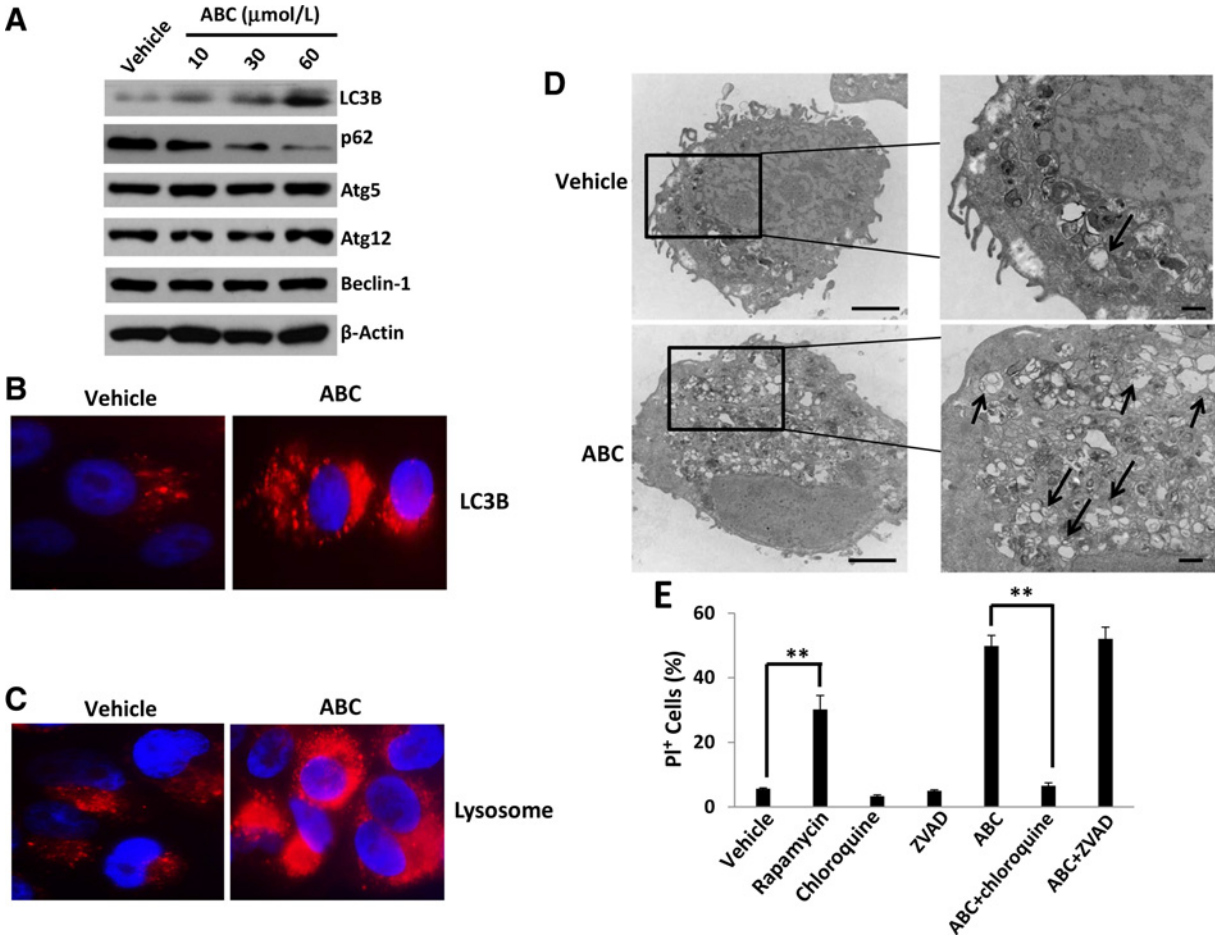

Figure 2.

ABC294640 treatment induces TIVE-LTC cell death through autophagy. **A,** TIVE-LTC were incubated with indicated concentrations of ABC294640 (ABC) for 24 hours, then protein expression was measured using immunoblots. **B** and **C,** TIVE-LTC were incubated with 60 μmol/L of ABC or vehicle for 24 h, then cellular LC3B expression and lysosome were detected using the immunofluorescence assay as described in Materials and Methods. **D,** Electron micrographs were generated as described in Materials and Methods, and representative micrographs at low magnification (left, scale bar = 2 μm) or high magnification (right, scale bar = 0.5 μm) depicting the ultrastructure of the cells were shown. Arrows indicate the autophagic vacuoles. **E,** TIVE-LTC were incubated with 60 μmol/L of ABC or vehicle in the presence of autophagy inhibitor chloroquine (1 μmol/L), rapamycin alone (1 μmol/L), the pan-caspase inhibitor Z-VAD-FMK (ZVAD, 10 μmol/L) or not for 24 hours, then cell viability was measured as above. Error bars, SD from three independent experiments. **, $P < 0.01$.

to ABC294640 for 24 hours resulted in the production of many large empty vacuoles and autophagic vacuoles containing residual digested material or intact organelles. In contrast, only a few small autophagic vacuoles were observed in the vehicle-treated cells (Fig. 2D). Finally, our findings were further supported by the evidence that one of the autophagy inhibitors, chloroquine, almost completely protected TIVE-LTC from ABC294640-induced autophagic death (Fig. 2E; Supplementary Fig. S3). We also observed the similar inhibitory effect of bafilomycin A1, a known autophagic flux inhibitor. In contrast, rapamycin, a known autophagy inducer, caused TIVE-LTC death, although with a less extent when compared with ABC294640 (Fig. 2E). Not surprisingly, the pan-caspase inhibitor, Z-VAD-FMK treatment cannot protect TIVE-LTC from cell death induced by ABC294640. Thus, our results suggest the potential role of autophagy as the mechanism of cell death induced by ABC294640 within TIVE-LTC.

Transcriptomic analysis of gene profile altered within ABC294640-treated TIVE-LTC

To determine the overall metabolic changes induced by ABC294640, we used the HumanHT-12 v4 Expression BeadChip (Illumina) which contains more than 47,000 probes derived from the NCBI RefSeq Release 38 and other sources to analyze the gene profile altered between vehicle- and ABC294640-treated TIVE-LTC. Our analysis indicated that 562 genes significantly upregulated and 444 genes downregulated in ABC294640-treated TIVE-LTC (≥2 folds and $P < 0.05$). The top 30 upregulated and downregulated candidate genes were listed in Tables 1 and 2, respectively. Among these candidates, there are several notable features: (i) some nuclear small RNA transcripts such as *RN7SK, RNU1G2, RNU1–5, RNU1–3,* and *RNU1A3* are highly upregulated, which has also been observed in c-MET inhibitor–treated KSHV+ PEL tumor cells in spite of unknown mechanisms or functions (20); (ii) multiple Metallothionein genes such as *MTE,*

Published OnlineFirst September 22, 2017; DOI: 10.1158/1535-7163.MCT-17-0485

Table 1. The top 30 candidate genes upregulated within ABC294640-treated TIVE-LTC

Gene symbol	Description	Fold change
RN7SK	7SK small nuclear, noncoding RNA	76.2
RNU1G2	U1G2 small nuclear, small nuclear RNA	45.0
MTE	Metallothionein E	42.7
RNU1-5	U1 small nuclear 5, small nuclear RNA	41.8
RNU1-3	U1 small nuclear 3, small nuclear RNA	41.7
MT1F	Metallothionein 1F	40.6
MT1E	Metallothionein 1E	38.7
RPPH1	Ribonuclease P RNA component H1	35.1
FOS	v-fos FBJ murine osteosarcoma viral oncogene homolog	25.7
MT1G	Metallothionein 1G	25.0
RNU1A3	U1A3 small nuclear, small nuclear RNA	21.3
HSPA6	Heat shock 70 kDa protein 6 (HSP70B')	20.7
RNU6-1	U6 small nuclear 1, small nuclear RNA	19.1
RNU6-15	U6 small nuclear 15, small nuclear RNA	17.7
MT2A	Metallothionein 2A	16.8
HSPA7	Heat shock 70 kDa protein 7 (HSP70B)	15.6
MT1A	Metallothionein 1A	13.6
IFIT2	Interferon-induced protein with tetratricopeptide repeats 2	12.9
SLC30A1	Solute carrier family 30 (zinc transporter), member 1	12.4
EGR1	Early growth response 1	11.6
RASD1	Dexamethasone-induced Ras-related protein 1	10.2
ISG15	Ubiquitin-like protein ISG15	9.4
RNU11	U11 small nuclear, small nuclear RNA	8.9
IL8	Interleukin 8	8.2
IFIT1	Interferon-induced protein with tetratricopeptide repeats 1	8.2
IFIT3	Interferon-induced protein with tetratricopeptide repeats 3	8.0
BAG3	BCL2-associated athanogene 3	7.5
CXCL2	Chemokine (C-X-C motif) ligand 2	6.5
TMEM106A	Transmembrane protein 106A	6.5
DNAJB1	DnaJ (Hsp40) homolog, subfamily B, member 1	6.0

MT1F/E/G, and *MT2A* are significantly upregulated, and they have been shown to be increased during oxidative stress (21, 22) to protect the cells against cytotoxicity (23, 24), radiation, and DNA damage (25, 26), and be increased in a variety of human tumors (27); 3) some genes have been reported related to tumor cell proliferation, such as *PPM1D*, silencing of which by RNAi inhibits lung cancer cells proliferation and the tumorigenicity of bladder cancer cells, respectively (28, 29). However, we found that the functional role of most genes listed here remains unclear for KSHV pathogenesis or tumorigenicity, which requires further investigation.

For validation of microarray analysis, we next selected 5 candidate genes from Tables 1 and 2, respectively, to perform qRT-PCR analysis. Our results indicated that all of the 10 selected genes were significantly altered in a manner comparable with those found in the microarray data, demonstrating the credibility of our results. Specifically, *EGR1*, *FOS*, *HSPA6*, *ISG15*, and *IFIT2* were significantly upregulated, while *FZD6*, *KLF10*, *PPM1D*, *TOP2A*, and *TXNIP* were significantly downregulated within ABC294640-treated TIVE-LTC, when compared with vehicle-treated cells (Fig. 3A and B). We also performed enrichment analysis of these significantly altered candidates by using the Gene Ontology (GO) Processes and Process Networks modules from Metacore Software. Our analysis showed that these proteins belong to several functional categories, including cellular response to stress, cell cycle/proliferation, and cellular metabolic process (Fig. 3C and D). In addition, the top 2 protein networks related to these candidates were shown in Supplementary Fig. S4A and S4B. For experimental and functional validation, we found that ABC294640 treatment significantly caused G_0–G_1 cell-cycle arrest as well as reducing S-phase subpopulation for TIVE-LTC (Supplementary Fig. S5A). Immunoblot analysis confirmed that ABC294640 reduced the expression of checkpoint regulatory proteins such as Cyclin D1, CDK6, and phospho-Rb, while increasing p21 expression (Supplementary Fig. S5B).

EGR1 is required for ABC294640-induced TIVE-LTC autophagic cell death

One of upregulated candidates found in our microarray data is *Egr1*, a transcriptional factor which has been previously found directly binding to the promoter region of *LC3B* and promoting its transcription and expression (30). Our data confirmed that the expression of EGR1 was gradually increased from ABC294640-treated TIVE-LTC in a dose-dependent manner (Fig. 4A). In addition, we found that directly silencing of *SphK2* by RNAi significantly increased EGR1 expression in TIVE-LTC, but not TIVE cells, probably because of higher basal expressional level of SphK2 in TIVE-LTC (Supplementary Fig. S6). Interestingly, we also found that directly silencing of *Egr1* by RNAi greatly reduced the expression of LC3B, Atg5, and Atg12, but not Beclin-1 within TIVE-LTC exposed to ABC294640 (Fig. 4B). Further analysis indicated that silencing of *Egr1* reduced *LC3B*, *Atg5*, and *Atg12*

Table 2. The top 30 candidate genes downregulated within ABC294640-treated TIVE-LTC

Gene symbol	Description	Fold change
TXNIP	Thioredoxin interacting protein	0.09
ARRDC4	Arrestin domain containing 4	0.12
ANKRD12	Ankyrin repeat domain 12, transcript variant 1	0.19
PDZD2	PDZ domain containing 2 (PDZD2)	0.19
ZFP30	Zinc finger protein 30 homolog (mouse)	0.19
ZNF45	Zinc finger protein 45	0.19
THBS1	Thrombospondin 1	0.22
KLF10	Kruppel-like factor 10, transcript variant 1	0.25
PLD6	Phospholipase D family, member 6	0.26
PPM1D	Protein phosphatase 1D magnesium-dependent, delta isoform (PPM1D)	0.26
TMEM133	Transmembrane protein 133	0.26
TOP2A	Topoisomerase (DNA) II alpha 170 kDa	0.26
ANKRA2	Ankyrin repeat, family A (RFXANK-like), 2	0.27
FSTL5	Follistatin-like 5	0.27
ABCB10	ATP-binding cassette, sub-family B (MDR/TAP), member 10, nuclear gene encoding mitochondrial protein	0.28
FZD6	Frizzled homolog 6 (Drosophila) (FZD6)	0.28
SLC38A2	Solute carrier family 38, member 2	0.28
CUL5	Cullin 5	0.29
MAT2A	Methionine adenosyltransferase II, alpha	0.29
TMEM2	Transmembrane protein 2	0.29
TP53INP1	Tumor protein p53 inducible nuclear protein 1	0.29
DHRS2	Dehydrogenase/reductase (SDR family) member 2, transcript variant 1	0.30
KLHL24	Kelch-like 24 (Drosophila)	0.30
PRKCA	Protein kinase C, alpha	0.30
TMEM19	Transmembrane protein 19	0.30
XPO1	Exportin 1 (CRM1 homolog, yeast)	0.30
ZNF670	Zinc finger protein 670	0.30
HERC1	Probable E3 ubiquitin-protein ligase HERC1	0.31
INTS2	Integrator complex subunit 2	0.31
DNM3	Dynamin 3	0.32

Published OnlineFirst September 22, 2017; DOI: 10.1158/1535-7163.MCT-17-0485

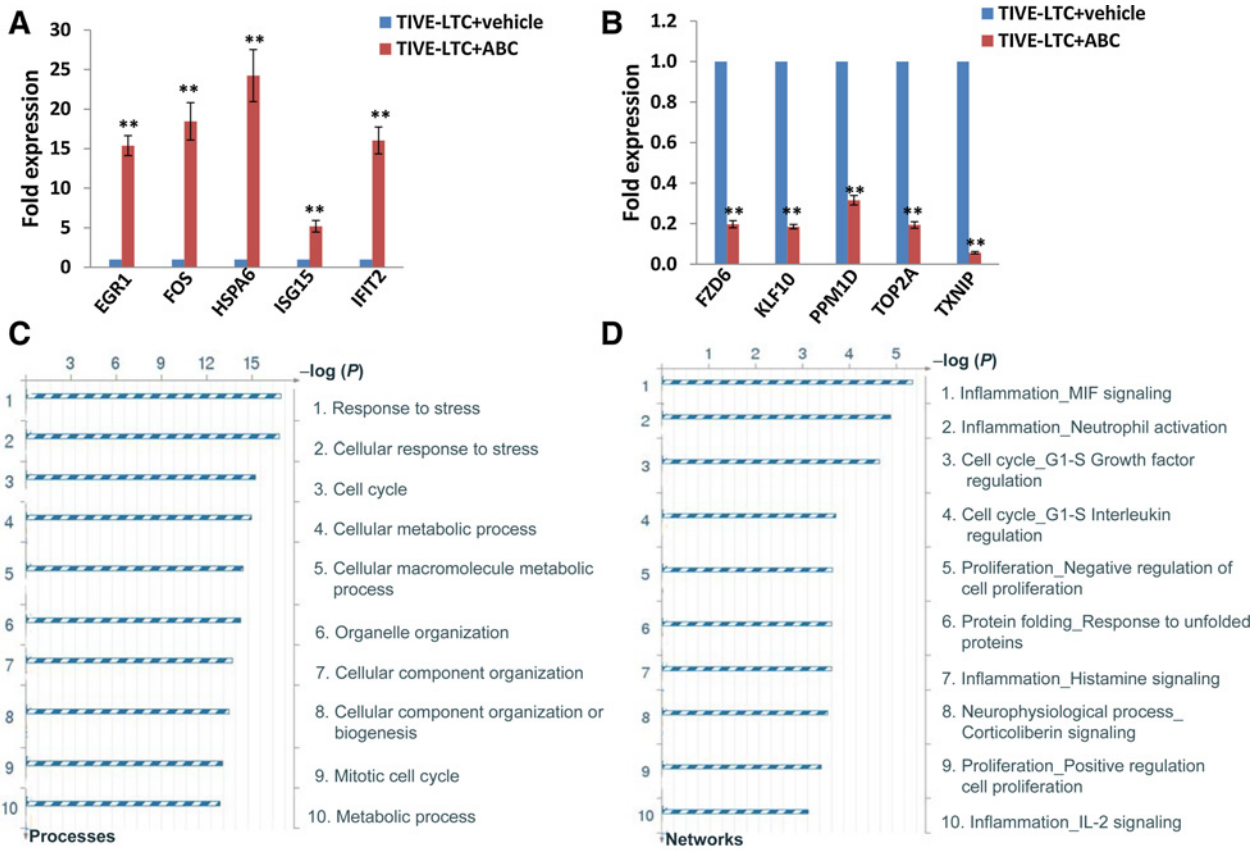

Figure 3.

Transcriptomic analysis of gene profile altered within TIVE-LTC exposed to ABC294640. **A** and **B,** The HumanHT-12 v4 Expression BeadChip was used to detect gene profile altered within ABC294640 (60 μmol/L)-treated TIVE-LTC when compared with vehicle-treated cells. The transcriptional levels of selected 5 candidate genes significantly upregulated or downregulated in microarray data were validated by using qRT-PCR, respectively. Error bars, SD from three independent experiments. **C** and **D,** The enrichment analysis of gene profile altered by ABC294640 was performed using the MetaCore Software Modules of Gene Ontology Processes and Process Networks.

at the transcriptional level as well (Fig. 4C). Finally, silencing of either *Egr1*, *LC3B*, or *Atg5* by RNAi, effectively protected TIVE-LTC from ABC294640 induced cell death (Fig. 4D; Supplementary Fig. S7A and S7B). Taken together, our data demonstrate that EGR1 is required for the ABC294640-induced TIVE-LTC autophagic cell death.

ABC294640 treatment effectively represses KSHV-induced tumor growth *in vivo*

By using an established Kaposi sarcoma–like nude mice model with TIVE-LTC (16), we tested the effect of ABC294640 on KSHV-induced tumor growth *in vivo*. We injected TIVE-LTC (5×10^5 cells 1:1 with growth factor-depleted Matrigel) subcutaneously into the right and left flanks of nude mice, respectively. When tumors reached 10–15 mm in diameter (~1.5 weeks), mice received *in situ* subcutaneous injection with either vehicle or ABC294640 (50 mg/kg of body weight), 5 days/week. The mice were observed every 2–3 days and palpable tumors were measured for additional 3 weeks. Our results indicated that ABC294640 treatment significantly repressed tumor growth in mice while the vehicle had no effects (Fig. 5A). After 3-week treatment, the tumors isolated from ABC294640-treated mice had significantly smaller size than those from vehicle-treated mice (Fig. 5B). IHC analysis confirmed the increased expression of LC3B, while the reduced expression of cellular proliferation indicator, Ki67, within tumor tissues from representative ABC294640-treated mice when compared with those from vehicle-treated mice (Fig. 5C). We then compared the expression of SphK2 and EGR1 within tumor tissues from representative vehicle- or ABC294640-treated mice by using immunoblots. We found that ABC294640 treatment reduced SphK2 while increasing EGR1 expression *in vivo* (Fig. 5D).

Discussion

Our previous studies showed that targeting SphK2 by a novel inhibitor, ABC294640, selectively induced the apoptosis of KSHV-infected primary endothelial cells (pDMVEC; ref. 13). In contrast, here we found that ABC294640 induced autophagic death of KSHV stably infected immortalized TIVE-LTC instead of apoptosis, implying different cellular response to ABC294640 by these KSHV-infected endothelial cells. Notably, only TIVE-LTC but not uninfected parental TIVE cells can form Kaposi sarcoma–like tumor in immunodeficiency mice (15, 16). Therefore, future work will focus on the mechanisms of cellular contents related to different programmed cell death caused by ABC294640. In fact,

Published OnlineFirst September 22, 2017; DOI: 10.1158/1535-7163.MCT-17-0485

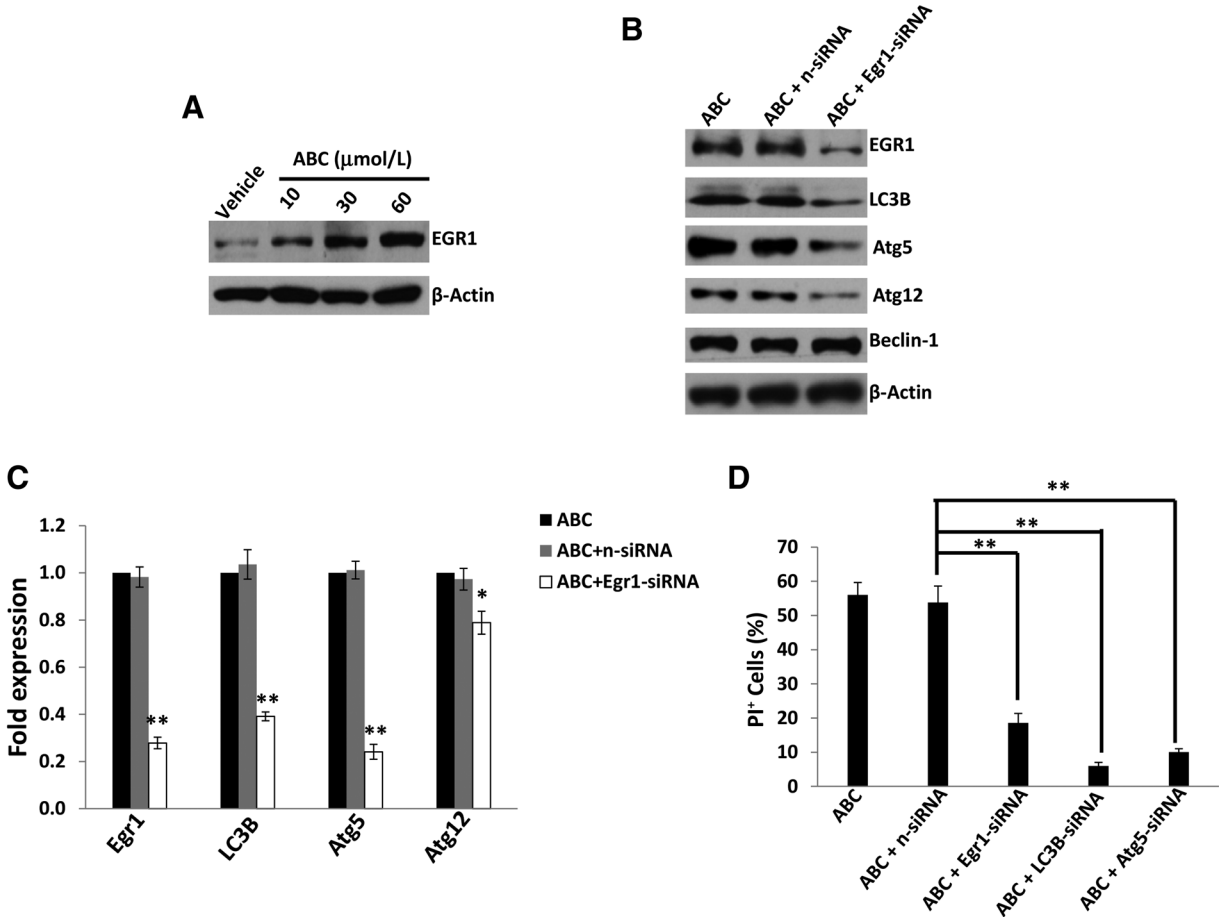

Figure 4.

EGR1 is required for ABC294640-induced autophagic cell death within TIVE-LTC. **A,** TIVE-LTC were incubated with indicated concentrations of ABC294640 (ABC) or vehicle for 24 hours, then protein expression was measured using immunoblots. **B** and **C,** TIVE-LTC were first transfected with either negative control siRNA (n-siRNA) or *Egr1*-siRNA for 48 hours, then incubated with 60 μmol/L of ABC294640 for 24 hours. The gene transcripts and protein expression were measured by using qRT-PCR and immunoblots. **D,** TIVE-LTC were first transfected with either n-siRNA or *Egr1*-siRNA, *LC3B*-siRNA, *Atg5*-siRNA, respectively, for 48 hours, then incubated with 60 μmol/L of ABC294640 for additional 24 hours. Cell viability was measured using flow cytometry. Error bars, SD from three independent experiments. *, $P < 0.05$; **, $P < 0.01$.

KSHV infection itself has been found connected to host cell autophagy. Lee and colleagues have reported that KSHV-encoded viral FLICE-like inhibitor protein (vFLIP) can suppress autophagy by preventing Atg3 from binding and processing LC3 (31). As a consequence, vFLIP expression effectively represses autophagic death induced by the mTOR inhibitor, rapamycin (31). Another recent study reveals that KSHV-encoded vCyclin and vFLIP proteins can induce or block autophagy and oncogene-induced senescence (OIS) process, respectively (32). In addition, KSHV infection can activate STAT3, which correlates with a decreased of autophagy in dendritic cells, as indicated by LC3B reduction and p62 accumulation (33). Therefore, it will be interested to understand which and how individual KSHV-encoded protein is involved in ABC294640-induced autophagic death of TIVE-LTC.

In this study, we found that ABC294640 treatment mainly increased LC3B and reduced p62 expression, but not Atg5, Atg12, Beclin-1, through the upregulation of EGR1, while silencing of *Egr1* downregulated LC3B, Atg5, Atg12, which implying additional negative regulators or compensated mechanisms are involved in the regulation of Atg5 and Atg12 expression from ABC294640-treated TIVE-LTC cells. ABC294640 exhibits little or no inhibitory activity for SphK1 at the concentrations up to 100 μmol/L (10) that exceeding those used in our *in vitro* studies, so our current study only focuses on SphK2. However, it will be interesting to investigate the role of SphK1 contributed to KSHV-infected cell survival and/or ABC294640-induced cell death in future study.

Our lipidomics analysis data indicated that ABC294640 treatment caused the accumulation of endogenous ceramide and dh-ceramide species within TIVE-LTC. Interestingly, it has been shown that exogenous ceramide stimulates autophagy in the human colon cancer HT-29 cells by increasing the accumulation of endogenous ceramides (34). Our recent data demonstrate that some exogenous ceramide or dh-ceramide species can induce significant apoptosis of KSHV+ PEL cells and effectively suppresses PEL tumor progression *in vivo* (35). However, it remains unknown how the components or molecules of sphingolipid metabolism can regulate KSHV-infected

Published OnlineFirst September 22, 2017; DOI: 10.1158/1535-7163.MCT-17-0485

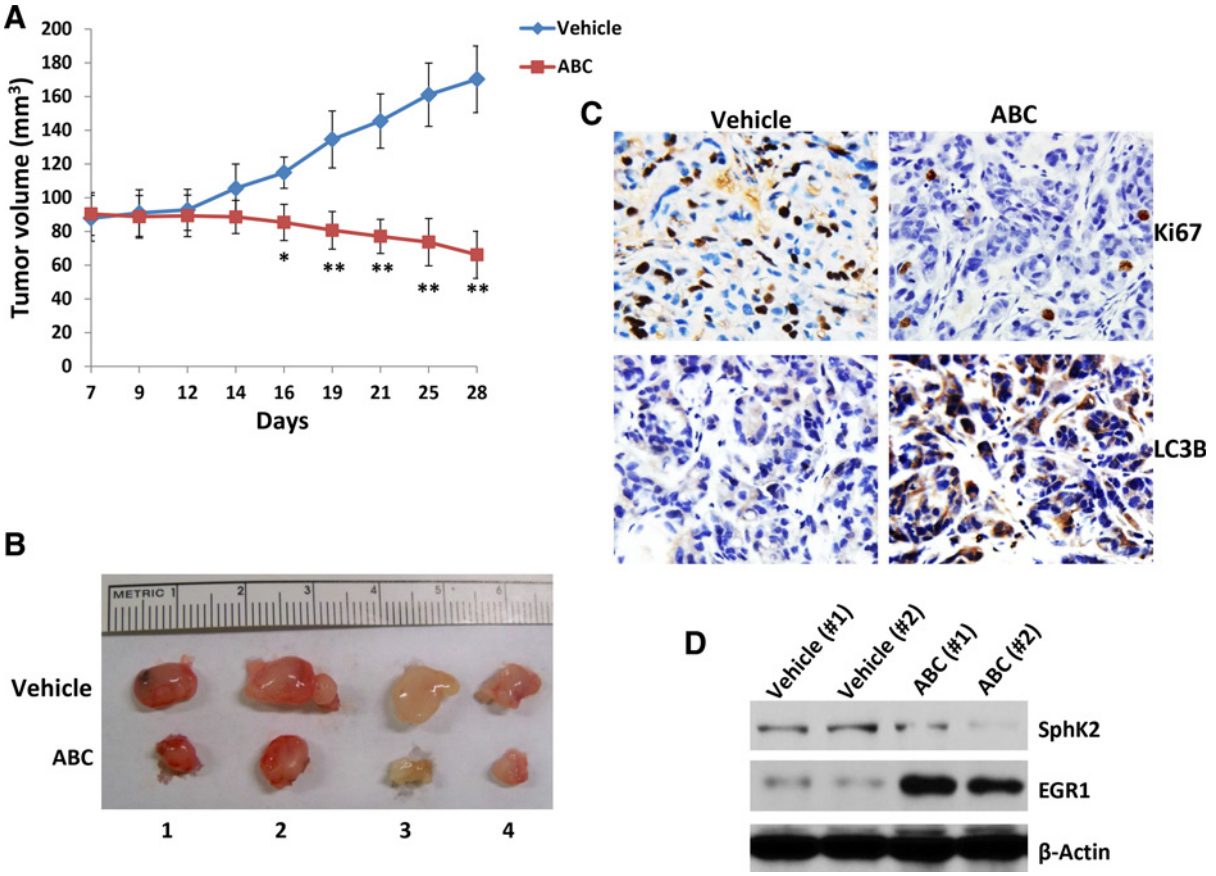

Figure 5.

Targeting SphK2 by ABC294640 significantly represses KSHV-induce tumor growth *in vivo*. **A** and **B,** TIVE-LTC (5×10^5 cells 1:1 with growth factor-depleted Matrigel) were injected subcutaneously into the right and left flanks of nude mice (4 mice per group), respectively. When tumors reached 10–15 mm in diameter (~1.5 weeks), mice received *in situ* subcutaneous injection with either vehicle or ABC294640 (50 mg/kg), 5 days/week. The mice were observed and measured every 2–3 days for the size of palpable tumors for additional 3 weeks. At the end of experiment, the tumors were excised from the site of injection for subsequent analysis. The number 1–4 represents different mice from the same group. Error bars, SD from one of two independent experiments. *, $P < 0.05$; **, $P < 0.01$. **C** and **D,** Protein expression in tumor tissues from representative mice was measured using the IHC or immunoblots assays as described in Materials and Methods.

cell survival, apoptosis, or autophagy. Also, we think that ABC294640-induced autophagic cell death for TIVE-LTC may involve other sphingolipid metabolism–independent mechanisms (or at least indirectly). Our recent transcriptomic analysis indicates that some exogenous ceramides upregulate a cluster of tumor suppressor genes (TSG) from KSHV-infected tumor cells, which are closely related to tumor cell survival or growth (36). Actually, ABC294640 has been reported to cause autophagic responses in A-498 kidney carcinoma, PC-3 prostate, and MDA-MB-231 breast adenocarcinoma cells (12). In addition, the involvement of MEK/ERK pathway in the antitumor activity of ABC294640 was demonstrated by decreased levels of phospho-Akt and phospho-ERK in ABC294640-treated A-498 cells (12). Even though the Akt and ERK pathways can activate the mTOR signaling, which blocks autophagy (37), ABC294640 did not significantly decrease phospho-mTOR levels. Therefore, the autophagy in A-498 cells induced by ABC294640 does not result from changes in the phosphorylation status of mTOR (12). However, the activities of these cell proliferation/survival–related signaling pathways have not been examined within ABC294640-treated TIVE-LTC, although we have observed the dose-dependent suppression of ERK, Akt, and NFκB p65 phosphorylation within KSHV+ PEL cells exposed to ABC294640 (13).

Anticancer chemotherapy is usually administered as a combination of different drugs by specific schedules to avoid quick occurrence of drug resistance (16). Previous studies have shown that ABC294640 combined with drugs that induce the unfolded protein response, such as proteasome inhibitors (e.g., MG-132) or HSP90 inhibitors (e.g., geldanamycin), can have synergistically cytotoxic to cancer cells (12). This is probably because some misfolded proteins are degraded by autophagy (38). Some proteasome inhibitors such as bortezomib have been found to effectively inhibit growth and induce apoptosis in KSHV+ PEL cells (39, 40). Other studies have reported that HSP90 inhibitors are efficacious against KSHV-related malignancies including Kaposi sarcoma and PEL (41, 42). Moreover, using PU-H71 (a purine-scaffold HSP90 inhibitor) affinity capture and proteomics analysis, many apoptosis and/or autophagy-related proteins are identified in HSP90 interactome within KSHV+ PEL cells (43). Therefore, it is interesting to test the synergistic effects of ABC294640 combined with these drugs on KSHV-induced tumor growth *in vivo*.

Disclosure of Potential Conflicts of Interest

C.D. Smith is a president and has ownership interest (including patents) in Apogee Biotechnology Corporation. No potential conflicts of interest were disclosed by the other authors.

Disclaimer

The funding sources had no role in study design, data collection and analysis, decision to publish, or preparation of the manuscript.

Authors' Contributions

Conception and design: L. Dai, Z. Qin
Development of methodology: L. Dai, A. Bai, Z. Qin
Acquisition of data (provided animals, acquired and managed patients, provided facilities, etc.): L. Dai, A. Bai
Analysis and interpretation of data (e.g., statistical analysis, biostatistics, computational analysis): L. Dai, A. Bai, P.C. Rodriguez, F. Yu, Z. Qin
Writing, review, and/or revision of the manuscript: L. Dai, C.D. Smith, P.C. Rodriguez, F. Yu, Z. Qin
Study supervision: Z. Qin

Acknowledgments

We thank Drs. Yuliya Y. Sokolova and Xiaochu Wu at Microscopy Center, Louisiana State University, for helping electron microscopy analysis. We also thank Dr. Rolf Renne at University of Florida for kindly providing TIVE and TIVE-LTC cells.

This work was supported by grants from a DOD Career Development Award to (CA140437, to Z. Qin), a Louisiana Clinical and Translational Science Center Pilot grant (U54GM104940 from NIH), a LSU LIFT^2 funding and NIH P20-GM121288-01 (principal investigator: Krzysztof Reiss) subproject to Z. Qin, as well as the awards from the National Natural Science Foundation of China (81472547 and 81672924, to Z. Qin; 81400164 and 81772930, to L. Dai).

The costs of publication of this article were defrayed in part by the payment of page charges. This article must therefore be hereby marked *advertisement* in accordance with 18 U.S.C. Section 1734 solely to indicate this fact.

Received May 25, 2017; revised July 13, 2017; accepted September 11, 2017; published OnlineFirst September 22, 2017.

References

1. Chang Y, Cesarman E, Pessin MS, Lee F, Culpepper J, Knowles DM, et al. Identification of herpesvirus-like DNA sequences in AIDS-associated Kaposi's sarcoma. Science 1994;266:1865–9.
2. Mesri EA, Cesarman E, Boshoff C. Kaposi's sarcoma and its associated herpesvirus. Nat Rev Cancer 2010;10:707–19.
3. Bonnet F, Lewden C, May T, Heripret L, Jougla E, Bevilacqua S, et al. Malignancy-related causes of death in human immunodeficiency virus-infected patients in the era of highly active antiretroviral therapy. Cancer 2004;101:317–24.
4. Nguyen HQ, Magaret AS, Kitahata MM, Van Rompaey SE, Wald A, Casper C. Persistent Kaposi sarcoma in the era of highly active antiretroviral therapy: characterizing the predictors of clinical response. AIDS 2008; 22:937–45.
5. Letang E, Lewis JJ, Bower M, Mosam A, Borok M, Campbell TB, et al. Immune reconstitution inflammatory syndrome associated with Kaposi sarcoma: higher incidence and mortality in Africa than in the UK. AIDS 2013;27:1603–13.
6. Mosam A, Shaik F, Uldrick TS, Esterhuizen T, Friedland GH, Scadden DT, et al. A randomized controlled trial of highly active antiretroviral therapy versus highly active antiretroviral therapy and chemotherapy in therapy-naive patients with HIV-associated Kaposi sarcoma in South Africa. J Acquir Immune Defic Syndr 2012;60:150–7.
7. Ogretmen B, Hannun YA. Biologically active sphingolipids in cancer pathogenesis and treatment. Nat Rev Cancer 2004;4:604–16.
8. Takabe K, Paugh SW, Milstien S, Spiegel S. "Inside-out" signaling of sphingosine-1-phosphate: therapeutic targets. Pharmacol Rev 2008;60: 181–95.
9. French KJ, Schrecengost RS, Lee BD, Zhuang Y, Smith SN, Eberly JL, et al. Discovery and evaluation of inhibitors of human sphingosine kinase. Cancer Res 2003;63:5962–9.
10. French KJ, Zhuang Y, Maines LW, Gao P, Wang W, Beljanski V, et al. Pharmacology and antitumor activity of ABC294640, a selective inhibitor of sphingosine kinase-2. J Pharmacol Exp Ther 2010;333:129–39.
11. French KJ, Upson JJ, Keller SN, Zhuang Y, Yun JK, Smith CD. Antitumor activity of sphingosine kinase inhibitors. J Pharmacol Exp Ther 2006;318: 596–603.
12. Beljanski V, Knaak C, Smith CD. A novel sphingosine kinase inhibitor induces autophagy in tumor cells. J Pharmacol Exp Ther 2010;333: 454–64.
13. Qin Z, Dai L, Trillo-Tinoco J, Senkal C, Wang W, Reske T, et al. Targeting sphingosine kinase induces apoptosis and tumor regression for KSHV-associated primary effusion lymphoma. Mol Cancer Ther 2014;13:154–64.
14. Dai L, Plaisance-Bonstaff K, Voelkel-Johnson C, Smith CD, Ogretmen B, Qin Z, et al. Sphingosine kinase-2 maintains viral latency and survival for KSHV-infected endothelial cells. PLoS One 2014;9:e102314.
15. An FQ, Folarin HM, Compitello N, Roth J, Gerson SL, McCrae KR, et al. Long-term-infected telomerase-immortalized endothelial cells: a model for Kaposi's sarcoma-associated herpesvirus latency in vitro and in vivo. J Virol 2006;80:4833–46.
16. Dai L, Trillo-Tinoco J, Chen Y, Bonstaff K, Del Valle L, Parsons C, et al. CD147 and downstream ADAMTSs promote the tumorigenicity of Kaposi's sarcoma-associated herpesvirus infected endothelial cells. Oncotarget 2016;7:3806–18.
17. Raval J, Lyman S, Nitta T, Mohuczy D, Lemasters JJ, Kim JS, et al. Basal reactive oxygen species determine the susceptibility to apoptosis in cirrhotic hepatocytes. Free Radic Biol Med 2006;41:1645–54.
18. Bielawski J, Szulc ZM, Hannun YA, Bielawska A. Simultaneous quantitative analysis of bioactive sphingolipids by high-performance liquid chromatography-tandem mass spectrometry. Methods 2006; 39:82–91.
19. Mullen TD, Hannun YA, Obeid LM. Ceramide synthases at the centre of sphingolipid metabolism and biology. Biochem J 2012;441:789–802.
20. Dai L, Trillo-Tinoco J, Cao Y, Bonstaff K, Doyle L, Del Valle L, et al. Targeting HGF/c-MET induces cell cycle arrest, DNA damage, and apoptosis for primary effusion lymphoma. Blood 2015;126:2821–31.
21. Sato M, Bremner I. Oxygen free radicals and metallothionein. Free Radic Biol Med 1993;14:325–37.
22. Iszard MB, Liu J, Klaassen CD. Effect of several metallothionein inducers on oxidative stress defense mechanisms in rats. Toxicology 1995; 104:25–33.
23. Aschner M, Conklin DR, Yao CP, Allen JW, Tan KH. Induction of astrocyte metallothioneins (MTs) by zinc confers resistance against the acute cytotoxic effects of methylmercury on cell swelling, Na+ uptake, and K+ release. Brain Res 1998;813:254–61.
24. Namdarghanbari M, Wobig W, Krezoski S, Tabatabai NM, Petering DH. Mammalian metallothionein in toxicology, cancer, and cancer chemotherapy. J Biol Inorg Chem 2011;16:1087–101.
25. Cai L, Koropatnick J, Cherian MG. Metallothionein protects DNA from copper-induced but not iron-induced cleavage in vitro. Chem Biol Interact 1995;96:143–55.
26. Shibuya K, Nishimura N, Suzuki JS, Tohyama C, Naganuma A, Satoh M. Role of metallothionein as a protective factor against radiation carcinogenesis. The J Toxicol Sci 2008;33:651–5.
27. Cherian MG, Jayasurya A, Bay BH. Metallothioneins in human tumors and potential roles in carcinogenesis. Mutat Res 2003;533:201–9.
28. Zhang C, Chen Y, Wang M, Chen X, Li Y, Song E, et al. PPM1D silencing by RNA interference inhibits the proliferation of lung cancer cells. World J Surg Oncol 2014;12:258.
29. Wang W, Zhu H, Zhang H, Zhang L, Ding Q, Jiang H. Targeting PPM1D by lentivirus-mediated RNA interference inhibits the tumorigenicity of bladder cancer cells. Braz J Med Biol Res 2014;47:1044–9.
30. Lee SJ, Smith A, Guo L, Alastalo TP, Li M, Sawada H, et al. Autophagic protein LC3B confers resistance against hypoxia-induced pulmonary hypertension. Am J Respir Crit Care Med 2011;183:649–58.

Published OnlineFirst September 22, 2017; DOI: 10.1158/1535-7163.MCT-17-0485

31. Lee JS, Li Q, Lee JY, Lee SH, Jeong JH, Lee HR, et al. FLIP-mediated autophagy regulation in cell death control. Nat Cell Biol 2009;11:1355–62.
32. Leidal AM, Cyr DP, Hill RJ, Lee PW, McCormick C. Subversion of autophagy by Kaposi's sarcoma-associated herpesvirus impairs oncogene-induced senescence. Cell Host Microbe 2012;11:167–80.
33. Santarelli R, Gonnella R, Di Giovenale G, Cuomo L, Capobianchi A, Granato M, et al. STAT3 activation by KSHV correlates with IL-10, IL-6 and IL-23 release and an autophagic block in dendritic cells. Sci Rep 2014;4:4241.
34. Scarlatti F, Bauvy C, Ventruti A, Sala G, Cluzeaud F, Vandewalle A, et al. Ceramide-mediated macroautophagy involves inhibition of protein kinase B and up-regulation of beclin 1. J Biol Chem 2004;279:18384–91.
35. Dai L, Trillo-Tinoco J, Bai A, Chen Y, Bielawski J, Del Valle L, et al. Ceramides promote apoptosis for virus-infected lymphoma cells through induction of ceramide synthases and viral lytic gene expression. Oncotarget 2015;6:24246–60.
36. Cao Y, Qiao J, Lin Z, Zabaleta J, Dai L, Qin Z. Up-regulation of tumor suppressor genes by exogenous dhC16-Cer contributes to its anti-cancer activity in primary effusion lymphoma. Oncotarget 2017;8:15220–9.
37. Meijer AJ, Codogno P. Signalling and autophagy regulation in health, aging and disease. Mol Aspects Med 2006;27:411–25.
38. Ding WX, Yin XM. Sorting, recognition and activation of the misfolded protein degradation pathways through macroautophagy and the proteasome. Autophagy 2008;4:141–50.
39. Matta H, Chaudhary PM. The proteasome inhibitor bortezomib (PS-341) inhibits growth and induces apoptosis in primary effusion lymphoma cells. Cancer Biol Ther 2005;4:77–82.
40. Bhatt S, Ashlock BM, Toomey NL, Diaz LA, Mesri EA, Lossos IS, et al. Efficacious proteasome/HDAC inhibitor combination therapy for primary effusion lymphoma. J Clin Invest 2013;123:2616–28.
41. Chen W, Sin SH, Wen KW, Damania B, Dittmer DP. Hsp90 inhibitors are efficacious against Kaposi sarcoma by enhancing the degradation of the essential viral gene LANA, of the viral co-receptor EphA2 as well as other client proteins. PLoS Pathog 2012;8:e1003048.
42. Gopalakrishnan R, Matta H, Chaudhary PM. A purine scaffold HSP90 inhibitor BIIB021 has selective activity against KSHV-associated primary effusion lymphoma and blocks vFLIP K13-induced NF-kappaB. Clin Cancer Res 2013;19:5016–26.
43. Nayar U, Lu P, Goldstein RL, Vider J, Ballon G, Rodina A, et al. Targeting the Hsp90-associated viral oncoproteome in gammaherpesvirus-associated malignancies. Blood 2013;122:2837–47.

AACR American Association for Cancer Research

Molecular Cancer Therapeutics

ABC294640, A Novel Sphingosine Kinase 2 Inhibitor, Induces Oncogenic Virus –Infected Cell Autophagic Death and Represses Tumor Growth

Lu Dai, Aiping Bai, Charles D. Smith, et al.

Mol Cancer Ther Published OnlineFirst September 22, 2017.

Epub ahead of print October 13, 2017 - doi:10.1189/jlb.5A0617-219R

JLB

Article

The effect of plasma auto-IgGs on CD4$^+$ T cell apoptosis and recovery in HIV-infected patients under antiretroviral therapy

Zhenwu Luo, Zejun Zhou,* Elizabeth Ogunrinde,* Tao Zhang,*,† Zhen Li,‡ Lisa Martin,§ Zhuang Wan,* Hao Wu,‡ Zhiqiang Qin,¶ Tongwen Ou,‖ Jiafeng Zhang,# Lei Ma,** Guoyang Liao,** Sonya Heath,†† Lei Huang,‡‡,1 and Wei Jiang*,†,2*

*Department of Microbiology and Immunology and §Division of Infectious Diseases, Department of Medicine, Medical University of South Carolina, Charleston, South Carolina, USA; †The First Affiliated Hospital of Hu-Nan University of Chinese Medicine, Changsha, China; ‡Beijing You'an Hospital, Capital Medical University, Fengtai District, Beijing, China; ¶Department of Genetics, Louisiana Cancer Research Center, Louisiana State University Health Sciences Center, New Orleans, Louisiana, USA; ‖Capital Medical University Affiliated XuanWu Hospital, Xicheng District, Beijing, China; #Zhejiang Provincial Center for Disease Control and Prevention, Hangzhou, China; **Biologicals Department, Institute of Medical Biology, Chinese Academy of Medical Sciences & Peking Union Medical College, Kuming, China; ††Division of Infectious Diseases, Department of Medicine, University of Alabama at Birmingham, Birmingham, Alabama, USA; and ‡‡The People's Liberation Army No. 302 Hospital, Treatment and Research Center for Infectious Diseases, Beijing, China

RECEIVED JUNE 2, 2017; REVISED SEPTEMBER 1, 2017; ACCEPTED SEPTEMBER 16, 2017. DOI: 10.1189/jlb.5A0617-219R

ABSTRACT

Although effective antiretroviral therapy (ART) suppresses HIV viral replication, prevents AIDS-related complications, and prolongs life, a proportion of patients fails to restore the patients' CD4$^+$ T cell number to the level of healthy individuals. Increased mortality and morbidity have been observed in these patients. In the current study, we have investigated the role of auto-IgGs in CD4$^+$ T cell apoptosis and recovery in a cross-sectional study. All HIV$^+$ subjects were on viral-suppressive ART treatment with a different degree of CD4$^+$ T cell reconstitution. Total auto-IgG binding on CD4$^+$ T cell surfaces and its associated apoptosis and CD4$^+$ T cell recovery were analyzed by flow cytometry ex vivo. Total IgGs from plasma were tested for their binding capacities to CD4$^+$ T cell surfaces and their mediation to CD4$^+$ T cell death through NK cell cytotoxicity in vitro. HIV$^+$ subjects had increased surface binding of auto-IgGs on CD4$^+$ T cells compared with healthy controls, and IgG binding was associated with elevated CD4$^+$ T cell apoptosis in HIV$^+$ subjects but not in healthy controls. Plasma IgGs from HIV$^+$ subjects bound to CD4$^+$ T cells and induced cell apoptosis through NK cytotoxicity in vitro. Soluble CD4 (sCD4) preincubation prevented NK cell-mediated CD4$^+$ T cell death. Our results suggest that plasma autoantibodies may play a role in some HIV$^+$ patients with poor CD4$^+$ T cell recovery under viral-suppressive ART. *J. Leukoc. Biol.* 102: 000–000; 2017.

Introduction

The advent of ART has dramatically improved survival and disease progression in HIV-infected individuals [1]. ART treatment suppresses HIV viral replication, improves immune function, restores peripheral CD4$^+$ T cell counts, and decreases morbidity and mortality [2–4]. However, long-term ART-treated patients exhibit an increased risk of cardiovascular diseases, cancer, osteoporosis, and other end-organ diseases [5]. Incomplete CD4$^+$ T cell reconstitution is mainly accounting for these aging-like complications.

The mechanisms of incomplete CD4$^+$ T cell recovery in HIV disease have been studied extensively, including direct viral cytopathogenicity, lymphoid fibrosis and thymic insufficiency [6, 7], indirect effects of persistent T cell activation and apoptosis [8–10], gut mucosal dysfunction, and elevated levels of microbial translocation and inflammation [11, 12]. However, the exact mechanism is not fully understood.

In the current study, we examined the potential role of auto-IgG binding on CD4$^+$ T cell surfaces in HIV$^+$ subjects after long-term, viral-suppressive ART treatment. We found that CD4$^+$ T cell apoptosis was elevated in HIV$^+$ subjects compared with healthy controls. The percentage of auto-IgG binding on CD4$^+$ T cell surfaces was inversely correlated with CD4$^+$ T cell counts in HIV$^+$ subjects. IgGs from plasma of HIV$^+$ subjects induced CD4$^+$ T cell death through NK cytotoxicity (ADCC) in vitro. sCD4 protein preincubation prevented IgG-mediated CD4$^+$ T cell death. Our results suggest that autoantibody-mediated CD4$^+$ T cell death

Abbreviations: ADCC = antibody-dependent cellular cytotoxicity, APC = allophycocyanin, ART = antiretroviral therapy, mCD = memory cluster of differentiation, nCD = naive cluster of differentiation, sCD = soluble cluster of differentiation

1. Correspondence: The PLA No. 302 Hospital, Treatment and Research Center for Infectious Diseases, Beijing, China, 100039. E-mail: huangleiwa@sina.com

2. Correspondence: Department of Microbiology and Immunology, Medical University of South Carolina, 173 Ashley Avenue, BSB208D, 9383, Charleston, SC 29466, USA. E-mail: jianw@musc.edu

may reveal an important mechanism of incomplete immune recovery in virologically suppressed HIV disease.

MATERIALS AND METHODS

Study subjects

Sixteen healthy controls and 26 HIV$^+$ ART-treated, aviremic, HIV-infected subjects were evaluated in a cross-sectional study. The clinical characteristics are shown in **Table 1**. All HIV$^+$ patients had been on ART treatment and had undetectable plasma HIV-1 RNA (<50 copies/ml) for at least 2 yr. The clinical characteristics of patients were shown in our previous study [13]. This study was approved by the Institutional Review Board from the Medical University of South Carolina.

Flow cytometry

The fluorochrome-labeled mAb used in this study included the following: anti-human CD3 (OKT3), anti-human CD4 (RPA-T4), anti-human CD8 (RPA-T8), anti-human CD27 (M-T271), anti-human CD45RA (HI100), annexin V (BD Pharmingen; BD Biosciences, San Jose, CA, USA), Ghost Dye Red 780 (Tonbo Biosciences, San Diego, CA, USA), and isotype control antibodies (BD Pharmingen; BD Biosciences). Cells were collected by a BD FACSVerse flow cytometer (BD Biosciences), and data were analyzed by FlowJo software (version 10.0.8; Ashland, OR, USA).

CD4 surface-bound IgG ex vivo

Plasma was isolated by centrifugation of EDTA-contained blood, aliquoted, and stored at −80°C. PBMCs were isolated over a Ficoll-Paque, and freshly isolated PBMCs were used for annexin V assays (see Fig. 1). Thawed PBMC samples were used for detecting surface-bound IgG on CD4$^+$ T cells (see Fig. 2B and C). Fluorescent-labeled antibodies were incubated with PBMCs at 4°C for 30 min for surface staining, and the cells were washed and stained with annexin V and then analyzed by flow cytometry immediately.

CD4 surface-bound IgG detection using plasmas in vitro

PBMCs from a healthy control donor were cultured with PHA (2 μg/ml) at 37°C for 24 h, and plasma from HIV$^+$ subjects or healthy controls was inactivated at 56°C for 30 min. Then, PHA-stimulated PBMCs (5×10^5 cells) were treated with 2.5 μl plasma in 50 μl buffer at 4°C for 60 min. After washing 3× with PBS, 50 μl aqua blue (Thermo Fisher Scientific, Waltham, MA, USA) was used at 4°C for 20 min to exclude dead cells. Next, 50 μl antibody cocktail containing anti CD3-PerCP (OKT3), CD4-BV421 (RPA-T4), CD8-PE-Cy7 (RPA-T8), CD27-APC-Cy7 (M-T271), CD45RA-FITC (HI100), IgM-APC (G20-127), and IgG-PE (G18-145) was surface stained at 4°C for 30 min. The cells were washed and analyzed by flow cytometry.

NK-mediated ADCC

CD4$^+$ T cells and NK cells were isolated from aviremic, ART-treated HIV$^+$ subjects or healthy controls for cytolysis and apoptosis assay. In brief, NK cells were isolated from PBMC using an NK cell enrichment kit (Stemcell Technologies, Vancouver, BC, Canada) and CD4$^+$ T cells were isolated from PBMC using a CD4 cell enrichment kit (Stemcell Technologies). The purities of CD4$^+$ T cells were above 93%, and the purities of NK cells were above 93%.

We pretreated CD4$^+$ T cells with sCD4 (Progenics Pharmaceuticals, New York, NY, USA) at a concentration of 25 μg/ml at 4°C for 60 min and stained with anti-CD4 antibody eBioscience eFluor 670 (Thermo Fisher Scientific). CD4$^+$ T cells were pretreated with sCD3 (Abcam, Cambridge, MA, USA) at a concentration of 25 μg/ml as Control 1. Anti-CD4 mAb (zanolimumab, 6G5) was cultured with CD4$^+$ T cells for 15 min and then treated with sCD4 (the concentration of 6G5:sCD4 is 1:5) as Control 2. 6G5 (5 μg/ml), cultured with CD4$^+$ T cells without sCD4 or sCD3, was set as a positive control. Next, CD4$^+$ T cells were cultured with autologous NK cells at a 3:1 ratio in Corning 96-well, V-bottom plates (Millipore-Sigma, St. Louis, MO, USA). The CD4$^+$ T cell cultures, in the absence of 6G5, sCD4, sCD3, and NK cells, were served as the additional negative controls. After incubation, $CaCl_2$ buffer and annexin V were added to the medium, which contained a constant number of flow cytometry particles (5×10^4/ml; AccuCount blank particles, 5.3 μm; Spherotech, Lake Forest, IL, USA). A constant number of particles (2.5×10^3) were counted during cytometry acquisition to normalize the number of CD4$^+$ T cells. The percentage of cytolysis was calculated using the following formula: %cytolysis = [(number of CD4$^+$ T cells of negative control) − (number of CD4$^+$ T cells in the presence of anti-CD4 IgGs, sCD4, or sCD3)]/(number of CD4$^+$ T cells of negative control) × 100. Cell apoptosis was analyzed by annexin V binding.

Statistical analysis

All data were analyzed and graphed using GraphPad Prism 6.0 (GraphPad Software, La Jolla, CA, USA) and SPSS (Version 23; IBM, Armonk, NY, USA). Statistical significance between 2 groups was determined by the Mann-Whitney *U* test (nonparametric) and the ANOVA test (paired test) for 3 or more groups. Associations between pairs of continuous variables were analyzed by Spearman correlation tests.

RESULTS

CD4$^+$ T cells are highly apoptotic and depleted in viral-suppressed, ART-treated HIV$^+$ subjects ex vivo

The absolute count and frequency of CD4$^+$ T cell subsets were assessed by flow cytometry. Total CD4$^+$ T cell, mCD4$^+$ T cell (CD3$^+$CD4$^+$CD45RA$^-$CD27$^{+/-}$), and nCD4$^+$ T cell (CD3$^+$CD4$^+$CD45RA$^+$CD27$^+$) absolute counts were still not fully recovered, even after long-term ART treatment in some HIV$^+$ subjects compared with healthy control (**Fig. 1A** and **B**; $P < 0.05$). T Cell apoptosis is an important immunologic parameter for HIV disease progression [14]. In untreated HIV patients, T cells undergo apoptosis, leading to an eventual T cell decline [15]. In this study, we analyzed CD4$^+$ T cell apoptosis using fresh blood samples. Consistent with the decline of CD4$^+$ T cell counts, CD4$^+$ T cells, including both nCD4$^+$ and mCD4$^+$ T cells from HIV$^+$ subjects,

TABLE 1. Clinical characteristics

Characteristic	Healthy control	HIV$^+$/ART treated	*P*
Total no. of subjects	16	26	
Sex, male/female	5/16	17/26	0.07
Age	38 (32–52)	43 (34–52)	0.99
CD4$^+$ T cell counts	765 (523–936)	540 (366–720)	0.02
Nadir CD4$^+$ T cell counts		294 (193–458)	
Years of ART		9 (6–11)	

CD4$^+$ T cell counts (cells per microliter). Data are medians (interquartile ranges).

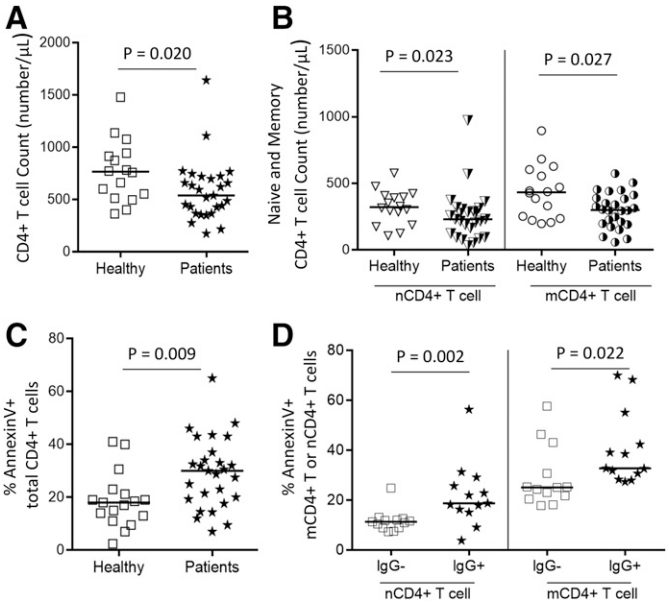

Figure 1. The absolute CD4$^+$ T cell counts and percentages of CD4$^+$ T cell apoptosis ex vivo. The median absolute counts of total CD4$^+$ T cells (A) and nCD4$^+$ (CD3$^+$CD4$^+$CD45RA$^+$CD27$^+$), and mCD4$^+$ (CD3$^+$CD4$^+$CD45RA$^-$CD27$^{+/-}$) T cells (B) in healthy controls and HIV$^+$ subjects ex vivo. The median percentages of annexin V binding on total CD4$^+$ T cells (C) and nCD4$^+$ and mCD4$^+$ T cells (D) in healthy controls and HIV$^+$ subjects ex vivo. Mann-Whitney *U* test (nonparametric).

experienced increased frequencies of T cell apoptosis compared with those from healthy controls (Fig. 1C and D). These results suggest that CD4$^+$ T cells are not fully recovered, and their function is not normal, even after long-term, viral-suppressive ART treatment.

Increased surface-bound IgG on CD4$^+$ T cells is associated with increased CD4$^+$ T cell apoptosis in HIV$^+$ subjects under viral-suppressed ART treatment

Increased surface binding of IgG on CD4$^+$ T cells and elevated levels of apoptotic IgG$^+$CD4$^+$ T cells have been reported in HIV-infected patients with hemophilia, suggesting that attachment of IgG to CD4$^+$ T cells may be associated with cell apoptosis [16]. To determine whether IgG-bound CD4$^+$ T cells could be detected in aviremic, ART-treated patients, we analyzed the percentages of surface IgG binding on CD4$^+$ T cells using anti-total IgG antibodies. Notably, we observed increased frequencies of IgG surface binding on both mCD4$^+$ and nCD4$^+$ T cells in HIV$^+$ subjects compared with healthy controls (**Fig. 2B**; $P < 0.05$). Moreover, nCD4$^+$ T cells had a higher frequency of IgG surface binding compared with mCD4$^+$ T cells in both healthy controls and HIV$^+$ subjects (Fig. 2B; $P < 0.05$).

Next, we chose samples with relatively higher frequencies of auto-IgG binding on total CD4$^+$ T cells (above 5 percentile in patients) and tested annexin V binding. We found that apoptosis was elevated in IgG$^+$CD4$^+$ T cells compared with IgG$-$CD4$^+$ T cells (Fig. 2C). Importantly, the percentage of IgG binding on CD4$^+$ T cells was inversely correlated with the absolute CD4$^+$ T cell counts in HIV$^+$ subjects ($r = -0.476$, $P = 0.016$) but not in healthy controls ($r = 0.093$, $P = 0.74$; Fig. 2D). These results suggest that auto-IgG binding on CD4$^+$ T cells may contribute to CD4$^+$ T cell apoptosis and depletion in ART-treated HIV disease in vivo.

Furthermore, to investigate the role of auto-IgGs from plasma of HIV$^+$ subjects in CD4$^+$ T cell apoptosis and recovery, total IgGs from plasma were tested for their binding abilities on CD4$^+$ T cell surfaces in vitro. Consistent with the amount of auto-IgGs on CD4$^+$ T cell surfaces ex vivo, the amount of auto-IgGs bound to CD4$^+$ T cells was increased significantly in plasma from ART-treated

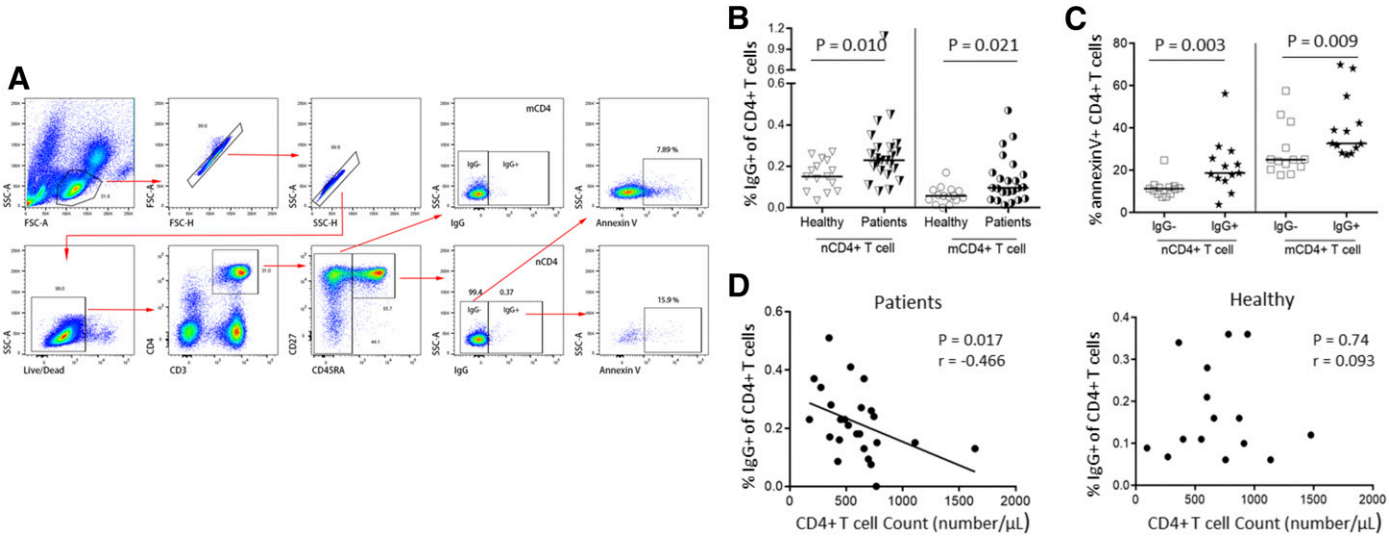

Figure 2. Surface-bound IgG on CD4$^+$ T cells and its association with cell apoptosis and recovery in HIV ex vivo. The percentages of IgG$^+$ on CD4$^+$ T cells and annexin V binding were analyzed by flow cytometry. (A) Representative dot plots showing the gating strategies were used to assess gating strategies of anti-IgG antibody surface binding and cell apoptosis (annexin V) on mCD4$^+$ T cells and nCD4$^+$ T cells. (B) The median frequencies of surface-bound IgG on mCD4$^+$ T cells and nCD4$^+$ T cells among healthy controls and HIV$^+$ subjects ex vivo. (C) The median frequencies of annexin V binding on IgG$^+$ and IgG$^-$ CD4$^+$ T cell subsets in HIV$^+$ subjects (50 percentile above the frequencies of auto-IgG binding on CD4$^+$ T cells in patients). (D) The correlations between surface-bound IgG and peripheral CD4$^+$ T cell counts in HIV$^+$ subjects and healthy controls. Mann-Whitney *U* test (nonparametric) and Spearman correlation tests. SSC-A, Side-scatter-area; FSC-A, forward-scatter-area; FSC-H, forward-scatter-height; SSC-H, side-scatter-height.

HIV+ subjects compared with healthy controls (**Fig. 3A**). To determine if the presence of auto-IgGs antibodies was represented specifically on CD4+ T cells, we assayed auto-IgGs on CD8+ T cells. Notably, plasma levels of IgG binding on anti-CD8+ T cells were not significantly different between healthy controls and HIV+ subjects (Fig. 3B; $P > 0.05$). Moreover, the frequencies of auto-IgG binding on CD8+ T cells were 0.93 ± 0.47 vs. 1.35 ± 0.94 in healthy controls and HIV+ subjects separately (means ± SD), which were much lower than those on CD4+ T cells (3.34 ± 1.11 vs. 4.45 ± 1.84 in healthy controls and HIV+ subjects separately; Fig. 3A and B).

NK cells purified from ART-treated HIV+ subjects exhibit cytotoxicity to CD4+ T cells via surface-bound auto-IgGs

To analyze further the potential impact of surface autoantibodies on CD4+ T cells, we purified NK cells and CD4+ T cells from ART-treated, HIV-infected subjects that had high amounts of autoantibody on the CD4+ T cell surface (above 5 percentile; Fig. 3A) or from healthy controls. Anti-CD4 IgGs (zanolimumab 6G5, a human mAb) served as the positive control. Surprisingly, coculture NK cells with autologous CD4+ T cells from HIV+ subjects resulted in the increases of CD4+ T cell apoptosis and cytolysis compared with cells from healthy controls (**Fig. 4A** and **B**).

To determine if the increased CD4 apoptosis is the result of greater proportions of auto-IgG antibodies, NK activation, or CD4+ T cell susceptibility, we cultured NK cells and autologous CD4+ T cells with purified total IgGs (50 μg/ml); the cells were from low auto-IgG HIV+ subjects or from healthy controls. Total IgGs were isolated from plasma of high auto-IgG HIV+ patients or healthy controls. Zanolimumab-6G5 antibody (5 μg/ml) was used a positive control. The CD4+ T cells and NK cells from HIV+ subjects were more sensitive than those from healthy controls in the presence of patients' IgGs (Fig. 4C and D; $P = 0.0002$). Notably, there was no significant induction of CD4+ T cell cytolysis in autologous NK cells and CD4+ T cells from healthy controls, cultured with total IgG either from controls or from high auto-IgG HIV+ subjects. There was also no significant induction of CD4+ T cell cytolysis in autologous NK cells and CD4+ T cells from HIV+ patients in the presence of total IgG from healthy controls (Fig. 4E). However, when autologous CD4+ T cells and NK cells from HIV+ subjects were cultured with total IgG from high auto-IgG HIV+ subjects, the induction of CD4+ T cell cytolysis was observed (Fig. 4E). These results may suggest that NK activation, CD4+ T cell susceptibility, and concentration of autoantibodies are all important for the induction of CD4+ T cell death.

To determine the antibody-binding specificity that mediated CD4+ T cell death from HIV+ subjects and whether this process is specific to CD4+ T cells, we assessed CD4+ T cell apoptosis and cytolysis after treatment with sCD4. Our results showed that the positive control anti-human mAb 6G5 mediated ADCC against CD4+ T cells, and sCD4 completely inhibited this effect (Fig. 4F and G). Furthermore, coculture of autologous NK cells and CD4+ T cells from HIV+ subjects resulted in NK-mediated CD4+ T cell death, and sCD4 significantly reduced this effect (Fig. 4F and G). Unlike sCD4, sCD3 failed to protect the CD4+ T cells of HIV+ subjects from death (Fig. 4F and G). These results implied that NK cell-mediated CD4+ T cell death in HIV disease is through CD4 binding.

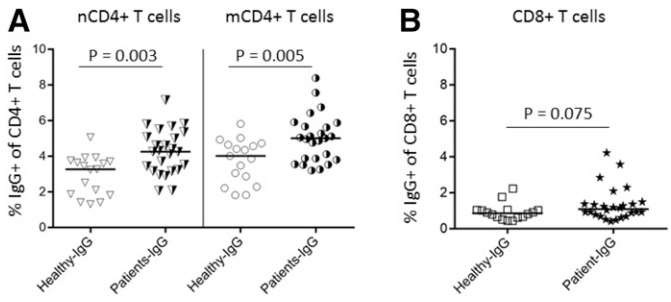

Figure 3. Binding abilities of auto-IgGs from plasma to CD4+ T cell surfaces in vitro. Total IgGs from plasmas of healthy controls and HIV+ subjects were cocultured with PBMCs from the same donor; surface IgG binding was tested by flow cytometry. (A) The median frequencies of IgG binding on nCD4+ and mCD4+ T cells of plasmas from healthy controls or HIV+ subjects. (B) The median frequencies of IgG binding on CD8+ T cells of plasmas from healthy controls or HIV+ subjects. Mann-Whitney *U* test (nonparametric).

DISCUSSION

In the current study, we found that elevated surface IgG binding on CD4+ T cells was inversely correlated with peripheral CD4+ T cell counts in aviremic, ART-treated subjects, and autoantibodies from plasma of HIV+ subjects induced CD4+ T cell death through NK-mediated ADCC and CD4 surface binding. These results suggest a possible role of these antibodies in incomplete immune reconstitution in HIV disease.

Previous studies in SIV and HIV have shown inverse correlations between plasma or serum autoantibody levels and peripheral CD4+ T cell counts, suggesting that autoantibodies against surface antigens on CD4+ T cells may play a role in CD4+ T cell decline [16–19]. However, these studies only investigated autoantibodies of diverse surface proteins on CD4+ T cells in untreated HIV patients or animal models. In the current study, we show clear evidence that even after long-term, viral-suppressive ART treatment, autoantibodies that bind onto CD4+ T cell surfaces are not only present but also facilitate CD4+ T cell death by NK cell-mediated ADCC. The different results between previous studies and ours can be a result of different patient populations (ART-naïve patients in previous studies vs. aviremic, ART-treated patients in our study). Although autoimmune diseases may present in the stage of acute HIV infection, they mainly occur in the immunologic reconstitution phase after ART [20, 21], suggesting that B cells may produce pathologic autoantibodies during immunologic recovery under ART.

The mechanism of NK cell-mediated ADCC against CD4+ T cells in vitro (Fig. 4E–G) may be a result of auto-IgG-activated NK cytotoxicity against IgG+CD4+ T cells. In addition, the inhibition effect of sCD4 indicates CD4-specific binding. Therefore, the percentages of NK cell-induced CD4+ T cell death in vitro were low from HIV+ subjects (Fig. 4E–G; interquartile ranges, 2–5%); however, the long-term effect of NK cells in CD4+ T cell recovery can be significant in vivo.

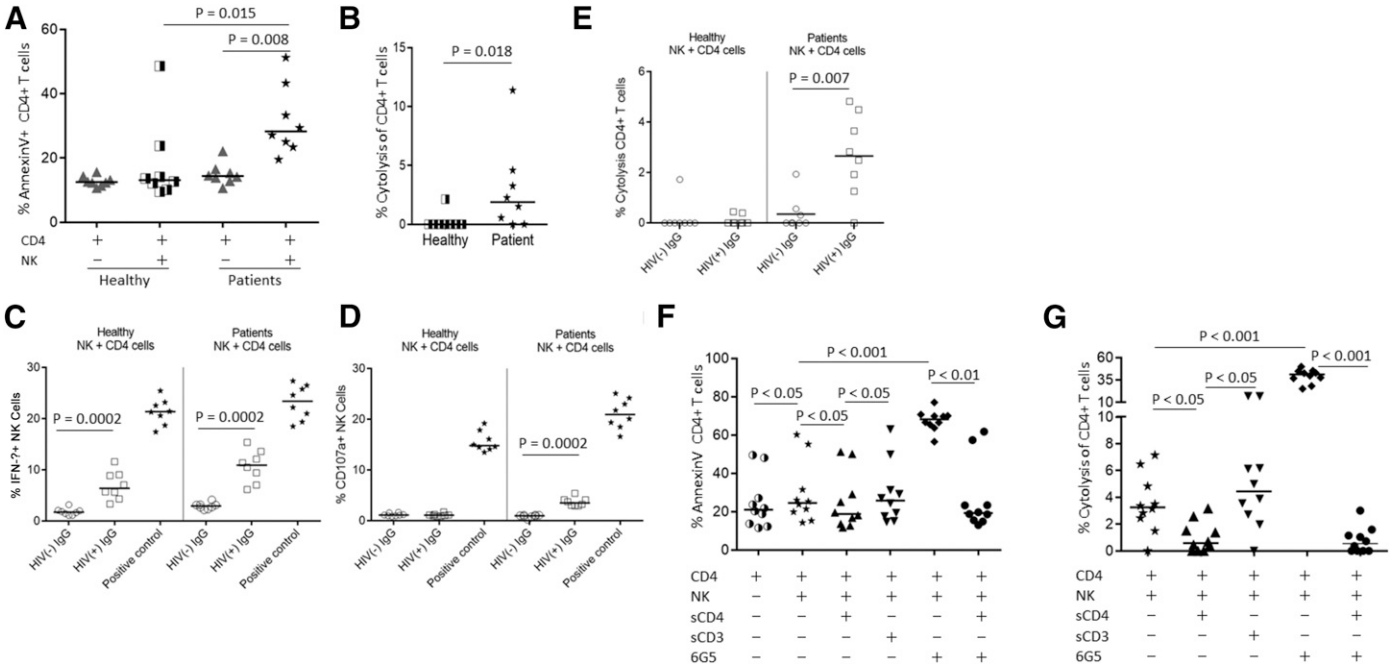

Figure 4. Autoantibody-dependent, NK cell-mediated cytolysis of primary CD4$^+$ T cells from HIV$^+$ subjects in vitro. CD4$^+$ T cells and NK cells were isolated from healthy controls or HIV$^+$ subjects. CD4$^+$ T cells were cultured with autologous NK cells at a ratio of 1:3 in the presence or absence of 6G5 or sCD4 protein, and the percentage of CD4$^+$ T cell apoptosis and cytolysis was analyzed by flow cytometry. The median percentages of annexin V binding (A) and cytolysis (B) of CD4$^+$ T cells from healthy controls or HIV$^+$ subjects cocultured with autologous NK cells in vitro. Mann-Whitney *U* test (nonparametric). The median percentages of IFN-γ^+ (C) and CD107a$^+$ (D) in NK cells and CD4$^+$ T cell apoptosis (E) were shown in culturing cells either from healthy control or HIV$^+$ subjects who had low auto-IgGs on CD4$^+$ T cells in the presence of total IgGs at 50 μg/ml from healthy controls or HIV$^+$ subjects with high frequency of auto-IgGs on CD4$^+$ T cells and zanolimumab (a positive control) at 5 μg/ml in vitro. Mann-Whitney *U* test (nonparametric). The median percentages of CD4$^+$ T cell apoptosis (F) or CD4$^+$ T cells cytolysis (G) from HIV$^+$ subjects cultured with autologous NK cells, with or without sCD4 (25 μg/ml), sCD3 (25 μg/ml), and zanolimumab-6G5 antibody (5 μg/ml) in vitro. ANOVA, paired.

Unlike HIV patients, healthy individuals have a low level of autoantibody bound to the surface of CD4$^+$ T cells, but their cocultured NK cells did not induce cell death of autologous CD4$^+$ T cells in vitro, suggesting a nonpathologic role of autoantibodies in plasma of healthy controls [22]. In addition, CD4$^+$ T cells from HIV$^+$ subjects may be more susceptible to NK-mediated cytotoxicity compared with controls [23]. Consistently, our recent study showed that NK cells are activated in HIV patients with CD4$^+$ T cell counts ≤350 cells/μl compared with healthy individuals and that the percentages of activated NK cells were inversely correlated with CD4$^+$ T cell counts [24]. Notably, sCD4 but not sCD3 inhibited CD4$^+$ T cell death induced by coculturing with autologous NK cells and autoantibodies, indicating a CD4-specific, autoantibody-mediated ADCC effect. However, whether other autoantibodies against surface antigens on CD4$^+$ T cells also play a role in the ADCC needs to be explored further.

The source of the autoantibodies against CD4$^+$ T cells still needs to be addressed. Notably, in recent studies found in lymph nodes and tissues, HIV still actively replicates, even in patients with complete viral suppression under ART [25]. As a consequence, HIV may lead to CD4$^+$ T cell death directly or indirectly. At the same time, the lower frequencies of macrophages and impaired macrophage function in HIV-infected subjects [26] failed to clear the apoptotic debris and immune complexes [27, 28], which may result in an increased level of self-antigens. Furthermore, CD4 antigens from apoptotic CD4$^+$ T cells or released HIV protein-bound CD4 may accumulate in the lymph nodes, providing the antigen stress for pathologic autoantibody generation in HIV patients after ART treatment.

In summary, we found that autoantibodies from HIV patients mediated ADCC against CD4$^+$ T cells through NK cytotoxicity. This may lead to incomplete CD4$^+$ T cell reconstitution from ART.

AUTHORSHIP

Z. Luo, H.W., L.H., and W.J. conceived of and directed the project. Z. Luo wrote the manuscript. Z.Z., E.O., T.Z., Z.Li, L. Martin, Z.W., J.Z., and L. Ma performed the laboratory sample testing and analyses. Z.Q., T.O., G.L., S.H., and W.J. were involved in critically revising the manuscript.

ACKNOWLEDGMENTS

This work was supported by U.S. National Institutes of Health (NIH; Grants AI091526 and AI128864 to W.J.), a U.S. Department of Defense Career Development Award (Grant CA140437; to Z.Q.), Louisiana Clinical and Translational Science Center Pilot (Grant U54GM104940), Saag/Health (NIH Grant P30 AI027767), the National Science Foundation of China–NIH Biomedical Collaborative Research Program (Grant 81761128001; to H.W.), the Beijing Key Laboratory for HIV/AIDS Research

(Grant BZ0089; to H.W.), Cells and Influenza Virus Attenuated Vaccine (Grant 2011DFR30420; to G.L.), Research on Genes Related to Adaptation of Influenza Virus in Vero Cell (Grant 2013FZ141; to G.L.), Research on the Key Technology of Influenza Virus Vaccine Demonstration and Industrialization (Grant 2014AE008; G.L.), Zhejiag Provincial Medicine Science and Technology Plan (Grants 2016RCB004 and 2013KYB059; to J. Zhang), Trivalent Influenza Virus Lysis Vaccine (Grant 2016-12M-1-019; to L. Ma), and the National Science Foundation of China (Grant 81772185; to L.H.). The authors thank NIH AIDS Reagent Program, Division of AIDS, National Institute of Allergy and Infectious Diseases, NIH: Human Soluble CD4 Recombinant Protein (sCD4) from Progenics. Human anti-CD4 mAb zanolimumab (HuMax-CD4) was kindly provided by Dr. Paul Parren from Genmab (Copenhagen, Denmark).

DISCLOSURES

The authors declare no conflicts of interest.

REFERENCES

1. Mocroft, A., Vella, S., Benfield, T. L., Chiesi, A., Miller, V., Gargalianos, P., d'Arminio Monforte, A., Yust, I., Bruun, J. N., Phillips, A. N., Lundgren, J. D. (1998) Changing patterns of mortality across Europe in patients infected with HIV-1. EuroSIDA study group. *Lancet* **352,** 1725–1730.
2. Battegay, M., Nüesch, R., Hirschel, B., Kaufmann, G. R. (2006) Immunological recovery and antiretroviral therapy in HIV-1 infection. *Lancet Infect. Dis.* **6,** 280–287.
3. May, M. T., Sterne, J. A., Costagliola, D., Sabin, C. A., Phillips, A. N., Justice, A. C., Dabis, F., Gill, J., Lundgren, J., Hogg, R. S., de Wolf, F., Fätkenheuer, G., Staszewski, S., d'Arminio Monforte, A., Egger, M.; Antiretroviral Therapy (ART) Cohort Collaboration. (2006) HIV treatment response and prognosis in Europe and North America in the first decade of highly active antiretroviral therapy: a collaborative analysis. *Lancet* **368,** 451–458.
4. Palella, F. J., Jr., Delaney, K. M., Moorman, A. C., Loveless, M. O., Fuhrer, J., Satten, G. A., Aschman, D. J., Holmberg, S. D.; HIV Outpatient Study Investigators. (1998) Declining morbidity and mortality among patients with advanced human immunodeficiency virus infection. *N. Engl. J. Med.* **338,** 853–860.
5. Deeks, S. G., Lewin, S. R., Havlir, D. V. (2013) The end of AIDS: HIV infection as a chronic disease. *Lancet* **382,** 1525–1533.
6. Teixeira, L., Valdez, H., McCune, J. M., Koup, R. A., Badley, A. D., Hellerstein, M. K., Napolitano, L. A., Douek, D. C., Mbisa, G., Deeks, S., Harris, J. M., Barbour, J. D., Gross, B. H., Francis, I. R., Halvorsen, R., Asaad, R., Lederman, M. M. (2001) Poor CD4 T cell restoration after suppression of HIV-1 replication may reflect lower thymic function. *AIDS* **15,** 1749–1756.
7. Diaz, A., Alós, L., León, A., Mozos, A., Caballero, M., Martinez, A., Plana, M., Gallart, T., Gil, C., Leal, M., Gatell, J. M., García, F.; Study Group of Lymphoid Tissue immunopathogenesis in HIV infection. (2010) Factors associated with collagen deposition in lymphoid tissue in long-term treated HIV-infected patients. *AIDS* **24,** 2029–2039.
8. Lederman, M. M., Calabrese, L., Funderburg, N. T., Clagett, B., Medvik, K., Bonilla, H., Gripshover, B., Salata, R. A., Taege, A., Lisgaris, M., McComsey, G. A., Kirchner, E., Baum, J., Shive, C., Asaad, R., Kalayjian, R. C., Sieg, S. F., Rodriguez, B. (2011) Immunologic failure despite suppressive antiretroviral therapy is related to activation and turnover of memory CD4 cells. *J. Infect. Dis.* **204,** 1217–1226.
9. Hunt, P. W., Martin, J. N., Sinclair, E., Bredt, B., Hagos, E., Lampiris, H., Deeks, S. G. (2003) T cell activation is associated with lower CD4+ T cell gains in human immunodeficiency virus-infected patients with sustained viral suppression during antiretroviral therapy. *J. Infect. Dis.* **187,** 1534–1543.
10. Hunt, P. W., Brenchley, J., Sinclair, E., McCune, J. M., Roland, M., Page-Shafer, K., Hsue, P., Emu, B., Krone, M., Lampiris, H., Douek, D., Martin, J. N., Deeks, S. G. (2008) Relationship between T cell activation and CD4+ T cell count in HIV-seropositive individuals with undetectable plasma HIV RNA levels in the absence of therapy. *J. Infect. Dis.* **197,** 126–133.
11. Mavigner, M., Cazabat, M., Dubois, M., L'Faqihi, F. E., Requena, M., Pasquier, C., Klopp, P., Amar, J., Alric, L., Barange, K., Vinel, J. P., Marchou, B., Massip, P., Izopet, J., Delobel, P. (2012) Altered CD4+ T cell homing to the gut impairs mucosal immune reconstitution in treated HIV-infected individuals. *J. Clin. Invest.* **122,** 62–69.
12. Marchetti, G., Bellistrì, G. M., Borghi, E., Tincati, C., Ferramosca, S., La Francesca, M., Morace, G., Gori, A., Monforte, A. D. (2008) Microbial translocation is associated with sustained failure in CD4+ T-cell reconstitution in HIV-infected patients on long-term highly active antiretroviral therapy. *AIDS* **22,** 2035–2038.
13. Luo, Z., Ma, L., Zhang, L., Martin, L., Wan, Z., Warth, S., Kilby, A., Gao, Y., Bhargava, P., Li, Z., Wu, H., Meissner, E. G., Li, Z., Kilby, J. M., Liao, G., Jiang, W. (2016) Key differences in B cell activation patterns and immune correlates among treated HIV-infected patients versus healthy controls following influenza vaccination. *Vaccine* **34,** 1945–1955.
14. Sousa, A. E., Carneiro, J., Meier-Schellersheim, M., Grossman, Z., Victorino, R. M. (2002) CD4 T cell depletion is linked directly to immune activation in the pathogenesis of HIV-1 and HIV-2 but only indirectly to the viral load. *J. Immunol.* **169,** 3400–3406.
15. Epple H. J, Allers K., Tröger H., Kühl A., Erben U., Fromm M., Zeitz M., Loddenkemper C., Schulzke J. D., Schneider T. (2010) Acute HIV infection induces mucosal infiltration with CD4+ and CD8+ T cells, epithelial apoptosis, and a mucosal barrier defect. *Gastroenterology* **139,** 1289–1300.
16. Daniel, V., Sadeghi, M., Naujokat, C., Weimer, R., Huth-Kühne, A., Zimmermann, R., Opelz, G. (2004) Evidence for autoantibody-induced CD4 depletion mediated by apoptotic and non-apoptotic mechanisms in HIV-positive long-term surviving haemophilia patients. *Clin. Exp. Immunol.* **135,** 94–104.
17. Stricker, R. B., McHugh, T. M., Moody, D. J., Morrow, W. J., Stites, D. P., Shuman, M. A., Levy, J. A. (1987) An AIDS-related cytotoxic autoantibody reacts with a specific antigen on stimulated CD4+ T cells. *Nature* **327,** 710–713.
18. Ardman, B., Mayer, K., Bristol, J., Ryan, M., Settles, M., Levy, E. (1990) Surface immunoglobulin-positive T lymphocytes in HIV-1 infection: relationship to CD4+ lymphocyte depletion. *Clin. Immunol. Immunopathol.* **56,** 249–258.
19. Müller, C., Kukel, S., Bauer, R. (1993) Relationship of antibodies against CD4+ T cells in HIV-infected patients to markers of activation and progression: autoantibodies are closely associated with CD4 cell depletion. *Immunology* **79,** 248–254.
20. Iordache, L., Launay, O., Bouchaud, O., Jeantils, V., Goujard, C., Boue, F., Cacoub, P., Hanslik, T., Mahr, A., Lambotte, O., Fain, O., associated authors: Delassus, J. L., Dhote, R., Fior, R., Galicier, L., Guillevin, L., Honore, P., Manea, M., Mekinian, A., de Menthon, M., Nunes, H., Pillebout, E., Raho, M., Weiss, L. (2014) Autoimmune diseases in HIV-infected patients: 52 cases and literature review. *Autoimmun. Rev.* **13,** 850–857.
21. Zandman-Goddard, G., Shoenfeld, Y. (2002) HIV and autoimmunity. *Autoimmun. Rev.* **1,** 329–337.
22. Elkon, K., Casali, P. (2008) Nature and functions of autoantibodies. *Nat. Clin. Pract. Rheumatol.* **4,** 491–498.
23. Doitsh, G., Galloway, N. L., Geng, X., Yang, Z., Monroe, K. M., Zepeda, O., Hunt, P. W., Hatano, H., Sowinski, S., Muñoz-Arias, I., Greene, W. C. (2014) Cell death by pyroptosis drives CD4 T-cell depletion in HIV-1 infection. *Nature* **505,** 509–514.
24. Luo, Z., Li, Z., Martin, L., Hu, Z., Wu, H., Wan, Z., Kilby, M., Heath, S. L., Huang, L., Jiang, W. (2017) Increased natural killer cell activation in HIV-infected immunologic non-responders correlates with CD4+ T cell recovery after antiretroviral therapy and viral suppression. *PLoS One* **12,** e0167640.
25. Lorenzo-Redondo, R., Fryer, H. R., Bedford, T., Kim, E. Y., Archer, J., Pond, S. L., Chung, Y. S., Penugonda, S., Chipman, J., Fletcher, C. V., Schacker, T. W., Malim, M. H., Rambaut, A., Haase, A. T., McLean, A. R., Wolinsky, S. M. (2016) Persistent HIV-1 replication maintains the tissue reservoir during therapy. *Nature* **530,** 51–56.
26. Brenchley, J. M., Paiardini, M., Knox, K. S., Asher, A. I., Cervasi, B., Asher, T. E., Scheinberg, P., Price, D. A., Hage, C. A., Kholi, L. M., Khoruts, A., Frank, I., Else, J., Schacker, T., Silvestri, G., Douek, D. C. (2008) Differential Th17 CD4 T-cell depletion in pathogenic and nonpathogenic lentiviral infections. *Blood* **112,** 2826–2835.
27. Koppensteiner, H., Brack-Werner, R., Schindler, M. (2012) Macrophages and their relevance in human immunodeficiency virus type I infection. *Retrovirology* **9,** 82.
28. Torre, D., Gennero, L., Baccino, F. M., Speranza, F., Biondi, G., Pugliese, A. (2002) Impaired macrophage phagocytosis of apoptotic neutrophils in patients with human immunodeficiency virus type 1 infection. *Clin. Diagn. Lab. Immunol.* **9,** 983–986.

KEY WORDS:
disease · autoantibody · HIV infection · ART

The effect of plasma auto-IgGs on CD4$^+$ T cell apoptosis and recovery in HIV-infected patients under antiretroviral therapy

Zhenwu Luo, Zejun Zhou, Elizabeth Ogunrinde, et al.

J Leukoc Biol published online October 13, 2017
Access the most recent version at doi:10.1189/jlb.5A0617-219R

VIROLOGICA SINICA 2017, 32 (5): 369–375
DOI: 10.1007/s12250-017-4027-2

REVIEW

Lipids, lipid metabolism and Kaposi's sarcoma-associated herpesvirus pathogenesis

Lu Dai[1,2,3]✉, Zhen Lin[4], Wei Jiang[5], Erik K. Flemington[4], Zhiqiang Qin[1,2,3]✉

1. Department of Genetics, Louisiana State University Health Sciences Center, Louisiana Cancer Research Center, New Orleans 70112, USA
2. Department of Pediatrics, East Hospital, Tongji University School of Medicine, Shanghai 200120, China
3. Research Center for Translational Medicine and Key Laboratory of Arrhythmias, East Hospital, Tongji University School of Medicine, Shanghai 200120, China
4. Department of Pathology, Tulane University Health Sciences Center, Tulane Cancer Center, New Orleans 70112, USA
5. Department of Microbiology and Immunology, Division of Infectious Diseases, Department of Medicine, Medical University of South Carolina, Charleston 29425, USA

Lipids are essential for mammalian cells to maintain many physiological functions. Emerging evidence has shown that cancer cells can develop specific alterations in lipid biosynthesis and metabolism to facilitate their survival and various malignant behaviors. To date, the precise role of cellular lipids and lipid metabolism in viral oncogenesis is still largely unclear with only a handful of literature covering this topic to implicate lipid metabolism in oncogenic virus associated pathogenesis. In this review, we focus on the role of lipid biosynthesis and metabolism in the pathogenesis of the Kaposi's sarcoma-associated herpesvirus, a common causative factor for cancers arising in the immunocompromised settings.

KEYWORDS **Kaposi's sarcoma-associated herpesvirus (KSHV); herpesvirus; lipid metabolism**

INTRODUCTION

Kaposi's sarcoma-associated herpesvirus (KSHV, also known as human herpes virus-8, HHV8) is the causative agent for a number of cancers, including Kaposi's sarcoma (KS), primary effusion lymphoma (PEL) and multicentric Castleman disease (MCD), all of which arise preferentially in immunocompromised patients (Chang et al., 1994; Cesarman et al., 1995; Soulier et al., 1995). Currently, there are four KS isoforms: classic KS affecting elderly men of the Mediterranean; endemic KS, existing in some countries of Central and Eastern Africa; iatrogenic KS, which usually develops in organ transplant recipients with immunosuppression; and epidemic or AIDS-KS, which typically presents with more aggressive features (Mesri et al., 2010). Even though the combined antiretroviral therapy (cART) helps to reduce the total incidence of KS in the western world, KS is still the most common AIDS-associated malignancy and a leading cause of cancer-related morbidity and mortality in AIDS patients (Bonnet et al., 2004). PEL is a B-cell malignancy harboring KSHV which arises preferentially within the pleural or peritoneal cavities of immunocompromised patients (Cesarman et al., 1995). PEL is a rapidly progressing malignancy with a median survival time of approximately 6 months, even after the combinational chemotherapy (Chen et al., 2007). KSHV-associated MCD is a rare lymphoproliferative disorder that frequently arises in HIV+ patients who have a suppressed HIV

Received: 2 June 2017, Accepted: 5 September 2017,
Published online: 10 October 2017
✉Correspondence:
Zhiqiang Qin, Phone: +1-504-210-3327, Fax: +1-504-210-2970,
Email: zqin@lsuhsc.edu
ORCID: 0000-0002-9905-1275
Lu Dai, Phone: +1-504-210-3327, Fax: +1-504-210-2970,
Email: ldai@lsuhsc.edu
ORCID: 0000-0002-6818-8535

activity and a relatively preserved CD4 count (Wang et al., 2016). Like other herpesviruses, KSHV establishes a lifelong infection in the host utilizing two major distinct phases: latent infection and lytic replication. During the latent infection–the predominant phase in the majority of infected cells–only a limited number of viral genes are expressed. Provocation by a variety of stimuli induces lytic replication, resulting in new virion assembly and release of infectious viral particles (Schulz, 2006). Previous studies suggest that the oncogenic potential of KSHV is largely dependent upon genes expressed during the viral latency, however, recent data demonstrate that the viral lytic reactivation is critical for infection of naïve cell targets, maintenance of the KSHV reservoir, and tumor development (Aluigi et al., 1996; Lebbe et al., 1997; Grundhoff and Ganem, 2014;).

Lipids form a diverse group of water-insoluble molecules that include triacylglycerides, phosphoglycerides, sterols and sphingolipids. Lipids are essential for mammalian cells to maintain their physiological functions. For instance, fatty acids are the major building blocks for the synthesis of triacylglycerides during the process of energy storage. Phosphoglycerides, together with sterols and sphingolipids are the major structural components of cellular membranes. In addition, lipids as second messengers and hormones also play important roles in many signal transduction pathways. For example, lipids in the cellular membranes have been linked to the functions of several signal transduction pathways, including immunoglobulin E signaling (Sheets et al., 1999), T-cell antigen receptor signaling (Janes et al., 2000), glial-cell-derived neurotrophic factor (GDNF) signaling (Tansey et al., 2000), Ras signaling (Roy et al., 1999) and Hedgehog signaling (Porter et al., 1996). Accumulating evidence has shown that cancer cells develop specific alterations in different aspects of lipid metabolism to facilitate their survival and various malignant behaviors. To date, there are only a handful of studies describing how an oncogenic virus such as KSHV can manipulate host cellular lipid biosynthesis and metabolism to promote viral infection, pathogenesis, and tumorigenesis. In the current review, we summarize recent findings in this new area of KSHV research.

ROLE OF LIPIDS IN THE PRIMARY AND LATENT KSHV INFECTION

In cell culture, KSHV is able to infect various types of human cells, such as B cells, endothelial cells, epithelial cells, and fibroblasts (Dai et al., 2012; Fontana et al., 2014; Kang and Myoung, 2017). Several membrane proteins including heparin sulfate proteoglycan (HSPG), DC-SIGN, integrin α3β1/αvβ3, EphA2 and xCT can act as cellular receptors for KSHV infection in a cell type-dependent manner (Birkmann et al., 2001; Akula et al., 2002; Kaleeba and Berger, 2006; Rappocciolo et al., 2006; Garrigues et al., 2008; Hahn et al., 2012). After binding with these receptors, KSHV can induce the phosphorylation of focal adhesion kinase (FAK) which subsequently leads to the activation of Src, phosphatidylinositol 3-kinase (PI3-K), protein kinase C-ζ (PKC-ζ), Rho-GTPases, mitogen-activated protein kinase kinase (MEK), and extracellular signal regulated kinase 1/2 (ERK1/2) (Naranatt et al., 2003; Sharma-Walia et al., 2004; 2005). Activation of these signaling cascades can facilitate virus entry, its movement in the cytoplasm, and the nuclear delivery of viral DNA. Many of these KSHV induced signaling molecules are associated with lipid rafts micro-domains in the membrane. Previously, Raghu *et al.* reported that lipid rafts of endothelial cells play critical roles in KSHV infection and gene expression (Raghu et al., 2007). They found that disruption of lipid rafts by methyl β-cyclo dextrin (MβCD) or nystatin significantly inhibited the expression of viral latent gene, *Lana* (Latency-associated nuclear antigen), and the lytic gene, *Rta* (Replication and transcription activator). Lana is the only viral protein consistently expressed in all KS-associated malignancies (Dupin et al., 1999) and its major function is to maintain the viral episome in the latently-infected cells (Ballestas et al., 1999; Avey et al., 2015). Rta is a key viral protein initially controlling virus "latent to lytic" switch (Sun et al., 1998). The inhibition of Lana and Rta expression was mainly achieved by suppressing the KSHV-induced PI3-K and RhoA-GTPases activation and reducing the co-localizations of PI3-K and RhoA-GTPases with lipid rafts (Raghu et al., 2007). Since disruption of lipid rafts did not affect KSHV binding and viral DNA internalization, the authors concluded that lipid rafts are mainly required for KSHV-induced microtubule dynamics, virus movement in the cytoplasm, nuclear delivery of viral DNA, and viral gene expression (Raghu et al., 2007). A later study from the same group indicates that at a very early time-point during infection (~1 min post-infection), an adaptor protein, c-Cbl, can induce the selective translocation of KSHV into the lipid rafts along with the α3β1, αVβ3, and x-CT receptors, leading to a productive infection (Chakraborty et al., 2011). Knock-down of c-Cbl was found to inhibit KSHV infection by preventing micropinocytosis and selective virus-receptor translocation, with KSHV being diverted toward a clathrin-lysosomal noninfectious pathway.

One recent study has shown that KSHV infection can activate several components of the lipoxygenase pathway, including 5-lipoxygenase (5LO), leukotriene (LT) A4 hylase (LTA4H), and leukotriene B4 (LTB4), a chemotactic lipid mediator of the 5LO pathway (Sharma-Walia et al., 2014). Interestingly, blocking the 5LO/LTB4

cascade can inhibit the expression of KSHV-encoded latent protein Lana, the immunomodulatory protein K5, the viral macrophage inflammatory protein 1 (MIP-1), and MIP-2 expression. Taken together, these results clearly indicate that cellular lipids, lipid metabolism and related signaling pathways are involved in KSHV primary infection and subsequent latency establishment. Given its critical role in KSHV infection cycle, the lipid pathway may represent a promising "drug target" to manage KSHV infection.

ROLE OF LIPIDS IN KSHV REACTIVATION AND LYTIC REPLICATION

Like latency, viral reactivation and lytic replication also play important roles in KSHV oncogenesis. A recent study has shown that reactivation can be induced by some short-chain fatty acids (SCFAs) such as phenylbutyrate through inhibiting histone deacetylase (HDAC) activities (Gorres et al., 2014). Consistently, Yu *et al.* have found that several SCFAs produced by periodontal pathogens such as *Porphyromonas gingivalis and Fusobacterium nucleatum* can also induce the KSHV lytic reactivation by suppressing HDACs as well as two histone N-lysine methyltransferases (HLMTs): enhancer of zeste homolog2 (EZH2) and suppressor of variegation 3–9 homolog1 (SUV39H1) (Yu et al., 2014). These findings indicate that periodontal pathogens may create a unique microenvironment in the oral cavity, which in turns favors KSHV replication and KS development. Indeed, oral cavity involvement represents the initial manifestation of KS in 20%–60% of HIV-associated cases (Flaitz et al., 1997; Lager et al., 2003; Reichart 2003).

We recently reported that targeting sphingolipid metabolism by either sphingosine kinase inhibitors or exogenous ceramides can dramatically induce viral lytic genes expression in KSHV-infected primary endothelial cells or PEL cells (Qin et al., 2014; Dai et al., 2014, 2015). Such induction is at least in part mediated by the suppression of pro-latency viral microRNAs (e.g., miR-K12-1 and miR-K12-11) as well as related signaling pathways (e.g., NF-κB) (Dai et al., 2014).

ROLE OF LIPIDS IN THE SURVIVAL OF KSHV-INFECTED CELLS

Recent studies have shown that cellular lipids and lipid metabolism can regulate the survival of KSHV-infected primary and tumor cells. Having analyzed the metabolic profiles of primary B cells and KSHV+ PEL cells, Bhatt *et al*. found that KSHV+ PEL cells exhibit greater aerobic glycolysis and fatty acid synthesis than primary B cells (Bhatt et al., 2012). Meanwhile, the major lipid components of eukaryotic cell walls (e.g., phosphatidylcholine and phosphatidylethanolamine) are also more abundant in PEL cells. The fatty acid synthase (FASN), a multienzyme complex involved in the cellular lipids synthesis (Kuhajda et al., 2000), is overexpressed in PEL cells. Moreover, treatment of KSHV+ PEL cells with the FASN inhibitor, C75, can reduce cell viability in a dose-dependent manner (Bhatt et al., 2012).

Delgado *et al.* have utilized a metabolomic approach to investigate the KSHV mediated global metabolic alterations in latently infected cells (Delgado et al., 2012). They found that ~60 analyzed metabolites were altered after latent infection. Among them, many long chain fatty acids were affected due to the alteration of fatty acid synthesis pathways. Previous studies have shown that fatty acid synthesis is also required for the survival of latently infected endothelial cells and inhibition of key enzymes (e.g., acetyl-CoA carboxylase (Wang et al., 2009) or FASN (Kuhajda et al., 2000)) in this pathway led to apoptosis of infected cells. In contrast, addition of palmitic acid (the fundamental fatty acid precursor) can protect latently infected cells from the acetyl-CoA carboxylase inhibitor, 5-(Tetradecyloxy)-2-Furoic Acid (TOFA)-induced cell death. The same group later reported that the KSHV latent infection also increases peroxisome biogenesis. Interestingly, the proteins involved in peroxisomal lipid metabolism of very long chain fatty acids, such as ABCD3 (a peroxisome-specific lipid transporter) and ACOX1 (Acyl-CoA Oxidase 1, a peroxisomal enzyme), are required for the survival of latently infected cells (Sychev et al., 2017).

Sphingolipid biosynthesis involves hydrolytic conversion of ceramide to sphingosine. Subsequently, sphingosine is phosphorylated by one of two sphingosine kinase isoforms (SphK1 or SphK2) to generate bioactive sphingosine-1-phosphate (S1P) (Ogretmen and Hannun, 2004) (Figure 1). The relative levels of ceramide and S1P ultimately determine the fate of tumor cells, with accumulation of ceramides favoring apoptosis, and accumulation of S1P favoring proliferation (Cuvillier et al., 1996; Ogretmen and Hannun, 2004). SphK can be activated by a variety of tumor-promoting cytokines and growth factors. SphK activation is responsible for a rapid accumulation of intracellular S1P and depletion of ceramide species (Maceyka et al., 2002). S1P can subsequently bind to one of five G protein-coupled S1P receptors (S1PR1-5) and then activate diverse downstream signaling pathways (Strub et al., 2010). Because of their pleiotropic roles, bioactive sphingolipids have evolved as promising therapeutic targets for cancer treatment over the past two decades (Saddoughi et al., 2013). We have recently reported that induction of intracellular ceramide using a novel SphK2 inhibitor (ABC294640) or exogenous ceramide/dihydro(dh)-ceramide species (e.g., C6-Cer or dhC16-Cer) can effectively kill KSHV+ primary endothelial cells or PEL tumor cells, but have little effect on KSHV non-infected cell controls (e.g., naïve endothelial cells or

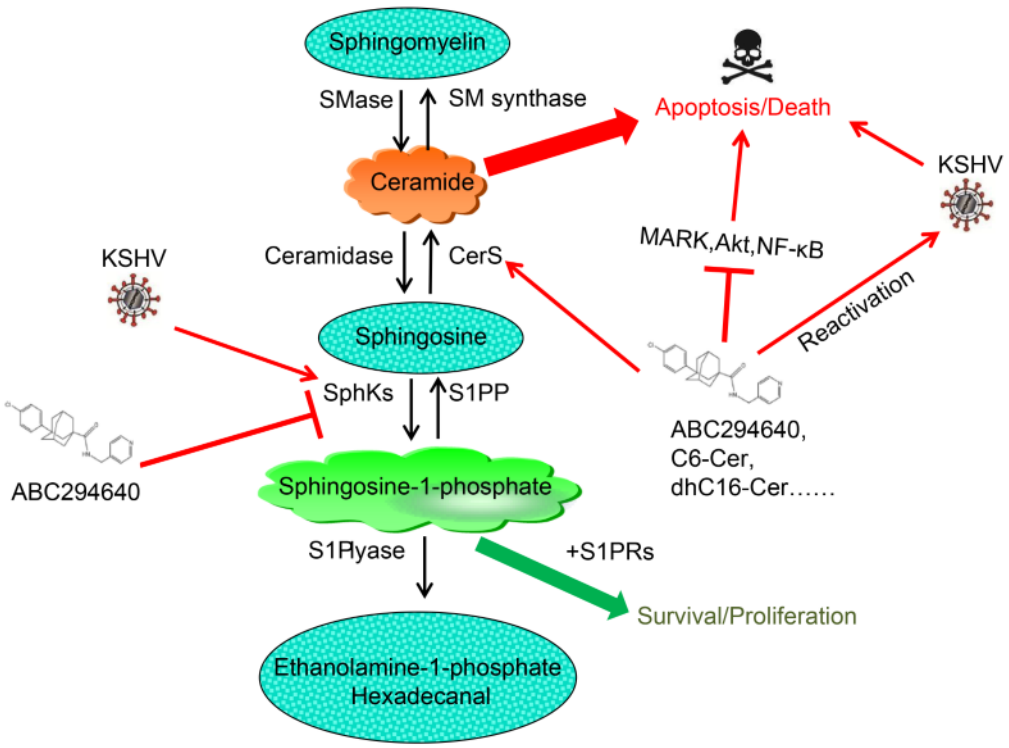

Figure 1. Targeting sphingolipid metabolism in KSHV-infected host cells. CerS, ceramide synthase; S1PP, S1P phosphatase; SphKs, sphingosine kinases; S1PRs, S1P receptors. ABC294640: A novel selective SPHK2 inhibitor; C6-Cer, dhC16-Cer etc: exogenous short- or long-chain ceramides.

B cells) (Qin et al., 2014; Dai et al., 2014, 2015). Further, these compounds can also repress KSHV+ PEL tumor progression *in vivo* and it is likely that this is mediated through interfering with several cell survival/proliferation-associated signaling pathways (e.g., MAPK/ERK, Akt and NF-κB) and up-regulating viral lytic genes and cellular tumor suppressor genes expression (Qin et al., 2014; Dai et al., 2015; Cao et al., 2017). In addition, the KSHV mediated up-regulation of SphK2 (Dai et al., 2014) may also help sensitize KSHV+ cells to sphingolipid targeted therapy.

LIPIDS AND KSHV- INDUCED ANGIOGENESIS/TRANSFORMATION

One recent study revealed that neutral lipid (NL) content is increased in KSHV-infected human umbilical vein endothelial cells (HUVEC) (Angius et al., 2015). In particular, triglyceride synthesis is boosted in the lytic phase, whereas the cholesteryl ester synthesis rises in the latent phase. Moreover, inhibition of cholesterol esterification significantly reduces neo-tubule formation mainly in latently infected cells, indicating that a reprogramming of cholesteryl ester metabolism is involved in KSHV-mediated neo-angiogenesis and that it may also contribute to the high metastatic potential of the derived-tumors.

It is believed that KSHV-encoded G protein-coupled receptor (vGPCR) is a key molecule in the pathogenesis of KS and that it plays a central role in promoting vascular endothelial growth factor-driven angiogenesis and spindle cell proliferation (Montaner et al., 2003; Grisotto et al., 2006; Wei et al., 2016). Several studies have shown that 1 Alpha, 25-dihydroxyvitamin D3 [1 alpha, 25(OH)(2)D(3)] and its TX527 analog inhibit the growth of vGPCR transformed endothelial cells *in vitro* and *in vivo*. The inhibition effects are achieved through a complex of mechanisms including an interaction with vitamin D receptor, down-regulation of the NF-κB pathway and up-regulation of the pro-apoptotic protein, Bim (Gonzalez-Pardo et al., 2010; 2012; 2013; Suares et al., 2015). Taken together, these data indicate the importance of vitamin D as a steroid signaling molecule in vGPCR-transformed endothelial cell proliferation.

CONCLUSION

Our group and others have recently shown that cellular lipids and lipid metabolism play important roles in KSHV-infected cell survival, pathogenesis, and tumorigenesis (summarized in Figure 2). Lipid research has become an

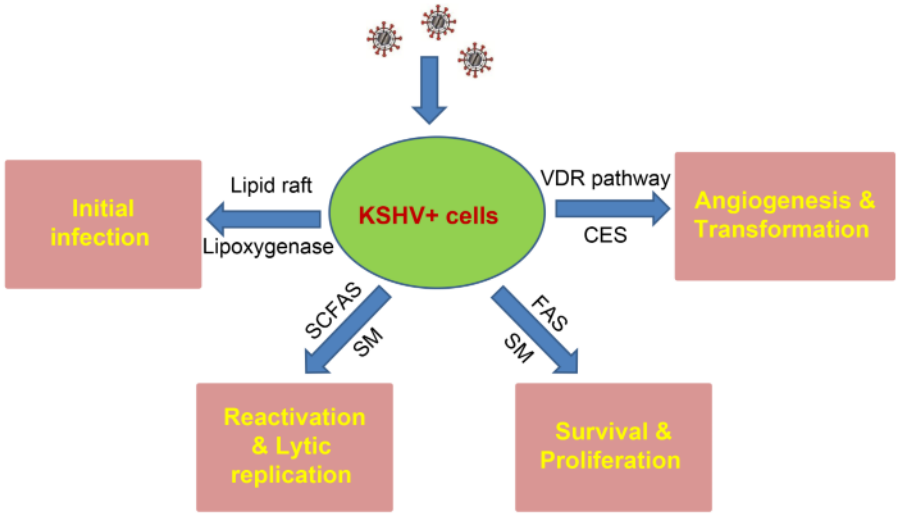

Figure 2. Schematic of recent findings about the contributions of cellular lipids and lipid metabolism to KSHV infection and pathogenesis. SCFAs: short-chain fatty acids; SM: sphingolipid metabolism; FAS: fatty acid synthesis; VDR: Vitamin D receptor; CES: cholesteryl ester synthesis.

exciting direction in the KSHV field. To date, it is still largely unclear how this oncogenic virus manipulates lipid biosynthesis and metabolism during *de novo* infection and KSHV mediated tumor development. Clinically, there are few data resulting from clinical trials testing the effectiveness of lipids-targeted therapeutics for KSHV-related malignancies. To the best of our knowledge, there's only one ongoing early phase trial for the evaluation of ABC294640 in patients with refractory/relapsed Diffuse Large B-cell Lymphoma (DLBCL) or Kaposi Sarcoma (KS) directed by Dr. Suki Subbiah (NCT0222 9981). How to accelerate the "bench to bedside" transition in this field is a key question needs to be addressed soon.

ACKNOWLEDGMENTS

This work was partially supported by grants from a DOD Career Development Award (CA140437), the Louisiana Clinical and Translational Science Center Pilot grants (U54GM104940 from NIH), a LSU LIFT2 funding, a NIH P20-GM121288-01 subproject, NIH RO1s (AI091526, AI128864, AI101046, and AI106676) as well as awards from the National Natural Science Foundation of China (81472547, 81400164, 81672924 and 81772930). Funding sources had no role in the study design, data collection/analysis, decision to publish, and/or manuscript preparation.

COMPLIANCE WITH ETHICS GUIDELINES

The authors declare that they have no conflicts of interest. This article does not contain any studies with human or animal subjects performed by any of the authors.

REFERENCES

Akula SM, Pramod NP, Wang FZ, Chandran B. 2002. Integrin alpha3beta1 (CD 49c/29) is a cellular receptor for Kaposi's sarcoma-associated herpesvirus (KSHV/HHV-8) entry into the target cells. Cell, 108: 407–419.

Aluigi MG, Albini A, Carlone S, Repetto L, De Marchi R, Icardi A, Moro M, Noonan D, Benelli R. 1996. KSHV sequences in biopsies and cultured spindle cells of epidemic, iatrogenic and Mediterranean forms of Kaposi's sarcoma. Res Virol, 147: 267–275.

Angius F, Uda S, Piras E, Spolitu S, Ingianni A, Batetta B, Pompei R. 2015. Neutral lipid alterations in human herpesvirus 8-infected HUVEC cells and their possible involvement in neo-angiogenesis. BMC Microbiol, 15: 74.

Avey D, Brewers B, Zhu F. 2015. Recent advances in the study of Kaposi's sarcoma-associated herpesvirus replication and pathogenesis. Virol Sin, 30: 130–145.

Ballestas ME, Chatis PA, Kaye KM. 1999. Efficient persistence of extrachromosomal KSHV DNA mediated by latency-associated nuclear antigen. Science, 284: 641–644.

Bhatt AP, Jacobs SR, Freemerman AJ, Makowski L, Rathmell JC, Dittmer DP, Damania B. 2012. Dysregulation of fatty acid synthesis and glycolysis in non-Hodgkin lymphoma. Proc Natl Acad Sci U S A, 109: 11818–11823.

Birkmann A, Mahr K, Ensser A, Yaguboglu S, Titgemeyer F, Fleckenstein B, Neipel F. 2001. Cell surface heparan sulfate is a receptor for human herpesvirus 8 and interacts with envelope glycoprotein K8. 1. J Virol, 75: 11583–11593.

Bonnet F, Lewden C, May T, Heripret L, Jougla E, Bevilacqua S, Costagliola D, Salmon D, Chene G, Morlat P. 2004. Malignancy-related causes of death in human immunodeficiency virus-infected patients in the era of highly active antiretroviral therapy. Cancer, 101: 317–324.

Cao Y, Qiao J, Lin Z, Zabaleta J, Dai L, Qin Z. 2017. Up-regulation of tumor suppressor genes by exogenous dhC16-Cer contributes to its anti-cancer activity in primary effusion lymphoma. Oncotarget, 8: 15220–15229.

Cesarman E, Chang Y, Moore PS, Said JW, Knowles DM. 1995. Kaposi's sarcoma-associated herpesvirus-like DNA sequences in AIDS-related body-cavity-based lymphomas. N Engl J Med, 332: 1186–1191.

Chakraborty S, ValiyaVeettil M, Sadagopan S, Paudel N, Chandran B. 2011. c-Cbl-mediated selective virus-receptor translocations into lipid rafts regulate productive Kaposi's sarcoma-associated herpesvirus infection in endothelial cells. J Virol, 85: 12410–12430.

Chang Y, Cesarman E, Pessin MS, Lee F, Culpepper J, Knowles DM, Moore PS. 1994. Identification of herpesvirus-like DNA sequences in AIDS-associated Kaposi's sarcoma. Science, 266: 1865–1869.

Chen YB, Rahemtullah A, Hochberg E. 2007. Primary effusion lymphoma. Oncologist, 12: 569–576.

Cuvillier O, Pirianov G, Kleuser B, Vanek PG, Coso OA, Gutkind S, Spiegel S. 1996. Suppression of ceramide-mediated programmed cell death by sphingosine-1-phosphate. Nature, 381: 800–803.

Dai L, Plaisance-Bonstaff K, Voelkel-Johnson C, Smith CD, Ogretmen B, Qin Z, Parsons C. 2014. Sphingosine kinase-2 maintains viral latency and survival for KSHV-infected endothelial cells. PLoS One, 9: e102314.

Dai L, Qin Z, Defee M, Toole BP, Kirkwood KL, Parsons C. 2012. Kaposi sarcoma-associated herpesvirus (KSHV) induces a functional tumor-associated phenotype for oral fibroblasts. Cancer Lett, 318: 214–220.

Dai L, Trillo-Tinoco J, Bai A, Chen Y, Bielawski J, Del Valle L, Smith CD, Ochoa AC, Qin Z, Parsons C. 2015. Ceramides promote apoptosis for virus-infected lymphoma cells through induction of ceramide synthases and viral lytic gene expression. Oncotarget, 6: 24246–24260.

Delgado T, Sanchez EL, Camarda R, Lagunoff M. 2012. Global metabolic profiling of infection by an oncogenic virus: KSHV induces and requires lipogenesis for survival of latent infection. PLoS Pathog, 8: e1002866.

Dupin N, Fisher C, Kellam P, Ariad S, Tulliez M, Franck N, van Marck E, Salmon D, Gorin I, Escande JP, Weiss RA, Alitalo K, Boshoff C. 1999. Distribution of human herpesvirus-8 latently infected cells in Kaposi's sarcoma, multicentric Castleman's disease, and primary effusion lymphoma. Proc Natl Acad Sci U S A, 96: 4546–4551.

Flaitz CM, Jin YT, Hicks MJ, Nichols CM, Wang YW, Su IJ. 1997. Kaposi's sarcoma-associated herpesvirus-like DNA sequences (KSHV/HHV-8) in oral AIDS-Kaposi's sarcoma: a PCR and clinicopathologic study. Oral Surg Oral Med Oral Pathol Oral Radiol Endod, 83: 259–264.

Fontana JM, Mygatt JG, Conant KL, Parsons CH, Kaleeba JA. 2014. Kaposi's Sarcoma-Associated Herpesvirus Subversion of the Anti-Inflammatory Response in Human Skin Cells Reveals Correlates of Latency and Disease Pathogenesis. J Skin Cancer, 2014: 246076.

Garrigues HJ, Rubinchikova YE, Dipersio CM, Rose TM. 2008. Integrin alphaVbeta3 Binds to the RGD motif of glycoprotein B of Kaposi's sarcoma-associated herpesvirus and functions as an RGD-dependent entry receptor. J Virol, 82: 1570–1580.

Gonzalez-Pardo V, D'Elia N, Verstuyf A, Boland R, Russo de Boland A. 2012. NFkappaB pathway is down-regulated by 1alpha, 25(OH)(2)-vitamin D(3) in endothelial cells transformed by Kaposi sarcoma-associated herpes virus G protein coupled receptor. Steroids, 77: 1025–1032.

Gonzalez-Pardo V, Martin D, Gutkind JS, Verstuyf A, Bouillon R, de Boland AR, Boland RL. 2010. 1 Alpha, 25-dihydroxyvitamin D3 and its TX527 analog inhibit the growth of endothelial cells transformed by Kaposi sarcoma-associated herpes virus G protein-coupled receptor in vitro and *in vivo*. Endocrinology, 151: 23–31.

Gonzalez-Pardo V, Verstuyf A, Boland R, Russo de Boland A. 2013. Vitamin D analogue TX 527 down-regulates the NF-kappaB pathway and controls the proliferation of endothelial cells transformed by Kaposi sarcoma herpesvirus. Br J Pharmacol, 169: 1635–1645.

Gorres KL, Daigle D, Mohanram S, Miller G. 2014. Activation and repression of Epstein-Barr Virus and Kaposi's sarcoma-associated herpesvirus lytic cycles by short- and medium-chain fatty acids. J Virol, 88: 8028–8044.

Grisotto MG, Garin A, Martin AP, Jensen KK, Chan P, Sealfon SC, Lira SA. 2006. The human herpesvirus 8 chemokine receptor vGPCR triggers autonomous proliferation of endothelial cells. J Clin Invest, 116: 1264–1273.

Grundhoff A, Ganem D. 2004. Inefficient establishment of KSHV latency suggests an additional role for continued lytic replication in Kaposi sarcoma pathogenesis. J Clin Invest, 113: 124–136.

Hahn AS, Kaufmann JK, Wies E, Naschberger E, Panteleev-Ivlev J, Schmidt K, Holzer A, Schmidt M, Chen J, Konig S, Ensser A, Myoung J, Brockmeyer NH, Sturzl M, Fleckenstein B, Neipel F. 2012. The ephrin receptor tyrosine kinase A2 is a cellular receptor for Kaposi's sarcoma-associated herpesvirus. Nat Med, 18: 961–966.

Janes PW, Ley SC, Magee AI, Kabouridis PS. 2000. The role of lipid rafts in T cell antigen receptor (TCR) signalling. Semin Immunol, 12: 23–34.

Kaleeba JA, Berger EA. 2006. Kaposi's sarcoma-associated herpesvirus fusion-entry receptor: cystine transporter xCT. Science, 311: 1921–1924.

Kang S, Myoung J. 2017. Primary lymphocyte infection models for KSHV and its putative tumorigenesis mechanisms in B cell lymphomas. J Microbiol, 55: 319–329.

Kuhajda FP, Pizer ES, Li JN, Mani NS, Frehywot GL, Townsend CA. 2000. Synthesis and antitumor activity of an inhibitor of fatty acid synthase. Proc Natl Acad Sci U S A, 97: 3450–3454.

Lager I, Altini M, Coleman H, Ali H. 2003. Oral Kaposi's sarcoma: a clinicopathologic study from South Africa. Oral Surg Oral Med Oral Pathol Oral Radiol Endod, 96: 701–710.

Lebbe C, de Cremoux P, Millot G, Podgorniak MP, Verola O, Berger R, Morel P, Calvo F. 1997. Characterization of in vitro culture of HIV-negative Kaposi's sarcoma-derived cells. In vitro responses to alfa interferon. Arch Dermatol Res, 289: 421–428.

Maceyka M, Payne SG, Milstien S, Spiegel S. 2002. Sphingosine kinase, sphingosine-1-phosphate, and apoptosis. Biochim Biophys Acta, 1585: 193–201.

Mesri EA, Cesarman E, Boshoff C. 2010. Kaposi's sarcoma and its associated herpesvirus. Nat Rev Cancer, 10: 707–719.

Montaner S, Sodhi A, Molinolo A, Bugge TH, Sawai ET, He Y, Li Y, Ray PE, Gutkind JS. 2003. Endothelial infection with KSHV genes in vivo reveals that vGPCR initiates Kaposi's sarcomagenesis and can promote the tumorigenic potential of viral latent genes. Cancer Cell, 3: 23–36.

Naranatt PP, Akula SM, Zien CA, Krishnan HH, Chandran B. 2003. Kaposi's sarcoma-associated herpesvirus induces the phosphatidylinositol 3-kinase-PKC-zeta-MEK-ERK signaling pathway in target cells early during infection: implications for infectivity. J Virol, 77: 1524–1539.

Ogretmen B, Hannun YA. 2004. Biologically active sphingolipids in cancer pathogenesis and treatment. Nat Rev Cancer, 4: 604–616.

Porter JA, Young KE, Beachy PA. 1996. Cholesterol modification of hedgehog signaling proteins in animal development. Science, 274: 255–259.

Qin Z, Dai L, Trillo-Tinoco J, Senkal C, Wang W, Reske T, Bonstaff K, Del Valle L, Rodriguez P, Flemington E, Voelkel-Johnson C, Smith CD, Ogretmen B, Parsons C. 2014. Targeting sphingosine kinase induces apoptosis and tumor regression for KSHV-associated primary effusion lymphoma. Mol Cancer Ther, 13: 154–164.

Raghu H, Sharma-Walia N, Veettil MV, Sadagopan S, Caballero A, Sivakumar R, Varga L, Bottero V, Chandran B. 2007. Lipid rafts of primary endothelial cells are essential for Kaposi's sarcoma-associated herpesvirus/human herpesvirus 8-induced phosphatidylinositol 3-kinase and RhoA-GTPases critical for microtubule dynamics and nuclear delivery of viral DNA but dispensable for binding and entry. J Virol, 81: 7941–7959.

Rappocciolo G, Jenkins FJ, Hensler HR, Piazza P, Jais M, Borowski L, Watkins SC, Rinaldo CR, Jr. 2006. DC-SIGN is a receptor for human herpesvirus 8 on dendritic cells and macrophages. J Immunol, 176: 1741–1749.

Reichart PA. 2003. Oral manifestations in HIV infection: fungal and bacterial infections, Kaposi's sarcoma. Med Microbiol Immunol, 192: 165–169.

Roy S, Luetterforst R, Harding A, Apolloni A, Etheridge M, Stang E, Rolls B, Hancock JF, Parton RG. 1999. Dominant-negative caveolin inhibits H-Ras function by disrupting cholesterol-rich plasma membrane domains. Nat Cell Biol, 1: 98–105.

Saddoughi SA, Ogretmen B. 2013. Diverse functions of ceramide in cancer cell death and proliferation. Adv Cancer Res, 117: 37–58.

Schulz TF. 2006. The pleiotropic effects of Kaposi's sarcoma herpesvirus. J Pathol, 208: 187–198.

Sharma-Walia N, Chandran K, Patel K, Veettil MV, Marginean A. 2014. The Kaposi's sarcoma-associated herpesvirus (KSHV)-induced 5-lipoxygenase-leukotriene B4 cascade plays key roles in KSHV latency, monocyte recruitment, and lipogenesis. J Virol, 88: 2131–2156.

Sharma-Walia N, Krishnan HH, Naranatt PP, Zeng L, Smith MS, Chandran B. 2005. ERK1/2 and MEK1/2 induced by Kaposi's sarcoma-associated herpesvirus (human herpesvirus 8) early during infection of target cells are essential for expression of viral genes and for establishment of infection. J Virol, 79: 10308–10329.

Sharma-Walia N, Naranatt PP, Krishnan HH, Zeng L, Chandran B. 2004. Kaposi's sarcoma-associated herpesvirus/human herpesvirus 8 envelope glycoprotein gB induces the integrin-dependent focal adhesion kinase-Src-phosphatidylinositol 3-kinase-rho GTPase signal pathways and cytoskeletal rearrangements. J Virol, 78: 4207–4223.

Sheets ED, Holowka D, Baird B. 1999. Critical role for cholesterol in Lyn-mediated tyrosine phosphorylation of FcepsilonRI and their association with detergent-resistant membranes. J Cell Biol, 145: 877–887.

Soulier J, Grollet L, Oksenhendler E, Cacoub P, Cazals-Hatem D, Babinet P, d'Agay MF, Clauvel JP, Raphael M, Degos L, et al. 1995. Kaposi's sarcoma-associated herpesvirus-like DNA sequences in multicentric Castleman's disease. Blood, 86: 1276–1280.

Strub GM, Maceyka M, Hait NC, Milstien S, Spiegel S. 2010. Extracellular and intracellular actions of sphingosine-1-phosphate. Adv Exp Med Biol, 688: 141–155.

Suares A, Russo de Boland A, Verstuyf A, Boland R, Gonzalez-Pardo V. 2015. The proapoptotic protein Bim is up regulated by 1alpha, 25-dihydroxyvitamin D3 and its receptor agonist in endothelial cells and transformed by viral GPCR associated to Kaposi sarcoma. Steroids, 102: 85–91.

Sun R, Lin SF, Gradoville L, Yuan Y, Zhu F, Miller G. 1998. A viral gene that activates lytic cycle expression of Kaposi's sarcoma-associated herpesvirus. Proc Natl Acad Sci U S A, 95: 10866–10871.

Sychev ZE, Hu A, DiMaio TA, Gitter A, Camp ND, Noble WS, Wolf-Yadlin A, Lagunoff M. 2017. Integrated systems biology analysis of KSHV latent infection reveals viral induction and reliance on peroxisome mediated lipid metabolism. PLoS Pathog, 13: e1006256.

Tansey MG, Baloh RH, Milbrandt J, Johnson EM, Jr. 2000. GFRalpha-mediated localization of RET to lipid rafts is required for effective downstream signaling, differentiation, and neuronal survival. Neuron, 25: 611–623.

Wang C, Xu C, Sun M, Luo D, Liao DF, Cao D. 2009. Acetyl-CoA carboxylase-alpha inhibitor TOFA induces human cancer cell apoptosis. Biochem Biophys Res Commun, 385: 302–306.

Wang HW, Pittaluga S, Jaffe ES. 2016. Multicentric Castleman disease: Where are we now?. Semin Diagn Pathol, 33: 294–306.

Wei F, Zhu Q, Ding L, Liang Q, Cai Q. 2016. Manipulation of the host cell membrane by human γ-herpesviruses EBV and KSHV for pathogenesis. Virol Sin, 31: 395–405.

Yu X, Shahir AM, Sha J, Feng Z, Eapen B, Nithianantham S, Das B, Karn J, Weinberg A, Bissada NF, Ye F. 2014. Short-Chain Fatty Acids from Periodontal Pathogens Suppress Histone Deacetylases, EZH2, and SUV39H1 To Promote Kaposi's Sarcoma-Associated Herpesvirus Replication. J Virol, 88: 4466–4479.